Genetic analyses of MAP kinase signalling in mouse gonad development

A thesis presented for the degree of Doctor of Philosophy (D.Phil)

Wolfson College, University of Oxford

Rachel Joan Elizabeth Brixey

MRC Mammalian Genetics Unit, Harwell

Department of Biochemistry, University of Oxford

Supervisors: Dr Andy Greenfield (MGU, MRC Harwell)
Dr Catherine Pears (Biochemistry, Oxford)

Trinity term 2011

Word count: 43,285

Genetic analyses of MAP kinase signalling in mouse gonad development

Rachel Brixey

Wolfson College, Oxford
MRC Mammalian Genetics Unit, Harwell
Department of Biochemistry, University of Oxford

A thesis presented for D.Phil, Trinity term, 2011

Abstract

Sexual development begins with the process by which the bipotential gonads of the embryonic urogenital ridge develop into either testes or ovaries. In the mouse, sex determination occurs at around 11.5 dpc and depends on the presence or absence of the Y chromosome and the associated activity of the testis-determining gene, *Sry*, in supporting cell precursors. The mutually antagonistic male and female developmental pathways are regulated by many cellular and molecular processes, disruption of which can lead to disorders of sex development (DSDs). However, many of the molecular mechanisms regulating the differentiation of the two gonads are still unknown.

The boygirl (*byg*) mutant was identified in an ENU-based forward genetic screen for embryos with gonadal abnormalities. On the C57BL/6J background, XY *byg/byg* homozygotes exhibited complete embryonic gonadal sex reversal. The defective gene in *byg*, *Map3k4*, is a component of the mitogen-activated protein (MAP) kinase signalling pathway and provides the first evidence for a function of this pathway in sex determination.

This thesis describes experiments aimed at investigating the cellular and molecular basis of the sex reversal phenotype associated with the XY *Map3k4*$^{byg/byg}$ mutant. Cellular characterisations revealed a defect in male-specific proliferation at 11.5 dpc, which was attributed to a defect in *Sry* up-regulation. Elucidation of the downstream kinases activated by MAP3K4 during sex determination was attempted, with particular focus on identifying a role for p38α MAP kinase (MAPK). Using a conditional knockout approach, the function of p38α in Steroidogenic factor-1 (*Sf1*)-positive somatic cells was assessed. However, specific inactivation in these cells did not affect gonad development. Conditional inactivation of *Map3k4* itself in these *Sf1*-positive cells also did not disrupt gonad development, suggesting that this pathway is either initiated in a different cell lineage or at an earlier stage than deletion driven by *Sf1-Cre* can disrupt. Conditional inactivation of p38α in the Müllerian duct mesenchyme and ovarian granulosa cells using *Amhr2-Cre* did reveal a function for p38α in female fertility, but did not disrupt embryonic sexual development. Gene knockdown in organ culture was attempted to determine a role for multiple p38 MAPKs in all cell types of the gonad. Therefore, this thesis details further characterisations of a novel signalling pathway important for the expression of *Sry*, focussing on the role of the p38 MAPKs.

Acknowledgements

First and foremost I extend my sincere gratitude to Dr Andy Greenfield, for being a fantastic supervisor throughout the 3½ years that I have spent on my DPhil and for motivating me when I've needed it. I would also not have been able to write this thesis in the short time I had remaining without his excellent advice and extremely quick proof reading.

I am extremely grateful to all of the laboratory members, past and present, particularly for making the 'Sex lab' such an enjoyable environment in which to work. Particular thanks go to Nick Warr, Pam Siggers and Deb Bogani for going out of their way to help me in the lab, and Nick for being a fellow perfectionist and a great dissection buddy since we both frequently left things to the last minute. Also, special thanks go to Nick and Pam for proof reading some first drafts of my thesis chapters, and Asha Dopplapudi for designing the *Mapk11* and *Mapk14* riboprobes for me. My thanks are also extended to all members of the development lab, particularly for contribution of ideas during my lab meetings.

The opportunity to use some of the core services present at MRC Harwell has been particularly beneficial. First, and most importantly, I'd like to thank all of the Ward 5 staff in the MLC who have looked after my mice and generated my colonies so (seemingly) effortlessly. Particularly Sara Wells and Jackie Harrison, without whom I could not have carried out the experiments detailed in this thesis. I am also grateful to Debbie Williams for all of her help with teaching me the basics of qRT-PCR and data analysis, the Histology team, Jim Humphreys and Dave Shipston in the Necropsy team, Martin Fray and the FESA team, Anne Southwell and Deb Brooker in GEMS who carried out my pyrosequencing analysis, Stuart Townsend and Jeremy Sanderson for teaching me how to use the confocal microscope and help with other imaging, and Michael Cheeseman for providing advice on my histology sections.

I'd like to thank all of the students at Harwell for making the unit such an enjoyable place to be. Particular thanks go to Vicki Patterson, Stuti Mehta, Laura Pastorelli, Dan Grimes, Anju Paudyal and Jonathan Stevens for help with various aspects of my work.

Lastly, I'd like to thank my family, most notably my parents, and Niall McCann for supporting and encouraging me so much in all that I do, not least during my long career as a student.

I thank the Medical Research Council for funding this research.

Contents

List of Figures

List of Tables

Abbreviations

AMH	Anti-Müllerian hormone
AMHR2	Anti-Müllerian hormone receptor 2
ATP	Adenosine triphosphate
BAC	bacterial artificial chromosome
β-gal	β-galactosidase
bp	base pairs
BrdU	bromodeoxyuridine
BSA	Bovine serum albumin
byg	boygirl
cDNA	complementary DNA
CGD	complete gonadal dysgenesis
Ct	cycle threshold
DIG	Digoxygenin
DMEM	Dulbecco's Minimal Eagle's Medium
DMRT1	double-sex and Mab-3 related transcription factor 1
DNA	deoxynucleic acid
dpc	days *post coitum*
dpp	days *post partum*
ds	double stranded
DSD	Disorder of sex development
ENU	*N*-ethyl-*N*-nitrosourea
ERK	extracellular signal-related kinase
FCS	Foetal calf serum
FESA	Frozen Embryo and Sperm Archive team at MRC Harwell
FGF9	fibroblast growth factor 9
FGFR2	FGF receptor 2
FOXL2	Forkhead box L2
FSH	Follicle stimulating hormone
G_0	Gap 0; mitotic arrest/quiescent phase of cell cycle
G_1	Gap 1; early interphase
G_2	Gap 2; late interphase
GATA4	member of the GATA family of transcription factors
GD	gonadal dysgenesis
H&E	haematoxylin and eosin
HISS	heat inactivated sheep serum
HMG	High mobility group
IHC	immunohistochemistry
JNK	c-Jun amino terminal kinases
kd	knockdown
LB	lysogeny broth medium
MeOH	methanol
MAP	mitogen activated protein
MAPK	MAP kinase
MAP2K	MAP kinase kinase
MAP3K	MAP kinase kinase kinase

mRNA	messenger RNA
miRNA	micro RNA
NP-40	Nonidet P-40
nt	nucleotide
O.C.T.	optimum cutting temperature compound
PBS	phosphate buffered saline
PBST	PBS with 1% Tween
PBS-BS	PBS with 1% BSA and 11% sucrose
PBS-BT	PBS with 1% BSA and 0.2% triton x-100
PCR	Polymerase chain reaction
PECAM	platelet/endothelial cell adhesion molecule
PFA	paraformaldehyde
PGD2	Prostaglandin D2
pHH3	phosphorylated histone H3
qRT-PCR	quantitative real-time reverse-transcriptase PCR
PK	Proteinase K
PGC	Primordial germ cell
R26R	Rosa-26 reporter line
RISC	RNA-induced silencing complex
RNA	ribonucleic acid
RNAi	RNA interference
rpm	revolutions per minute
RQ	Relative quantification; method to calculate the fold change
RSPO1	R-spondin 1
SDS	sodium dodecyl sulphate
SEM	standard error of the mean
SF1	Steroidogenic factor 1
shRNA	short hairpin
siRNA	short interfering RNA
SNP	single nucleotide polymorphism
SOX9	SRY-related HMG box 9
SRY	Sex-determining region on the Y Chromosome
ss	single-stranded
SSC	Saline-sodium citrate buffer
STRA8	Stimulated by retinoic acid 8
TBE	Tris/Borate/EDTA buffer
TBST	Tris buffered saline with Tween
TESCO	Testis-specific enhancer of *Sox9* core
TGF-β	transforming growth factor β
ts	tail somites
UGR	urogenital ridge
UTR	untranslated region
UV	ultra violet
WMISH	wholemount *in situ* hybridisation
WNT	wingless-type MMTV integration site family
wt	wild-type
WT1	Wilms tumour suppressor 1

Mitogen-activated protein kinase-related nomenclature

Due to the discrepancies found in the literature over the nomenclature used when describing mitogen-activated protein kinase-related research, this section clarifies the nomenclature used in this thesis.

The mitogen-activated protein kinase signalling cascade as a whole is referred to as the 'MAP kinase' pathway. This is to allow differentiation from referral to particular components of the pathway.

The MAP kinase kinase kinases are referred to as the MAP3Ks, with specific members named as MAP3K1, MAP3K2 etc.

The MAP kinase kinases are referred to as the MAP2Ks, and in this case, specific members are named as MKK1, MKK2 etc to enable easy differentiation from the MAP3Ks at a quick glance.

The MAP kinases are referred to as the MAPKs, with specific member proteins named by family group; JNK1/2/3, ERK1/2, ERK5 and p38α/β/γ/δ, for ease of family identification. Specific genes encoding these MAPKs are used in their official form (*Mapk11*, *Mapk12* etc) to comply with official Mouse Genome Informatics (MGI) nomenclature guidelines.

Chapter 1. Introduction

1.1. Overview

Sex determination is the process by which an organism develops as either male or female. There are a number of diverse sex determination systems in nature; the sex of some species is determined chromosomally, whilst others are non-genetic and depend on the environment. The most well characterised system is that of mammals, such as mice and humans. In this case, the Y chromosome is a dominant male determinant: males are usually heterogametic (XY) and females homogametic (XX). This chromosomal sex is determined at the moment of fertilisation due to the inheritance of either the paternal X or Y chromosome. Gonadal sex describes the development of bipotential gonads into either testes or ovaries. This is determined by the presence or absence of the sex-determining gene on the Y chromosome (*SRY*) and in the mouse, this sex-determining period is around 11.5 days *post coitum* (dpc) (Gubbay et al. 1990; Koopman et al. 1990; Sinclair et al. 1990). Lastly, phenotypic sex describes the development of the reproductive tracts, external genitalia and secondary sexual characteristics, mediated predominantly by gonadal hormones.

The sexual development process is extremely complex, largely due to the unique bipotential nature of the gonadal primordium, the genital ridge. Many key genes and signalling pathways involved in sex determination are still being identified, and some of these will be discussed below. One recently identified component of the mammalian sex-determining pathway is the mitogen-activated protein (MAP) kinase signalling cascade. The role of this pathway was implicated by the discovery of a function for the molecule, MAP3K4, in mouse testis determination (Bogani et al. 2009). The research described in this thesis attempts to characterise the cellular and molecular basis of the

gonadal defects in *Map3k4*-deficient XY embryos and identify the downstream components of the pathway that are involved in sex determination. Before discussing MAP3K4, however, I will describe important recent developments in our understanding of mammalian sex determination, with an emphasis on mouse development.

1.2. Mammalian sex determination

1.2.1. Formation of the urogenital ridge

In the mouse, the urogenital ridge (UGR) forms around 9.0 dpc from the intermediate mesoderm, between the somitic and lateral plate mesoderm, on the dorsal side of the embryo (Karl and Capel 1995). It forms as a pair of mounds along the length of the anteroposterior axis within the body cavity, on either side of the neural tube and dorsal aorta. This mesodermal region is initially comprised of three distinct regions: the pronephros, mesonephros and metanephros. The pronephros forms at the anterior end, but has no known function and regresses soon after it has formed. The mesonephros, the mid-section, gives rise to the mesonephric ducts and gonadal region, while the metanephros at the posterior end forms the definitive kidney (Figure 1.1).

The first event in the development of the urogenital ridge is the formation of the mesonephric (or Wolffian) duct (Smith and Mackay 1991; Torres et al. 1995). This develops along the intermediate mesoderm in an anterior to posterior direction to meet the cloaca. The initial anterior portion, along with a few non-functional tubules, represents the pronephros region. By 9.5 dpc the mesonephric duct has extended further down the mesenchyme defining the mesonephric region and mesonephric tubules begin to form. The mesonephric duct reaches the cloaca by 10.0 dpc and the epithelial cells that form the duct are then surrounded by mesenchymal cells. At this stage, the bipotential genital ridge also begins to form as a thickening of the coelomic epithelium

on the ventromedial surface of the mesonephros. Mesonephric tubules become more extensive and convoluted, and tubules from the anterior end of the mesonephros connect the mesonephric duct with the gonad (Karl and Capel 1995). However, by 12.5 dpc these connections have degenerated. The metanephric region forms when the ureteric buds develop out from the posterior end of the mesonephric duct around 11.0 dpc. These induce the differentiation of the kidney within the metanephric region (Saxén 1987).

1.2.2. The bipotential gonad

The early bipotential gonad consists of primordial germ cells (PGCs), coelomic epithelial cells, and gonadal blastema, containing somatic cells. The PGCs are first observed in the embryo at 7.2 dpc and are found in a region posterior to the primitive streak in the extraembryonic mesoderm, separated from the embryo by the amniotic fold (Ginsburg et al. 1990). These PGCs proliferate and individuals migrate anteriorly through the hindgut towards the site of the genital ridge. They populate the gonads between 10.5 and 11.5 dpc, shortly after the gonad has formed from the mesonephros (Tam and Snow 1981; Gomperts et al. 1994). This accumulation of PGCs in to the gonad is assisted by a change in shape, enabling the PGCs to link together and form aggregates (Gomperts et al. 1994). Once in the gonadal ridge, the PGCs become less motile, continue to proliferate and by 13.5 dpc, the gonad is fully colonised by the PGCs. Following this stage, the PGCs respond to sexually dimorphic cues in the surrounding somatic cells to begin differentiation into either oocytes or spermatocytes. This will be discussed further later on (see section 1.2.6.2 and 1.2.7).

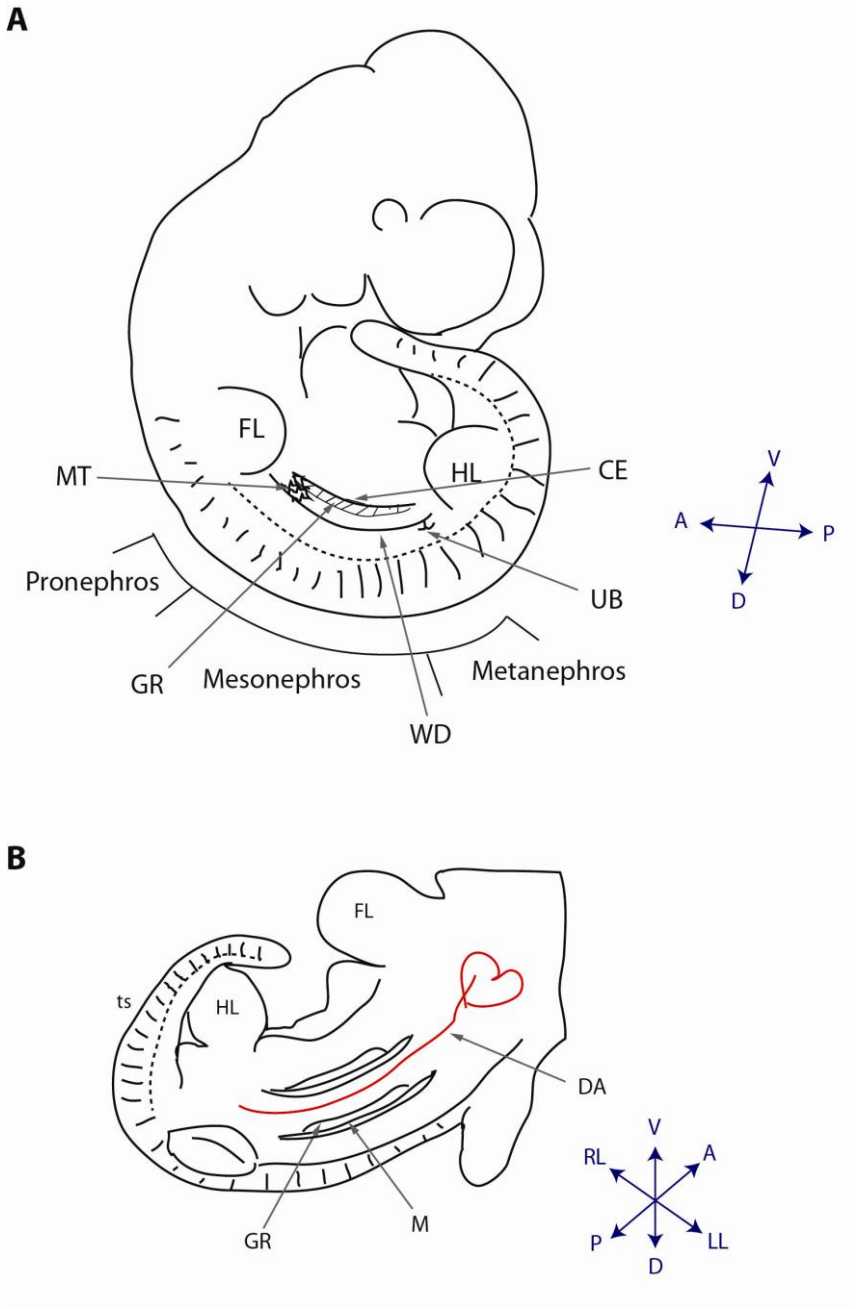

Figure 1.1: Schematic of the position of the urogenital ridge at 10.5 dpc
(A) The urogenital ridges are located in the intermediate mesoderm along the dorsal side of the embryo, either side of the dorsal aorta. The mesonephric duct (Wolffian duct, WD) forms between the forelimb (FL) and the hindlimb (HL) in an anterior to posterior direction. It is comprised of three regions: the pronephros, which has no function and regresses; the mesonephros, which gives rise to the mesonephric tubules (MT) and gonadal ridge (GR); and the metanephros, from which the ureteric buds (UB) form to give rise to the kidney.
(B) The gonadal ridge forms from the ventromedial surface of the mesonephroi (M). CE, coelomic epithelium; DA, dorsal aorta; ts, tail somites; A↔P, anteroposterior axis; D↔V, dorsoventral axis; RL↔LL, right lateral to medial to left lateral axis.

The somatic cells are comprised of three important precursor cell lineages: the steroidogenic cells, supporting cells and connective tissue. These are bipotential in nature until genetic cues, depending on the presence or absence of the Y chromosome, drive their sex-specific differentiation from 11.5 dpc. The connective tissue lineage includes the stromal cells, endothelial cells and male-specific peritubular myoid cells and these cells are important for the organisational structure and formation of either the testis or ovary. The supporting cell lineage gives rise to either the testis-specific Sertoli cells or the ovary-specific granulosa cells, which play an important role in supporting the healthy development of germ cells. Lastly, the steroidogenic lineage gives rise to the steroid hormone-producing cells such as the Leydig cells in the testis and theca cells in the ovary and these contribute to the secondary sexual characteristics of the embryo (Swain and Lovell-Badge 1999).

1.2.3. Genetic regulation of gonad formation

There are several genes, particularly transcription factors, which are essential for the formation and development of the early bipotential gonad before the expression of the testis-determining gene, *Sry*, at around 10.5 dpc. These include *Sf1* (also known as *Nr5a1/Ad4BP)*, *Wt1*, *Gata4*, *Fog2 (Zfpm2)*, *Emx2*, *Lhx9*, *Dax1 (Nr0b1)* and *M33 (Cbx2)*. Whether they are also required for subsequent sex-specific development is not always clear, but mice carrying disruptions to these genes all display early gonad development and/or kidney and adrenal developmental defects. Some of the genes that are relevant to the rest of this thesis are discussed in further detail below.

The steroidogenic factor 1 (SF1)/nuclear receptor subfamily 5, group A, member 1 (NR5A1)/adrenal 4-binding protein (Ad4BP) transcription factor is expressed in the developing gonadal ridge at the earliest stage of development between 9.0 and 9.5 dpc

(Ikeda et al. 1994). In later stage embryos, the transcript encoding SF1 is expressed in both the gonadal and adrenal primordia; reflecting its steroidogenic function. It is also expressed in the diencephalon region of the forebrain, containing the hypothalamic primordium, which further confirms its endocrine-related function. The targeted disruption of the gene encoding this nuclear receptor results in the development of mice that lack adrenal glands and gonads, and consequently have a severe deficiency in corticosterone, a steroid produced by the adrenal cortex (Luo et al. 1994). They also have impaired formation of the ventromedial hypothalamic nucleus (Ikeda et al. 1995). The gonads form initially but degenerate between 11.0 and 11.5 dpc due to increased apoptosis. This suggests that SF1 is not involved in the initial formation of the urogenital ridge, or the migration of germ cells, but has a role in the growth and differentiation of the bipotential somatic cells (Swain and Lovell-Badge 1999). *In vitro* data has also shown that SF1 is a potential activator of *Sry* because it can bind to and activate both the human and pig *SRY* promoter (Pilon et al. 2003). In support of this, recent data reveal a role for SF1 in the regulation of *Sry* expression in the mouse: reduced dosage of *Sf1*, when combined with the loss of CITED2 (a transcriptional co-factor), can result in partial or complete sex reversal due to disruption of *Sry* expression (Buaas et al. 2009).

Wilms tumour suppressor 1 (WT1) is another transcription factor that is expressed from 9.0 dpc in the urogenital ridge (Armstrong et al. 1993). Later, it is expressed in the coelomic epithelium and in either Sertoli cells or granulosa cells. WT1 functions in epithelial-mesenchymal transitions found in the developing gonad and kidney and the homozygous knockout of *Wt1* results in early embryonic lethality and the failure to form gonads or kidneys (Kreidberg et al. 1993). The *Wt1* gene encodes at least 24 different isoforms through alternative splicing but all contain four zinc fingers at the C-

terminal domain. It has been found that splice variants leading to the insertion or omission of a three-amino acid-sequence (KTS) between zinc fingers 3 and 4 (designated as either +KTS or −KTS variants) lead to distinct functions (Hammes et al. 2001). Targeted disruption of the −KTS form results in streak gonads in both XX and XY embryos, highlighting a function for this spliced isoform in early gonad formation and development. In contrast, the targeted disruption of the +KTS isoform (which causes Frasier's syndrome in humans as characterised by feminisation of external XY genitalia) caused XY sex reversal, but did not affect XX development, suggesting a role for WT1 (+KTS) that is specific to testis determination. It has been suggested that the −KTS form can bind to and activate the *Sf1* promoter (Wilhelm and Englert 2002), while the +KTS form is involved in the direct cell-autonomous regulation of *Sry* expression (Bradford et al. 2009). Thus, both WT1 (+KTS) and WT1 (−KTS) display a role in gonad development, but have different functions at different stages.

GATA4 is a member of the GATA zinc-finger family of transcription factors and is the only member active in the somatic cells of the early gonad (Viger et al. 1998). *Gata4* expression has been detected in somatic cells of the urogenital ridge from the earliest stage examined (10.5 dpc) (Ketola et al. 2002). The GATA proteins require a physical interaction with multitype zinc-finger co-factors of the FOG (Friend of GATA) family for normal function. The FOG associated with GATA4 is FOG2 (also known as ZFPM2), which is also expressed in the somatic cells of the urogenital ridge at the same stages as GATA4 (Tevosian et al. 2002). The knockout of FOG2, which is embryonic lethal by 14.5 dpc, did not affect the initial formation of the urogenital ridge and wild-type levels of *Wt1* and *Sf1* were present. However, the expression of *Sry* at 11.5 dpc was significantly decreased, which consequently caused disruption to later testis development (Tevosian et al. 2002). In contrast, the *Gata4*$^{-/-}$ knockout mutant dies

between 7.0 and 9.5 dpc but the generation of a *Gata4* knock-in allele that abrogates the interaction between GATA4 and FOG2 survives until 13.5 dpc (Crispino et al. 2001). Analysis of gonad development in these mutants revealed a similar disruption to testis development as displayed with the *Fog2*$^{-/-}$, confirming that the GATA4/FOG2 complex is involved in the regulation of *Sry* expression (Tevosian et al. 2002).

1.2.4. Sex determination

The mammalian testis-determining pathway begins with the expression of *Sry* in somatic cells of the XY gonadal ridge from 10.5 dpc (Koopman et al. 1990). This gene on the Y chromosome was identified in 1990, some thirty years after the Y chromosome was identified as the dominant male determinant in humans and mice (Welshons and Russell 1959; Gubbay et al. 1990; Sekido and Lovell-Badge 2009). The expression of *Sry* drives the gonad towards the testicular fate, whilst its absence promotes ovarian development. This was confirmed by experiments in which XX embryos that carried a transgene of *Sry* developed as infertile males (Koopman et al. 1991).

Sry is transcribed as a single exon and is expressed in both a temporal and spatial wave-like pattern. It is restricted to the urogenital ridge and is only expressed between 10.5 and 12.5 dpc, reaching its peak at 11.5 dpc (Koopman et al. 1990; Jeske et al. 1995). The expression is initiated in the central portion of the gonadal ridge before extending out to the anterior and posterior poles over the course of a few hours. Following the peak expression along the length of the genital ridge at 11.5 dpc, expression then decreases in the central and anterior portions prior to loss of expression in the posterior region (Bullejos and Koopman 2001). This window of expression is critical for the subsequent activation of the SRY target, *Sox9*, which is required for Sertoli cell differentiation and the cascade of downstream testis development events. If the

initiation of *Sry* expression is delayed, even by 6 hours, testis development fails to be initiated (Hiramatsu et al. 2009). The SRY protein contains a conserved high mobility group (HMG) DNA-binding domain. This 79 amino acid motif enables the protein to bind to the (A/T)ACAA(T/A) consensus sequence in the minor groove of DNA causing a 60-85° bend (as reviewed in (Polanco and Koopman 2007)). The rest of the protein is not highly conserved, therefore it is mutations in the HMG box domain that lead to a non-functioning protein and XY sex reversal. There are other domains of SRY that mediate protein-protein interactions and transcriptional *trans*-activation or -repression. This suggests, along with evidence from *Sry*-negative XX maleness in human patients, that it is likely that SRY may also be involved in the repression of certain female-specific proteins that act as male development suppressors (McElreavey et al. 1993; Polanco and Koopman 2007).

SRY is a member of the SOX (SRY-related HMG box) family of transcription factors and one of these, *Sox9*, is thought to be the only target of SRY (Sekido and Lovell-Badge 2008). *Sox9* is expressed in several organ systems of the mouse embryo, including the skeleton, heart, kidneys and brain (Wright et al. 1995). However, it is also strongly expressed in the somatic cells of the XY urogenital ridge shortly after the expression of SRY, mimicking the same wave-like pattern, but persisting beyond 12.5 dpc (Morais da Silva et al. 1996; Sekido et al. 2004). SOX9 is important for bone formation in mammals and mutations in human *SOX9* lead to a skeletal dysmorphology syndrome, campomelic dysplasia (CD). Patients with CD often display XY sex reversal and this provided the first evidence that SOX9 is involved in sex determination (Wright et al. 1995). This has been further supported by loss- and gain-of-function studies in mice in which the homozygous deletion of *Sox9* causes XY sex reversal, whilst the transgenic activation of *Sox9* causes XX sex reversal (Vidal et al. 2001; Chaboissier et

al. 2004; Barrionuevo et al. 2006). Therefore, *Sox9* is sufficient and necessary for testis development.

Sox9 is activated by SRY through the binding of SRY, along with SF1, to an enhancer region (called TESCO; testis-specific enhancer of *Sox9* core) upstream of the *Sox9* transcription start-site (Sekido and Lovell-Badge 2008). The initiation of low-level expression of *Sox9* is mediated by SF1 and occurs in both XY and XX somatic cells. At 11.5 dpc, once SRY has reached a critical level of expression, SRY acts synergistically with SF1 to upregulate *Sox9* in the XY somatic cells. Once SOX9 has subsequently reached a critical threshold of expression, *Sry* is repressed via a SOX9-dependent negative-feedback loop (Chaboissier et al. 2004). SOX9 levels are then maintained through various positive-feedback loops with other genes (discussed in detail in the next section), and also by auto-regulation, since SOX9 is also an HMG-family transcription factor, and can bind to the TESCO region on *Sox9* to maintain its own expression (Sekido and Lovell-Badge 2008).

The up-regulation of *Sry* and *Sox9* promotes the testis-specific pathway of gonad development. They trigger the activation of numerous other genes that are involved in this process, which will be discussed in more detail throughout this introduction. They also initiate the cellular differentiation and organisation that are important to testis development and function. In the absence of *Sry* and the up-regulation of *Sox9*, the ovarian pathway is initiated. These two pathways are mutually antagonistic; the activation of one also drives the repression of the other and consequently sex determination is a strongly canalised developmental process. This is discussed further in section 1.2.7. A summary of the testis- and ovary-specific events is shown in Figure 1.2.

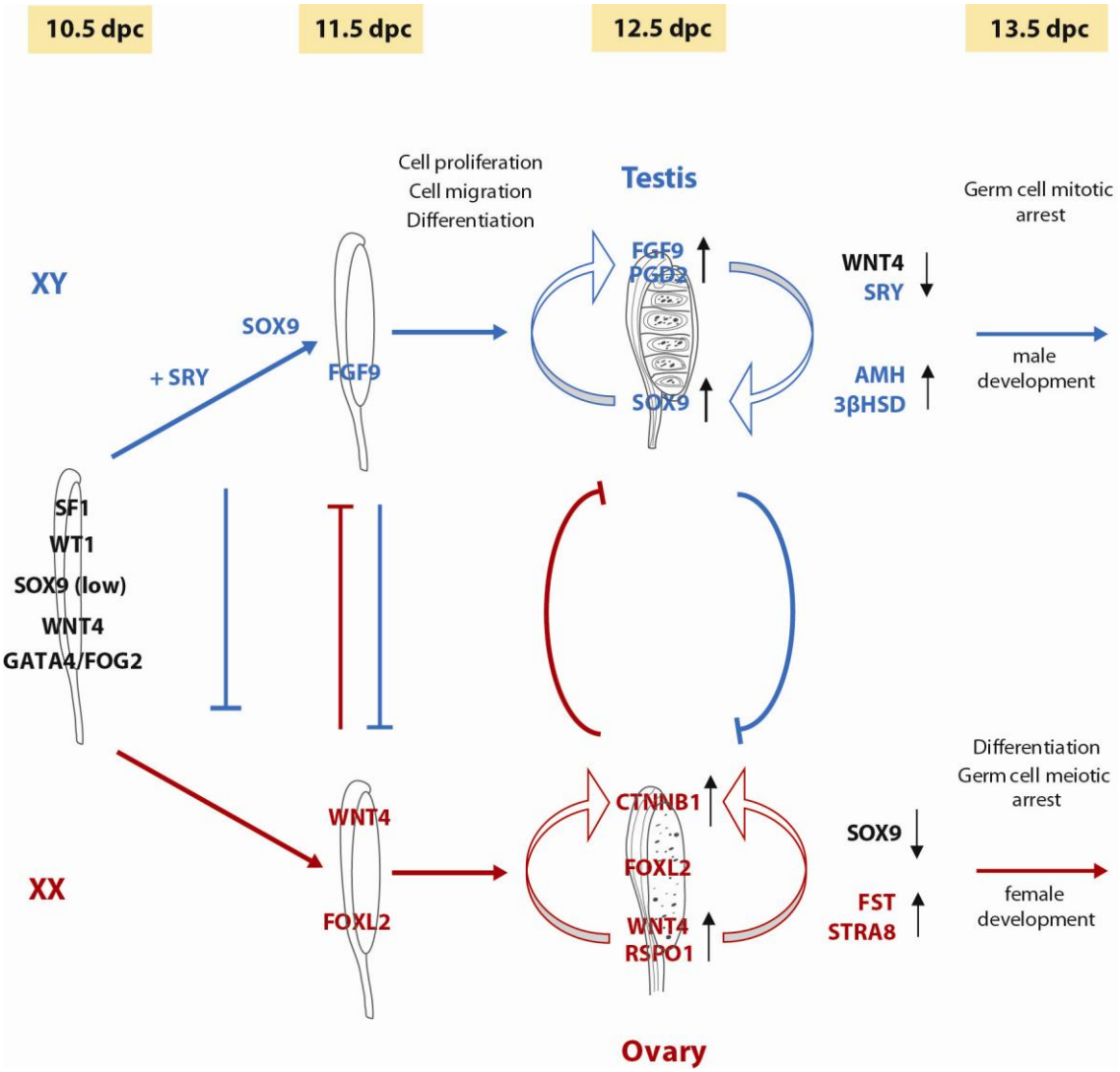

Figure 1.2: Schematic representation of the key cellular and molecular events driving sex determination

The presence of SRY from 10.5 dpc drives the differentiation of the bipotential gonad down the testis development pathway with subsequent up-regulation of other testis-determining genes. Key cellular events including cell proliferation and migration induce morphological changes and the development of testis cords. Hormones produced from the testis direct development of the secondary male characteristics. In the absence of SRY, the female development pathway is initiated with the up-regulation of the canonical Wnt pathway members and FOXL2. Germ cells enter meiotic arrest, and the absence of male hormones permits the development of secondary female characteristics. Multiple feedback loops and mutual antagonistic interactions exist to support normal development of either pathway. Only molecules and interactions relevant to this thesis are shown.

1.2.5. Molecular events driving testis development

The activation of SRY in the developing testis triggers the differentiation of the bipotential somatic supporting cell lineage into Sertoli cells (Burgoyne et al. 1988; Sekido et al. 2004). These Sertoli cells then cluster around germ cells and, in conjunction with migratory endothelial cells and peritubular myoid cells, form testis cords that subsequently contribute to the sex-specific development of germ cells. Sertoli cells are also thought to regulate the development of Leydig cells from the steroidogenic lineage (Wilhelm and Koopman 2006).

Due to the vital role of Sertoli cells in the organisation and development of the testis, there are a number of mechanisms employed to ensure that the Sertoli cell numbers do not fall below the critical level required for normal development. First, is the auto-regulation of *Sox9* mentioned previously. Second, is the ability of cells that have expressed sufficient *Sox9* to induce *Sox9* expression in neighbouring cells, in which the expression of *Sry* alone may be insufficient. This paracrine recruitment mechanism is facilitated by testis-specific prostaglandin D2 (PGD2) and *Ptgds*, which encodes the enzyme required for PGD2 production, is itself activated by SOX9 (Wilhelm et al. 2005; Wilhelm et al. 2007; Moniot et al. 2009; Koopman 2010). The role of PGD2 was confirmed by an experiment that showed PGD2 could induce *Sox9* expression and thus Sertoli cell differentiation in XX cells from aggregated XX and XY gonads (Wilhelm et al. 2005). This system is not reported to be necessary for testis development based on the phenotype of the *Ptgds* knockout, but is thought to act as a backup or reinforcement (Moniot et al. 2009). A SOX9 positive-feedback loop is also established with fibroblast growth factor 9 (FGF9) (Kim et al. 2006). FGF9 is a secreted growth factor that is expressed in pre-Sertoli cells following SOX9 up-regulation (Sekido and Lovell-Badge 2009). *Fgf9* expression is thought to be activated by SOX9, and in turn FGF9 functions

to maintain expression of *Sox9*. Contrary to the backup role of PGD2, FGF9 has a more vital function in the maintenance of SOX9 expression and subsequent Sertoli cell differentiation. Mice harbouring a homozygous deletion of *Fgf9* display XY sex reversal and decreased levels of SOX9 after 11.5 dpc (Colvin et al. 2001; Kim et al. 2006). In addition, the loss of FGFR2, the receptor for FGF9, leads to testis developmental defects and XY sex reversal (Kim et al. 2007; Bagheri-Fam et al. 2008).

1.2.6. Cellular events driving testis development

Following *Sry* expression and the initiation of Sertoli cell differentiation, a number of cellular events specific to testis development take place. These include increased cell proliferation of coelomic epithelial cells, migration of mesonephric cells into the body of the gonad, and differentiation of other precursor cells into testis-specific lineages. All of these events cause the developing testis to increase in size relative to the XX gonad and develop testis cords. These specific cellular differences are visible by 12.5 dpc (see Figure 1.3 for an overview of the cellular structure).

1.2.6.1. Cell proliferation

Pre-Sertoli cells and pre-granulosa cells proliferate between 10.5 and 11.5 dpc in XY and XX gonads. Increased cell proliferation in the coelomic epithelium of the XY gonad then occurs from 11.25 dpc and this testis-specific event is induced directly by *Sry* (Schmahl et al. 2000). However, it is cell proliferation events prior to this stage that are vital to testis determination. A classic experiment in which embryonic cell proliferation was blocked at different stages of development showed that only proliferation in the XY gonad between 10.8 and 11.2 dpc was vital for testis development (Schmahl and Capel 2003). If proliferation was inhibited either side of this period, testis development was not disrupted, but inhibition during this window led to a complete absence of testis

cords and disruption to Sertoli cell differentiation. The cell lineage in which this testis-determining proliferation occurs has not yet been determined. The fact that a difference in the cell proliferation rate between XX and XY gonads cannot be detected within this 10.8 to 11.2 dpc window suggests that it is not dependent on *Sry*, but may be required to prime the gonad for appropriate *Sry* expression.

The detectable, male-enhanced, coelomic epithelial cell proliferation occurs in different stages (Schmahl et al. 2000). The initial *Sry*-dependent stage occurs from 11.25 dpc in SF1-positive cells until 11.5 dpc (16-18 tail somites (ts)). A second stage of proliferation follows in SF1-negative cells at or near the coelomic epithelium between 19 and 25 ts, with a final stage after 25 ts in a mixture of SF1-positive and -negative cells throughout the gonad, not just concentrated to the coelomic region. SF1 is expressed in somatic cells of the bipotential gonad, and in XY gonads these are the precursors of both Sertoli cells (due to the role of SF1 in the expression of *Sox9*) and Leydig cells (due to the steroidogenic function of SF1) (Ikeda et al. 1994). Therefore, the different stages of cell proliferation are thought to give rise to different cell lineages. The first stage gives rise to Sertoli cells, which then migrate into the gonad to form testis cords during the SF1-negative proliferative phase, before proliferating again after 25 ts. Precursors to interstitial cells proliferated during both the SF1-positive and -negative phases and were tentatively identified as Leydig cells and vascular cells, respectively. These cell lineage observations are also consistent with previous work that identified Sertoli cells as originating from the coelomic epithelium and migrating into the body of the gonad between 15 and 17 ts (Karl and Capel 1998). Migrating coelomic epithelial cells from 18-20 ts stage gonads stayed in the interstitium.

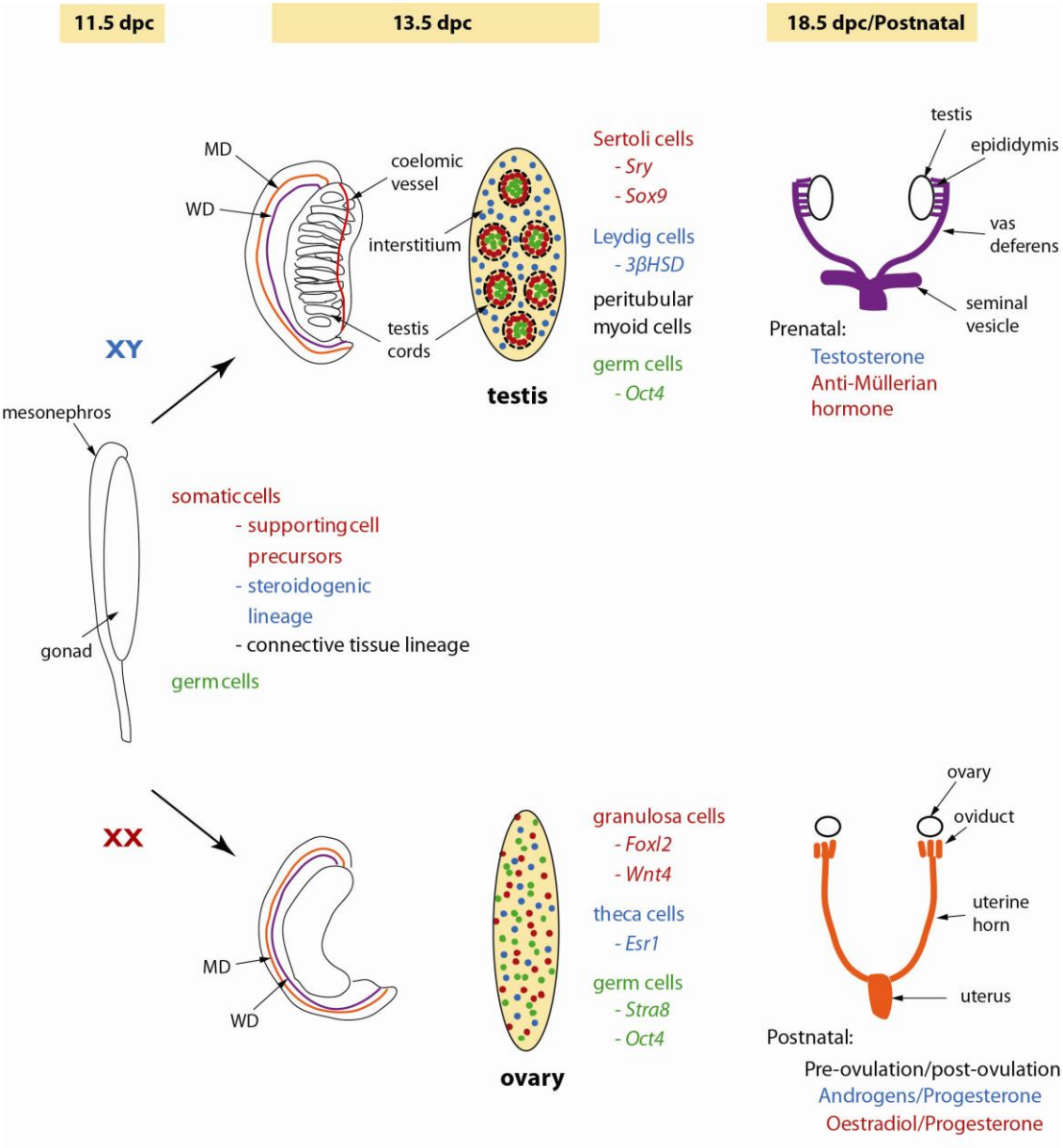

Figure 1.3: Cellular events guiding sexual development
By 13.5 dpc, both the Wolffian duct (WD, purple) and Müllerian duct (MD, orange) are present in both XX and XY mesonephroi. Testis cords in the male develop from 12.5 dpc. Endothelial cells migrate into the gonad from the mesonephros and develop the testis-specific vasculature and coelomic vessel (red). Sertoli cells cluster around germ cells and are encapsulated by peritubular myoid cells to form testis cords, which are directed by endothelial cells. Leydig cells differentiate in the interstitium. Sertoli cells produce anti-Müllerian hormone (AMH), which drives MD regression, and Leydig cells produce testosterone, which directs differentiation of the WD into the structures marked. In the ovary, precursors to granulosa cells and theca cells, and germ cells (which enter meiosis at 13.5 dpc) are present. Absence of testosterone and AMH directs the differentiation of the MD into the structures marked, while the WD regresses. In the postnatal ovary, the differentiated theca cells form around the follicle and are stimulated by luteinising hormone (LH) to produce androgens. The differentiated granulosa cells support oocyte development in the follicles. They are stimulated by follicle-stimulating hormone (FSH) to convert the androgens into oestradiol. Post-ovulation, both cells produce progesterone. Key markers for each sex-specific cell lineage are marked, and each lineage is colour-coded throughout.

The main functions of elevated testis-specific proliferation are to i) increase the size of the XY gonad and ii) establish the necessary numbers of precursor cells to enable testis development to continue. FGF9, along with its receptor FGFR2, are necessary for the Sertoli cell-specific proliferation and the subsequent differentiation. FGFR2 is initially localised to the plasma membrane of pre-Sertoli coelomic epithelial cells, and this is characteristic of a role in cell proliferation mediated by FGF9 (Kim et al. 2007). However, by 11.0 dpc, FGFR2 becomes sexually dimorphic following nuclear localisation in Sertoli cells within the body of the XY gonad (Schmahl et al. 2004). This XY specific localisation is important for Sertoli cell differentiation, leading to the conclusion that FGF9 is not just important for the maintenance of SOX9 expression levels, but also for Sertoli cell proliferation and differentiation (Kim et al. 2007).

1.2.6.2. Differentiation and migration

Following the proliferation and differentiation of Sertoli cells, differentiation of the other important cell types for testis development occurs. Cells from the connective tissue lineage are important for the formation of testis cords and the vascularisation of the testis. The stromal cells and peritubular myoid cells are thought to arise from differentiation within the mesenchyme of the gonad, while endothelial cells migrate in from the mesonephros in a testis-specific fashion (Martineau et al. 1997; Cool et al. 2008; Archambeault et al. 2009). These endothelial cells form a characteristic vasculature for the embryonic testis, comprising a prominent coelomic vessel along the ventral surface of the coelomic epithelium (Wilhelm and Koopman 2006), and are also required to direct testis cord formation (Combes et al. 2009b; Cool et al. 2011).

Peritubular myoid cells are flat, elongated cells that help to direct the development of testis cords. They form a single layer of cells around Sertoli cells, encapsulating the testis cords containing XY germ cells. In this environment, XY germ cells enter G_0/G_1 quiescence (mitotic arrest) from 12.5 dpc. They remain in this state until after birth at which point they then resume mitosis and differentiate into spermatogonia (Kocer et al. 2009). Significantly, XY germ cells are not required for testis cord formation or the maintenance of testis development since it has been shown that the testis cords can form even in the absence of germ cells, as in the W/W^v germ cell-free gonad (Kurohmaru et al. 1992). However, it is likely that one of the functions of the testis cord structure is to protect the XY germ cells from meiosis-inducing effects of retinoic acid, a secretion molecule that is produced in the mesonephros. Sertoli cells express CYP26B1, an enzyme that breaks down retinoic acid, allowing the germ cells to remain in mitotic arrest (Bowles et al. 2006). FGF9 has also been shown to direct XY germ cell fate by repressing the action of retinoic acid in an antagonistic mechanism (Bowles et al. 2010).

Leydig cells develop as distinct foetal and adult lineages, but both are responsible for steroidogenesis in the testis. Foetal Leydig cells differentiate from early SF1-positive cells and are present in the interstitium surrounding the testis cords from 12.5 dpc (Brennan and Capel 2004). Their role is to produce testosterone that is required for subsequent development and maturation of the testis and internal/external male genitalia. Leydig cell precursors have been shown to arise from the coelomic epithelium and also through migration from the mesonephros before 11.0 dpc (Karl and Capel 1998; Jeays-Ward et al. 2003; DeFalco et al. 2011).

1.2.7. Ovarian determination and antagonism

In the absence of *Sry*, XX gonads develop as ovaries. Contrary to original proposals, ovarian development is an active process and defined genetic programmes are initiated in the XX gonad as early as 11.5 dpc, despite cellular differences not being apparent until after 13.5 dpc (Nef et al. 2005). The main cellular event is the induction of meiosis in XX germ cells. This can be detected by the expression of *Stra8* (Stimulated by retinoic acid), a marker of meiosis that is triggered by retinoic acid (Koubova et al. 2006). XX germ cells must enter meiosis at this stage during embryogenesis to initiate oocyte differentiation; in contrast to the germ cells in XY gonads, which are not required for testis development, the absence of germ cells in XX gonads leads to ovarian dysgenesis and follicle abnormalities with no function (McLaren 1991).

The main genes that are activated during early ovarian development encode members of the canonical Wnt signalling pathway (WNT4, β-catenin (CTNNB1) and RSPO1), transcription factor FOXL2, and a glycoprotein, FST. All have been postulated as the female-sex-determining factor; however, the mouse knockouts of each produce only partial XX sex reversal, with the formation of ovotestes, rather than complete XX sex reversal as would be expected. Instead, it is likely that a combination of RSPO1, CTNNB1, WNT4 and FOXL2 (potentially with other unidentified genes) is required to maintain ovarian development and repress the testis pathway. The antagonism between the male and female pathways has been shown to exist throughout development but also during reproductive life, and this is discussed briefly below.

Wnt4 is initially expressed in the bipotential urogenital ridge from 9.5 dpc in the mesonephros and from 11.0 dpc in the coelomic epithelium, but from 11.5 dpc, becomes restricted to the XX gonad although it is still present in the mesonephros of

both sexes (Vainio et al. 1999). In XX *Wnt4*$^{-/-}$ mutant gonads, partial XX sex reversal occurs with the up-regulation of *Sox9* and *Fgf9* despite the absence of *Sry* (Vainio et al. 1999; Jeays-Ward et al. 2003; Yao et al. 2004; Kim et al. 2006). As a result, WNT4 and FGF9 were shown to act with mutual antagonism to repress the development of the opposing pathway. In XY *Fgf9*$^{-/-}$ mutant gonads, the expression of *Wnt4* was upregulated (Kim et al. 2006). WNT4 has also been shown to activate follistatin (*Fst*), a glycoprotein that inhibits the formation of the XY-specific vasculature and coelomic vessel, and promotes germ cell survival (Yao et al. 2004).

The role for R-spondin1 (RSPO1) in ovary development emerged recently following evidence from a human study in which members of an Italian family with incidences of XX, *SRY*-negative, sex reversal, carried mutations in the *RSPO1* gene (Parma et al. 2006). However, in mice, the homozygous deletion of *Rspo1* resulted in the development of XX ovotestes; the gonads were partially masculinised with a very similar phenotype to that found from the *Wnt4*$^{-/-}$ mutants (Chassot et al. 2008; Tomizuka et al. 2008), suggesting that RSPO1 was directly involved in WNT4 signalling in the gonad. This was confirmed in the analysis of the *Rspo1*$^{-/-}$ XX mutant, in which *Wnt4* and genes involved in β-catenin signalling were downregulated, suggesting that RSPO1 positively regulated both *Wnt4* and *Ctnnb1* (Chassot et al. 2008; Tomizuka et al. 2008). The role of β-catenin in ovary development was confirmed following the conditional inactivation in *Sf1*-positive somatic cells: disruption to ovary development in XX gonads occurred with a strikingly similar phenotype to that observed with both *Wnt4*$^{-/-}$ and *Rspo1*$^{-/-}$ XX mutants (Liu et al. 2009).

Forkhead box L2 (FOXL2) is a transcription factor that is ovary specific with activation in pre-granulosa cells occurring from 11.5 dpc and increasing expression levels until

early postnatal life specifically in primordial follicles (Ottolenghi et al. 2007). Homozygous null mutations of *Foxl2* in mice caused partial sex reversal in postnatal XX animals but no abnormalities were detected during development (Ottolenghi et al. 2005). Perinatal expression of *Sox9* was upregulated in the XX *Foxl2*$^{-/-}$ gonads suggesting a role for FOXL2 in the repression of *Sox9* postnatally.

Antagonism between the testis- and ovary-determining genetic networks was only recently discovered to be essential for maintenance of gonadal identity throughout reproductive life, rather than just being restricted to sex determination in the embryo. This later function of FOXL2 was confirmed by a study utilising the conditional knockout strategy to inactivate *Foxl2* in the adult ovary (Uhlenhaut et al. 2009). The loss of FOXL2 in adult granulosa cells caused these cells to reprogram to become Sertoli cells, with the up-regulation of *Sox9* and *Dmrt1*, which consequently triggered complete transdifferentiation of theca cells to Leydig cells and the production of testosterone. More recently, a second report demonstrated that the loss of DMRT1 in adult males activated *Foxl2* and reprogrammed Sertoli cells into granulosa cells (Matson et al. 2011). Theca cells also formed in these mutant mice, producing oestrogen and germ cells became feminised.

1.3. Development of the reproductive tracts

Before sexual differentiation, the mesonephros contains two pairs of genital ducts, the Wolffian (mesonephric) duct and the Müllerian (paramesonephric) duct (Kobayashi and Behringer 2003). The Wolffian duct is the precursor of the male reproductive tracts and matures to form the epididymides, vasa deferentia and seminal vesicles, while the Müllerian duct is the precursor of the female reproductive tracts and differentiates into the oviducts, uterus, cervix and upper vagina. The differentiation of the sex-specific

ducts into the respective reproductive tracts is dependent on hormonal signalling; testosterone produced from Leydig cells drives the differentiation of the Wolffian duct, while anti-Müllerian hormone (AMH) produced from Sertoli cells drives the regression of the Müllerian duct through interaction with its receptor, AMHR2, in the Müllerian duct mesenchyme (Behringer et al. 1994; Wilhelm and Koopman 2006). The absence of these hormones in females allows the Müllerian duct to differentiate and the Wolffian duct to degenerate (Kobayashi and Behringer 2003). However, this section focuses specifically on the Müllerian duct.

1.3.1. Formation of the Müllerian duct

The Müllerian duct develops in both sexes from 11.75 dpc and is completed by 13.5 dpc (Orvis and Behringer 2007). Initially, cells in the coelomic epithelium first become specialised to the Müllerian duct fate and then invaginate from the coelomic epithelium out to the Wolffian duct. This occurs by 12.0 dpc and is driven by WNT4 expression in the mesonephros (Vainio et al. 1999). These primordial cells then proliferate to enable elongation of the duct alongside the Wolffian duct towards the cloaca. This process is dependent on the expression of WNT9B in the Wolffian duct, which acts as a guide for the extending duct (Carroll et al. 2005).

1.3.2. Male-specific regression of the Müllerian duct

The regression of the unrequired duct begins shortly after the Müllerian duct has fully formed. In females, in the absence of testosterone, the Wolffian duct begins to regress passively from 13.5 dpc through the loss of cells: no specific female hormone is associated with this process. In males, the presence of AMH drives the regression of the Müllerian duct from the same stage (Orvis and Behringer 2007). AMH is both necessary and sufficient for the regression of the Müllerian duct as evidenced by the formation of

uteri and oviducts alongside normal male reproductive tract derivatives in XY *Amh*$^{-/-}$ mutant mice (Behringer et al. 1994), and the absence of Müllerian duct derivatives in XX mice with overexpressed *Amh* (Behringer et al. 1990). In humans, mutations in *AMH* have been identified in patients with Persistent Müllerian duct syndrome (PMDS). This is a rare disorder of sex development (DSD), in which the female reproductive tract is retained in an otherwise virilised male (Josso et al. 1997).

AMH is a member of the transforming growth factor-β (TGF-β) superfamily that is secreted by Sertoli cells (Josso and Clemente 2003). In XY mice, *Amh* is expressed from 11.5 dpc, levels then increase until birth but decrease dramatically at puberty (Münsterberg and Lovell-Badge 1991). The expression of *Amh* is directly regulated by SOX9, SF1, GATA4 and WT1. In females, expression is not detected until 6 days post partum in the granulosa cells of the ovary.

AMH signalling is mediated by its type II receptor, AMHR2. In mice, the mutation of *Amhr2* causes an identical XY phenotype to that seen with loss of *Amh* (Mishina et al. 1996). Moreover, in humans, mutations in *Amhr2* have also been identified in patients with PMDS (Josso et al. 1997). AMHR2 is therefore the only type II receptor required to mediate the AMH-induced regression of the Müllerian duct, but also mediates signalling from AMH for other functions within the testis and ovary. *Amhr2* is expressed in the Müllerian duct mesenchyme from 13.5 dpc, and also in the embryonic and postnatal gonad (Arango et al. 2008). Expression studies of *Amhr2* in the rat revealed embryonic localisation to Sertoli cells and granulosa cells and, in the adult, testicular expression was observed in Sertoli and Leydig cells and ovarian expression in the granulosa cells of preantral and small antral follicles, but not primordial (Baarends et al. 1994; Baarends et al. 1995a; Baarends et al. 1995b; Racine et al. 1998). The

Amhr2-expressing cells are initially present in the coelomic epithelium of both male and female mesonephroi, and then migrate into the mesenchyme surrounding the male Müllerian duct under the influence of AMH (Zhan et al. 2006). This mesenchymal expression of *Amhr2* is also regulated by WNT7A from the Müllerian duct epithelium and in XY *Wnt7a*$^{-/-}$ knockouts, the Müllerian duct fails to regress (Parr and McMahon 1998).

Two type I receptors have also been linked to AMH signalling: BMPR1A (also known as ALK3) and ACVR1 (ALK2). The deletion of *Bmpr1a* in *Amhr2*-expressing cells in the Müllerian duct mesenchyme inhibited the regression of the Müllerian duct in males (Jamin et al. 2002). The knockdown of *Acvr1* in gonad organ culture prevented the transition of *Amhr2* expression from the coelomic epithelium of the mesonephros to the mesenchyme surrounding the Müllerian duct and also prevented Müllerian duct regression (Zhan et al. 2006). This suggests that different type I receptors are recruited by AMH/AMHR2 at different stages of development. To determine the downstream signalling of AMH activation during Müllerian duct regression, the role of WNT/β-catenin signalling was investigated through the conditional ablation of β-catenin in *Amhr2*-expressing cells in the Müllerian duct mesenchyme (Kobayashi et al. 2011). In XY mutants, Müllerian duct regression was inhibited. Conversely, the ablation in *Wnt7a*-expressing cells in the Müllerian duct epithelium did not affect the regression, suggesting that the canonical WNT pathway regulates the regression in the mesenchyme by mediating AMH signalling.

1.3.3. Female-specific Müllerian duct differentiation

In female mice, the Müllerian duct differentiates into the oviduct, uterus, cervix and upper vagina. This differentiation occurs in an anterior to posterior fashion and is not

completed until 2 weeks after birth (Yin and Ma 2005). Epithelial-to-mesenchymal interactions direct the cellular fate of the Müllerian duct epithelium, which changes along the anterior-posterior axis depending on the tissue being formed. A number of genes with region-specific expression along the female reproductive tract have been identified, which are likely to control the epithelial cell fate (Kobayashi and Behringer 2003). Amongst others, these include certain WNT proteins.

Wnt4 is expressed in the stroma of the uterine horns at birth and this expression subsequently extends to the epithelium of the vagina (Miller et al. 1998). However, a function of this gene in the patterning of the Müllerian duct has not yet been determined due to the vital role of *Wnt4* in Müllerian duct formation (Vainio et al. 1999). *Wnt5a* is initially expressed in the stroma throughout the reproductive tract but is restricted to the uterine horns postnatally (Miller et al. 1998). The uterine horns of *Wnt5a* mutant reproductive tracts were shortened and coiled and the cervical/vaginal structures were poorly defined (Mericskay et al. 2004). Endometrial glands in the uterine horns also failed to develop, which are essential for embryo implantation and development. Lastly, *Wnt7a* is initially expressed throughout the epithelium of the reproductive tract but, like *Wnt5a*, becomes restricted to the uterine horns postnally (Miller et al. 1998). In the absence of *Wnt7a*, the female reproductive tracts undergo posterior transformations; the oviduct lacks coiling and acquires characteristics of the uterus, and the uterus of the vagina (Miller and Sassoon 1998; Parr and McMahon 1998). It has been found that *Wnt7a* acts to regulate the boundaries of expression of *Wnt5a* and *Wnt4*, and also to maintain the correct expression levels of certain *Hox* genes required to pattern the reproductive tract (Miller and Sassoon 1998; Mericskay et al. 2004).

The conditional inactivation of β-catenin in *Amhr2*-positive cells of the Müllerian duct mesenchyme in XX mice disrupted the coiling of the oviduct, and the female phenotype closely resembled that of the *Wnt7a* mutant (Deutscher and Yao 2007). It is therefore suggested that β-catenin mediates the signalling of *Wnt7a* to pattern the reproductive tract, in addition to the role in Müllerian duct regression in males already mentioned. These data provide evidence for the mesenchymal-epithelial interactions required for the correct patterning and development of the female reproductive tract; however, the actual morphogenetic mechanism is not fully understood.

1.4. Disorders of sexual development (DSDs)

Ultimately, sex determination is controlled by the presence or absence of *Sry* and the subsequent differentiation of gonadal supporting cell precursors into either Sertoli cells or granulosa cells during development. The sexual differentiation process that has been described here is controlled by different gene networks: the SRY/SOX9/FGF9 network in males, and FOXL2/WNT/β-catenin signalling in females. Both these networks have an antagonistic function as previously mentioned and, therefore, any disruption to the normal development of testes or ovaries can cause disorders of sexual development (DSDs).

In humans, DSDs account for approximately 7.5% of all congenital defects and individuals with these disorders suffer from the added effect that these DSDs can have on the quality of life (A.Sinclair, personal communication). The causes of DSDs range from aneuploidy of the sex chromosomes, such as XXY (Klinefelter's syndrome), XYY ('supermales'), or XO (Turners syndrome), to causative mutations in key sex-determining genes, such as in 46,XX or 46,XY gonadal dysgenesis (GD) syndromes

(White et al. 2011). Abnormalities in the development of the phenotypic sex can also occur, but the focus in this section will be on 46,XX and 46,XY GD.

46,XX GD mainly occurs by the translocation of *SRY* onto the X chromosome, giving rise to XX males (McElreavey et al. 1993). Incidences of *SRY*-negative XX female-to-male sex reversal are much less common, but have been described in cases with loss-of-function mutations in genes that act to antagonise the male pathway such as *RSPO1* (Parma et al. 2006) and *WNT4* (Mandel et al. 2008).

46,XY GD is characterised by abnormal testicular determination which can manifest with complete masculinisation, feminisation or with ambiguous genitalia. In cases of complete GD (CGD), testes are absent and bilateral streak gonads are present, along with female internal and external genitalia. The causative mutations can lead to the loss-of-function of critical male-determining genes, such as in *SRY* (Cameron and Sinclair 1997), *SOX9* (Wright et al. 1995), and *SF1* (Lin and Achermann 2008), or the gain-of-function (due to duplication) of female-determining genes, such as *WNT4* (Jordan et al. 2001). As well as mutations in sex-determining genes, GD can occur as a result of the inability to respond to male hormones as in androgen insensitivity syndrome (AIS). However, about 70% of 46,XY GD cases have no accurate diagnosis since many of the molecular mechanisms remain unknown (White et al. 2011).

Previously, sequencing for the causative mutations in patients with GD led to the identification of a number of the transcription factors and secreted signalling molecules that are now known to have key roles in sexual development. However, many of the molecular mechanisms important for the function of these genes are not yet known. For example, it is not yet clear how extracellular signals such as FGF9 or WNT4 control intracellular signal transduction pathways to produce sex-specific cellular responses in

gonadal cells. It is likely that intracellular signalling pathways are essential to mediate such effects. Further analyses of the unexplained cases of GD are likely to help provide some of these clues. Further genetic studies in mice, such as the use of random mutagenesis in forward genetic screens, are also likely to lead to the identification of novel key players. A very good example of this forms the main focus of this thesis.

1.5. A requirement for MAP kinase signalling in mouse sex determination

During an *N*-ethyl-*N*-nitrosourea (ENU)-induced forward genetic screen for gonadal abnormalities, which was carried out at MRC Harwell, evidence of a key role for mitogen activated protein (MAP) kinase signalling in mouse sex determination was recently provided. The boygirl (*byg*) mutant was initially identified by dissection of embryos derived from a G3 pedigree (RECB/31) segregating ENU-induced mutations on a mixed C3H/HeH × C57BL/6J genetic background (Bogani et al. 2009). Mutant embryos, homozygous for the *byg* mutation, exhibited spina bifida, mild oedema, and XY gonadal abnormalities, including disrupted testis cord development or ovotestis formation (Figure 1.4A-D). Once backcrossed onto the C57BL/6J background, XY *byg/byg* gonads always had an ovarian morphology, lacked markers of the embryonic testis and exhibited up-regulation of ovarian markers (Figure 1.4E-G). Positional cloning identified the ENU-induced point mutation (an A to T transversion) on the proximal region of mouse Chromosome (Chr) 17 in the gene *Map3k4* (also known as *Mekk4*). This mutation caused an arginine to stop-codon change in the open reading frame at position 382 of 1597. *Map3k4* encodes a MAP kinase kinase kinase (MAP3K/MAPKKK/MEKK), and this early truncation of the mutant protein occurs before the critical kinase domain (Figure 1.4H-I). Analysis of MAP3K4 by Western blot

using an anti-MAP3K4 antibody confirmed that full-length (180 kDa) protein was absent in homozygous tissue (Figure 1.4J). To test the functionality of this truncated protein, and confirm that no other mutations contributed to the *byg*/*byg* phenotype, a complementation test was carried out in which mice heterozygous for the *byg* allele (*Map3k4*^{byg}) were crossed to heterozygous mice carrying a constitutive knockout allele of *Map3k4* (*Map3k4*^{tm1Flv}, denoted henceforth as *Map3k4*$^{-}$), which was a kind gift from H.Chi and R.Flavell (Chi et al. 2005). Resultant embryos that carried both *Map3k4* mutant alleles (*Map3k4*$^{byg/-}$) exhibited the same spina bifida and XY gonadal abnormalities as homozygous individuals of either mutant allele (Figure 1.4K-L). This confirmed that *Map3k4* contained the causative ENU-induced mutation and that *byg* is also a null allele. Subsequent studies showed that, at 11.5 dpc, XY *byg/byg* gonads show dramatic loss of SRY and SOX9 expression (Figure 1.4M-O). This important observation of lack of *Sry* expression, both at the mRNA and protein level, and the subsequent loss of SOX9 expression, establishes a role for MAP kinase signalling during early mouse sex determination.

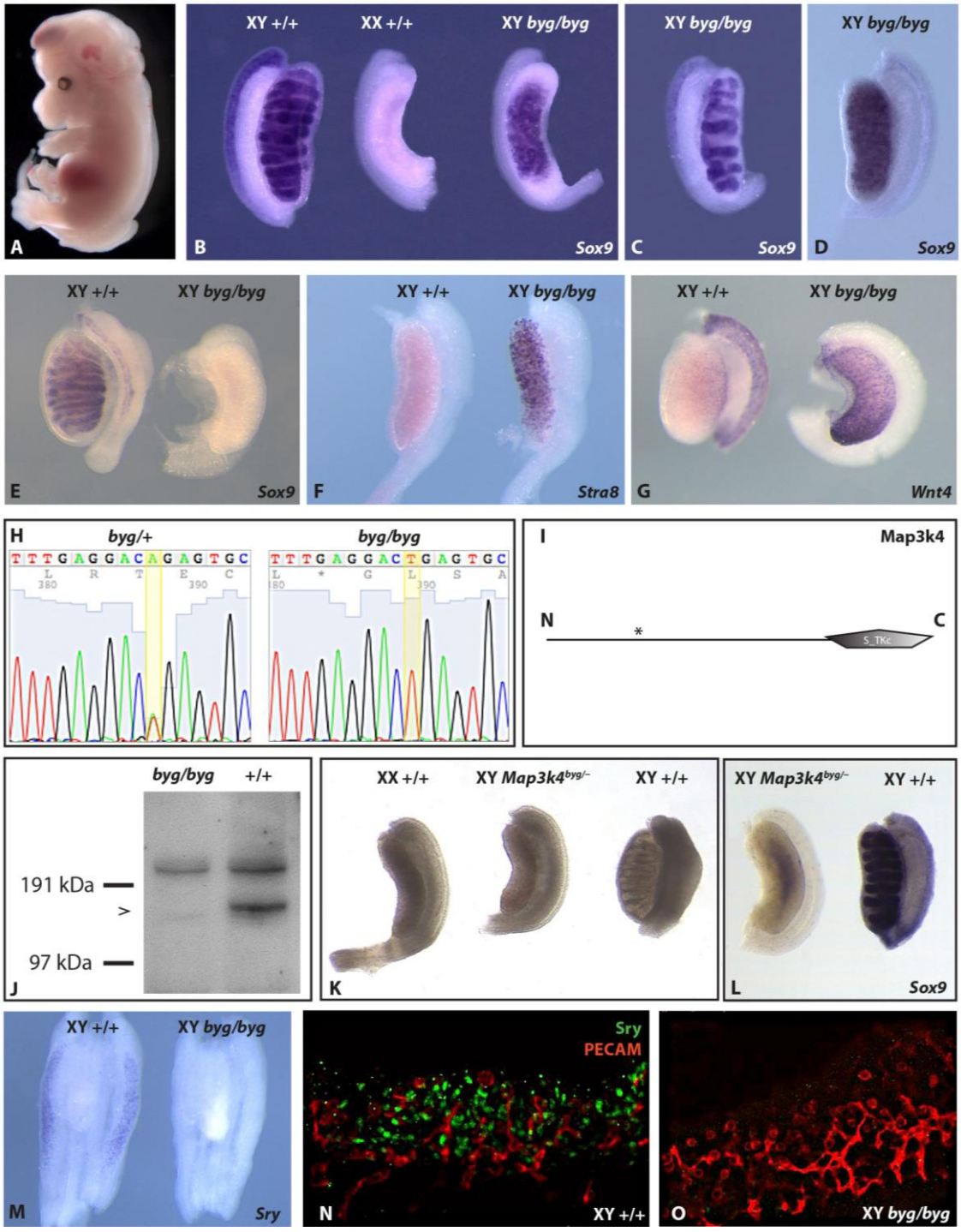

Figure 1.4: Embryonic phenotyping of the ENU mutant, boygirl (*byg*)
(**A**) External phenotype of 13.5 dpc *byg* homozygote, exhibiting neural tube defects and oedema. (**B-D**) On a mixed genetic background from the original screen, XY *byg/byg* gonads exhibit abnormal expression of *Sox9*, which marks Sertoli cells, as shown by wholemount *in situ* hybridisation (WMISH). Phenotypes at 13.5 dpc range from ovotestis development (right, B) to disrupted testis cord development (C) and testes without cords (D). (**E-G**) On the C57BL/6J background, XY *byg/byg* always exhibit complete gonadal sex reversal as shown by expression of: *Sox9* (E), *Stra8*, which marks female meiotic germ cells (F), and *Wnt4*, an ovarian somatic cell marker (G). (**H-J**) The ENU point mutation was mapped to *Map3k4* and causes an arginine to stop codon amino acid change (H). This mutation results in early truncation of the protein (asterisk, I) before the critical kinase domain and loss of protein expression, as shown by Western blotting (J). (**K-L**) To check complementation of the *byg* allele with a known knockout null allele, $Map3k4^{byg/+}$ mice were crossed with $Map3k4^{-/+}$ mice and the phenotype of the resulting embryos carrying both alleles ($Map3k4^{byg/-}$) was assessed. Double heterozygotes exhibited neural tube defects, and XY individuals were sex-reversed as shown by lack of testis cords (K), and loss of *Sox9* expression (L). (**M-O**) Lack of *Sry* mRNA expression at 11.5 dpc (M), and SRY protein expression at 11.0 dpc (O) was observed in XY *byg/byg* gonads.

1.6. MAP kinase signalling

MAP kinase signalling is vital for a great number of cellular activities. MAP kinases participate in intracellular cascades that transduce extracellular signals from the plasma membrane to nuclear transcription factors and other proteins (Wilkinson and Millar 2000). These pathways relay signals from a variety of stimuli to regulate multiple different cellular responses such as cell proliferation, survival, transcription and translation (Cuevas et al. 2007). The MAP kinase cascade contains a core, evolutionary conserved, three-component module which relays the signal through phosphorylation. The MAP3Ks are dual-specific kinases that activate a MAP kinase kinase (MAP2K/MAPKK/MEK/MKK) by phosphorylation of conserved serine and threonine residues. In turn, MAP2Ks activate a MAP kinase (MAPK) by phosphorylation of conserved tyrosine and threonine residues. Activated MAPKs can either phosphorylate cytoplasmic targets to regulate diverse processes including protein degradation and localisation, apoptosis or cell migration, or are translocated to the nucleus in which they can directly activate transcription factors to regulate gene expression or other nuclear proteins such as regulators of chromatin remodelling (Wilkinson and Millar 2000). See Figure 1.5 for a summary of the MAP kinase pathway.

The three-component MAP3K-MAP2K-MAPK signalling modules are directed by scaffold proteins that bring the signalling partners into close proximity to enable the rapid transmission of signals (Aouadi et al. 2006; Dhanasekaran et al. 2007). These scaffold proteins also function to protect the components within the relevant MAP kinase modules from irrelevant stimuli and to minimise crosstalk from other modules (Iwanaga et al. 2008). The importance of scaffold proteins becomes more apparent with the observation that there are a disproportionately large number of MAP3Ks to regulate a limited number of MAPKs in mammalian cells, and at each level of the relay, the

specific component is able to activate more than one downstream kinase (Yoshioka 2004; Dhanasekaran et al. 2007). Scaffold proteins also have the ability to enhance, decrease or redirect the signal flux through inhibitor or adaptor properties (Aouadi et al. 2006).

In mammalian cells there are four main families of MAPKs: extracellular signal-regulated kinase (ERK) 1/2 (or p42/p44 MAPK), c-jun amino-terminal kinases (JNK1/2/3), p38 kinases (p38α/β/γ/δ), and ERK5 (Cuevas et al. 2007). The ERK1/2 family is the most characterised and mediates signals from growth factors such as the Ras-mediated growth factor receptor tyrosine kinases via the Raf-family of MAP3Ks and the MKK1 and MKK2 MAP2Ks (Wilkinson and Millar 2000). The p38 and JNK families are associated with apoptosis, cell proliferation, and the cell's response to stress and inflammation.

1.6.1. MAP3K4-activated pathways

MAP3K4-activated signalling modules are thought to regulate the cell's response to stress from ultraviolet radiation, heat shock or osmotic stress (Winter-Vann and Johnson 2007). Functional MAP3K4 can lead to the activation of either the p38 or JNK kinase, following selective phosphorylation of either the MAP2K subgroups MKK3/6 or MKK4/7, respectively (Gerwins et al. 1997; Takekawa et al. 1997). MKK3 and MKK6 both lead to the specific activation of p38 MAPKs, MKK7 is specific to JNK activation, while MKK4 mainly activates JNK, but can also phosphorylate p38 (Dérijard et al. 1995; Han et al. 1996; Enslen et al. 1998). *In vivo* evidence for the ability of MAP3K4 to phosphorylate MKK3, MKK6 and MKK4 has been reported (Gerwins et al. 1997; Takekawa et al. 1997); however, MKK7 had not been identified by this point and was therefore not tested (Tournier et al. 1997; Yao et al. 1997). There are multiple MAP3K

proteins that belong to structurally diverse families, yet all lead to the activation of a comparatively small set of MAPKs. The use of scaffolding proteins is one mechanism to direct the specificity, but another important mechanism is the contribution of docking interactions between the kinases. These specific docking interactions exist between both the MAP2Ks and MAPKs, and the MAP3Ks and MAP2Ks. The interactions between MAP2Ks and MAP3Ks were investigated using an *in vitro* yeast two-hybrid protein interaction method (Takekawa et al. 2005). These experiments confirmed the ability of MAP3K4 to bind with MKK3, MKK6 and MKK4, which was sufficient to phosphorylate and activate the MAP2Ks. However, the docking site on MKK7 was not recognised by MAP3K4 and therefore MKK7 was not activated by MAP3K4 (Takekawa et al. 2005).

1.6.2. Analysis of MAP3K4 function

Previous inactivation of *Map3k4* by gene targeting has provided an insight into the function of this gene. Studies have shown that the homozygous inactivation of *Map3k4* (*Map3k4*$^{-/-}$) leads to perinatal lethality of embryos with severe neural tube defects when on the C57BL/6J background (Chi et al. 2005). However, when on a mixed C57BL/6J × 129/SvE background the homozygous mutants were viable with no obvious defects other than a slightly reduced body size; they were born, however, with a reduced Mendelian ratio of 15%, instead of the predicted 25% (Chi et al. 2004). Using the homozygous embryos from the C57BL/6J background, it was shown that MAP3K4, via MKK4, had an anti-apoptotic role at sites of neural tube closure in the neuroepithelium (Chi et al. 2005): the expression of activated MKK4 (pMKK4) was decreased and increased apoptosis was observed from 8.5 dpc, before the initiation of neural tube closure. However, no changes in JNK or p38 levels were observed.

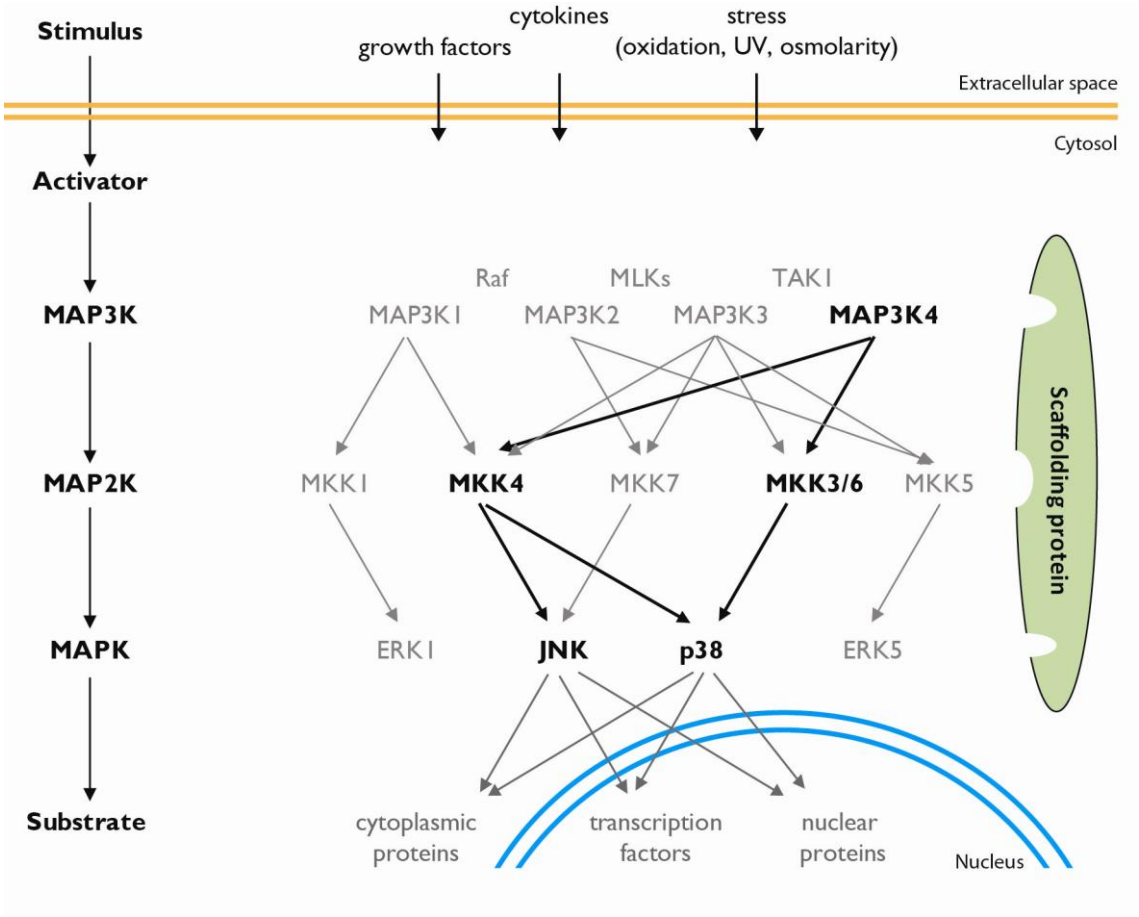

Figure 1.5: Schematic representation of the MAP kinase pathway
The MAP kinase cascade functions to transduce specific extracellular signals to nuclear transcription factors or other proteins. The three-component MAP3K-MAP2K-MAPK signalling module is directed by a specific scaffold protein. There are many different MAP3Ks (not all are shown), which activate a limited number of MAP2Ks and MAPKs. Most interactions are taken from an accumulation of *in vitro* data; however some have also been confirmed by mouse knockout studies. The proposed MAP3K4-activated pathway is highlighted. Each MAPK can activate a large variety of target proteins ranging from cytoplasmic proteins to nuclear transcription factors. Some target proteins can be activated by more than one MAPK, while others are specific. MAP3K4 is known to be a stress-activated MAP kinase. MLKs, mixed lineage kinases; TAK1, TGF-β-activated kinase 1.

A different, kinase-inactive, mutant allele of *Map3k4* (*Map3k4*^{K1361R}, referred to henceforth as *Map3k4*^{ki}) was also generated in order to focus specifically on the consequences of removing the enzyme activity while MAP3K4 protein is still present (Abell et al. 2005). This variant was maintained on a mixed C57BL/6J × 129/SvE background and embryos also died at birth with severe neural tube defects, similar to the knockout on the C57BL/6J background. However, instead of loss of phosphorylation of MKK4 in the mutants, they observed inhibition of MKK3 and MAPK-activated protein kinase 2 (MAPKAPK-2) activation in hindbrains and fibroblasts, and also detected skeletal defects and infertility. This loss of phosphorylation of both downstream kinases suggests that MAP3K4 activates the p38 MAPK pathway in hindbrain tissue and fibroblasts.

The discrepancies observed with the inhibition of different MAP2Ks in the absence of functional MAP3K4 suggest that MAP3K4 activates different MAP kinase pathways in different tissues during different stages of development. During the study of *Map3k4*$^{byg/byg}$, the expression of different MAPK signalling components was also assessed in the embryonic gonads using antibodies against activated MKK4 (pMKK4), p38 (pp38) and JNK (pJNK) by immunohistochemistry (Bogani et al. 2009). However, no clear differences between XY *Map3k4*$^{byg/byg}$ mutants and XY controls were observed. It is possible that an inappropriate stage of gonad development was analysed, or that differences were very subtle. It could also be that other MAP2Ks and MAPKs are disrupted.

FGFs, which play a key role in sex determination as has been described throughout this Introduction, are known to signal through tyrosine kinase receptors. These activated receptors, in turn, activate the MAP kinase signalling cascade through the ERK1/2

pathway (Schlessinger 2000; Lanner and Rossant 2010). This provides a strong link between MAP kinase signalling and extracellular signalling that occurs in the gonad. Also, evidence that the MAP kinase cascade mediates the up-regulation of *Sox9* expression by FGF2 has been reported in chondrocytes (Murakami et al. 2000). A link between the MAP kinase pathway and *Sox9* expression was also reported in the gonad; MAP kinases mediated the activation of *Sox9* by Vinexin γ, a scaffolding protein of the ERK family of MAP kinases (Matsuyama et al. 2005). However, the targeted disruption of the gene encoding Vinexin γ caused only slight down-regulation of *Sox9* and did not disrupt sex determination. Analysis of *Map3k4*$^{byg/byg}$ mutants also showed that the FGF pathway was still active since *Map3k4*$^{byg/byg}$ mutants could respond to exogenous FGF9 (Bogani et al. 2009).

1.7. A requirement for MAP kinase signalling in human sex determination

A role for MAP kinase signalling in human testis determination has also recently been established, although in this case the relevant MAP3K was MAP3K1, not MAP3K4 (Pearlman et al. 2010). Mutations in *MAP3K1* have been associated with both familial and sporadic cases of 46,XY DSDs, including cases of both GD and CGD. The type of mutation identified varies from an intron splice-acceptor mutation, which inserts two amino acid residues, to missense point mutations located at sites of both highly conserved and less conserved amino acids. The function of these mutated proteins was assessed in lymphoblastoid cell lines derived from the patients and the regulation of downstream MAPKs was found to be disrupted; the phosphorylation of p38 and ERK1/2 was upregulated, while increased binding of RHOA to the mutant MAP3K1 was observed. However, whether these observations in heterologous cell lines are

relevant to human sex determination *in vivo* has not yet been determined. The link between MAP kinase signalling and human sex determination highlights the importance of this pathway and the necessity to understand the mechanism involved.

1.8. Main aims

A role for the MAP3K4-activated MAP kinase signalling pathway in mammalian sex determination has been identified. However, the mechanism involved is likely to be extremely complex, given the complexity of the MAP kinase pathway and the number of different aspects of development that it regulates. This thesis focuses on analysing the phenotype of the *Map3k4*^{byg} null mutant in more detail by specifically focusing on the cell proliferation aspect of gonad development and by using genetic methods to address the role of downstream MAP kinase pathway molecules. It also attempts to address a role for p38 MAPK in sexual development. The ultimate aim of the project is to piece together the MAP kinase pathway along with the molecules it regulates to determine how it acts on the known regulators of gonad development and how disruptions to the pathway affect sex determination.

Chapter 2. Materials and Methods

2.1. General methods and solutions

Standard solutions were prepared according to (Sambrook et al. 1989). Deionised RNase-free AnalaR water (VWR) was used as standard. All thermocycling reactions were performed using a G-Storm GS-4 thermocycler.

2.2. Mouse lines

Mouse work was conducted under the authority of the Home Office Project Licence number 30/2381.

Experiments conducted on wild-type tissue used either the C57BL/6J background or 3H1 embryos resulting from timed matings between female C3H/HeH and male 101 mice.

2.2.1. Stock maintenance

Experimental mice were maintained as heterozygous stock on the C57BL/6J background unless otherwise stated. The C57B6/J background was specifically chosen due to its increased sensitivity to XY sex reversal (Bouma et al. 2007). Primer sequences and reaction conditions used to genotype each line are shown in Table 2-1. Most lines were genotyped using a standard polymerase chain reaction (PCR) followed by gel electrophoresis (unless otherwise stated).

The boygirl (*byg*) line (*Map3k4*^{byg}) was identified from an ENU-based, three-generation (G3) genetic screen for recessive mutant alleles causing gonadal abnormalities when homozygous, performed at MRC Harwell (Bogani et al. 2009). The line was genotyped

using a PCR-based pyrosequencing assay in which the PCR products were generated using a biotinylated reverse primer, and then analysed by pyrosequencing for the single nucleotide polymorphism (SNP) using a specific sequencing primer as detailed (Table 2-1).

Cre transgenic mouse lines: *Sf1-Cre* was a kind gift from K.Parker (Bingham et al. 2006) and was generated by the insertion of a *Cre* cassette into an *Sf1* BAC (bacterial artificial chromosome), which in transgenic mice drives the expression of *Cre* in somatic cells of the gonads, adrenal cortex and ventromedial hypothalamic nucleus; *Amhr2-Cre* was a kind gift from R.Behringer (Jamin et al. 2002) and was generated using a 'knock-in' approach in which a *Cre* recombinase expression cassette was targeted into exon 5 of the *Amhr2* locus using mouse embryonic stem cells. *Amhr2-Cre* is expressed in somatic cells of the embryonic gonad and the mesenchyme of the Müllerian duct epithelium; *β-Actin-Cre* is a ubiquitous *Cre* expressing line (Lewandoski and Martin 1997) and a colony was already established at MRC Harwell. All *Cre* lines were genotyped using generic *Cre*-specific primers in a duplex reaction to detect the presence of the *Cre* transgene, and also a positive control product (using IL2 primers). This reaction was designed by L.Pastorelli, a previous PhD student in the laboratory.

Mice carrying floxed alleles: $Mapk14^{flox}$, a kind gift from M.Pasparakis (Ventura et al. 2007), contains two LoxP sites flanking exons 2 and 3; $Map3k4^{flox}$, a kind gift from H.Chi (Chi et al. 2004), contains two LoxP sites flanking exon 3. Both lines were maintained as heterozygous and homozygous stocks on C57BL/6J. They were genotyped using a three-primer reaction in which two primers flank one of the LoxP sites (to detect the floxed allele) and the third primer anneals to the genomic DNA close

to the other LoxP site. Successful recombination and deletion of the floxed region will result in a product from the third primer.

The *Mapk11*$^{-/-}$ knockout (KO) line was a kind gift from J.S.Arthur (Beardmore et al. 2005). It was generated by replacing exons 2-7 with a neomycin cassette, resulting in a null allele. The line was genotyped using a three-primer reaction: one primer is located in genomic DNA within the region that is deleted (to detect the wild-type allele), whilst another is located in the inserted neomycin cassette (to detect the KO allele), and the third anneals to genomic DNA outside of the targeted region and common to both primers.

The *Map3k4*$^{-/-}$ KO line was a kind gift from H.Chi and R.Flavell (Chi et al. 2004). It was generated by the insertion of LoxP sites either side of exon 3. Exon 3 was then deleted following homologous recombination driven by a ubiquitously expressed *Cre* transgene. This resulted in a frame-shift and premature termination of the coding sequence before the critical kinase domain, creating a null allele. The line was genotyped using a three-primer reaction: two primers span the location of the 1st LoxP site to detect the wild-type allele, while a third anneals downstream of the location of the 2nd LoxP site to detect the KO allele.

2.2.2. Fertility testing

Fertility testing of adult mice was conducted as follows. Male experimental mice were mated with female C57BL/6J controls in triplicate. These females were checked for vaginal plugs to confirm normal mating behaviour. At 14.5 days *post coitum* (dpc) pregnant females (verified by palpating) were culled and the number of embryos recorded (see section 2.3 for details on plug checking and uterus removal). The experimental males were compared to control males in identical tests. Experimental

females were mated with male C57BL/6J mice. If the number of experimental females available for testing was limited (as with *Mapk14*$^{flox/flox}$; *Amhr2-Cre*), fertility was tested by counting the number of newborn pups. Females were subsequently mated again until they had produced two or three litters or had been in matings for approximately two months. If more than eight experimental females were available, females were checked for vaginal plugs and were then sacrificed at 14.5 dpc to record the number of embryos.

2.2.3. Morulae collection

To check for signs of fertilisation of oocytes, a separate group of experimental females and control littermates were mated to C57BL/6J males. The females were sacrificed at 2.5 dpc and the uterus and oviducts removed. The oviducts and uterine horns were flushed with culture media for collection of morulae. The number and quality of morulae collected was recorded and any healthy morulae were subsequently cultured to the hatching blastocyst stage by the Frozen Embryo and Sperm Archive (FESA) team.

2.3. Tissue collection

For embryo collection, timed matings were set up at approximately 3pm and vaginal plugs were checked the following morning. Noon on the day of the plug was counted as 0.5 dpc. Some embryos were collected from mice maintained in a reverse light-dark cycle, where the 12-hour light cycle began at 4pm, rather than the usual 7am. In such cases, noon on the day of the plug was counted as 1.0 dpc. Pregnant females were culled by cervical dislocation (Schedule one) under the Home Office regulations. Their uteri, containing the embryos, were removed through an opening in the abdomen. Embryos were dissected in phosphate buffered saline (PBS) using a Leica MZ6 dissection microscope. Embryos were first decapitated (under Home Office guidelines) before the urogenital ridges (UGRs) were collected (unless otherwise stated).

To determine the exact stage of an embryo 12.5 dpc or younger, tail somites (ts) were always counted. This was conducted by counting the number of somites between the hindlimb and the tail tip. The stages were characterised as follows: 8 ts = 10.5 dpc; 18 ts = 11.5 dpc; 28 ts = 12.5 dpc.

For the collection of adult tissue, mice were culled by cervical dislocation and the reproductive organs (ovaries, oviduct, uterine horns and vagina from females or testes, epididymis, vas deferens and seminal vesicles from males) were removed through an opening in the abdomen and collected.

2.4. Tissue processing

2.4.1. Wholemount *in situ* hybridisation (WMISH)

Collected embryonic tissue was placed in Eppendorf tubes and fixed in 4% paraformaldehyde (PFA) in PBS overnight. Once fixed, the tissue was taken through a methanol (MeOH) dehydration series for 5 minutes each step (2x PBS, 1x 25% MeOH in PBS, 1x 50%, 1x 75%, and 2x 100%) and then stored in 100% MeOH at -20°C until required.

2.4.2. Immunohistochemistry (IHC)

For wholemount IHC, 11.0 dpc to 12.0 dpc tissue was collected and processed as in section 2.4.1. However, dehydrated tissue was only stored for a maximum of 7 days before being used, as longer storage duration affected the quality of the staining.

For section IHC, embryonic tissue was dissected and fixed in 4% PFA overnight, then washed in 30% sucrose/PBS at 4°C for 24 hrs, prior to embedding for cryosectioning (see section 2.8.4 and 2.10.3).

2.4.3. RNA extractions

Single embryonic gonads (C57BL/6J) staged at 11.5 dpc, 12.5 dpc or 13.5 dpc were subdissected to remove the mesonephros. The separated gonads were collected in Eppendorf tubes (paired gonads together) and snap frozen immediately using dry ice. All tissue for RNA extraction was stored at -70°C until required.

2.4.4. *LacZ* expression

For *LacZ* expression analysis of embryonic samples, whole embryos from 11.5 dpc to 13.5 dpc stages, and caudal regions, including the reproductive tracts/gonads, of 17.5 dpc embryos were collected in PBS and placed in a 24-well plate to separate the samples. Either the yolk sac or tail sample was collected for genotyping.

For *LacZ* expression analysis of adult tissue, male and female reproductive organs were washed twice in PBS. These samples were then placed into wells of a 12-well plate.

2.4.5. Organ cultures

For standard organ cultures, UGR tissue was collected from 11.5 dpc embryos in PBS, placed in a 24-well plate in organ culture media (see section 2.11) and then incubated at 37°C with 5% CO_2.

For knockdown organ cultures, whole embryos (C57BL/6J) from 10.5 dpc to 11.5 dpc (unless otherwise stated) were collected in Opti-MEM reduced-serum media (Invitrogen) in an RNase-free environment. Samples were initially placed in a 24-well plate and kept on ice.

2.4.6. Histology

Ovaries and testes from 17.5 dpc embryos were removed and fixed in 10% formalin. These were then processed by the histology team at MRC Harwell for paraffin wax sectioning and haematoxylin and eosin (H&E) staining.

Adult ovaries and testes, along with the respective reproductive tracts, were analysed by the necropsy team at MRC Harwell for gross morphological defects. The testes were weighed, then fixed in Bouin's fixative, which allows improved nuclear detail necessary for analysing testicular sections (Ananthanarayanan et al. 2005), for a minimum of 6 hours. Other tissues collected, which included the ovaries, oviducts, uterus, and occasionally the adrenal glands, were fixed in 10% buffered formalin. All tissue was then washed in 70% ethanol and processed by the histology team for paraffin wax sectioning and H&E staining.

2.4.7. Genotyping

Depending on the size of embryo, or experimental tissue required, either the head, part of the head, or the yolk sac was collected in a PCR plate and stored at -20°C ready for genotyping.

2.5. Genotyping

Mouse colonies were genotyped to identify the relevant allele (section 2.2.1 and Table 2-1). Embryos were genotyped for their chromosomal sex if this could not be determined visually by the presence/absence of testis cords in the gonads (12.5 dpc or younger) and also for the presence of the experimental alleles if relevant (Table 2-1).

2.5.1. Genomic DNA extraction

DNA, from either ear biopsies of 4-week old mice or a small section of embryonic tissue collected during dissections, was extracted by Proteinase K (PK) digestion. A solution of 0.75 mg/ml PK (Roche) in TE-Tween (50 mM Tris, pH 8.0 / 1 mM EDTA / 0.5% Tween-20) was added to each sample and incubated at 55°C for 90 minutes then at 95°C for 5 minutes to denature the PK. Following disruption of the tissue by vortexing thoroughly, the tissue debris was pelleted by centrifugation at 4,000 rpm for 3 minutes. A working dilution (1:10 in H_2O) of the released DNA was prepared.

2.5.2. Polymerase chain reaction (PCR)

New primers were designed using the primer3 programme (http://frodo.wi.mit.edu/primer3/). Primers were synthesised by either Sigma Aldrich or Eurogentec and primer pairs with corresponding thermocycling reaction conditions are listed in Table 2-1. Standard reactions were set up using 2x PCR Reddymix (Thermo Scientific) consisting of 0.5 units Thermoprime Plus DNA Polymerase, 10 mM Tris-HCl, 50 mM KCl, 1.5 mM $MgCl_2$ and 0.2 mM each of dATP, dCTP, dGTP and dTTP, with 1 µl DNA (approximately 30 ng) and 0.2 µM of each gene-specific primer in a total volume of 20 µl. PCR reactions for pyrosequencing analysis (to distinguish SNPs) used 1.1x PCR SuperMix (Invitrogen) consisting of 0.44 units recombinant *Taq* DNA Polymerase, 22 mM Tris-HCl, 55 mM KCl, 1.65 mM $MgCl_2$, 0.22 mM each of dATP, dCTP, dGTP and dTTP, with 1.5 µl DNA and 0.3 µM of each gene-specific primer in a total volume of 20 µl.

2.5.3. Gel Electrophoresis

DNA was analysed by standard gel electrophoresis. PCR products or DNA/RNA mixed with loading buffer (1x TE, pH 8.0 / 10% glycerol / 0.08% Orange G), were loaded into

a 1.5% Ultrapore™ Agarose (Invitrogen)/TBE gel containing 1:10,000 SYBR Safe DNA stain (Invitrogen). A 1kb Plus DNA ladder (Invitrogen) was also loaded to assess product sizes. The gel was electrophoresed for 20-30 minutes at 90 V, and products were visualised using an Ultra Violet (UV) gel doc system (BioRad).

2.5.4. PCR Purification

PCR products to be sequenced, or used for a subsequent ligation reaction, were purified by one of the following methods, following the manufacturer's instructions.

QIAquick PCR Purification kit (Qiagen): This kit removes the primers and buffer salts from the reaction and recovers DNA fragments from 100 bp to 10 kb. Briefly, PCR reactions were pooled and applied to a column in which the DNA is bound to the silica membrane in the presence of high salt concentrations, and the unwanted components pass through. After a series of ethanol washes to remove salts, the DNA was eluted in 30 µl of elution buffer.

QIAquick Gel extraction kit (Qiagen): This kit was used to isolate DNA fragments from a gel and therefore purify a specific product of a PCR reaction, avoiding the contamination of any non-specific products. The gel slice containing the DNA was first dissolved in a buffer that provided the necessary conditions to facilitate binding of the DNA to the silica membrane.

2.5.5. Sequencing

Purified DNA (following PCR purification) or Plasmid DNA was sent to GATC (http://www.gatc-biotech.com/en/home.html) along with specific sequencing primers if required. Sequences were returned by email and analysed using BLAST tools from Ensembl (http://www.ensembl.org/Mus_musculus/blastview) or sequence alignment tools (http://www.ebi.ac.uk/Tools/msa/clustalw2/).

Table 2-1: Details of genotyping assays and PCR conditions

Assay	Forward primer(s)	Reverse primer(s)	Genotyping method	*PCR programme (# of cycles & annealing temp)	Product sizes	SNP	Assay design
XY sexing	TGGATGGTGTGGCCAATG	CACCTGCACGTTGCCCTT	Standard	†x36 57°C x34 'fast'	253 bp X 335 bp Y		N. Warr (Warr et al. 2009)
boygirl	AGGACTATGAACGGTACGC	Bio-CGCAGCTTCTGATTTAGATC	Pyrosequencing GCCAAGGACTTTGAGG	Pyros** x40 60°C		A wt T mut	GEMS,Harwell (Bogani et al. 2009)
Mapk14-flox	X:CTACAGAATGCACCTCGGATG Z:CCAGCACTTGGAAGGCTATTC AltZ:AAGCTGAGGAGTTGTGTCAGG	Y:AGAAGGCTGGATTTGCACAAG	Standard	NO* x35 58°C Z 61°C AltZ	wt: 121 bp floxed: 188 bp del: 411 bp Alt del: 214 bp		(Ventura et al. 2007) Primer3
Map3k4-flox	X:CAGACGGAACTTGGATGTTAGTAGG Z:GTCTGCTTGAATGGCATTTGG	Y:ACCCTGAGCAGTATTGTGGATTTC	Standard	NO* 61°C	wt: 138 bp floxed: 190 bp del: 280 bp		Hongbo Chi (personal communication) Primer3
Map3k4-KO	X:TAAGACAGAGGCAGGGATTGGC	Y:CCGTTGTTCTCAGAGTTGCTCG Z:GAGCAGTATTGTGGATTTCCGAAG	Standard	NO* 65°C	wt: 463 bp KO: 180 bp		Hongbo Chi (personal communication)
Cre	Cre:CGTACTGACGGTGGGAGAAT IL2:CTAGGCCACAGAATTGAAAGATCT	Cre:CCCGGCAAAACAGGTAGTTA IL2:GTAGGTGGAAATTCTAGCATCATC	Standard	†x36 56°C	Cre: ~80 bp IL2: ~220 bp		L. Pastorelli (Pastorelli et al. 2009)
Mapk11-KO	X:GCATCTCTGGAGCTCTGTGAGAGG Z:GGCGATGCCTGCTTGCCGAATATCATGG	Y:GGAGACTATCAGTCTGCCAACCC	Standard	NO* 65°C	wt: 220 bp KO: ~600 bp		(Beardmore et al. 2005)

*Standard PCR programme 'NO': 95°C for 5 min, 36 cycles of [95°C 30 sec, X°C 30 sec, 72°C 30 sec], then 72°C for 5 min. Annealing temp & variations to # of cycles stated.
**Pyros PCR programme: 95°C for 5 min, 40 cycles of [95°C 15 sec, 60°C 30 sec, 72°C 15 sec], then 72°C for 5 min.
†Alternatives to NO: XY sexing: As NO, but 95°C for 15 sec within cycles. 'Fast' XY sexing: x34 with 10 sec each step (15 sec for 72°C). *Cre:* as NO, but 72°C for 15 sec.

2.6. Cloning

2.6.1. TA Cloning

Double-stranded DNA fragments (e.g. from PCR Purification) were ligated into a pGEM-T Easy vector (Promega) following the manufacturer's standard protocol. The pGEM-T Easy vector is supplied as a linearised vector with a 3' T overhang on both ends. This overhang prevents recircularisation of the vector and facilitates easy ligation of a PCR product generated by a *Taq* polymerase. When DNA is amplified by *Taq* polymerase during PCR, an A overhang on the 3' end of the fragment is produced. The compatible A and T overhangs anneal and the complete ligation of the insert into the vector to generate circular plasmid DNA is facilitated by T4 DNA ligase.

Firstly, the amount of insert (PCR product) per vector was calculated using a molar ratio of 3:1. The pGEM-T Easy vector is 3 kb in size and 50 ng is required. The amount of insert was calculated as follows:

$$\frac{ng\ of\ \ vector \times kb\ of\ \ insert}{kb\ of\ \ vector} \times insert : vector\ \ molar\ \ ratio = ng\ of\ \ insert$$

The 10 µl reaction (1X Rapid ligation buffer, 50 ng vector, PCR product and 3 units T4 DNA ligase in H_2O), was then incubated for either 1 hour at 25°C, or overnight at 4°C. 2 µl of the ligation reaction was used for transformations.

2.6.2. Transformations

Plasmid DNA was transformed with subcloning efficiency DH5α chemically competent cells (Invitrogen) following the manufacturer's guidelines. Approximately 10 ng of plasmid DNA was added to 25-50 µl of DH5α competent cells and incubated for 30 min on ice. For transformation, the cells were heat-shocked for 20 seconds in a 42°C water

bath, and then immediately cooled on ice for 2 min. 950 µl of pre-warmed lysogeny broth (LB) medium was added, and the samples were then incubated at 37°C for 1 hour in a shaker at 225 rpm. To ensure well separated colonies, volumes of 20 µl and 200 µl of each transformation were spread on LB-agar selective plates containing the appropriate antibiotic (either 100 µg/ml ampicillin or 50 µg/ml kanamycin) for the vector being transformed, and incubated overnight at 37°C.

2.6.3. DNA preparation

Three individual colonies from each transformation were selected and used to inoculate 3 ml LB medium and appropriate antibiotic in separate universal tubes. These single colony cultures were incubated overnight at 37°C in the shaker at 225 rpm. The plasmid DNA from these single colony cultures was purified using either a Miniprep kit (Roche) or a Midiprep kit (Qiagen) according to the manufacturer's instructions. However, for the Midiprep kit, the single colony culture was first inoculated again in a 1:1000 dilution: 30 µl of starter culture was added to a conical flask containing 30 ml of LB and appropriate antibiotic and incubated overnight at 37°C in a shaker.

The concentration of eluted plasmid DNA was determined by analysing the absorbance at 260 nm on a Nanodrop ND-8000 (Thermo scientific).

2.7. Quantitative real-time PCR (qRT-PCR)

2.7.1. RNA extraction and cDNA synthesis

Total RNA and protein was extracted from frozen embryonic gonadal tissue processed as described in section 2.4.3. Due to the small amount of tissue from which RNA needed to be extracted, three pairs of 11.5 dpc gonads were pooled together at the beginning of the RNA extraction procedure, whilst two pairs of 12.5 dpc and 13.5 dpc

gonads were pooled. Each pool represents one sample. The Nucleospin RNA/protein isolation kit (MACHEREY-NAGEL) was used following the manufacturer's instructions. Briefly, a buffer containing guanidine thiocyanate (a cell lysis and protein denaturing agent) along with 1% β-mercaptoethanol (denatures disulphide bonds in RNases) was added to the frozen tissue. The tissue was vortexed vigorously and the resulting lysate filtered. 70% ethanol was added to the lysate before it was then passed through a Nucleospin column; this binds RNA/DNA but allows protein to be eluted. A membrane desalting buffer was added to the column and then the DNA was digested by rDNase. A series of membrane washes followed; firstly, to inactivate the rDNase and remove salts, then to dry the membrane. Finally, the pure RNA was eluted in 2x 20 µl of RNase-free H_2O (or in 1x 20 µl applied twice if the yield of RNA was expected to be low). The quantity and quality of the RNA was analysed using the Nanodrop ND-8000 and gel electrophoresis.

For qRT-PCR analysis of RNA from cultured gonads (section 2.11 and 2.12.2), the Micro RNA extraction kit (Qiagen) was used. This allowed elution of quality RNA in 14 µl H_2O (applied to the column twice) from a single cultured gonad to avoid the necessity of pooling samples. The basic principles of this kit are exactly the same as described for the Nucleospin kit, however the membrane in the spin column is smaller allowing for elution of more RNA in a smaller volume.

500 ng of cDNA was synthesised from 500 ng of RNA using the High capacity cDNA Reverse Transcription kit (Applied Biosystems). Briefly, 500 ng RNA was diluted to 50 ng/µl, then combined with 10 µl of reaction mix (1x reverse transcriptase buffer, 100 mM dNTP mix, 1x random primers, 1 µl Multiscribe reverse transcriptase and H_2O),

and finally subjected to the following thermocycler conditions for cDNA synthesis: 25°C for 10 min, 37°C for 120 min, and 85°C for 5 min.

2.7.2. Plate set-up

Each qRT-PCR plate was set up using 10 ng of cDNA per well, which was added to a pre-aliquoted reaction mix of 1x Fast Mastermix (Applied Biosystems), 1x TaqMan assay (Applied Biosystems) and nuclease-free H_2O, to make a final volume of 20 µl. Real-time amplification was performed on a 7500 Fast machine (Applied Biosystems) using a Fast programme of: 95°C for 20 sec, then 40 cycles of 95°C for 3 sec and 60°C for 30 sec. The following TaqMan assays were used: *Mapk11* (Mm00440955_m1); *Mapk12* (Mm00443518_m1); *Mapk13* (Mm00442488_m1); *Mapk14* (Mm00442497_m1); *Sox9* (Mm03003574_s1); *Fst* (Mm00514982_m1); *Stra8* (Mm01165142_m1); *Wnt4* (Mm00437341_m1); *Fgf9* (Mm00442795_m1) and *Hprt1* (Mm01545399_m1), all from Applied Biosystems.

2.7.3. Analysis of qRT-PCR results

TaqMan assays contain three target-specific oligonucleotides: two primers for the cDNA to be amplified, and a probe containing a FAM™ fluorophore at the 5' end and a quencher at the 3' end. This probe is designed to anneal to the cDNA between the two primers. During the PCR reaction, the Taq polymerase extends the primers and causes the degradation of the TaqMan probe, which results in the release of the fluorophore. The separation of the fluorophore from the quencher allows it to emit excitation energy, which is detected as fluorescence by the real-time thermocycler. The amount of fluorescence detected is directly correlated to the amount of cDNA present in the reaction, which is doubling for every PCR cycle. qRT-PCR measures the number of cycles it takes to reach a specific threshold of fluorescence at which the levels can be

detected: this is called the cycle threshold (Ct). Following this principle, original samples, in which the mRNA (and therefore cDNA) being analysed is more abundant, would reach the specific threshold more quickly and so have a smaller Ct value.

Standard curves were generated using a range of cDNA concentrations from both male and female 13.5 dpc gonads, to assess the efficiencies of the TaqMan assays. Five cDNA dilution points of 30 ng, 10 ng, 1 ng, 0.1 ng and 0.01 ng were used per sample and assay tested, with three technical replicates. The standard curve was generated by plotting Ct over log of the cDNA concentration, and the gradient of the resulting linear regression was used to calculate the efficiency of the assay (Equation 1).

Equation 1: Efficiency (%)

$$\left(10^{\left(-1/slope\right)}-1\right)\times 100$$

The optimal slope gradient is -3.32 since this is equivalent to 100% efficiency. However, an assay with efficiency between 90-110% is acceptable to use.

The relative quantification (RQ) method was used to analyse expression levels of the genes of interest in the sample tissue. This method assumes that all assays have efficiencies between 90-110% so that they can be directly compared, and results are calibrated to a specific reference sample; usually a wild-type sample. To calculate the fold change against the calibrator sample (RQ), the following method was used:

i) The average Ct for each biological sample and assay is normalised against the endogenous control: $Ct_{target} - Ct_{endogenous} = \Delta Ct$

ii) These normalised results of the sample are then calibrated against those of the reference: $\Delta Ct_{sample} - \Delta Ct_{reference} = \Delta\Delta Ct$

iii) The fold change (RQ) of expression can then be calculated: $2^{-\Delta\Delta Ct}$

This gives the relative expression levels with respect to the reference sample. RQ min and RQ max were used to calculate the error for each result:

i) The standard deviation for each ΔCt value is calculated, which is then used to determine the standard error of the mean for each (Equation 2).

ii) RQ min (Equation 3) and max (Equation 4) are then calculated using the respective formulae, where t equals the value from the student *t*-test tables for a given degree of freedom using 95% confidence. The degree of freedom used is generally equal to: (# biological samples × 2) – 2

Equation 2: Standard error of the mean

$$SE\Delta Ct = \sqrt{\frac{Stdev_{sample}^{2}}{n} + \frac{Stdev_{calibrator}^{2}}{n}}$$

Equation 3: RQ min

$$RQ\ \text{min} = 2^{-[av\Delta\Delta Ct + (SE\Delta Ct \times t)]}$$

Equation 4: RQ max

$$RQ\ \text{max} = 2^{-[av\Delta\Delta Ct - (SE\Delta Ct \times t)]}$$

Analysis of results was performed using Applied Biosystems software, comparing fold change values (RQ) of each assay, with the gene *Hprt1* as the endogenous control. For each assay, three to six biological replicates and three technical replicates were performed.

2.8. Wholemount in situ hybridisation (WMISH)

2.8.1. 3' UTR riboprobe design

Where possible, riboprobes were designed to hybridise to the 3' untranslated region (UTR) of the gene of interest to reduce the possibility of off-target effects, since this region is unique to each gene. A region greater or equal to 400 bp in size was amplified by designing primers using the primer3 programme (http://frodo.wi.mit.edu/primer3/). See Table 2-2 for details of specific primer sequences for riboprobes designed using the primer3 programme. Other riboprobes used are detailed in previous reports (see Table 2-3). Following a standard PCR reaction to amplify this region, the products were purified as detailed in section 2.5.4. The purified PCR product was then ligated into the pGEM-T Easy vector and cloned using DH5α competent cells (section 2.6). The resulting purified plasmid DNA was sequenced in both directions using the RNA polymerase promoters either side of the polylinker/cloning region (section 2.5.5). This was to confirm the presence of the intended insert, but also to determine the orientation of the insert so that the appropriate restriction enzyme and RNA polymerase could be selected to linearise and transcribe the DNA in an antisense direction.

Table 2-2: Primer sequences for riboprobes designed by 3'UTR amplification

RNA probe	Forward primer	Reverse primer	Product size
Mapk11	5′-ATGGTCCCTGGAGACTCTGA-3′	5′-TCACAGCTGGGATTCAAGAC-3′	369 bp
Mapk12	5′-GGGTATCCAAAGGAGGTTGG-3′	5′-CACCAAATGGCTGGTTCG-3′	489 bp
Mapk13	5′-GACCTGCTCGACAAGATGC-3′	5′-CACCACCCAGGTAACAGAGG-3′	420 bp
Foxl2	5′-GTTCGAGAAGGGCAACTACC-3′	5′-AGGCCGTTGTAGGAGTTCAC-3′	420 bp

2.8.2. DIG-labelled riboprobe synthesis

In summary, 500 ng to 1 µg of linearised DNA was labelled in a total volume of 20 µl: the plasmid DNA sample was digested using a restriction enzyme located at the 5' end of the sense strand (Table 2-3); the resulting linearised DNA was then precipitated with ethanol and resuspended in H_2O; and finally, the DNA was transcribed into DIG-labelled RNA using the relevant RNA polymerase (Table 2-3).

Table 2-3: RNA probes used and synthesis conditions

RNA probe	Restriction enzyme	RNA polymerase	Sequence details	Reference
Sox9	*Hin*dIII	T7		(Wright et al. 1995)
Wnt4	*Eco*RV	SP6	IMAGE #40044945	(Bogani et al. 2009)
Stra8	*Bam*HI or *Hin*dIII	T7	IMAGE #40045823	(Bogani et al. 2009)
Oct4	*Bam*HI	T7	IMAGE #AA522407	(Siggers et al. 2002)
Hsd3b	*Xho*I	T3	IMAGE #580043	(Smith et al. 2008)
Insl3	*Sal*I	T7	3'UTR from IMAGE #6773462	(Warr et al. 2009)
Foxl2	*Nco*I	SP6	PCR 3'UTR	N.Warr; unpublished
Pax2	*Bam*HI	T3		(Dressler et al. 1990)
Mapk11	*Not*I or *Sal*I	T7	PCR 3'UTR	unpublished
Mapk12	*Nco*I or *Sac*II	SP6	PCR 3'UTR	unpublished
Mapk13	*Not*I or *Sac*I	T7	PCR 3'UTR	unpublished
Mapk14	*Sal*I	T7	IMAGE #5389457	unpublished

The DNA digestion was performed in a 50 µl reaction: 15 µl of plasmid DNA (at approximately 1 µg/µl), 5 µl of 10x buffer, 2 µl of relevant restriction enzyme, and 0.5 µl of BSA (if required) (all reagents from New England Biolabs). The reaction was incubated for 2 hours at the optimum temperature for the restriction enzyme used (but was usually 37°C). To check that the linearisation was successful, 5 µl was electrophoresed on a 1% agarose/TBE gel alongside plasmid DNA.

To precipitate the linearised DNA, 10% volume of 3 M sodium acetate (pH 4.5) and 2.5x 100% ethanol was added. The solution was incubated for 30 min on dry ice, and

then centrifuged at 14,000 rpm, 4°C for 30 min. The ethanol solution was removed and replaced with 200 µl 70% ethanol. This was centrifuged again at 4°C for 10 min, then the ethanol was removed and the DNA pellet resuspended in 20 µl H_2O.

For the DIG labelling and transcription reaction (RNase-free), approximately 3 µl of linearised DNA was added to a 20 µl total reaction comprising 2 µl 10x transcription buffer, 2 µl 10x DIG labelling mix, 1 µl 40 U/µl Rnasin, 2 µl 20 U/µl RNA polymerase (SP6, T7 or T3) (all reagents from Roche) and H_2O. The reaction was incubated at 37°C for 2 hours. Any remaining DNA was digested by the addition of 2 µl 20 U/µl DNase 1 (RNase-free; Roche) and a further 20 min incubation at 37°C. To stop the reaction and precipitate the RNA, 2 µl of 200 mM EDTA, 2.5 µl of 4 M LiCl, and 75 µl of 100% EtOH were added to the reaction before incubating at either -70°C on dry ice for 30 min or at -20°C overnight. The reaction was centrifuged at 4°C for 20 min, then 200 µl ice cold 70% ethanol was added to the pellet and centrifuged again for 2 min. The pellet was air-dried for up to one minute before the RNA was resuspended in 100 µl H_2O. To check the quality of the probe, 5 µl was electrophoresed on a 1% agarose gel as described previously (section 2.5.3). The probe was stored at -20°C.

2.8.3. WMISH protocol

All steps were performed at room temperature (RT) unless otherwise stated. The experiment was performed using 12-well cell culture dishes with Netwell (Fisher) inserts, in which the tissue was contained so that the wells (plus tissue) could be moved into the next solution easily. The following solutions were used:

PBST:	PBS plus 1% Tween.
20x SSC:	(Saline-sodium citrate) 3 M NaCl, 0.3 M sodium citrate in H_2O, pH 4.5 (autoclave sterilised).
Pre-hybridisation sol:	50% formamide, 5x SSC, 0.1% Tween-20, 50 µg/ml Heparin in H_2O.

Hybridisation sol:	Pre-hybridisation sol, 100 µg/ml yeast RNA, 100 µg/ml salmon sperm DNA, and 5 µl/ml denatured probe.
TBST:	140 mM NaCl, 2.7 mM KCl, 25 mM Tris-HCl (pH 7.5), 50 mM $MgCl_2$, 0.1% Tween-20 in H_2O.
Solution 1:	50% formamide, 4x SSC, 2 ml 1% SDS in H_2O.
Solution 2:	50% formamide, 2x SSC in H_2O.
NTMT:	100 mM NaCl, 100 mM Tris-HCl (pH 9.5), 50 mM $MgCl_2$, 0.1% Tween-20 in H_2O (filter sterilised).
Alkaline Phosphatase stain:	20 µl/ml of NBT/BCIP in NTMT.

Embryonic tissue, processed as described in section 2.4.1, was rehydrated through a 5-min/step methanol series into PBST (twice) and then bleached with 6% H_2O_2 in PBST for 40 min. After 3x 5 min PBST washes, the tissue was digested with 10 µg/ml Proteinase K (Roche) for 12-20 min (depending on the size of the tissue), and then stopped with 2 mg/ml glycine for 5 min. Tissue was washed again for 2x 5 min in PBST and then post-fixed in 0.2% gluteraldehyde in 4% PFA in PBST for 20 min. After a further 2 washes in PBST, the tissue was placed in pre-hybridisation solution at 70°C for 1 hour or more. Meanwhile, the RNA probe (10 µl per 2 ml reaction well) was denatured at 70°C for 10 min. The denatured probe was spun down, cooled on ice, and transferred to pre-aliquoted hybridisation solution. Tissue was transferred to this hybridisation solution containing denatured RNA probe and incubated at 70°C overnight.

The next day, the samples were washed for 2x 30 min in solution 1 at 70°C, and then 2x 30 min in solution 2 at 65°C. Following 3x 5 min in 1x TBST at RT, samples were transferred to 10% heat inactivated sheep serum (HISS) in TBST to pre-block (prevent non-specific binding of the antibody) for at least 3 hours at RT. Meanwhile, 1% HISS in TBST was prepared to allow for 2 ml per sample. Antibody solution was then pre-prepared in which embryo powder (made from homogenised 12.5-14.5 dpc embryos,

washed with acetone, dried and ground to a powder with a pestle and mortar) was heat-inactivated for 30 min at 70°C in 1 ml TBST. The powder was pulsed down to a pellet and TBST removed. The powder was then resuspended in 1 ml cold 1% HISS in TBST. 1 µl of anti-digoxigenin-alkaline-phosphatase conjugated Fab fragments (Roche) per reaction sample was added to the embryo powder, and this antibody-HISS-embryo powder mix was then placed on a rotator for 1 hour+ at 4°C to pre-absorb the antibody. The TBST supernatant containing the HISS and antibody was then transferred back into the remaining 1% HISS in TBST and the samples hybridised in 2 ml of this pre-prepared antibody solution overnight at 4°C.

The following day, samples were washed in TBST for 3x 5 min at RT, and then 5x 1 hour before being left overnight in TBST at 4°C. The colour was developed the following day by washing the samples 3x 10 min in NTMT. The samples were then transferred to a watch glass and incubated in alkaline phosphatase staining solution in the dark for colour development. The reaction was stopped with PBST. To remove any background staining, the samples were left in PBST for one to three days before being fixed in 4% PFA for one hour. The samples were stored at 4°C in PBST with 0.4% PFA.

2.8.4. Imaging and cryosectioning

To photograph the WMISHs, 1% agarose/H_2O plates were used: the samples to image were placed on the agarose covered with PBST, and imaged using a Leica MZ16 dissection microscope with a camera attached.

Some samples were subsequently processed for cryosectioning by embedding in the orientation of choice in optimal cutting temperature (O.C.T.) compound (Sakura) in small Beem capsules (Agar scientific). These were snap-frozen in dry ice and stored at

-80°C until ready to cut. 12 µm thick sections were cut using a Microm cryostat (HM 560). Cryosections were imaged using a Zeiss Axiophot 2.

2.9. *LacZ* expression

To confirm the expression pattern of a *Cre* transgenic mouse line, the *Cre* line was crossed to R26R – a reporter line containing a *LacZ* gene downstream of a neomycin cassette flanked by two LoxP sites, which is driven by the ubiquitous Rosa26 promoter (Soriano 1999). Site-specific recombination between the LoxP sites in the presence of *Cre* recombinase causes the deletion of the neomycin cassette and transcription of the *LacZ* gene. The expression of the product, β-galactosidase, and subsequent enzymatic activity, can be assessed by staining with X-Gal. Active β-galactosidase cleaves X-Gal to release a blue product that can be detected, and thus the cell-specific location of the active *Cre* promoter can be determined.

Tissue that was dissected and processed according to section 2.4.4 was fixed (1% PFA, 0.2% gluteraldehyde, 2 mM $MgCl_2$, 5 mM EGTA, and 0.02% Nonidet P-40 (NP-40) in PBS) for 30 min on ice with shaking. This was followed by 3 washes in PBS + 0.02% NP-40 before adding the staining solution (5 mM $K_3Fe(CN)_6$, 5 mM $K_4Fe(CN)_6$, 2 mM $MgCl_2$, 0.01% Deoxycholate, 0.02% NP-40, and 1 mg/ml X-GAL in PBS). The colour developed in the dark overnight (at RT). Colouring was halted by washing in 3x PBS and post-fixing in 4% PFA for 20 min. The stained tissues were stored in 0.4% PFA in PBS at 4°C.

2.10. Immunohistochemistry (IHC)

The antibodies used to study protein expression by this method (and their corresponding concentrations) are detailed below (Table 2-4):

Table 2-4: Details of antibodies used and corresponding IHC conditions

1° Antibody	Company	Species	Conc^{n}	2° Antibody Alexa fluor	Method
Phospho-histone H3 (pHH3) (pSer^{10})	Upstate #06-570	Rabbit	1:500	α-rabbit 1:400	Wholemount
Phospho-histone H3 (pHH3) (pSer^{28})	Sigma #H9908	Rat	1:2000	α-rat 1:300	Wholemount
PECAM-1/CD31	BD Bioscience #550274	Rat	1:250 or 1:200	α-rat 1:200	Wholemount Cryosections
SF1	Gift from K.Morohashi	Rabbit	1:750	α-rabbit 1:200	Wholemount
Phospho-SF1 (pSF1)	Gift from H.Ingraham	Rabbit	1:500	α-rabbit 1:500	Wholemount
Cleaved caspase-3	Cell signalling #9661S	Rabbit	1:250	α-rabbit 1:500	Cryosections
phospho-p38 (pp38)	Cell signalling #4631	Rabbit	1:100	α-rabbit 1:500	Wholemount

2.10.1. Wholemount IHC

To investigate protein expression in wholemount tissue, samples stored in 100% methanol for less than 7 days were used. All incubation steps were performed with agitation. The samples (11.5 dpc UGRs) were washed for 3x 5 min in freshly made PBS-BS (PBS with 1% BSA and 11% sucrose). They were then incubated in primary antibody (diluted in PBS-BS) overnight at 4°C. The following day, the samples were washed in PBS for 3x 2 hours (4°C) and then incubated in secondary antibody in PBS-BS overnight at 4°C. The samples were washed the next day 3x 2 hours in PBS at 4°C and then overnight in PBS at 4°C. If a cell nuclear marker was required, aqueous DAPI (1:300 in PBS; Sigma Aldrich) was added to the samples for 15 min the following morning. To image the samples, they were first sub-dissected to two single gonads and then mounted on slides in PBS, in a sagittal orientation, using silicone grease to support the coverslip. They were imaged using a Leica TCS SP5 confocal microscope with either a 20X or 40X objective.

2.10.2. Imaging and cell counts for pHH3 staining

The central third of each gonad was imaged using a Leica TCS SP5 confocal microscope (40X). For cell counts in the coelomic region, a Z-stack series (10 µm steps) was generated for sagittal sections of each sample. Three central sections were then chosen 20 µm apart to ensure no cell was counted twice. The number of cells positive for pHH3 within the coelomic epithelium of all three sections per sample was calculated. The total number of cells within this region was also calculated by counting the number of cell nuclei situated above the line of germ cells. Differences between samples were assessed using a two-tailed student's *t*-test.

2.10.3. Section IHC

Cryosections were primarily used because they were more compatible with the majority of antibodies being used for protein expression analysis. However, this is very much dependent on the antibody used. The method outlined below is specifically for use with cryosections.

Cryosections of tissue, processed as described in section 2.4.2 and using the method outlined in 2.8.4, were air-dried for 1 hour. To limit the antibody solution required to cover the sections, the sections were encircled with wax by using a wax pen (Vector Labs), to contain the solutions. The sections were then re-hydrated in PBS for 10 min and blocked in PBS-BT (PBS with 1% BSA and 0.2% triton x-100) for 1 hour. Primary antibody in PBS-BT was added and left to incubate overnight at 4°C. The next day, slides were washed 4x PBS for 5 min. Secondary antibody in PBS-BT was added for 45 min at RT, then slides were washed in PBS again for 2x 5 min. Slides were mounted in Vectashield with DAPI (Vector Labs) and imaged using a Zeiss Axiophot 2.

2.11. Organ cultures

Prior to the day of use, organ culture agar blocks were prepared using 1.5% bacto-agar (DIFCO) in Dulbecco's Minimal Eagle's Medium (DMEM) (#21969, Invitrogen) and set in a 35 mm culture dish. The agar blocks were equilibrated in 3 ml of organ culture medium (10% foetal calf serum, 200 mM L-Glutamine and 50 µg/ml ampicillin in DMEM) overnight at 37°C/5% CO_2.

For standard organ cultures, on the day of dissection, samples prepared as in section 2.4.5 were genotyped for their sex. XX and XY UGRs were then sub-dissected into single gonads in organ culture medium. The medium surrounding the agar blocks was replaced with 400 µl of fresh medium and the individual gonads were placed in the grooves of the agar blocks, with excess medium removed. These were then cultured at the air/medium interface in a 37°C/5% CO_2 incubator for 48 hours. The cultured gonads were subsequently removed from the agar blocks and either fixed in 4% PFA overnight before dehydration into 100% methanol for WMISH analysis, or snap frozen in dry ice and stored at -70°C for RNA extraction and qRT-PCR analysis.

For knockdown organ culture, the main principles of the standard culturing apply, but the initial preparation before the samples go into culture differs (see section 2.12).

2.12. Knockdowns

To optimise a gene knockdown technique in mouse gonads two different methods were trialled.

2.12.1. Magnetofections

Knockdown using an shRNA, which is taken up by cells of the tissue following a magnetofection technique, was attempted following a published protocol (Svingen et al.

2009). 11.5 dpc UGRs were collected as described for standard cultures in section 2.4.5 but in a 12-well plate in L15 medium (Invitrogen). The samples were left on ice while they were genotyped for their sex and the plasmid DNA/CombiMAG mix was prepared. For each 1 µg expression plasmid, 2.5 µl Lipofectamine 2000 (Invitrogen) was added, incubated for 20 min at RT, mixed with 3.5 µl CombiMAG (Chemicell) and incubated for a further 20 min. This compound was then injected into the gonadal ridge by trialling a variety of methods including a hand-held Transferpette with pulled glass capillaries (Fisherbrand), and a mouth-pipette with thin-walled borosilicate capillaries (Harvard apparatus). The 12-well plate containing the injected gonads in L15 medium was placed on a magnetic plate (Chemicell) for 1 hour at RT. The gonads were transferred to pre-equilibrated 1.5% agar blocks (section 2.11) and cultured for 48 hours at 37°C/5% CO_2. Initially, a pEGFP-C1 expression plasmid (Clonetech #6084-1) was used to assess efficiency of uptake into cells. This was assessed by imaging the cultured gonads with an Olympus IX81 microscope. Uptake of an *Sry*-expressing plasmid (*pcHA-Sry*, a kind gift from P.Koopman) into XX gonads was also tested. This method was discontinued before use of an shRNA for knockdown was tested.

2.12.2. Transfections

For siRNA knockdown, whole embryos were collected in a 24-well plate in Opti-MEM reduced-serum medium as described in section 2.4.5. The samples were left on ice for approximately 3 hours while they were genotyped for their sex. The UGRs were then extracted from the embryos and transfected overnight at 37°C in a 5% CO_2 incubator in the presence of two siRNAs both at 200 nM, and 20 nM Lipofectamine RNAiMAX (Invitrogen) in the Opti-MEM reduced-serum medium. Two different Silencer Select siRNAs (Invitrogen) per targeted gene were used together to increase the chances of efficient knockdown. These were as follows: *Sox9* (s74192 and s74193), *Mapk11*

(s72152 and s72153), *Mapk12* (s78078 and s78079), *Mapk13* (s77110 and s77111), and *Mapk14* (s77113 and s77114). The siRNA/Lipofectamine/Opti-MEM medium solution was prepared according to the manufacturer's recommendations following the 'Forward Transfection' protocol. Briefly, the amount of siRNA required to make a final concentration of 200 nM in 600 µl was made up to 50 µl volume per sample in Opti-MEM medium. In the same manner, the Lipofectamine RNAiMAX was also made up to 50 µl volume per sample. These were incubated for 5 min, before the Lipofectamine/Opti-MEM compound was combined with the siRNA/Opti-MEM compound. These were incubated for 20 min, before 100 µl was added to each well containing 500 µl of Opti-MEM medium and the sample. Samples of the same sex, tail somite stage and siRNA conditions were pooled together in the same well to save reagents.

The next morning, the samples were sub-dissected into individual gonads in organ culture medium (see section 2.11), transferred to a pre-equilibrated 1.5% agar block and cultured for 48 hours at 37°C/5% CO_2 as described in section 2.11. Following culture, the gonads were processed depending on the method of choice to determine the effects of the gene knockdown. However, for qRT-PCR analysis, the Qiagen Micro RNA extraction kit was used instead of the Nucleospin kit, as it could extract better quality RNA in a smaller volume, enabling RNA extraction from single cultured gonads (see section 2.7 for details). 5 ng cDNA was subsequently used per qRT-PCR reaction.

Negative control siRNA samples were always cultured simultaneously using a standard non-specific negative control Silencer Select siRNA (Invitrogen). A 200 nM Block-iT Alexa Fluor Red Oligo (Invitrogen) was also used to assess transfection efficiency by observing the uptake of the Alexa Fluor into the gonad using confocal microscopy.

Chapter 3. The role of MAP kinase signalling in gonad development: analysis of the boygirl (*byg*) mutant

3.1. Introduction

This chapter focuses on the cellular and molecular characterisations of gonad development in the ENU-induced *Map3k4* null mutant, *byg*, on the C57BL/6J background. The C57BL/6J background is always preferentially used for studies of testis determination, since it is known to be sensitised to disruptions to XY gonad development and exhibit high frequencies of XY gonadal sex reversal in some genetic contexts in comparison to other strains (Bouma et al. 2007; Bogani et al. 2009). The exact cause of this increased susceptibility to XY sex reversal is not confirmed, but a report has shown, through expression profiling analysis between C57BL/6J and 129S1/SvImJ wild-type mice, that higher levels of expression of ovary-determining genes are detected in C57BL/6J samples (Munger et al. 2009). Higher levels of *Sox9* expression were also detected, therefore it is likely that in the C57BL/6J wild-type mice; the elevated *Sox9* counteracts the ovary-determining genes, but in the presence of allelic variants that weaken the *Sox9* expression, ovary development is more likely to ensue.

3.1.1. Role of proliferation during sexual differentiation

Cell proliferation is one of the cellular activities that MAP kinases regulate and it is also a vital part of gonad development. Sufficient rates of cell proliferation between 10.8 dpc and 11.2 dpc in the gonad are vital for subsequent testis determination in XY gonads; inhibition of proliferation within this developmental period prevents the formation of testis cords and reduces the expression of testis-specific genes *Sox9* and *Amh* (Schmahl and Capel 2003). However, a detectable difference in cell proliferation between XX and XY gonads only becomes apparent after 11.25 dpc, since this testis-specific

proliferation is part of the testis differentiation process and is induced by *Sry* (Schmahl et al. 2000).

Proliferating cells are those that are actively undergoing growth and division through the cell cycle. The cell cycle consists of two important stages: interphase and mitosis. Mitosis is the point at which the cell splits into two identical daughter cells, while interphase includes the preparation for mitosis, which is split into three sections: Gap 1 (G_1), synthesis (S), and Gap 2 (G_2). G_1 immediately follows mitosis, and is when the cell starts to increase in size and synthesise proteins and enzymes required for synthesis. This is followed by a G_1/S checkpoint, to ensure that the cell is ready for DNA synthesis (S-phase) and to check for any DNA damage. G_1 also contains the exit point for quiescent cells which no longer divide; they enter Gap zero (G_0), the resting phase, in which cells can remain for a long period of time. This quiescent phase is common for fully differentiated cells, such as neurons. For cells that are still proliferating, following the G_1 checkpoint, they enter S-phase during which the chromosomes duplicate such that each chromosome consists of two sister chromatids. The cell then enters G_2, when it again increases in size and prepares for mitosis by synthesising the required molecules, such as microtubules. This is followed by a second checkpoint, G_2/M, to again ensure that the cell cycle can continue, and no errors are present. Mitosis then follows, which is split into four different stages: prophase, metaphase, anaphase and telophase.

During mitosis, the chromatin condenses into highly ordered mitotic chromosomes and it is the subsequent correct segregation of sister chromatids into two identical daughter cells that is essential (Koshland and Strunnikov 1996). Chromatin is highly organised to facilitate the packaging of DNA into the nucleus. DNA is wrapped around core histone proteins to form nucleosomes. These nucleosomes then coil around each other into

euchromatin, which is the chromosome structure where genes are actively transcribed. Chromatin can also be more tightly coiled into heterochromatin structures, which prevent the active transcription of genes as the sister chromatids prepare for mitotic division. During the prophase stage of mitosis, the chromatin condenses even further into metaphase chromatin, which is a very strong structure allowing the separation of the sister chromatids into two daughter cells without damaging the DNA. During metaphase, the chromatin aligns in the centre of the nucleus, which is mediated by microtubules between the centrioles at either end of the nucleus and kinetochores on the centrioles of the chromosomes. The sister chromatids are pulled apart and separated during anaphase, and the nuclear envelope forms around each pair of chromatids to generate two separate daughter cells during telophase. Cytokinesis occurs after mitosis, and is the separation of the cytoplasm into the two daughter cells.

A cluster of four pairs of histone proteins are found within a nucleosome: histone H2A, H2B, H3 and H4. A fifth, H1, is a linker histone which links adjacent nucleosome cores to further compact the chromatin. These histones have vital roles in the condensation of the chromatins during mitosis, and two phosphorylation sites within the N-terminal of histone H3 have been identified. Phosphorylation at both serine-10 ($pSer^{10}$) and serine-28 ($pSer^{28}$) coincides with the induction of mitotic chromosome condensation and so antibodies against either of these phosphorylation sites have been developed for use as markers for proliferating cells that are undergoing mitosis (Goto et al. 1999). These anti-phospho-histone H3 (pHH3) antibodies detect phosphorylation at either the Ser^{10} or Ser^{28} sites. Ser^{10} phosphorylation is initiated during G_2 (late interphase) on pericentromeric heterochromatin and then increases during prophase until maximum phosphorylation in metaphase. Dephosphorylation is initiated in anaphase and is completed by decondensation of the chromatin, therefore showing that it is a mitosis-

specific event (Hendzel et al. 1997). Ser^{28} phosphorylation is initiated in prophase, the onset of mitosis, which is slightly later than the initiation of $pSer^{10}$ (Goto et al. 1999). Detection of phosphorylated histone H3, at Ser^{10}, forms the core of the cell proliferation analysis in this results chapter (section 3.2.1).

Another method of detecting proliferating cells is based on incorporation of bromodeoxyuridine (BrdU), an analogue of thymidine, into the DNA of cells during S-phase (Lengronne et al. 2001). An antibody can then be used to detect BrdU and therefore identify cells undergoing DNA replication. However, this method of detection cannot be directly compared to methods using pHH3 antibodies, since BrdU detects cells that were in S-phase during the application of BrdU, and pHH3 antibodies only detect cells currently in mitosis. S-phase occupies a longer period of the cell-cycle than mitosis, meaning that more cells will be in S-phase than mitosis at any given time of detection.

The MAP kinase cascade can regulate the cell cycle and proliferation in a variety of ways. G_1 progression is controlled by the D group of cyclins, and ERK1/2 is known to activate D1 cyclin, allowing progression of the cell cycle through to mitosis. In contrast, p38 MAPKs inhibit D1 cyclin, which causes G_1 mitotic arrest, blocking the cell cycle (Lavoie et al. 1996). Therefore, gonadal cell proliferation in the *Mapk3k4*$^{byg/byg}$ mutant was examined in detail between 11.5 dpc and 12.1 dpc, when a significant divergence in rates between male and female was expected. This analysis assessed the expression of pHH3 to specifically detect cells in the mitotic phase of the cell cycle.

3.1.2. *Sry* transcriptional regulators

Sry expression was found to be significantly reduced at 11.5 dpc in the XY *Map3k4*$^{byg/byg}$ mutant (Bogani et al. 2009). One approach to study the molecular basis of

this defect is to study potential *Sry* transcriptional regulators via a candidate approach. There are a number of such potential regulators that have been identified over recent years. Steroidogenic factor 1 (SF1 or NR5A1) is an orphan nuclear receptor and a critical regulator of sex determination (Luo et al. 1994). *Sf1* expression in somatic precursor cells is vital for the expression of *Sox9*, and therefore testis differentiation (Sekido and Lovell-Badge 2008). *In vitro* transfection studies have shown that SF1 binds and activates both the human and pig *SRY* promoter, while *in vivo* studies in mice have shown that SF1, with CITED2, can regulate *Sry* expression making SF1 a good candidate for an *Sry* activator in mice (Pilon et al. 2003; Buaas et al. 2009; Sekido and Lovell-Badge 2009).

An interesting link exists between SF1 and MAP kinase signalling in that SF1 is activated following phosphorylation of a single serine residue (Ser^{203}), which is located within the activation function domain in the hinge of the protein (Hammer et al. 1999). This Ser^{203} residue also resides within a consensus MAPK activating site, which means that the phosphorylation of this residue, and therefore the SF1 protein, is stimulated directly by a MAPK protein, likely to be ERK2 (Hammer et al. 1999).

Other putative *Sry* transcriptional regulators include WT1(+KTS), GATA4 and CBX2 (M33). WT1 and GATA4 are also known to be activated through phosphorylation so also provide good candidates for further study. However, work in this thesis focuses on SF1 and its activated form.

3.2. Results

3.2.1. Analysis of cell proliferation in boygirl embryonic gonads

Due to the association between MAPK activity and growth, and previous studies on the role of cell proliferation in XY gonad development (Schmahl et al. 2000; Schmahl and Capel 2003), a detailed analysis of cell proliferation in the gonadal coelomic region of this mutant was performed using wholemount immunohistochemical analysis and confocal imaging. Using the mutation on the C57BL/6J background, embryos from *byg*/+ intercross matings were collected at 11.5 dpc (17-18 tail somites (ts)), 11.8 dpc (20-22 ts) and 12.1 dpc (24 ts). To visualise cells in the mitotic phase of the cell cycle, an antibody raised in rabbits against phosphorylated histone H3 (pHH3) was used. This antibody detects HH3 phosphorylated at Ser^{10} ($pSer^{10}$), which is restricted to early mitotic cells and some cells during G_2 interphase (see section 3.1.1 for more information). To distinguish somatic cells from germ cells, a rat-developed antibody against platelet/endothelial cell adhesion molecule (PECAM), which marks the membrane of primordial germ cells and endothelial cells, was used at the same time. Following immunohistochemistry and confocal imaging, detailed cell counts in the coelomic region were performed at each stage in XY +/+, XX +/+ and XY *byg/byg* gonads (see 2.10.2 in the Materials and Methods for details). Somatic cell proliferation in XY *byg*/*byg* gonads appeared reduced in comparison to wild-type XY embryonic gonads at all stages examined (Figure 3.1 and Table 3-1). From 11.8 dpc onwards, the coelomic region of XY wild-type gonads was thickened and contained a larger number of somatic cells compared with XY *byg*/*byg* gonads, which resembled XX wild-type gonads of the same stage. It is possible to conclude from these data that cellular proliferation, and thus gonadal growth, in the coelomic region is severely compromised in XY *byg*/*byg* gonads.

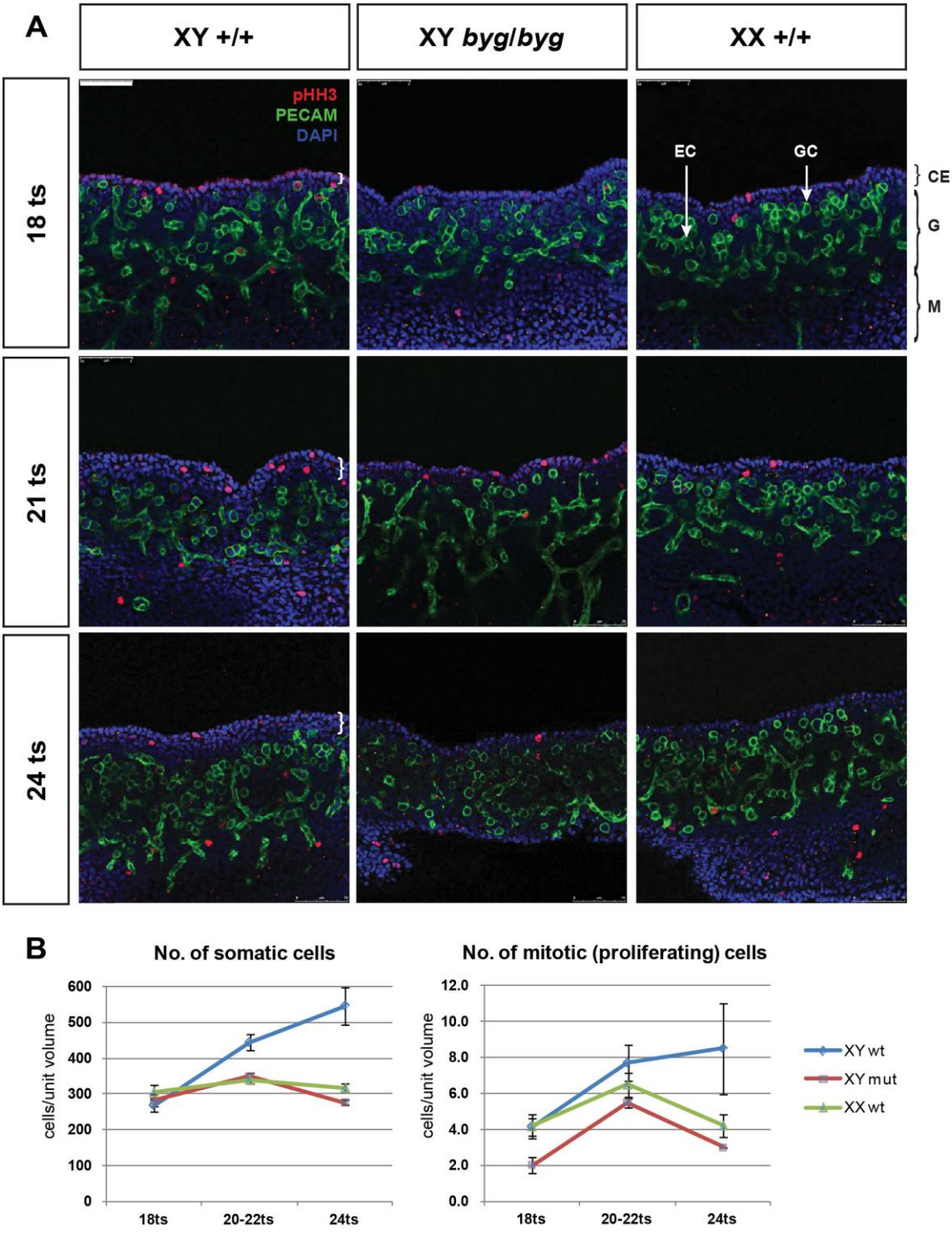

Figure 3.1: Reduced gonadal growth in XY *byg/byg* embryos between 11.5 and 12.1 dpc
(**A**) Somatic cell proliferation within the coelomic region of XY *byg/byg* gonads was analysed by confocal imaging following wholemount immunostaining with anti-pHH3 (red, mitotic cells) and anti-PECAM (green, germ cells), and results compared to XY +/+ and XX +/+ gonads. Cell nuclei were visualised using aqueous DAPI (blue). Embryos were accurately staged by counting the tail somites (ts). The coelomic growth zone in the epithelium of XY +/+ gonads is shown in white brackets. Both the coelomic region and number of proliferating cells are reduced in the XY *byg/byg* gonads. Images were taken with a 40x objective. Gonads were mounted in a sagittal orientation as shown by labelling in the top right. Scale bar = 75 µm. CE, coelomic epithelium; EC, endothelial cell; G, gonad; GC, germ cell; M, mesonephros.
(**B**) Graphical representation of cell numbers. Error bars represent standard error of the mean.

Table 3-1: Cell proliferation in the XY *byg/byg* gonad
Cell counts for the number of mitotic and total somatic cells within the coelomic region of wild-type (+/+) and *byg/byg* gonads between 13 and 24 tail somite (ts) stages. Average of *N* number of samples is shown.

	13 ts			18 ts			20-22 ts			24 ts		
	N	Mitotic	Somatic	*N*	Mitotic	Somatic	*N*	Mitotic	Somatic	*N*	Mitotic	Somatic
XY +/+	4	6.00	216.0	6	4.17	268.0	7	7.71	444.0	2	8.50	546.0
XY *byg/byg*	4	6.25	195.3	5	2.00*[a]	281.4	8	5.50*[b]	349.3*[c]	2	3.00	277.0*[d]
XX +/+	3	4.00	211.0	5	4.20	306.6	6	6.50	340.0*[e]	4	4.25	317.8*[f]

* Values are significantly different from respective XY wild-type data using a two-tailed student *t*-test where p=<0.05. Individual p values: a=0.01, b=0.043, c=0.001, d=0.038, e=0.002, f=0.003

To ascertain whether the proliferation in the XY *byg/byg* gonads was also reduced during the stage critical for testis determination (10.8 – 11.2 dpc), 13 ts gonad samples were also analysed. Preliminary cell counts of 4 samples per genotype suggests that there is no significant difference between both the number of mitotic and the number of somatic cells within the coelomic region of XY *byg/byg* samples and XX +/+ controls in comparison with XY +/+ controls (Table 3-1 and Figure 3.2A). Therefore, the difference in proliferation that is observed in the XY *byg/byg* gonads at 11.5 dpc is most likely a consequence of the failure to appropriately up-regulate *Sry* expression and activate cellular pathways of testis morphogenesis. An earlier defect in cellular proliferation as the cause of reduced *Sry* expression cannot be excluded, but such a defect was not obviously detectable with the assays and reagents used here.

3.2.2. Apoptosis

Another potential explanation for the decreased volume of cells in the coelomic region in *byg*/*byg* XY gonads is increased apoptosis. Also, increased levels of apoptosis have been described previously in the neural tube of mice lacking *Map3k4* (Abell et al. 2005; Chi et al. 2005). To detect apoptotic cells, an antibody against cleaved caspase-3 was used. Caspase-3 is a protein that is activated specifically during the process of apoptosis and is one of the 'effector' caspases required to trigger the cell death programme. This

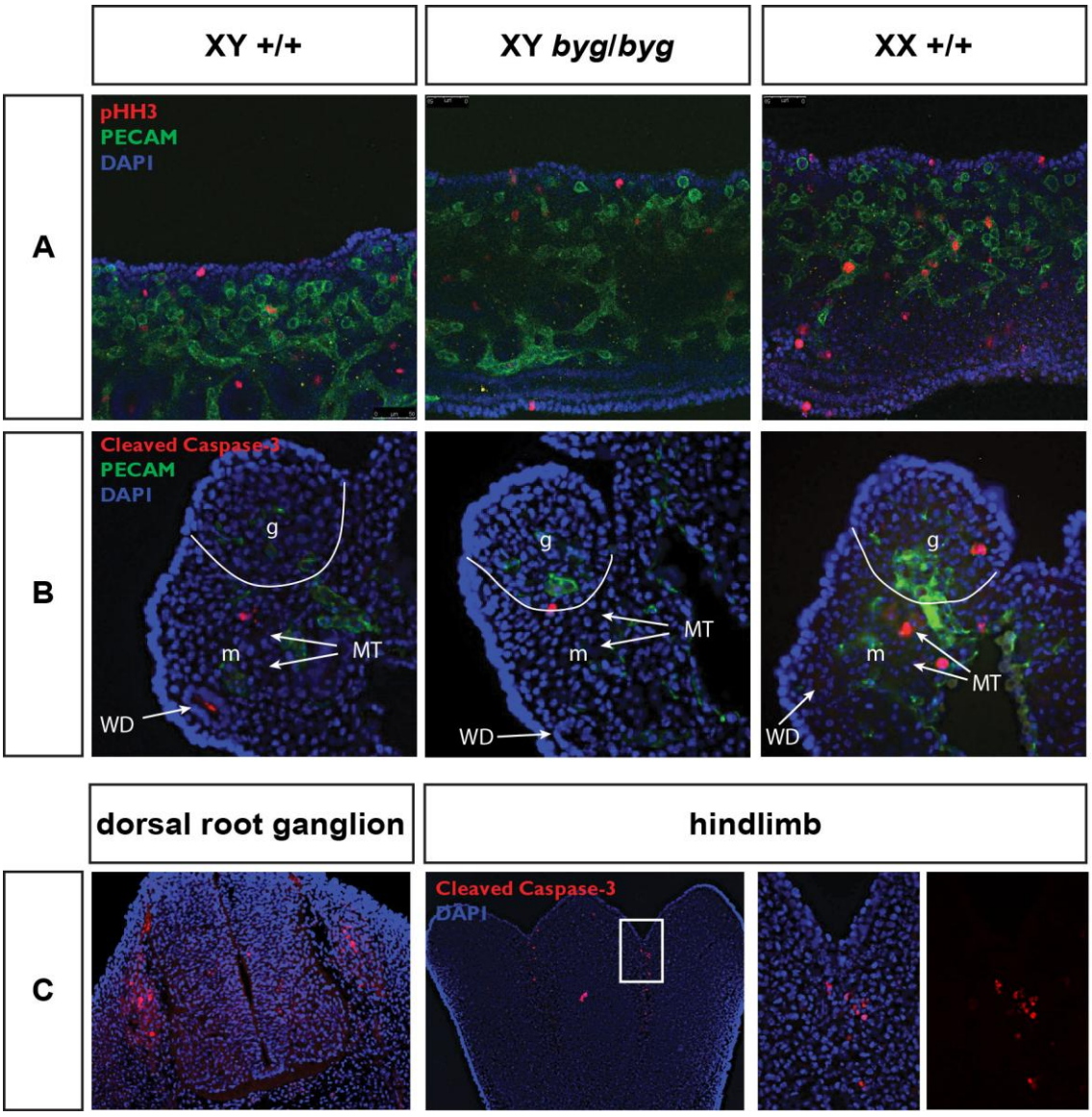

Figure 3.2: Analysis of proliferation at 11.0 dpc and apoptosis at 11.5 dpc
(**A**) Cell proliferation was examined at 11.0 dpc (13 ts) in the same way as for Figure 3.1A. The number of mitotic cells in the coelomic epithelium, and the number of somatic cells, were counted in all three samples. No obvious difference was observed.
(**B**) Apoptosis was examined in transverse cryosections of 11.5 dpc *byg* tissue using an anti-cleaved caspase-3 antibody (red). Anti-PECAM antibody (green) was used to detect germ cells in the gonad, while nuclei were counterstained with DAPI (blue). The gonadal area (g) is highlighted within the white semi-circle. Hardly any apoptotic cells were observed in any sample, and most apoptotic cells that were present resided in the mesonephric tubules (MT). WD, Wolffian duct; m, mesonephros.
(**C**) The antibody was first tested on control tissue to check efficiency. Sections were through dorsal root ganglion (transverse) and the interdigital mesenchyme of 14.0 dpc hindlimb (transverse).

activation occurs by cleavage of the inactive zymogen into two subunits which dimerise to form an active enzyme that the anti-cleaved caspase-3 antibody recognises. The number of apoptotic cells was studied in XY *byg*/*byg* gonads compared to controls at 17 ts by immunohistochemistry on transverse cryosections (Figure 3.2B). Very few positive cells were observed in either mutant or control samples, suggesting that apoptosis is unlikely to play a role in the reduced growth of the XY *byg/byg* gonads. The activity of the antibody was validated by analysing the interdigital mesenchyme of the developing limb, as well as sections of the dorsal root ganglion, as positive controls (Figure 3.2C). The few apoptotic cells that were observed in the gonadal samples were usually found in the mesonephric tubules and duct, or on the gonad/mesonephros border. This is consistent with previous studies of apoptosis in the developing mouse gonad (Schmahl and Capel 2003).

3.2.3. SF1: a missing link between MAP kinase signalling and *Sry*?

Due to the reduction of SRY expression in XY *byg/byg* gonads, the expression of SF1 (a potential transcriptional regulator of *Sry*) in XY *byg/byg* and control gonads was investigated using an anti-SF1 antibody (a kind gift from K.Morohashi). Analysis at 11 ts (just before the normal up-regulation of *Sry* (Koopman et al. 1990; Hacker et al. 1995; Bullejos and Koopman 2001)) revealed nuclear expression in the somatic cells throughout the gonad with no obvious differences with respect to either the number of cells expressing the protein or the sub-cellular localisation of the protein in any samples examined (Figure 3.3A-D). Expression of SF1 at 11.5 dpc (20 ts) in wild-type XY and XX gonads was also tested (Figure 3.3E-F). Expression was seen in somatic cells throughout the gonad with no sex-specific differences observed at this stage, which is consistent with previous reports (Ikeda et al. 1994).

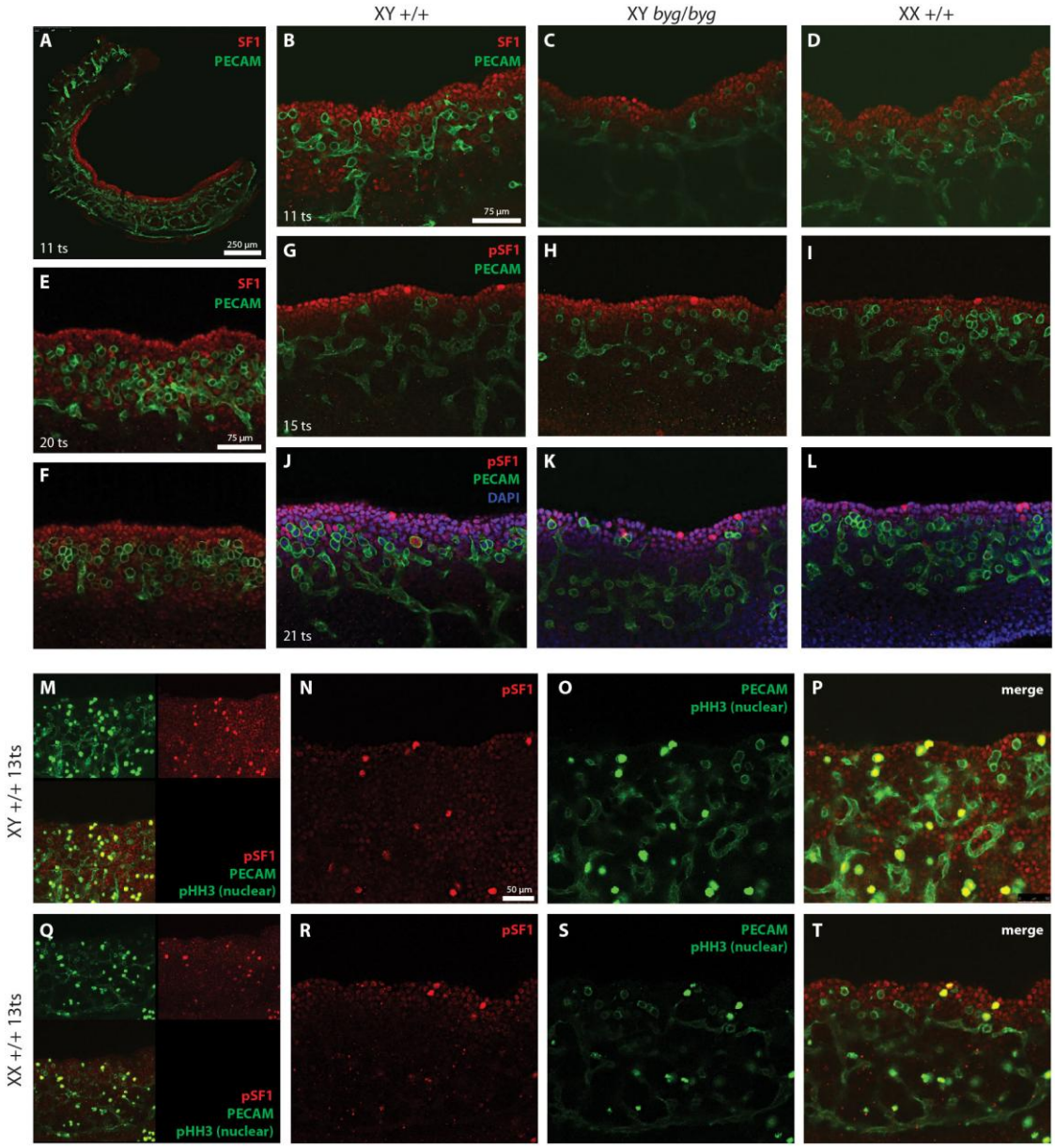

Figure 3.3: Analysis of SF1 expression in XY *byg/byg* gonads

Wholemount immunohistochemistry using antibodies against both SF1 and activated SF1 (pSF1) were performed to show the location of SF1-positive somatic cells in the gonad, in comparison with pSF1 cells. The colocalisation of pSF1 with mitotic cells was also determined using a rat anti-pHH3. Images show sagittal confocal (optical) sections taken with a 40x objective, unless otherwise stated.

(**A**-**D**) Anti-SF1 (red) with anti-PECAM (green) on 11 ts gonads: (A) Control sample taken with a 10x lens to show full size of 11 ts gonad. Gonadal tissue is highlighted by SF1 expression, and at this stage is a thin layer of cells along the top of the urogenital ridge structure. (B-D) Expression of SF1 in XY +/+, XY *byg/byg* and XX +/+ samples respectively. No qualitative difference observed between either the number of cells expressing SF1 or the subcellular localisation. (**E**-**F**) Expression of SF1 in XY (E) and XX (F) wild-type 20 ts samples confirms no difference between sexes at this stage. (**G**-**I**) Expression of pSF1 (red) in XY +/+, XY *byg/byg* and XX +/+ samples, respectively, at 15 ts stage. Expression seems to be localised to the coelomic epithelium (large bright cells). This anti-pSF1 antibody also appears to highlight unphosphorylated-SF1 (smaller cells). (**J**-**L**) Expression of pSF1 at 21 ts with nuclei marked with DAPI. (**M**-**T**) Samples were co-stained with a rat anti-pHH3 (nuclear, green) to determine if pSF1 cells colocalised with mitotic cells. Rat anti-PECAM (membrane marker, green) was also used to distinguish the gonad from the mesonephros. (M) and (Q) are maximum projection images; (N-P) and (R-T) are single section images showing colocalisation of pSF1 with pHH3. All pSF1-positive cells were also pHH3-positive, but pHH3-positive cells were not always pSF1-positive. XY *byg/byg* samples are not shown because there was no difference.

Scale bars represent: 250 µm (A), 75 µm (B-L), and 50 µm (N-P and R-T).

The activated form of SF1, which is phosphorylated at Ser^{203}, was also examined using a specific antibody against this phosphorylated form (pSF1; a kind gift from H.Ingraham). XY *byg/byg*, XY +/+ and XX +/+ samples at both 15 ts and 21 ts stages were assessed and a subset of pSF1-positive cells were observed mainly within the coelomic epithelium at both stages, with no difference between the XY *byg/byg* and controls (Figure 3.3G-L). However, the antibody also appeared to detect other cells within the coelomic epithelium (albeit with a reduced intensity), which are potentially unphosphorylated SF1-positive cells, so the specificity and reliability of this antibody is questionable.

As most expression of pSF1 appeared to be localised to the coelomic epithelium, some samples were co-immunostained with rat anti-pHH3 ($pSer^{28}$) to determine if the positive cells co-localised. Rat anti-pHH3 antibody was used rather than the rabbit $pSer^{10}$ anti-pHH3 used in the previous proliferation studies since anti-pSF1 was also raised in rabbit: the distinct secondary antibodies could then detect each in a different colour, and overlapping cells would be detected. However, expression of PECAM was also required to detect germ cells and differentiate the gonadal tissue from the mesonephros, and anti-PECAM was raised in rat. Due to the different subcellular localisations of both anti-PECAM (membrane marker of germ cells) and anti-pHH3 (nuclear marker of mitotic cells) though, it was possible to use antibodies raised in the same species. At 11.0 dpc, all pSF1-positive cells were also positive for pHH3 in both XY and XX wild-type samples. However, not all pHH3-positive cells were positive for pSF1 (Figure 3.3M-T). Using the maximum projection confocal images, where the Z stacks are flattened into one image enabling all positive cells to be visualised together, cell counts of both pSF1- and pHH3-positive cells in the coelomic epithelium of 12-14 ts samples were counted

(Table 3-2). No significant difference was observed between either XY *byg/byg* and XY +/+, or XX +/+ and XY +/+, with respect to both average pHH3- or pSF1-positive cells.

Table 3-2: pSF1-postive cells versus mitotic cells in the XY *byg/byg* gonad
Cell counts in the coelomic epithelium of 12-14 ts samples using maximum projection confocal images. The results are an average across the number (*N*) of samples analysed. Statistical analysis was performed with a two-tailed student's *t*-test compared to XY +/+ samples, at 95% confidence (*p* value).

	N	pHH3		pSF1	
		Average	*p*	Average	*p*
XY +/+	7	12.00		7.00	
XY *byg/byg*	4	9.75	0.439	6.25	0.695
XX +/+	4	15.25	0.324	6.75	0.924

3.3. Discussion

A point mutation in the open reading frame of *Map3k4*, which causes an early truncation of the protein before the critical kinase domain, has been identified in *byg* mutants. This null mutation causes embryonic phenotypes including neural tube defects, oedema and, on the C57BL/6J background, complete male-to-female XY gonadal sex reversal. To analyse the cellular effects of this $Map3k4^{byg}$ mutation on gonad development at the sex-determining stage, cell proliferation was examined. Most of the theory and planning of these experiments was prepared in the light of publications showing that cell proliferation in the male gonad is not only induced by *Sry*, but at an earlier stage, cell proliferation is also necessary for testis development (Schmahl et al. 2000; Schmahl and Capel 2003). This critical stage of proliferation was identified between 10.8 and 11.2 dpc. Inhibition of embryonic cell proliferation between this time-frame blocked testis cord formation in XY gonads and, therefore, the testis pathway (Schmahl and Capel 2003). However, as noted by the authors, a difference in cell proliferation between XX and XY gonads could not be detected at this stage. The detectable male-specific proliferation occurs in the coelomic epithelium after 16 ts (11.25 dpc) (using the genetic background and detection methods the authors describe), but in two different stages (Schmahl et al. 2000). Coelomic epithelial cell proliferation prior to 18 ts occurred in SF1-positive cells; precursors for Sertoli cells and Leydig cells. Cell proliferation after 18 ts occurred in SF1-negative cells which differentiated into interstitial cells. Both stages of male-specific cell proliferation were found to be *Sry*-dependent, and the authors therefore concluded that it was induced by *Sry*. These two stages of proliferation were supported by earlier cell lineage tracer experiments using DiI labelled cells (Karl and Capel 1998). Pre-Sertoli cells arose from the coelomic

epithelium prior to 18 ts, whilst cells labelled from 18 ts onwards differentiated into unidentified interstitial cells.

To ensure an adequate time-frame to observe potential differences between XY *byg/byg* mutant gonads and XY controls, 17 ts to 24 ts gonads were chosen for the main analysis of cell proliferation. The levels of proliferation observed during these experiments, even in XY wild-type gonads, never reached the numbers reported by Schmahl *et al* (2000). Also, no significant differences with either the number of proliferating cells, or the total number of somatic cells, between wild-type male and female at 11.5 dpc (17-18 ts) were observed. The reason that significant increases in XY cell proliferation at 11.5 dpc could not be replicated here may be due to region- or stage-specific differences in different genetic backgrounds or the different methods used to detect proliferative cells. The original experiments used BrdU (Schmahl et al. 2000), and as mentioned in the Introduction to this chapter, BrdU-labelling would detect a higher proportion of proliferating cells due to its incorporation into S-phase. While another group did detect a sexually dimorphic difference at 13 ts between XX samples with an inducible *Sry* transgene and XX controls, they only achieved this during organ culture with BrdU labelling under very specific conditions (Hiramatsu et al. 2009). They were unable to replicate this difference between 11.5 dpc XX and XY wild-type embryonic gonads *in vivo* using either pHH3 or BrdU (Y.Kanai, personal communication).

Whatever the details of the sex-specific differences in cell proliferation are in different contexts, it is clear that XY *byg/byg* gonads do not grow to the same extent as their wild-type counterparts. The results presented established that the total number of cells in the coelomic region of XY *byg/byg* gonads was significantly reduced compared to XY wild-type littermates, and was instead very characteristic of the XX wild-type

control at 22 ts onwards. The number of mitotic cells in this region was also decreased in the *byg/byg* XY gonads from 18 ts onwards (therefore meaning a significant reduction in the rate of proliferation at this stage). During analysis at 13 ts, to determine if the mutation in *Map3k4* affected cell proliferation rates before the *Sry*-dependent stage, no significant differences were observed in the coelomic epithelium between XY +/+ and XY *byg/byg* samples (or XY +/+ and XX +/+ samples). Since the cells that are sensitive to the inhibition of proliferation during the critical proliferative phase have not yet been identified (Schmahl and Capel 2003), a defect in proliferation in these cells of the *byg* mutant cannot be ruled out, but obvious differences throughout the gonad were not observed.

Examination of SRY expression in XY *byg/byg* gonads at 11.0 dpc reveals reduced numbers of SRY-positive cells and reduced levels of SRY within these cells (Bogani et al. 2009). However, the relationship between proliferation in the coelomic region and *Sry* expression in pre-Sertoli cells is unclear. Even though no difference in cell proliferation between mutant and wild-type gonads is observed at 13 ts, taking into account how difficult it is to observe subtle differences, it is not easy to conclude whether i) the initiation of the female pathway in XY *byg/byg* gonads and the reduced proliferation rate at 18 ts is due to reduced *Sry* expression within the critical time window of 11.0 to 11.25 dpc failing to initiate testis development (Hiramatsu et al. 2009); or ii) whether the disrupted MAPK pathway is affecting proliferation through inhibition of cyclin D1, and thus the necessary rate of proliferation required in the critical window of 10.8 to 11.2 dpc to initiate testis development is not achieved (Schmahl and Capel 2003). Even so, testis-specific proliferation is a result of *Sry* up-regulation, rather than *Sry* up-regulation being a result of increased proliferation (Schmahl et al. 2000). Therefore, the MAPK pathway may well affect cell proliferation,

but the reduction of *Sry* expression is most likely the real cause of the failure to initiate the testis pathway.

In an attempt to determine how the MAP3K4-activated signalling pathway activates *Sry* transcription, I assessed the levels and patterning of SF1 expression during similar stages of development. No abnormalities in either the levels of SF1, the number of cells expressing SF1, or the cellular localisation of SF1 were observed between 10.5 and 11.5 dpc. It is therefore necessary to look at the expression profiles of other potential *Sry* transcriptional regulators, such as GATA4/FOG2, CBX2 and WT1 (+KTS). This work is being addressed by other members of the laboratory.

It is impossible to determine the cell-type specificity of MAPK activity during testis determination by using a constitutive *Map3k4* knockout. One way to address this would have been to make conditional knockouts of *Map3k4* in specific gonadal cell-types using different *Cre* deleters. However, during the early stages of this project, the floxed allele of *Map3k4* was not available, so efforts were targeted on the downstream MAPKs instead to try and ascertain the cellular and molecular mechanisms.

Chapter 4. Expression of p38 MAPKs in gonad development

4.1. Introduction

The *byg* mutant has revealed a completely novel aspect of gonad development, but the mechanistic details of MAP kinase signalling during the process of sex determination still remain unclear. As mentioned in the main Introduction, MAP3K4 can phosphorylate three different downstream MAP2Ks (MKK3, MKK4 and MKK6), which lead to the activation of either p38 or JNK MAPKs. To further elucidate the downstream MAP kinase components functioning during testis determination, analysis was focused at the MAPK level. MAP3K4 can indirectly activate either JNK or p38 MAPKs, so either could be worthy candidates for further study. However, they are not simple protein families to investigate because each is encoded by multiple genes.

There are three different JNKs: JNK1, JNK2 and JNK3, which are comprehensively reviewed by Aouadi *et al* and Davis (Davis 2000; Aouadi et al. 2006). Each MAPK group has its own characteristic Thr-X-Tyr phosphoacceptor loop, and for the JNK family this is Thr-183-Pro-Tyr-185 (Kyriakis et al. 1991; Kyriakis et al. 1994). This dual phosphorylation motif can be specifically activated by either MKK4 or MKK7 MAP2Ks. The *Jnk1* and *Jnk2* genes (officially designated *Mapk8* and *Mapk9*, respectively) are expressed ubiquitously while *Jnk3* (*Mapk10*) is restricted to the heart, brain and testis (Martin et al. 1996). However, there is a great deal of functional redundancy between the three *Jnk* genes, which, alongside the many different alternatively spliced variants of each gene, highlights the difficulty in studying the function of each by simple targeted gene disruption. Single knockouts of each gene have been generated and result in no detrimental effects to development or fertility, although the differentiation of some immune cells was altered (Yang et al. 1997; Dong et al.

1998; Yang et al. 1998). However, double knockouts generated for each combination revealed that JNK1 and JNK2 were vital to embryonic development, as this double knockout was lethal by 11.5 dpc due to exencephaly and apoptosis defects in the brain. Neither of the other two double knockouts exhibited a detectable developmental defect as both survived normally, although fertility tests were not reported (Kuan et al. 1999).

In contrast, there are four different p38 MAPKs: p38alpha (p38α), p38beta (p38β), p38gamma (p38γ) and p38delta (p38δ). These members of the p38 MAPK family are approximately 60% identical in their amino acid sequences; p38α and p38β share 75% homology, p38γ and p38δ are approximately 65% identical, and approximately 60% identity is observed between the other pair combinations (Jiang et al. 1997). These kinases represent related, but distinct, MAPK subgroups which arose through ancestral duplication (Caffrey et al. 1999). This is clarified by the observation that the genes encoding the p38α/β/γ/δ MAPKs (*Mapk14*, *Mapk11*, *Mapk12* and *Mapk13*, respectively) are found on two different mouse chromosomes: *Mapk14* and *Mapk13* (the genes encoding p38α and p38δ, respectively) are located next to each other on Chr 17, while *Mapk11* and *Mapk12* (the genes encoding p38β and p38γ, respectively) are found on Chr 15. These syntenic groups are also conserved in humans on Chr 6 and Chr 22.

The specific phosphoacceptor loop for the p38 family of MAPKs is Thr-180-Gly-Tyr-182, which is activated predominately by the MAP2Ks MKK3 and MKK6, but can also be activated by MKK4 (Dérijard et al. 1995; Raingeaud et al. 1995; Han et al. 1996). These MAP2Ks have distinct specificities for the p38 MAPKs. MKK3 selectively activates p38α, p38γ and p38δ, while MKK6 can activate all four p38 MAPKs (Enslen et al. 1998). MKK4 is specific to p38α but can also activate p38δ (Jiang et al. 1997). The p38 MAPKs also have different expression patterns, with p38α being relatively

ubiquitous while the others are more tissue-specific, such as, p38β in the brain, p38γ in skeletal muscle and p38δ in endocrine glands including the testes (Hu et al. 1999; Beardmore et al. 2005). A mouse knockout of each isoform has been generated but the knockout of *Mapk14* (p38α) is the only one that is embryonically lethal. The *Mapk14*$^{-/-}$ embryos die by 10.5 dpc due to a placental defect (Adams et al. 2000; Mudgett et al. 2000; Tamura et al. 2000). All the other knockouts develop normally and are viable and fertile (Beardmore et al. 2005; Sabio et al. 2005), although a more recent knockout of *Mapk13* (p38δ) suggests the involvement of this kinase with enhanced glucose tolerance (Sumara et al. 2009).

Data from our laboratory indicates that inhibition of p38 MAPK signalling disrupts XY testis development *in vitro*. Culturing of wild-type 11.5 dpc XY gonads for 48h in the presence of a highly selective inhibitor of p38α and p38β (SB202190) dramatically reduced the expression of *Sox9* and caused up-regulation of the ovarian marker, *Wnt4*, suggesting that inhibition of this p38 activity causes partial XY gonadal sex reversal (Bogani et al. 2009). Moreover, evidence suggests that human SRY is a possible target of p38 MAPK signalling in cultured keratinocytes (Gazel et al. 2008). Previous reports suggest that interleukin-1 induces Sertoli cell proliferation via p38 MAPK signalling in *in vitro* rat Sertoli cell cultures (Petersen et al. 2005), and a function of p38 MAPK in control of *SOX9* mRNA stability has been shown in both human THP-1 monocytes and human chondrocytes (Frevel et al. 2003; Tew and Hardingham 2006). For these reasons, I decided to focus on the p38 MAPK pathway instead of the JNK pathway, and so first determined the expression of all four p38 MAPK genes in the embryonic gonad.

4.2. Results

4.2.1. Expression of p38 MAPK genes during development

To investigate the expression of the different p38 isoforms during gonad development, digoxygenin (DIG)-labelled RNA riboprobes were designed to the 3'-untranslated region (UTR) of each gene. All 3'UTR probes (except for *Mapk14*) were then hybridised to the relevant gene transcript through wholemount *in situ* hybridisation (WMISH). For *Mapk14*, hybridisation of a 3'UTR probe was not successful, so a probe generated from an IMAGE clone of this gene was used instead. Expression of all genes was analysed in 10.5 dpc whole embryos and gonads between 11.0 and 13.5 dpc, using C57BL/6J wild-type tissue.

The expression of *Mapk14* (the gene encoding p38α) had previously been identified in many regions of the 10.5 dpc embryo, including the heart, limb buds and somites (Adams et al. 2000). In adult mice, p38α is relatively ubiquitous, with expression shown by Western blot in the spleen, liver, lung, brain, thymus, heart, kidney, adrenal glands, skeletal muscle and within the follicles of the ovary (Lee et al. 2000; Beardmore et al. 2005; Ventura et al. 2007; Liu et al. 2010). However, expression had not previously been assessed in embryonic gonads. During my analysis of *Mapk14* by WMISH, expression was found throughout the whole 10.5 dpc embryo within the ventral region of the rostral-caudal axis, with strong expression in the heart and limb buds (Figure 4.1A). In gonadal tissue, *Mapk14* was expressed at all stages examined between 11.0 and 13.5 dpc (Figure 4.1B). At 13.5 dpc this expression seemed stronger within the testis cords, and was also strong in ovaries (Figure 4.1C). Cryosection data of 13.5 dpc stained testes and ovaries confirmed that while expression was weak, it was present

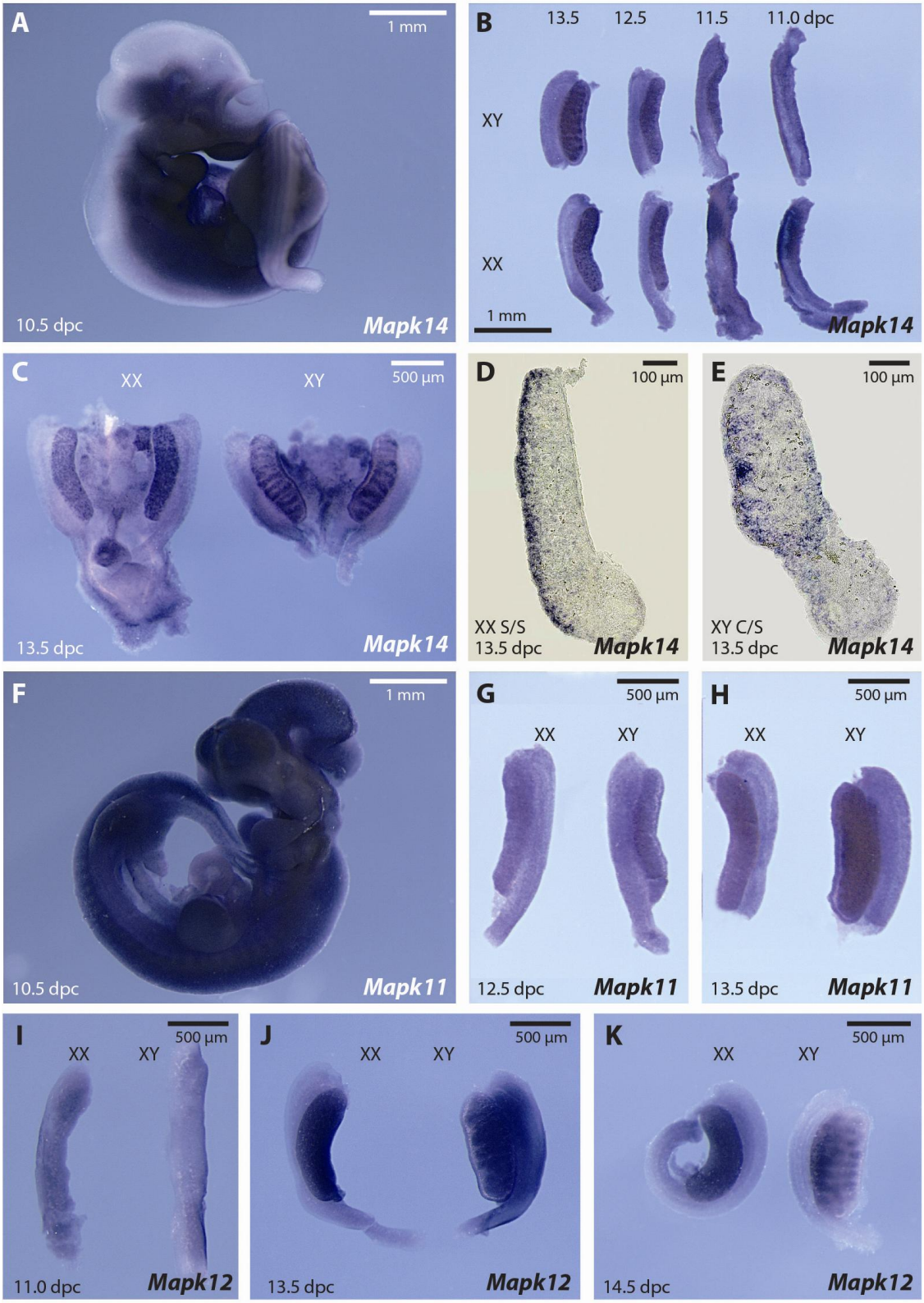

Figure 4.1: Analysis of *Mapk14*, *Mapk11* and *Mapk12* by WMISH
WMISHs were performed on C57BL/6J wild-type tissue. (**A**-**E**) Expression of *Mapk14* (p38α). (A) At 10.5 dpc, expression is localised to the ventral side of the rostral-caudal axis of the whole embryo. (B) Expression in the gonads between 11.0 and 13.5 dpc. In 13.5 dpc tissue, expression is localised to the ovary and cords of the testis (C). This expression is confirmed by cryosections cut in a sagittal orientation for the ovary (D), and in a coronal orientation for the testis (E). (**F**-**H**) Expression of *Mapk11* (p38β) in whole 10.5 dpc embryos (F) and gonads at 12.5 dpc (G) and 13.5 dpc (H) seems to be ubiquitous. (**I**-**K**) Expression of *Mapk12* (p38γ) is not detected in 11.0 dpc gonads (I), but is at 13.5 dpc (J) and 14.5 dpc (K), where it is visible in the cords of the testes. Scale bars are shown with the size marked.

within testis cords of coronal sections and on the outer surface of the ovary from sagittal sections (Figure 4.1D-E).

Mapk11 (the gene encoding p38β) is less well characterised than *Mapk14*. Western blot analysis of adult tissue has found high levels of expression in the brain, thymus and spleen, with lower levels in kidney, heart, adrenals, liver and lung (Beardmore et al. 2005). My analysis of *Mapk11* shows ubiquitous expression throughout the whole 10.5 dpc embryo and also in 12.5 dpc and 13.5 dpc testes and ovaries (Figure 4.1F-H).

Mapk12 (*p38γ*) expression is less widespread and highest in skeletal muscle and lung (Beardmore et al. 2005). My analysis by WMISH shows that in the gonad, expression of *Mapk12* seems to be similar to *Mapk11* expression, although by 13.5 dpc expression was visible within the testis cords (Figure 4.1I-K).

Previously published analyses of *Mapk13* (the gene encoding p38δ) suggest more relevance to developmental processes. It is less widespread than the other genes, as protein expression seems to be restricted to the heart, kidney, adrenals, thymus and brain in the tissues analysed from adult mice (Beardmore et al. 2005). Also, RNA analysis by Northern blot has shown strong expression in adult testes, lung and kidney, and using WMISH in embryos expression is seen in increasing numbers of epithelial tissues as the embryo develops, suggesting that *Mapk13* is a developmentally regulated MAPK (Hu et al. 1999). During my embryonic gonad WMISH analyses, expression was seen in the gonad by 11.5 dpc. At 10.5 dpc there was little, if any, expression in the gonads, while some was seen at 16 ts (Figure 4.2A-B). From 11.5 dpc onwards, strong expression was seen in the XY gonad and Wolffian duct, and while WMISH cannot provide quantitative results, expression in the XX gonad did appear weaker (Figure 4.2C-D). Cryosection data confirmed the gonadal expression, which in females was

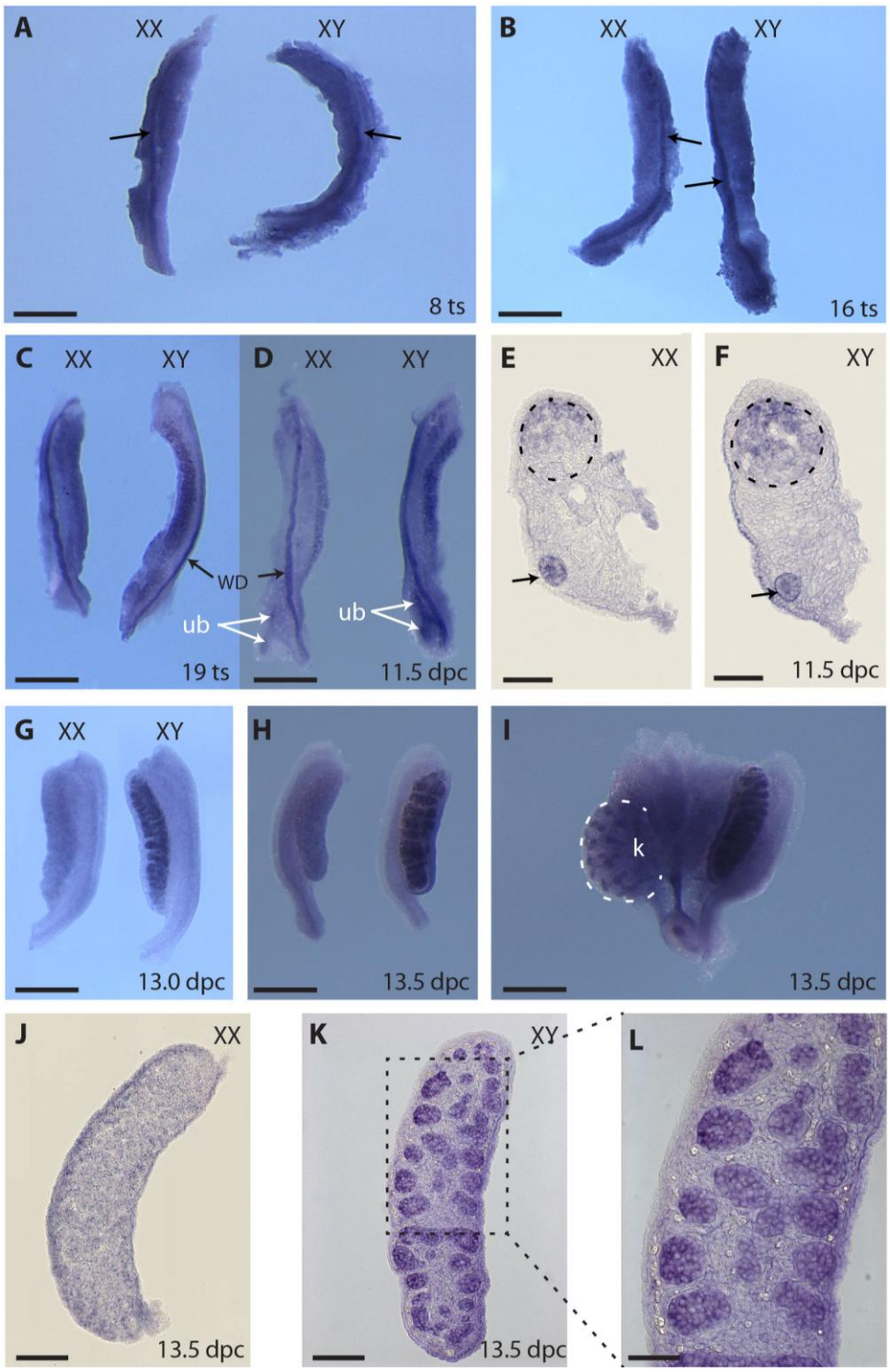

Figure 4.2: Analysis of *Mapk13* by WMISH
WMISH was performed on C57BL/6J wild-type tissue between 10.5 dpc and 13.5 dpc. (**A**) At 10.5 dpc (8 ts), expression was not detected in the gonads, but was in the Wolffian duct (arrows). (**B**) By 16ts, expression was more visible in the gonads, particularly of the male (XY). (**C-D**) Expression was overt from 11.5 dpc (18 ts) onwards in both male and female gonads, with apparent stronger expression in the male. Strong expression is visible in the Wolffian ducts (black arrows) and also in the ureteric buds (white arrows) where the kidneys are starting to form. (**E-F**) Transverse cryosection data confirms the strong expression in the Wolffian duct (black arrows), and within the gonads of both sexes (area within dotted line). Expression is not in the coelomic epithelium of either sex (area outside dotted line), and in the female (E) it seems to be in the outer half of the gonad only. (**G-H**) At 13.0 dpc (G) and 13.5 dpc (H), expression is very strong in the testis cords. (**I**) Expression is also strong in the kidney (k, area within dotted line). (**J-L**) Cryosection data in a coronal orientation of 13.5 dpc ovaries (J) and testes (K,L) shows expression primarily within the testis cords. Scale bars = 500 µm (A-D, G-I), 100 µm (J-K) and 50 µm (E,F,L).

localised to the outer half of the gonad in comparison with full gonadal expression in the male (Figure 4.2E-F). Expression was also absent from the coelomic epithelium, comprising the outer few layers of cells surrounding the gonad in both sexes. By 13.5 dpc, expression was very strong in the testis, and was found predominantly in the cords, while less expression was visible in the ovary (Figure 4.2G-H). Expression was also very strong in the kidney (Figure 4.2I). Cryosection data of testes at 13.5 dpc, in a coronal orientation, revealed strong expression within the testis cords (Figure 4.2J-L). It was not possible to determine the cell-type specificity of this expression, as signal seemed to be present throughout the whole cord. This could suggest that it was expressed in both Sertoli cells and germ cells, but this would have to be confirmed by further analysis, such as expression analysis in germ cell-free gonads.

4.2.2. Analysis of p38 MAPK expression levels using qRT-PCR

To validate the observations from the WMISH data, quantitative real-time reverse-transcriptase PCR (qRT-PCR) was performed using TaqMan gene expression assays for each gene (see section 2.7 in Materials and Methods for details).

XX and XY gonads, with the mesonephros removed, were collected at 11.5, 12.5 and 13.5 dpc. Due to the small amount of tissue from which RNA needed to be extracted, three pairs of 11.5 dpc gonads were pooled together at the beginning of the RNA extraction procedure, whilst two pairs of 12.5 dpc and 13.5 dpc gonads were pooled. Each pool represents one sample, and three to four samples were analysed for each stage, sex and TaqMan assay. *Sox9* was used as a positive (male-enhanced) control to ensure the sample collection procedure was accurate, and *Hprt1*, a house-keeping gene, was used as an endogenous control. Each sample was performed in triplicate for three technical replicates.

To assess the efficiencies of the TaqMan assays with the RNA extracted from the gonadal samples, standard curves were generated as per section 2.7.3 of the Materials and Methods using 13.5 dpc XX and XY samples. All efficiencies fell within the acceptable range of 90-110% (Figure 4.3 and Table 4-1).

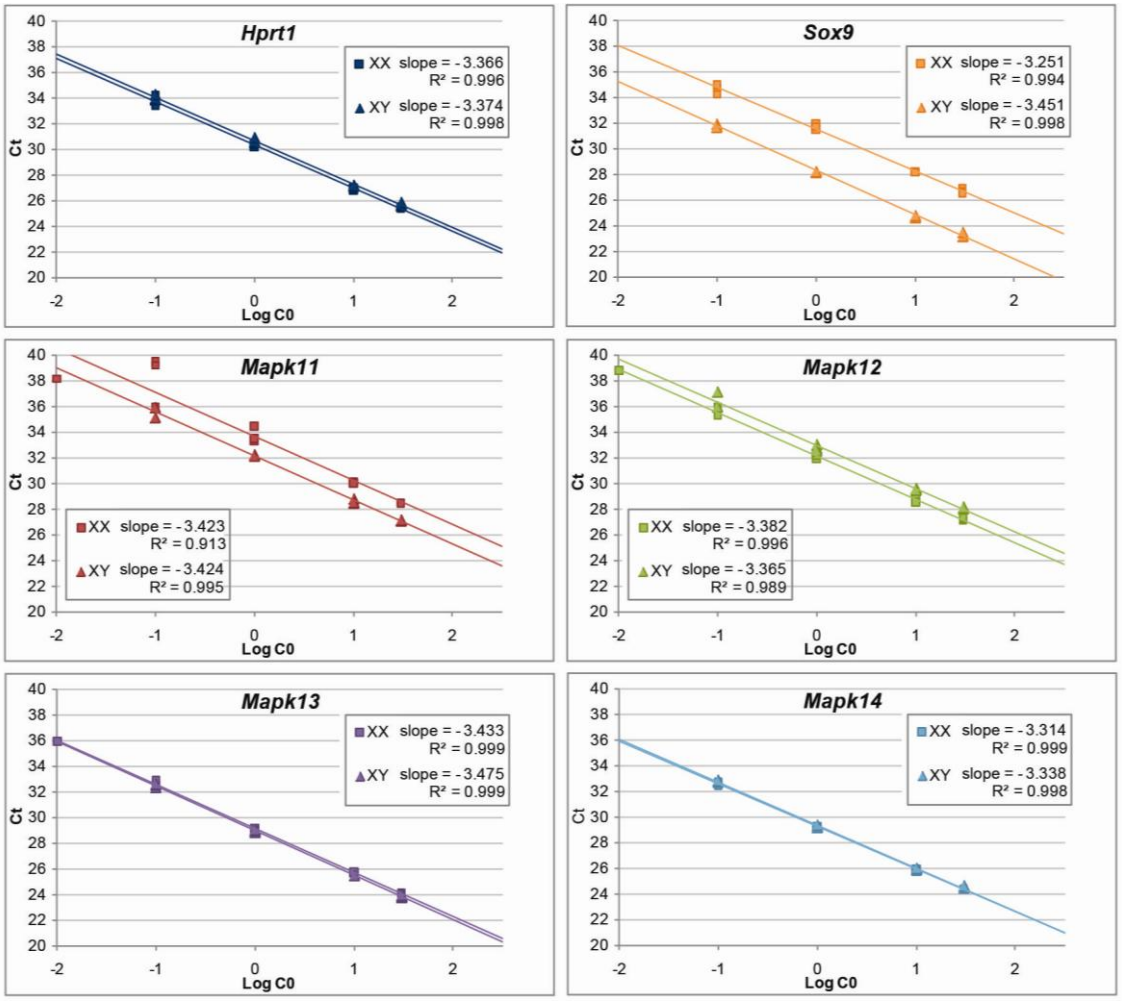

Figure 4.3: Standard curves to assess the PCR efficiencies of the TaqMan assays
Standard curves were generated using a five-step serial dilution of 13.5 dpc cDNA from both XX and XY samples. The cDNA concentrations used were: 30 ng, 10 ng, 1 ng, 0.1 ng and 0.01 ng, and the Ct was plotted over the log of the cDNA concentration (C0). The lowest dilution of 0.01 ng (-2 log C0), frequently had to be omitted from the analysis as either the threshold was not reached within the 40 cycles, or it was reached very late, causing significant variation between the technical replicates, and affecting the results. The gradient of the slope for each line is marked and is used to calculate the PCR efficiency; a slope of −3.32 would be 100% efficient. The R^2 value is also marked, which reflects how well the data fit the linear regression line. A value of one would mean no regression from the line i.e. the regression line perfectly fits the data.

The endogenous control chosen should ideally be a ubiquitous gene that is highly expressed in the tissue being analysed. Expression levels should also not vary between different samples. *Hprt1* was chosen because it is a well characterised housekeeping gene that has been used previously by our laboratory as an endogenous control.

Table 4-1: PCR efficiencies of each TaqMan assay

PCR efficiencies for the four p38 MAPKs, *Sox9* and *Hprt1* TaqMan assays, were calculated from the slope of the line of regression from the standard curves. A slope of −3.32 would be 100% efficient.

	Slope of line		% Efficiency	
	XX	XY	XX	XY
Hprt1	−3.366	−3.374	98.1%	97.9%
Sox9	−3.251	−3.451	103.0%	94.9%
Mapk11	−3.423	−3.424	95.9%	95.9%
Mapk12	−3.382	−3.365	97.6%	98.2%
Mapk13	−3.433	−3.475	95.6%	94.0%
Mapk14	−3.314	−3.338	100.3%	99.3%

4.2.3. Confirmation of expression of the p38 MAPKs in the embryonic gonad by qRT-PCR

To analyse the expression levels of the different p38 MAPKs in the 11.5 dpc to 13.5 dpc gonads by qRT-PCR, the relative quantification (RQ) method was used as described in section 2.7.3 of the Materials and Methods.

The data are presented as levels of transcript relative to the XX 11.5 dpc, so that any changes in transcript levels in older samples, or in the opposite sex, can be assessed (Figure 4.4). The significance of the data was calculated using a two-tailed student's *t*-test at 95% confidence, comparing the ΔΔCt values of the samples (see asterisks on Figure 4.4 and Table 4-2). Using these values, the following data were observed:

Table 4-2: Statistical analysis using –ΔΔCt values calibrated to XX 11.5 dpc
Average Ct value and average −ΔΔCt value for each sample are shown for the p38 MAPK genes. Significance was calculated using a two-tailed Student's *t*-test with –ΔΔCt values at 95% confidence. Each sample was compared to 11.5, 12.5 or 13.5 dpc data. Significant *p* values (≤0.05) are in red.

Mapk11	XX			XY		
dpc	11.5	12.5	13.5	11.5	12.5	13.5
Av Ct	31.20	31.97	32.28	30.90	31.77	31.58
Av ΔΔCt	-0.18	-1.20	-1.17	-0.38	-0.53	-0.37
t-test:						
c.f. 11.5		**0.0040**	**0.0025**	0.2117	0.6162	0.9611
c.f. 12.5			0.7650		0.0648	0.5559
c.f. 13.5						**0.0042**

Mapk12	XX			XY		
dpc	11.5	12.5	13.5	11.5	12.5	13.5
Av Ct	29.27	29.25	30.31	28.72	30.56	31.23
Av ΔΔCt	-0.02	-0.27	-0.97	0.03	-1.09	-1.80
t-test:						
c.f. 11.5		0.0514	**0.0163**	0.8330	**0.0083**	**0.0006**
c.f. 12.5			0.0540		**0.0118**	**0.0161**
c.f. 13.5						**0.0198**

Mapk13	XX			XY		
dpc	11.5	12.5	13.5	11.5	12.5	13.5
Av Ct	28.89	28.03	28.13	27.45	25.47	25.17
Av ΔΔCt	-0.12	0.46	0.72	0.82	3.51	3.78
t-test:						
c.f. 11.5		**0.0327**	**0.0001**	0.0506	**0.0008**	**0.0003**
c.f. 12.5			0.1345		**0.0001**	0.2841
c.f. 13.5						**0.0000**

Mapk14	XX			XY		
dpc	11.5	12.5	13.5	11.5	12.5	13.5
Av Ct	25.07	24.62	24.82	24.61	25.01	24.86
Av ΔΔCt	-0.17	0.00	0.17	-0.22	0.09	0.21
t-test:						
c.f. 11.5		0.3725	**0.0463**	0.8734	0.3059	0.1499
c.f. 12.5			0.2846		0.6981	0.5214
c.f. 13.5						0.7649

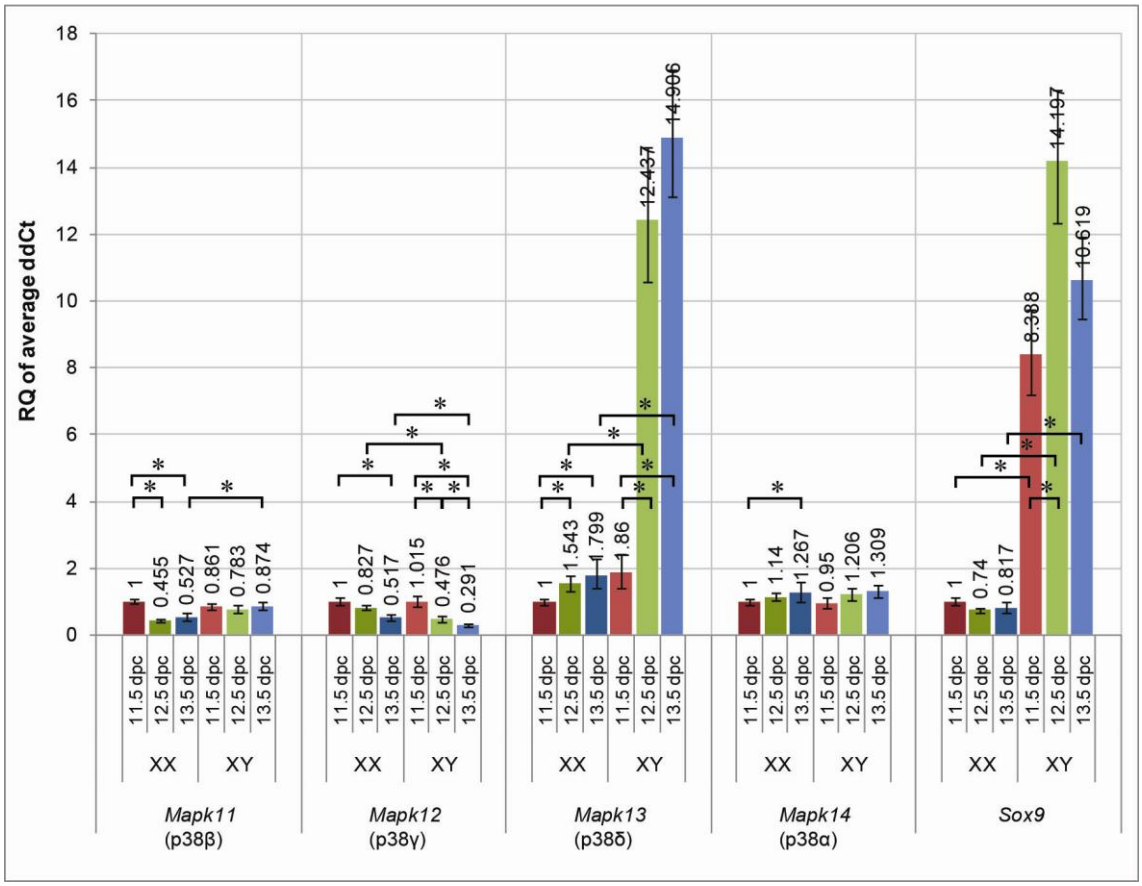

Figure 4.4: Comparative relative quantification of p38 MAPK isoform gene expression
Relative quantification (RQ), shown as the fold-change of the average ΔΔCt, compared against the XX 11.5 dpc sample data (transcript level calibrated to XX 11.5 dpc). Significance between the samples was calculated using a two-tailed student's *t*-test at 95 % confidence (see Table 4-2 above). Error bars are shown as RQ min and RQ max.

Mapk11 (p38β) is expressed in both female (XX) and male (XY) samples at all stages, although in females, expression appears to decrease significantly after 11.5 dpc. In male samples, levels remain constant across all stages and are equivalent to the XX 11.5 dpc values. *Mapk12* (p38γ) is expressed in both female and male samples at 11.5 dpc at the same level, but from 12.5 dpc onwards in males, and at 13.5 dpc in females, this expression decreases significantly. After 11.5 dpc, male expression is significantly lower than that of females at corresponding stages. *Mapk13* (p38δ) is expressed in both male and female samples at all stages, but in males this expression is always significantly higher than in females of the comparable stage, and dramatically so from 12.5 dpc onwards. This sexually dimorphic expression profile confirms that seen by WMISH. *Mapk14* (p38α) is expressed in both sexes and in all stages at a constant level. Lastly, *Sox9* is expressed strongly in the male from 11.5 dpc onwards, with levels approximately 10-fold higher than that observed in females. This observation validates the experimental strategy and confirms that the samples were not contaminated or otherwise abnormal.

Comparative expression levels do not give an indication of the actual amount of transcript present in each tissue: they are only an indicator of the difference in levels when compared to the calibrator sample. To ascertain the levels of expression between the different tissues without calibration to a particular sample, it is possible to directly compare the Ct values after normalisation to the endogenous control (the ΔCt), without calculating the ΔΔCt. To do this, the fold-change of the ΔCt (rather than of the ΔΔCt) is calculated using $2^{-\Delta Ct}$ (Figure 4.5). From these results it is clear that *Mapk13* in the male is expressed as strongly as *Sox9*, and *Mapk14* is expressed strongly in all samples. On the other hand, *Mapk11* and *Mapk12* are expressed at only low levels.

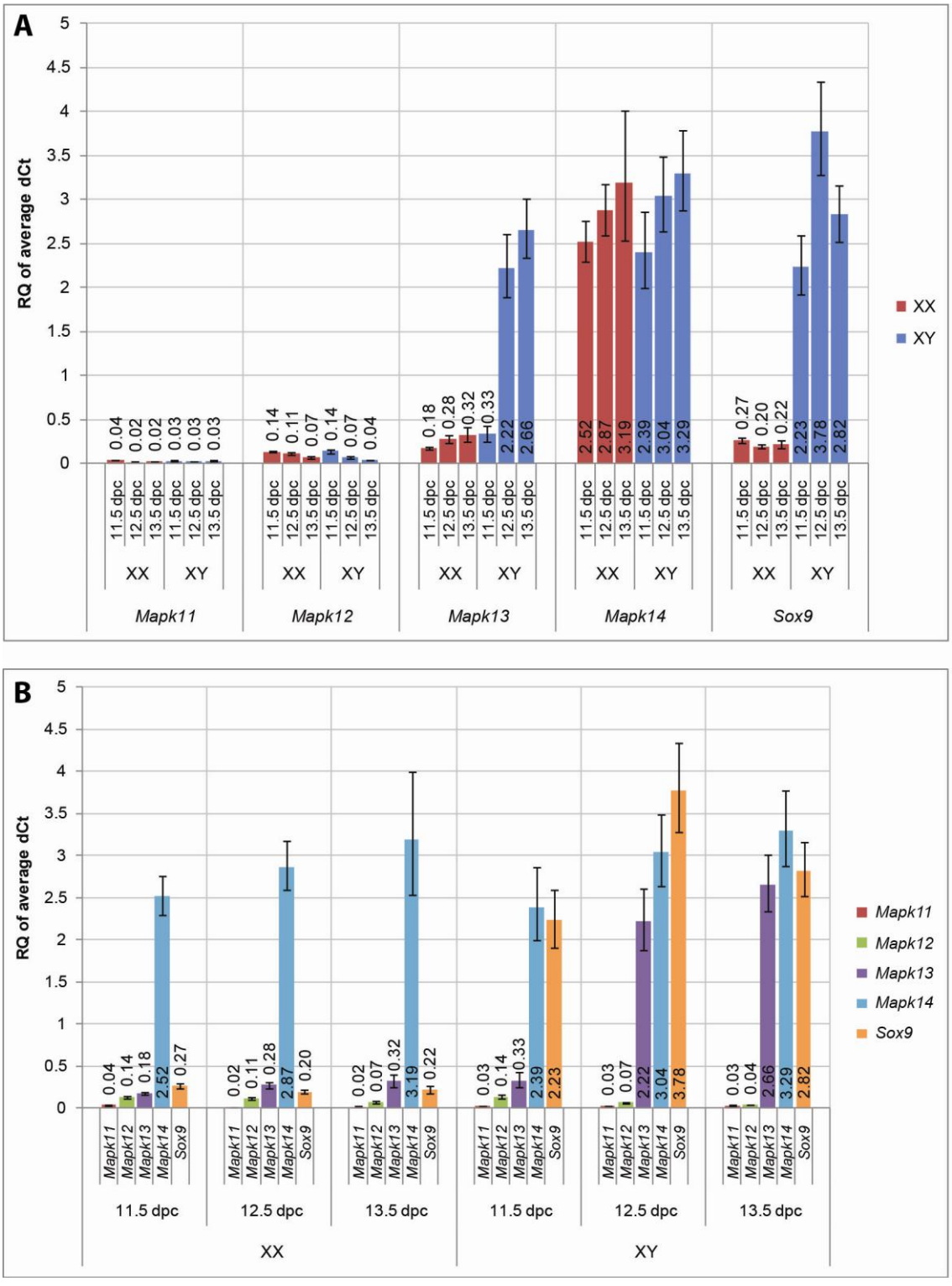

Figure 4.5: Relative quantification showing transcript levels before calibration
Results are displayed as the fold change of the average ΔCt rather than of the ΔΔCt, to show the different levels of the transcripts within the same tissue. (**A**) Graph showing the results grouped by gene assayed. (**B**) Shows the results grouped by sex and gonad stage. Error bars are RQ min and RQ max.

4.3. Discussion

Identifying the expression pattern of the different p38 MAPK genes in the embryonic gonad was crucial before attempting to determine their function in this tissue. Although many different groups have previously analysed the p38 MAPKs, when I started this section of work p38 had not been studied in the embryonic gonad. Following WMISH and qRT-PCR to analyse this expression, the two most interesting profiles were that of *Mapk14* and *Mapk13*. *Mapk14* is expressed strongly in the developing gonad between 11.5 and 13.5 dpc in both sexes, which suggests that this gene has a particular function in both ovary and testis development. In males, *Mapk14* is expressed predominantly in the testis cords, which contain both germ cells and Sertoli cells and seem to have a similar expression profile as that of *Map3k4*, which was reported previously (Bogani et al. 2009). The absence of a sexually dimorphic expression profile for *Mapk14* does not rule out the possibility of a role in sex determination due to the sexually dimorphic expression of the key testis-determining molecules, SRY, SOX9 and FGF9. As an example, *Gata4* is expressed in the somatic cells of both XX and XY gonads at all stages of development, and in postnatal ovaries and testes (Ketola et al. 2002; Anttonen et al. 2003; Manuylov et al. 2011). In XY gonads, the somatic cell expression becomes restricted to Sertoli cells from 13.5 dpc onwards. Conditional inactivation of *Gata4* from 10.5 dpc in somatic cells of the gonad caused XY sex reversal, confirming that it has a vital role in testis determination despite expression also in the XX somatic cells (Manuylov et al. 2011). Expression of *Mapk14* in both somatic cells and germ cells suggests that it is involved in a number of different aspects of gonad development.

Mapk13, on the other hand, is sexually dimorphic. This difference in expression level between male and female gonads occurs as early as 11.5 dpc, during the sex-determining period, so may play an important role in this process. The qRT-PCR profile

of *Mapk13* in comparison with *Sox9* suggests that the activation of *Mapk13* in males may occur after that of *Sox9*, since even though there are higher levels of *Mapk13* in males at 11.5 dpc when compared to females, the dramatic difference is only seen from 12.5 dpc. *Mapk13* is also strongly expressed in the early Wolffian duct, which could indicate either a function in kidney development or a function in later male reproductive tract development. However, since this expression is strongest at 11.5 dpc, and is seen in the ureteric bud and the 13.5 dpc kidney, it is likely to reflect the former potential function. *Mapk13* is also very strongly expressed in the testis cords at 13.5 dpc and strong protein expression has been reported in adult mouse testes. This suggests that it has an important role in testis development. Unfortunately, it has not been possible to elucidate the cell-type within the testis cords in which it is expressed, but it is either Sertoli cells or germ cells (or a combination of both).

Testis determination occurs in the somatic pre-Sertoli lineage following the expression of *Sry* and the consequent up-regulation of *Sox9*, which along with *Fgf9* drives the differentiation of these cells into Sertoli cells. The Sertoli cells then cluster around the germ cells and, in a complex morphogenetic process involving migratory endothelial cells and peritubular myoid cells, form testis cords (Wilhelm and Koopman 2006; Combes et al. 2009a; Combes et al. 2009b). Sertoli cells then secrete AMH to drive the regression of the Müllerian duct and inhibit female development. During spermatogenesis, Sertoli cells function to nurture the developing sperm. Therefore, Sertoli cells are vital for normal male development and inappropriate expression of a vital gene involved in their function could result in major developmental defects. On the other hand, germ cells are also required for the proper function of the adult testis, or more specifically, the production of sperm and therefore fertility. However, it is established that a testis can develop in the absence of germ cells, so functioning germ

cells are only required for production of sperm and not testis development itself (McLaren 1991; Kurohmaru et al. 1992).

Whilst my expression analysis was being performed, another group published qRT-PCR data of the different p38 MAPKs in embryonic gonads (Ewen et al. 2010). They sorted the cells in the developing gonad to analyse expression in somatic cells and germ cells separately. Microarray data using whole gonads between 11.5 dpc and 13.5 dpc gave very similar expression profiles to those described above. Briefly, they found that all four p38 MAPKs were expressed in all stages examined, and in both sexes. Specific changes observed included decreased *Mapk12* in males over the period examined, while *Mapk13* was sexually dimorphic, with higher expression in the males at all stages examined. In the germ cell- and somatic cell-sorted samples all four p38 MAPKs were expressed in every stage of both germ cells and somatic cells. However, *Mapk14* was found to be higher in XX germ cells than XY germ cells and somatic cells of either sex. In contrast, *Mapk11* was higher in XY germ cells than XX germ cells, but expression in somatic cells of both sexes was found to be higher still (except XX 13.5 dpc somatic cells, in which expression was reduced). *Mapk12* had equal expression in the germ cells of both sexes, but had higher expression in XX somatic cells than XY somatic cells, while *Mapk13* was found to be higher in all XY cells (both germ and somatic) than XX cells. A summary of these levels of expression is shown below, where the darker grey depicts strongest expression, down to white, which denotes very low expression (Table 4-3). Due to the method of cell sorting, the somatic cell population comprises all cells in the gonad that are not germ cells. Therefore, these results do not help to determine the exact somatic cell population in which expression is detected. However, in combination with my WMISH analysis, it suggests that the *Mapk13* expression I observed in the

testis cords is a result of expression in both Sertoli cells and germ cells. This is also the case for the *Mapk14* expression.

Table 4-3: Summary of expression analysis of p38 MAPKs in MACS sorted gonads
Amount of expression observed following qRT-PCR of germ cells and somatic cells of XX and XY gonads between 12.5 dpc and 13.5 dpc. Amount of expression is shown by both the number of asterisks (more = high) and by the colour of each box (darker = high). Data taken from (Ewen et al. 2010).

	XX		XY	
	Germ cells	Somatic cells	Germ cells	Somatic cells
Mapk14 (p38α)	********	****	****	****
Mapk11 (p38β)	*	***	**	***
Mapk12 (p38γ)	**	***	**	*
Mapk13 (p38δ)	****	***	******	******

Interestingly, the description of *Mapk13* expression in both XX and XY gonads between 11.5 and 13.5 dpc is remarkably similar to that for *Dmrt1* (Lei et al. 2007). *Dmrt1* is expressed in both somatic cells and germ cells of the 10.5 to 11.5 dpc bipotential gonad in both sexes. By 12.5 dpc, expression of *Dmrt1* is strongly sexually dimorphic, with increased expression in XY gonads in Sertoli cells and germ cells. In XX gonads, expression is reduced in somatic cells compared to germ cells at 12.5 dpc, and somatic expression is lost by 13.5 dpc. DMRT1 (double-sex and Mab-3 related transcription factor-1) is an evolutionarily conserved transcription factor that has a role in regulating sexual differentiation in many different organisms. As mentioned in the Introduction, adult-specific deletion of *Dmrt1* in mice causes transdifferentiation of testis-specific cells into ovary-like cells, demonstrating that *Dmrt1* is required for maintenance of the adult testicular state by continued antagonism of the female gonadal pathway (Matson et al. 2011). Also, the constitutive knockout of *Dmrt1* does not affect sex determination, but impairs the ability of postnatal Sertoli cells to differentiate and mature, such that the seminiferous tubules in the testis become crowded and germ cells die during meiosis (Raymond et al. 2000).

In addition, Ewen *et al* also looked at the localisation of activated p38 MAPK using an antibody specific for phospho-p38 (pp38). Staining together with an antibody against OCT4, an undifferentiated germ cell marker, they concluded that activated p38 was found in all XY germ cells from 12.5 dpc onwards, but not in XX, concluding that p38 is involved primarily with the differentiation of XY germ cells as it is activated in these cells before they differentiate. However, the use of the pp38 antibody does not differentiate between the different p38 MAPKs since it detects all activated forms. Therefore, the exact isoform involved with male germ cell development is still not known, although they suggest that it is likely to be the p38δ and p38β isoforms since those are the two that have higher expression in male versus female germ cells. They also conducted the same p38 MAPK small-molecule inhibitor cultures of XY gonads that were performed by our laboratory and described previously (Bogani et al. 2009). They observed a decrease in expression of OCT4 at the protein level, and at the gene level by qRT-PCR. This correlated with an increase in expression of *Stra8*, which marks female meiotic germ cells, suggesting that this inhibition of p38α and p38β causes the XY germ cells to enter meiosis and thus, inhibits the male germ cell differentiation pathway. However, our inhibitor studies confirmed the sex reversal associated with somatic cells; *Sox9* is decreased and *Wnt4* is increased and these are male and female somatic cell markers, respectively. Therefore, it seems much more likely that the inhibition of p38α and p38β is primarily disrupting sex determination and as a consequence of this, early somatic cell sex reversal in the cultured gonad causes the XY germ cells to sex reverse. Further experiments will be required to clarify the roles of MAPK signalling in somatic and germ cells in the developing gonad. In the next chapter I describe experiments aimed at addressing the function of one p38 isoform, p38α, in gonadal somatic cells.

Chapter 5. Function of p38α in sexual development

5.1. Introduction

At least four independent groups have generated *Mapk14* null mice, all of whom published their findings in the same year (Adams et al. 2000; Allen et al. 2000; Mudgett et al. 2000; Tamura et al. 2000). In all cases, embryonic lethality was observed between 10.5 dpc and 12.5 dpc, except in one, when lethality was recorded up to 16.5 dpc. Homozygous embryos appeared to develop normally until 10.5 dpc, following which, they became retarded in growth in comparison with controls, paler, had defects in the myocardium, and showed vascularisation deficiencies. In two studies, the authors attributed this early lethality to a placental defect because the labyrinth layer was absent due to a failure of vascularisation; in one case the spongiotrophoblast layer was also severely reduced (Adams et al. 2000; Mudgett et al. 2000). Any other defects seen in the *Mapk14* null embryos were secondary to the placental defects; *Mapk14*$^{-/-}$ mutants developed to term and were reported to be normal and viable at 18.5 dpc when the placental defect was rescued (Adams et al. 2000). This placental defect was rescued by an established strategy of aggregating tetraploid (*Mapk14*$^{+/+}$) and diploid (*Mapk14*$^{-/-}$) morulae. The tetraploid cells give rise to the primitive endoderm and the trophoblast lineages, while the diploid cells exclusively contribute to the extra-embryonic mesoderm and the embryo (Nagy et al. 1990; Ihle 2000).

In contrast, a different study by Tamura *et al*, revealed slightly different phenotypes to the ones already mentioned (Tamura et al. 2000). Surprisingly, small subsets of homozygote embryos were found live and viable between 13.5 dpc and 16.5 dpc. The embryos that died by 11.5 dpc were slightly growth-retarded and had placental defects similar to that already described. However, embryos still alive from 12.5 dpc onwards

looked morphologically normal in comparison with their wild-type littermates, although they were slightly paler. This anaemia was a result of smaller livers that contained significantly reduced numbers of circulating haemoglobinised red blood cells and enucleated erythrocytes; the number of immature nucleated erythrocytes within the haematopoietic tissue was also decreased. The yolk sacs also lacked circulating red blood cells in the vasculature, contributing to the anaemia of the embryos. This defect in erythropoiesis was found to be a result of decreased erythropoietin (*Epo*) gene expression. So, embryos that bypassed the placental defect still died during development due to an important function of p38α in erythropoiesis. It is unclear why such a discrepancy in the different constitutive knockouts was observed, although genetic background may be important since Tamura *et al*. were the only group to study the effects on a C57BL/6J background rather than a mixed genetic background as with the other studies. As discussed by J.Ihle, the fact that the tetraploid rescue of the placental defect resulted in healthy embryos, without anaemia or vascularisation defects, suggests that the decrease in *Epo* is also a direct result of defects in the placenta (Ihle 2000). Another plausible explanation is that *Epo* is also produced in either the endoderm or trophoblast lineages, meaning that the deficiency of *Epo* in the liver is rescued with the wild-type tetraploid cells.

To study the function of *Mapk14* in other tissues more carefully and avoid the lethality of the constitutive knockout, conditional alleles of the gene have been generated to study the consequences of deletion in specific tissues. Several groups have focused on the role of *Mapk14* in cardiac function and it has been reported that *Mapk14* functions by negatively regulating proliferation of cardiomyocytes, both embryonically and postnatally; overexpression of *Mapk14* causes reduced growth of the heart in the embryo, while inactivation of *Mapk14* causes the induction of cardiomyocyte

proliferation in neo-natal hearts (Engel et al. 2005). Other groups have used conditional alleles of *Mapk14* to study alternative functions through specific deletions. These include embryo-specific deletions (avoiding the effects of ablation in extra-embryonic lineages) to investigate the role in muscle formation through myoblast proliferation (Perdiguero et al. 2007), and to study the general post-natal function (Hui et al. 2007). In both cases, the embryo-specific deletions resulted in early postnatal lethality by 4 days post *partum* (dpp). Hui *et al* attribute this phenotype to a severe defect in lung function: they show significantly more nucleated blood cells in peripheral blood of the mutants than those contained in wild-type blood. This is due to increased myeloid cell proliferation during foetal haematopoiesis, which is a result of JNK activation. At the same time, a separate study reported the deletion of a different *Mapk14* conditional allele in adult mice (Ventura et al. 2007). This also found that *Mapk14* had an important role in lung since deletion resulted in severe disruption of the pulmonary morphology due to reduced differentiation of lung progenitor cells. In addition to these roles of p38α in the regulation of proliferation and differentiation, this pathway has also been implicated in cytokine production and inflammatory responses following the specific deletion of *Mapk14* in myeloid or epithelial cells (Kim et al. 2008), while support for the function of p38α as a tumour suppressor was provided with the observation that tissue-specific *Mapk14*-deficient mice were sensitised to both lung- and liver-induced tumours (Hui et al. 2007; Ventura et al. 2007). Finally, the targeted disruption of *Mapk14* in granulosa cells and cumulus cells caused changes in certain gene expression profiles within the adult ovary (Liu et al. 2010).

In summary, *Mapk14* has many reported functions during development and also postnatally as a tumour suppressor. In contrast, knockout mice generated for the other p38 MAPKs do not have any overt developmental defects, suggesting that they are not

vital in development or that p38α can compensate for their loss (Beardmore et al. 2005; Sabio et al. 2005). Along with the knowledge that the inhibition of p38α and β in gonad organ culture results in XY gonadal sex reversal, the genetic function of *Mapk14* (the gene encoding p38α) during sexual development was investigated thoroughly through conditional ablation on the C57BL/6J background.

The *Cre/*LoxP system for conditional ablation works through the ability of a *Cre* recombinase to initiate site-specific recombination of a target gene containing two LoxP sites, such that the region between these sites (the floxed region) is deleted. This ablation can be targeted to specific tissue types by controlling the expression of a *Cre* transgene, usually through use of the promoter of a gene specifically expressed in that tissue (Figure 5.1). The *Mapk14* floxed allele (*Mapk14*^{flox}) was obtained from M.Pasparakis (Ventura et al. 2007); in this allele the LoxP sites flank exons 2 and 3 of *Mapk14*. The deletion of these exons results in a *Mapk14* null allele due to the removal of the entire amino-terminal lobe of the catalytic domain, including the glycine-rich ATP-binding loop as previously described (Adams et al. 2000).

The *Sf1-Cre* transgenic line (a kind gift from K.Parker) targets *Cre* expression to steroidogenic tissues including the cortical cells of the adrenal glands, Leydig and Sertoli cells in the testis, and theca and granulosa cells in the ovary. It is also expressed in the pituitary and other parts of the brain (Bingham et al. 2006). The bacterial artificial chromosome (BAC) transgene contains the *Cre* recombinase gene inserted into the *Sf1* (*Nr5a1*) locus at the ATG initiator methionine along with 23 kb 5' of the *Sf1* transcription initiation site upstream, and 88 kb of the *Sf1* gene and 3' region downstream of the *Cre* cassette. Endogenous *Sf1* expression can be detected in the gonad as early as 9.5 dpc in the somatic cells (Ikeda et al. 1994). However, studies to

determine when the *Cre* expression from *Sf1-Cre* mice was initiated only detected *Cre* after 10.5 dpc. By 11.5 dpc this expression was consistent throughout the somatic cells of the gonad, but with less expression within cells of the coelomic epithelium (Bingham et al. 2006; Kim et al. 2007). This somatic cell localisation is specific to Sertoli and Leydig cell lineages. At the outset of this project, the *Sf1-Cre* line had previously been used to knockout β-catenin (Liu et al. 2009) and *Fgfr2* (Kim et al. 2007) in the gonads.

The *Amhr2-Cre* colony was already established in the MLC due to previous use by our group (Pastorelli et al. 2009). It was originally obtained from R.Behringer and it targets *Cre* expression to the somatic cells of the gonad from 11.5 dpc and the Müllerian duct mesenchyme of the mesonephros from 12.5 dpc (Jamin et al. 2002; Kobayashi et al. 2011). The somatic cell expression has been identified in both Sertoli cells and Leydig cells of prenatal and postnatal testis and also in granulosa cells of the adult ovary (Jeyasuria et al. 2004; Jorgez et al. 2004; Tanwar et al. 2010). The *Amhr2-Cre* allele was generated by a knock-in of a *Cre-neo* cassette into exon 5 of *Amhr2,* which encodes the Type II receptor for anti-Müllerian hormone. *Amhr2-Cre* has been used to successfully delete β-catenin (Hernandez Gifford et al. 2009), *Fst* (Jorgez et al. 2004) and *Gata4* (Kyrönlahti et al. 2011b) in female mice, resulting in fertility defects and late-onset morphological defects of the oviduct and uterine horns or histological defects of the ovary and follicle development. In males, *Amhr2-Cre* has been used to drive the deletion of *Bmrp1a* (Jamin et al. 2002) and β-catenin (Kobayashi et al. 2011) in Müllerian duct mesenchymal cells to disrupt ductal regression, and the deletion of *Sf1* (Jeyasuria et al. 2004) and *Gata4* (Kyrönlahti et al. 2011a) to disrupt the function in Leydig cells and Sertoli cells, respectively.

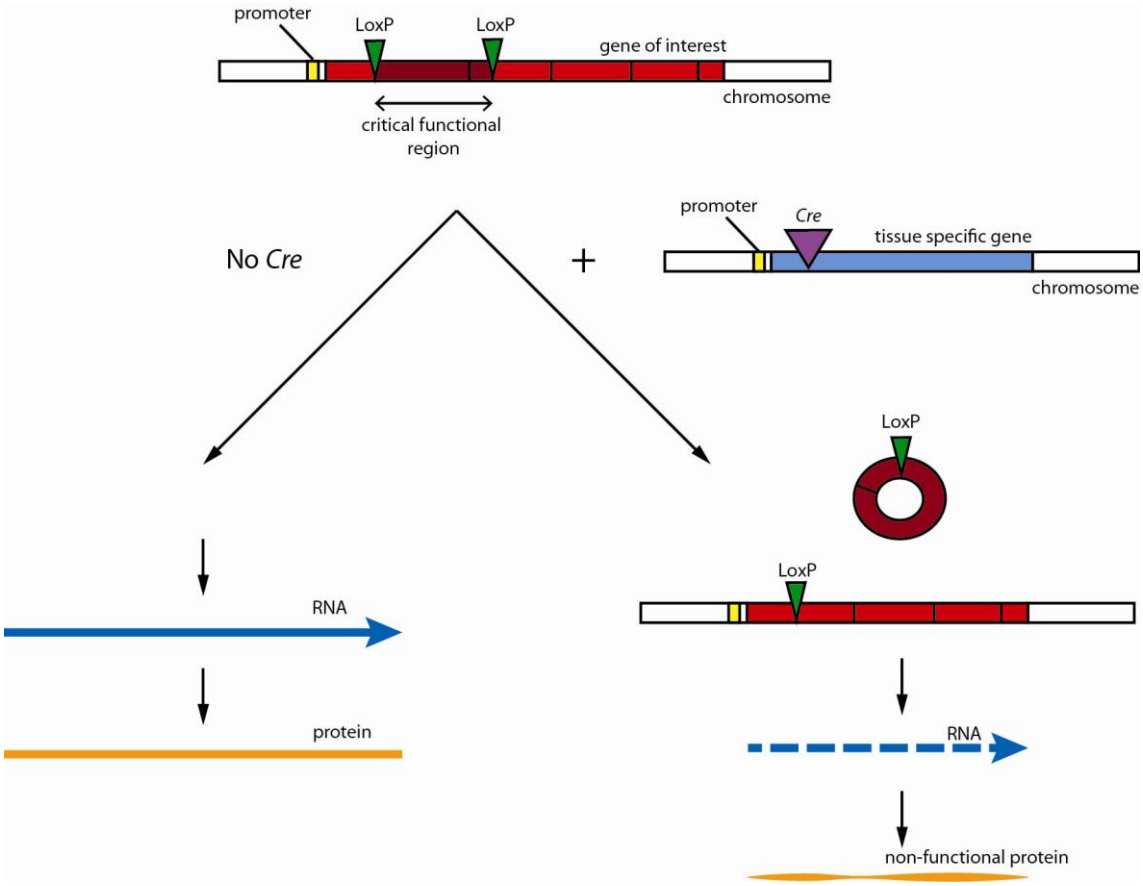

Figure 5.1: *Cre*/LoxP site-specific recombination
Diagram to show the *Cre*/LoxP system modelled on the *Mapk14* floxed allele which contains two LoxP sites flanking exons 2 and 3; the floxed region encodes the critical functional domain of the kinase. In the absence of *Cre*, transcription and translation occur normally because the two 34 bp LoxP sites do not affect the function of the transcript. The *Cre* gene is inserted after the tissue- or cell-specific gene promoter and activation of this results in the transcription and translation of the active recombinase enzyme. In cells containing this *Cre* recombinase, the enzyme recognises the specific LoxP sequence and drives site-specific recombination causing the region between the LoxP sites to be deleted. This results in deletion of the critical functional region and the translation of a non-functional protein.
Not all floxed alleles work by the same principle. For example, the R26R locus (described in section 5.2.2) contains a floxed stop-cassette after the ubiquitous *Rosa26* promoter, the deletion of which results in activation of expression. Other alternatives can include the whole gene being deleted (or the transcriptional start site), therefore preventing any transcription or protein product at all.

5.2. Results

5.2.1. Confirmation of ubiquitous *Mapk14* deletion

To confirm the identity of the imported *Mapk14*^{flox} allele and test for its successful deletion in our hands, a cross was set up with a ubiquitously expressed *Cre* recombinase, *β-actin-Cre*. A standard breeding strategy was followed as detailed below (Figure 5.2). Briefly, first generation (G1) *Cre*-positive heterozygote mice were crossed to G1 *flox*/+ heterozygote mice, to generate *flox*/+; *Cre*/+ double heterozygotes in the G2 progeny. Meanwhile, G1 *flox*/+ heterozygotes were also intercrossed to produce G2 *flox/flox* homozygotes. The G2 female *flox/flox* mice were then set up in timed matings with G2 *flox*/+; *Cre*/+ double heterozygous males to allow for G3 embryo collection at a specific gestation point.

The G3 embryos from the *β-actin-Cre* G2 timed matings were collected at 11.5 dpc, the stage at which the constitutive knockout embryos die (Table 5-1). A total of 52 embryos, not including resorptions, were collected from six litters. Of these, 4 XY and 5 XX were ubiquitously deleted conditional knockouts (*Mapk14*$^{\Delta/\Delta}$; *Cre*/+) and all were dead at the time of dissection. All other embryos appeared healthy. Statistical analysis using both a Pearson's chi-squared goodness-of-fit test and a binomial distribution test confirmed that the 17% of the experimental class observed was not significantly lower than the 25% expected, therefore embryos of this genotypic class were viable until 10.5-11.5 dpc.

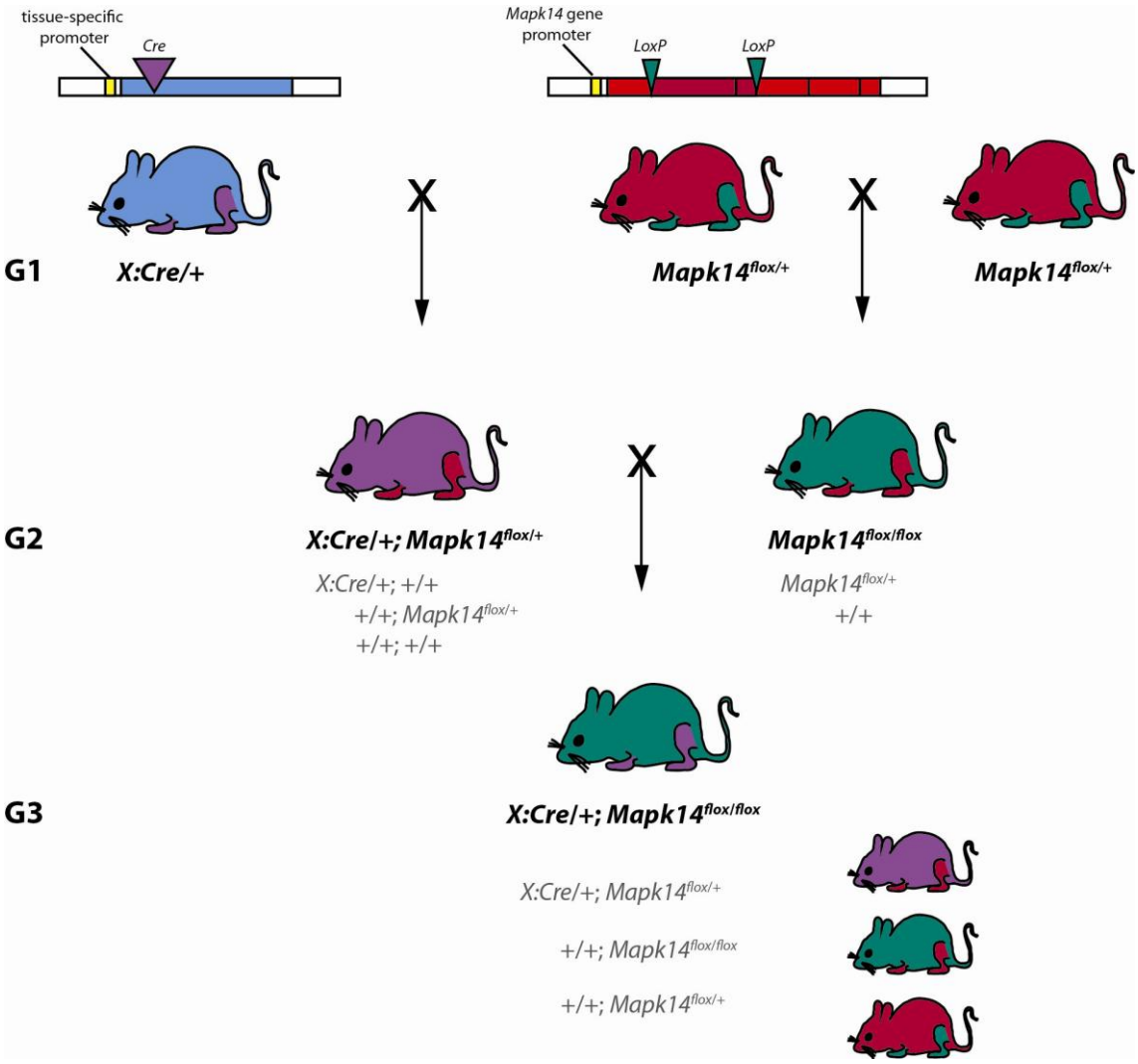

Figure 5.2: The *Cre*/LoxP breeding scheme
First generation (G1) *Cre*-positive heterozygotes were mated with G1 *Mapk14*$^{flox/+}$ heterozygotes to produce second generation (G2) progeny. G1 *Mapk14*$^{flox/+}$ heterozygotes were also intercrossed to produce G2 *Mapk14*$^{flox/flox}$ homozygotes. G2 *Cre*/+; *Mapk14*$^{flox/+}$ double heterozygous males were then crossed with female *Mapk14*$^{flox/flox}$ homozygotes in a timed mating for embryo collection of the third generation (G3) progeny at a specific stage post *coitum*. The phenotype of the G3 *Cre*/+; *Mapk14*$^{flox/flox}$ experimental class was analysed in comparison with littermate controls (either heterozygous *Cre*/+; *Mapk14*$^{flox/+}$ or homozygous *Cre*-negative *Mapk14*$^{flox/flox}$). Some G3 progeny were also allowed to litter down to assess the adult phenotype and viability.
Since G3 progeny were generally collected as embryos, the pregnant females had to be sacrificed to collect each litter, meaning a large cohort of G2 females was required. Therefore, a homozygous *Mapk14*$^{flox/flox}$ colony was set up to produce the *Mapk14*$^{flox/flox}$ females, thus avoiding the need to genotype so many animals.

Table 5-1: Observed Mendelian ratios at 11.5 dpc from *Mapk14* ubiquitous deletion
Numbers obtained from six litters. Statistical analysis performed on distribution of all genotypes using a Pearson's chi-squared goodness-of-fit test that shows no significant variation from expected ratios. A binomial distribution was also calculated for the experimental genotype, and the 17% observed was not found to be significantly lower than the 25% expected.

Mapk14*; *β-actin-Cre	XX	XY	Total	%	*p*
Δ/Δ; *Cre*/+	5	4	9	17.3	0.1292
Δ/*flox*; +/+	9	6	15	28.9	
Δ/+; *Cre*/+	7	3	10	19.2	
flox/+; +/+	8	10	18	34.6	
Total	29	23	52	100%	0.2453

To confirm successful recombination of the *Mapk14*^{flox} allele in the presence of *β-actin-Cre*, a standard PCR reaction was performed. The possible genotypes are detailed separately to those in Figure 5.2 due to the complexity of inheriting the deletion allele through the germline, as is the case with the deletion driven by *β-actin-Cre* (Table 5-2). Three different products were amplified in the three-primer reaction (sequences of which were obtained from M.Pasparakis), which corresponded to the wild-type (121 bp), floxed (188 bp) and deletion (411 bp) alleles of *Mapk14* (Figure 5.3). The presence of the *Cre* recombinase was also detected by PCR using a duplex reaction to amplify the *Cre* transgene, and also a ubiquitous gene, IL2, for a positive control. This genotyping reaction was designed by L.Pastorelli, a previous PhD student, and can detect any *Cre* allele (Pastorelli et al. 2009). The genotyping results confirmed 100% deletion of *Mapk14*^{flox} in all cells of the conditional knockout since no floxed alleles remained (red marked samples, Figure 5.3). This confirmed successful recombination of the *Mapk14*^{flox} allele, corroborated by the non-viability of the *Mapk14*$^{\Delta/flox}$; *β-actin-Cre*/+ embryos by 11.5 dpc in line with the phenotype of constitutive knockouts (Adams et al. 2000).

Table 5-2: Possible genotypes of G3 progeny resulting from *β-actin-Cre* G2 heterozygotes

Mapk14*; *β-actin-Cre ♂ \ ♀		***Mapk14*$^{flox/flox}$; +/+** flox; +	*Cre* deletes *flox*:
***Mapk14*$^{\Delta/+}$; *Cre*/+**	Δ; *Cre*	Δ/*flox*; *Cre*/+ →	Δ/ Δ; *Cre*/+
	Δ; +	Δ/*flox*; +/+	Δ/*flox*; +/+
	+; *Cre*	+/*flox*; *Cre*/+ →	+/ Δ; *Cre*/+
	+; +	+/*flox*; +/+	+/*flox*; +/+

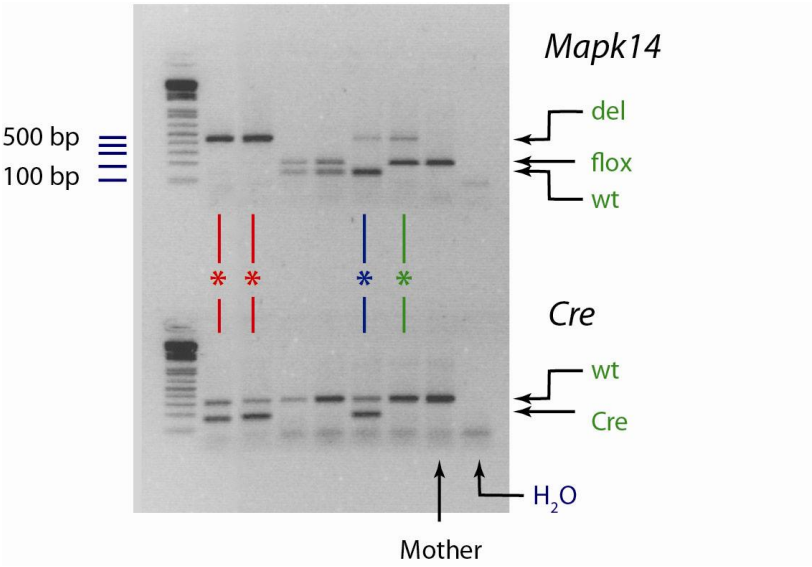

Figure 5.3: *β-actin-Cre*-driven ubiquitous deletion of the *Mapk14*^{flox} allele
Genotyping of G3 progeny was performed using a standard PCR-based assay. Presence of the *Cre* transgene was determined at the same time using a separate assay. Samples marked in red show total deletion of the floxed allele in the presence of *Cre* and are from the experimental class. Except for the last sample, which is the mother, all other samples depict the three possible genotypes when the floxed allele is deleted through the germ line of *β-actin-Cre*-positive samples. For example, the deletion allele present in sample 6 (green) has been inherited from the G2 father and is not a result of site-specific recombination in this sample as no *Cre* recombinase is present, unlike the deletion allele in sample 5 (blue).

5.2.2. Targeted deletion of *Mapk14* in somatic cells of the developing gonad

5.2.2.1. Use of an Sf1-Cre deleter

Testis determination occurs in the somatic cells of the gonad, specifically the pre-Sertoli cells, due to the expression of *Sry*, *Sox9* and *Fgf9*. Therefore, to disrupt sex determination, somatic cells are the most important cell-type in which to target the *Mapk14* deletion. The expression of *Mapk14* in these cells was confirmed previously (see Chapter 4). A useful *Cre* deleter for this purpose is *Sf1-Cre*, which is driven by the *Sf1* regulatory sequences (Bingham et al. 2006). As discussed earlier, *Sf1* encodes a transcription factor involved with regulating *Sry* and *Sox9* expression. Endogenous *Sf1* is expressed solely in somatic cells from 9.5 dpc onwards, while *Sf1-Cre* expression has been observed from 10.5 dpc onwards.

To characterise the expression of *Sf1-Cre* in our hands, *Cre*-positive females were crossed to *Rosa26*-reporter (R26R) homozygous males. The R26R line carries the *LacZ* gene with a neomycin cassette flanked by two LoxP sites upstream, and is driven by the ubiquitous *Rosa26* promoter (Soriano 1999). The insertion of the neomycin cassette acts as a premature stop codon since the neomycin resistance gene contains polyadenylation sequences which block transcription of the 3' region of the gene (Wiggin et al. 2002). Deletion of the region between the LoxP sites following recombination driven by a *Cre* recombinase results in the expression of the *LacZ* gene and subsequent β-galactosidase (β-gal) activity. The β-gal activity can be detected through staining with X-Gal due to the production of a blue product formed following the cleavage of X-Gal by β-gal. This in turn identifies the cells that express *Cre* recombinase or those that are descended from cells that have expressed *Cre* recombinase: once recombination has occurred in a cell, *LacZ* expression continues in its descendents. Therefore, *Cre*-directed β-gal

activity also acts as a lineage tracer and presence of β-gal activity only confirms that *Cre* has been expressed in cells of that tissue at some point, and is not necessarily identifying current activity of the *Cre*-driven promoter. The presence of the blue staining produced from cleavage of X-Gal by active β-gal will sometimes be referred to as β-gal activity and sometimes as expression.

Embryos were collected from 10.5 to 13.5 dpc and stained with X-Gal to show β-gal activity (Figure 5.4). At 10.5 dpc, *Sf1-Cre* expression was detectable in the forebrain, eyes, and the urogenital ridge (Figure 5.4A). At 7 ts (the earliest stage examined) this urogenital expression was confined to the anterior end of the gonad, which is likely to be the anlage of the adrenal gland (Figure 5.4B). By 8 ts, expression was observed in the somatic cells of the gonad, albeit only a scattering of cells, but at 10 ts was more pronounced (Figure 5.4C-D). In 11.0 dpc embryos expression was stronger still in the aforementioned locations, with definitive expression also visible in the adrenal gland (Figure 5.4E-F). Transverse cryosection data of the 13 ts gonads revealed strong staining in the body of the gonad, with some coelomic epithelial cells also showing β-gal activity (Figure 5.4G). Cryosection data of 13.5 dpc gonads confirm the expression in somatic cells of both testes and ovaries and absence in germ cells within the testis cords (Figure 5.4L,N). These expression patterns are consistent with the published reports, confirming the *Sf1*-driven *Cre* activity (Bingham et al. 2006).

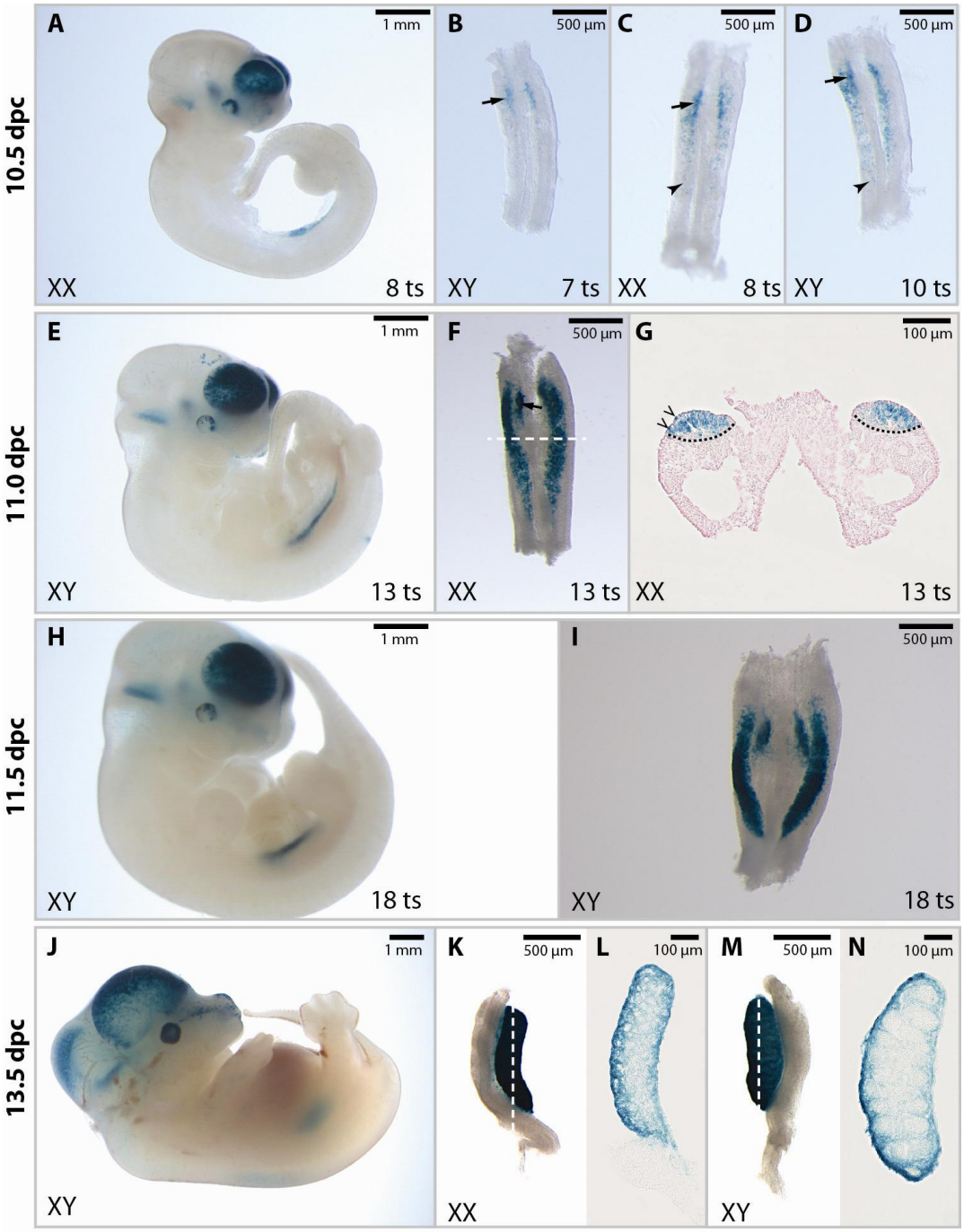

Figure 5.4: *Sf1-Cre* expression profile as shown by β-galactosidase (β-gal) activity
Sf1-Cre-positive females were mated with R26R males whom carry a *LacZ* gene that is activated in the presence of *Cre*, due to deletion of a stop cassette. The β-gal product is detected by staining with X-Gal, therefore the activity corresponds to the *Cre* positive cells. (**A-D**) β-gal activity at 10.5 dpc. (A) In the whole embryo activity was detected in the forebrain, eyes and urogenital ridge. (B) Expression in the urogenital ridge initiates in the adrenal anlagen at 7ts (arrow). (C) By 8ts, expression extends into a few somatic cells down the length of the gonad (arrowhead). (D) By 10ts, expression is visible in more somatic cells (arrowhead). (**E-G**) At 11.0 dpc, β-gal activity is stronger in the forebrain (E) and urogenital ridge, and separate expression was visible in the adrenal gland (arrow, F). Transverse cryosections (from white-dotted line, F) confirms expression throughout the 13 ts gonad, including some positive cells in the coelomic epithelium ('v' arrow heads, G). (**H-I**) At 11.5 dpc, the separation and expression in the adrenal glands is very obvious (I). (**J-N**) At 13.5 dpc, expression was more diffuse in the brain and eyes (J), and there was strong activity in both ovaries (K-L) and testes (M-N). No expression is present in the mesonephros. Coronal cryosections (L and N, orientation depicted by white dotted lines in K and M respectively) confirm expression is present in the somatic cells of the gonad, with no expression visible in the germ cells of the testis cords.

5.2.2.2. Use of Sf1-Cre to drive Mapk14 deletion

Following the confirmation that the *Mapk14*^{flox} allele could be successfully deleted, and that *Sf1-Cre* could successfully delete the R26R locus by 11.0 dpc in the gonad, it was possible to generate *Mapk14* conditional knockouts driven by the *Sf1-Cre* recombinase (referred to as *Sf1Cre-Mapk14*-cKO or 'mutants' within section 5.2.2 only). The same breeding strategy was followed as for the *β-actin-Cre*-driven deletion: G3 embryos from timed matings between female *Mapk14*$^{flox/flox}$ and male *Mapk14*$^{flox/+}$; *Sf1-Cre*/+ mice were assessed.

5.2.2.3. Determining successful recombination

To ensure successful recombination of the *Mapk14*^{flox} allele within the embryonic gonad, one gonad from each 14.5 dpc embryo collected for phenotypic analysis was put aside for genotyping. The deletion allele was detected in all *Cre*-positive gonads, including *flox/+*; *Cre*/+ heterozygous embryos, except in two mutants (out of 36), in which the deletion band was too weak to detect (Figure 5.5A). Moreover, the deletion allele was absent from all hindbrain samples, confirming the specificity of deletion.

However, because the deletion is only occurring in *Sf1*-positive cells of the gonad, some floxed alleles were still detected in these whole-gonad samples. For this reason it was not possible to determine the efficiency of the recombination. However, to try and determine the percentage of total cells within the gonad that had successfully recombined, a PCR reaction was performed in which *Mapk14*$^{flox/flox}$ DNA was "spiked" with either *Mapk14*$^{\Delta/flox}$ or *Mapk14*$^{\Delta/\Delta}$ DNA from the ubiquitous *β-actin-Cre*-driven *Mapk14*^{flox} deletion samples (see Table 5-2 for genotypes). The DNA was added in increasing amounts to achieve a range of concentrations from 0% *Mapk14*$^{\Delta/\Delta}$ DNA to 100% *Mapk14*$^{\Delta/\Delta}$ DNA (Figure 5.5B). From this experiment it was then possible to

compare the ratio of intensities of the deletion product to the floxed product (Δ-to-flox) in the experimental samples with those ratios of the spiked DNA samples and thus determine the approximate level of floxed allele recombination that had occurred (Figure 5.5B). While slight variation in the Δ-to-flox ratio was seen in experimental samples, in the majority of cases both products were approximately equal in intensity, which suggests approximately 50% of the cells in the gonad underwent recombination in the presence of *Cre*. Unfortunately, this analysis could not help determine the overall efficiency of the recombination since it was not possible to determine the percentage of cells in the gonad that were *Sf1*-positive.

To ascertain the stage by which the recombination had occurred, 10.5 dpc embryos were collected and gonads removed for genotyping. At this stage, the deletion allele was not detectable in any *Cre*-positive samples (N = 4, out of 15 embryos). Either the recombination event had not occurred this early, or insufficient numbers of cells in the gonad at this stage contained the deletion allele for it to be detected by the PCR assay. The deletion allele was successfully detected by 11.5 dpc, but any attempts to identify the deletion allele between 10.5 and 11.5 dpc failed due to a failure to obtain embryos at the appropriate stages.

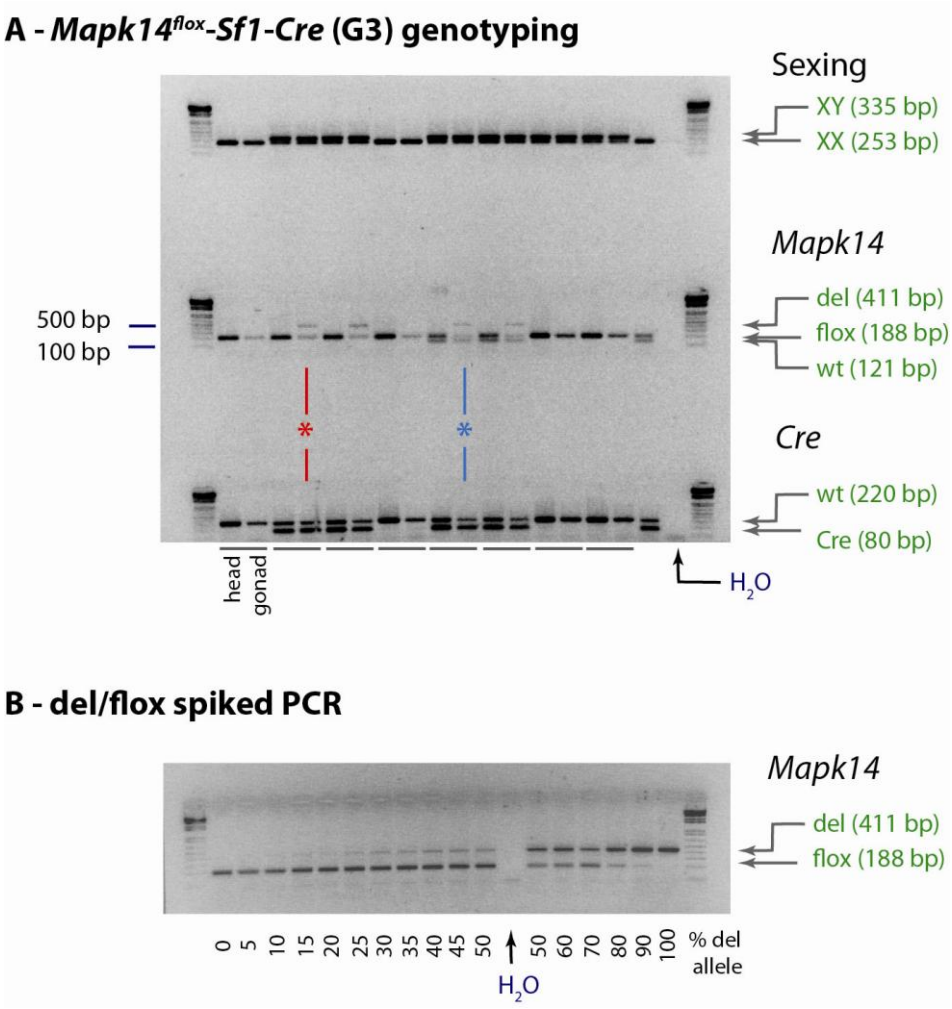

Figure 5.5: *Sf1Cre-Mapk14*-cKO genotyping
(**A**) Example of genotyping results from a G3 *Mapk14*^{flox}*-Sf1-Cre* litter. Two lanes per sample: first is the hindbrain tissue, second is the gonadal tissue. *Sf1Cre-Mapk14*-cKO individuals contain the deletion allele in the gonad sample but not the hindbrain sample (e.g. sample highlighted by red line). Heterozygous controls (*Mapk14*$^{flox/+}$*; Cre/+*), also contain the deletion allele as well as the *flox* and wild-type (wt) alleles due to mosaicism of the deletion (e.g. sample highlighted by the blue line).
(**B**) Results of the deletion allele and floxed allele DNA spiking reaction. *Mapk14*$^{flox/flox}$ DNA was spiked with an increasing percentage of *Mapk14*$^{\Delta/flox}$ DNA to produce a concentration range of 0% to 50% deletion allele DNA. The 50% sample contains 100% *Mapk14*$^{\Delta/flox}$ DNA from the *β-actin-Cre*-driven deletions and therefore all cells contain 50% deletion allele and 50% floxed allele. *Mapk14*$^{flox/flox}$ DNA was also spiked with an increasing percentage of *Mapk14*$^{\Delta/\Delta}$ DNA to produce a concentration range of 50% to 100% deletion allele DNA. In this case, the 50% sample contains 50% of the *Mapk14*$^{flox/flox}$ DNA and 50% of the *Mapk14*$^{\Delta/\Delta}$ DNA, which is therefore equivalent to half the cells containing 100% of the floxed allele and the other half containing 100% of the deletion allele. Assessing the Δ-to-flox ratio of product intensity, it is possible to assume that in the experimental samples from (A) slightly less than 50% of cells in the gonad contain 100% *Mapk14*$^{\Delta/\Delta}$ DNA.

5.2.2.4. Phenotypic analysis

To analyse sex determination and gonadal development in the mutants, 17 litters were collected at 14.5 dpc for phenotypic analysis, all of which were genotyped for the sex chromosomes, and in 14 litters, one gonad from each embryo was collected for genotyping to confirm the deletion of the *Mapk14*^{flox} allele. Out of the 17 litters, there were 20 female mutants and 16 male mutants, with no apparent gonadal sex reversal (Table 5-3).

Table 5-3: Mendelian ratios observed at 14.5 dpc from *Sf1-Cre*-driven *Mapk14*^{flox} deletions

Mapk14*; *Sf1-Cre	XX	XY	Total	%
flox/flox; *Cre*/+	20	16	36	24.8
flox/flox; +/+	19	22	41	28.3
flox/+; *Cre*/+	15	21	36	24.8
flox/+; +/+	15	17	32	22.1
Total	69	76	145	100%

WMISH was performed on the gonads to assess *Sox9*, *Wnt4*, *Stra8*, *Oct4* and *Hsd3b* (3βHSD) expression. No phenotypic difference between the mutants or the homozygous controls (*flox*/*flox*; +/+) was observed (Figure 5.6). *Oct4* expression appeared slightly abnormal and suggested that primordial germ cell numbers were sparse; however, this was also observed to the same degree in controls (Figure 5.6E-F). Despite the WMISH being sub-optimal, germ cells were present in both mutant and control samples. The expression of *Stra8* (which marks female meiotic germ cells) was also normal, which confirms that there is no defect in terms of germ cell number or differentiation. This is further confirmed by the normal fertility of both mutant and control mice (see next section).

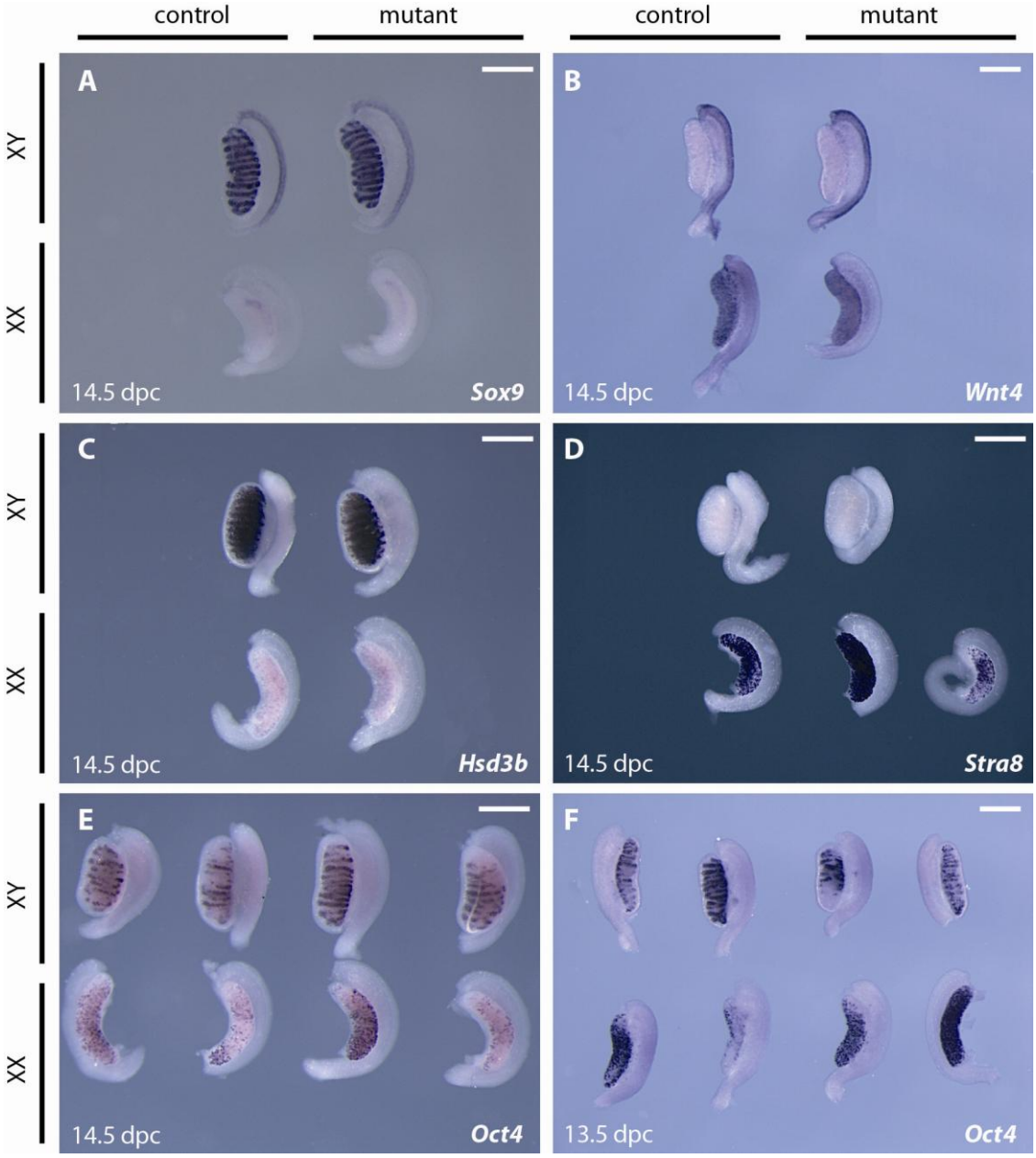

Figure 5.6: Phenotypic analysis of *Sf1Cre-Mapk14*-cKOs by WMISH
14.5 dpc *Mapk14*$^{flox/flox}$*; Sf1-Cre/+* mutant and *Mapk14*$^{flox/flox}$*; +/+* control gonads were analysed by WMISH for expression of cell-type-specific gene markers. In all cases, the gonads on the left-hand side are the controls, and the gonads on the right-hand side are mutants. Male gonads are on the top row of each image and female gonads along the bottom. (**A**-**D**) The following sex-specific markers were assessed at 14.5 dpc: *Sox9*, which marks male Sertoli cells (A); *Wnt4*, to mark female somatic cells (B); *Hsd3b*, which marks male Leydig cells (C); and *Stra8*, which marks female meiotic germ cells. (**E**-**F**) The expression of *Oct4*, which marks primordial germ cells in both sexes, was analysed at both 14.5 dpc (E) and 13.5 dpc (F). All scale bars are 500 µm.

5.2.2.5. Adult viability and fertility

To ensure there were no age-related defects or infertility in adult *Sf1-Cre*-driven *Mapk14* deletion mice, some G3 progeny were allowed to litter down. The mutants were viable, with no age-related defects observed in the stages studied, up until approximately six months of age. To assess fertility, males (four mutants and six *flox*/+;*Cre*/+ heterozygous controls) were placed into fertility testing at approximately 8 weeks of age with C57BL/6J females with known fertility, for 2-3 months (Table 5-4). Embryos were collected from pregnant females at 13.5 dpc to determine the size of each litter. Approximately 4-5 females were mated with each male during this time. An average litter of 8.46 embryos was observed from the mutant male matings, and 9.00 embryos from the control male matings. This was not a significant difference. At the end of the 2-3 month fertility testing, males were culled at approximately 20 weeks of age and analysed internally for any gross morphological defects.

Females were also mated to test their fertility (Table 5-4). Eight mutant females at approximately 11 weeks old were mated with C57BL/6J males of known fertility. Embryos were collected from pregnant females at 13.5 dpc to determine the size of each litter. Females were fertile with an average litter size of 7.63 embryos.

Table 5-4: Results from fertility testing of XY and XX mutants compared to controls
N is number of mice. Values are expressed as average ± standard error of the mean (SEM). Statistical analysis was performed using a two-tailed *t*-test at 95% confidence, and mutant samples were compared with XY controls in both cases.

p38α*; *Sf1-Cre	Sex	*N*	Total litters	Total embryos	Average litter size	*p* (*t*-test) c.f. XY control
flox/flox; *Cre*/+	M	4	13	110	8.46 ± 0.45	0.362
flox/+; *Cre*/+	M	4	16	144	9.00 ± 0.38	
flox/flox; *Cre*/+	F	8	8	58	7.63 ± 1.07	0.146

5.2.2.6. Morphological and histological analysis

Following fertility testing, three male mutants and three male controls were examined internally for any gross morphological defects (Table 5-5). No abnormalities were obvious with any constituents of the reproductive tract (vas deferens, epididymis and seminal vesicles). Testes were of normal size and analysis of H&E-stained sections showed normal seminiferous tubules and healthy sperm (Figure 5.7A-B). Due to strong expression of *Sf1-Cre* in the adrenal glands, and known presence of p38α protein, these were also analysed for any defects (Figure 5.7C-F). In adult mice, adrenal glands are much smaller in relation to kidneys and so are difficult to detect. In some cases, the adrenal glands in the male mutants were displaced further from the kidney than normal. However, there was also variation with the location of the adrenal glands in the controls, so this was discounted as a phenotype.

Three female mutants and controls were also analysed for gross morphological defects. The mutants were of similar size and weight as controls (Table 5-5) and the ovaries and uterus were normal. H&E-stained sections showed that the ovaries were undergoing normal follicle cycling, as all stages of folliculogenesis could be detected (Figure 5.7J). The oviducts, uterine horns and uterus body also had no overt defects (Figure 5.7K-L).

Table 5-5: Average mouse and testes weights
N is number of mice. Values are expressed as average ± SEM

Mapk14*; *Sf1-Cre	Sex	*N*	Average terminal weight (g)	Average weight left testis (g)	Average weight right testis (g)
flox/flox; Cre/+	M	3	30.95 ± 1.34	0.10 ± 0.01	0.10 ± 0.01
flox/+; Cre/+	M	3	31.47 ± 1.02	0.10 ± 0.01	0.10 ± 0.00
flox/flox; Cre/+	F	3	23.90 ± 0.96		
flox/+; Cre/+	F	3	23.71 ± 0.74		

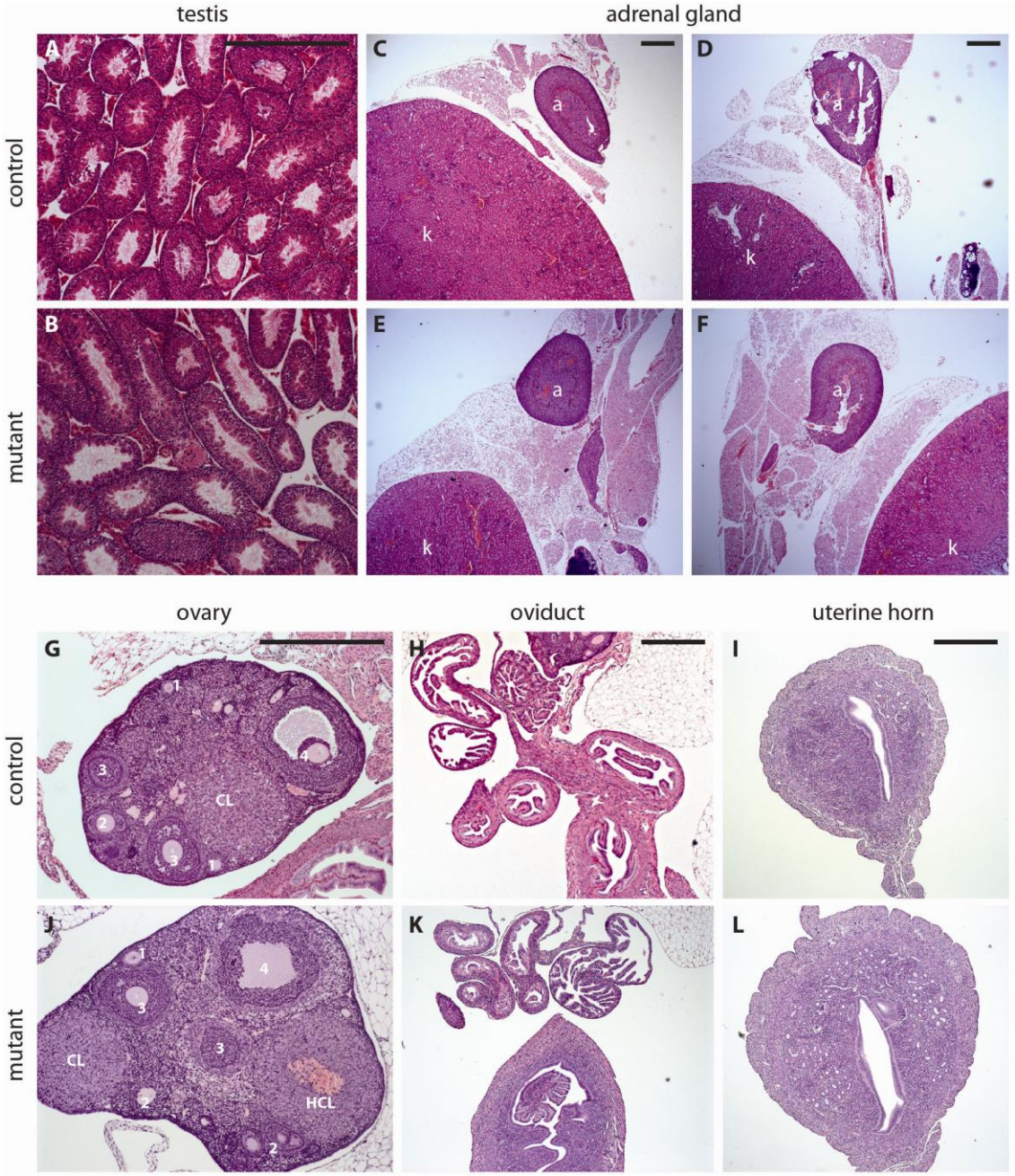

Figure 5.7: *Sf1Cre-Mapk14*-cKO histology analysis
H&E-stained histology sections of adult *Mapk14*$^{flox/flox}$*; Sf1-Cre/+* mutants in comparison with *Mapk14*$^{flox/+}$*; Sf1-Cre/+* heterozygous controls for male (**A-F**) and female (**G-L**) reproductive tissues. (**A-B**) Section though a testis to show the seminiferous tubules containing sperm in both controls and mutants. No abnormalities of testis structure or sperm production were visible in the mutants. (**C-F**) Sections through the adrenal glands (a) and part of the kidney (k), in controls (C-D) and mutants (E-F). The distance between the adrenal gland and kidney varies in both. (**G-L**) Sections of female control tissues: ovary (G), oviduct (H) and uterine horn (I) and sections of the mutant tissues: ovary (J), oviduct (K) and uterine horn (L). Mutant ovaries appear to cycle normally with all stages of follicle development visible. Cross-sections of the oviducts and uterine horns reveal no changes. Stages of folliculogenesis labelled: 1) Primary follicle; 2) Secondary follicle (preantral); 3) Tertiary follicle (antral); 4) Late tertiary follicle (preovulatory); CL, corpus luteum; HCL, haemorrhagic corpus luteum. All scale bars are 500 µm.

5.2.3. *Amhr2-Cre*-mediated deletion of *Mapk14*

5.2.3.1. Use of an Amhr2-Cre deleter

AMHR2 is a receptor located in the mesonephric mesenchyme that binds AMH and drives the regression of the Müllerian duct in males from around 14.5 dpc. The *Amhr2-Cre* mouse line had been used previously in our laboratory so was easily available to use to generate a separate tissue-specific knockout of *Mapk14*.

To ascertain the expression profile of *Amhr2-Cre* this line was crossed to R26R and the resultant progeny stained with X-Gal to assess the *LacZ* expression pattern determined by β-gal activity, as previously described in section 5.2.2.1. Embryos were collected at 13.5 dpc and 17.5 dpc, and adults from these matings were also examined at 6 weeks of age. Following X-Gal staining, at 13.5 dpc, β-gal activity was restricted to the urogenital ridge of the embryo (arrow, Figure 5.8A). This expression was strong in both the mesonephros and gonad of male and female samples at 13.5 dpc (Figure 5.8B-G), with mesonephric expression restricted to the Müllerian duct mesenchyme (double arrows, Figure 5.8D,G). At 17.5 dpc, β-gal activity was present in both male and female reproductive tracts but was stronger in the testis than the ovary (Figure 5.8H-M). No β-gal activity was observed in *Cre*-negative samples. Despite the clear, restricted expression observed in the majority of *Cre*-positive samples, at 13.5 dpc some *Amhr2-Cre*-positive embryos exhibited widespread, non-specific expression (Figure 5.8N). Analysis of expression in the gonads of these samples revealed reduced levels, although some was still present in the mesonephros (Figure 5.8O). This type of expression was termed ‘leaky’ and was also observed in some 17.5 dpc embryos (Figure 5.8P-Q). It appeared that the expression was limited to the outer surface of the stained tissue and due to the lack of any non-specific staining in *Cre*-negative samples, it is most likely a result of inappropriate *Cre* recombinase activity, perhaps at earlier embryonic stages.

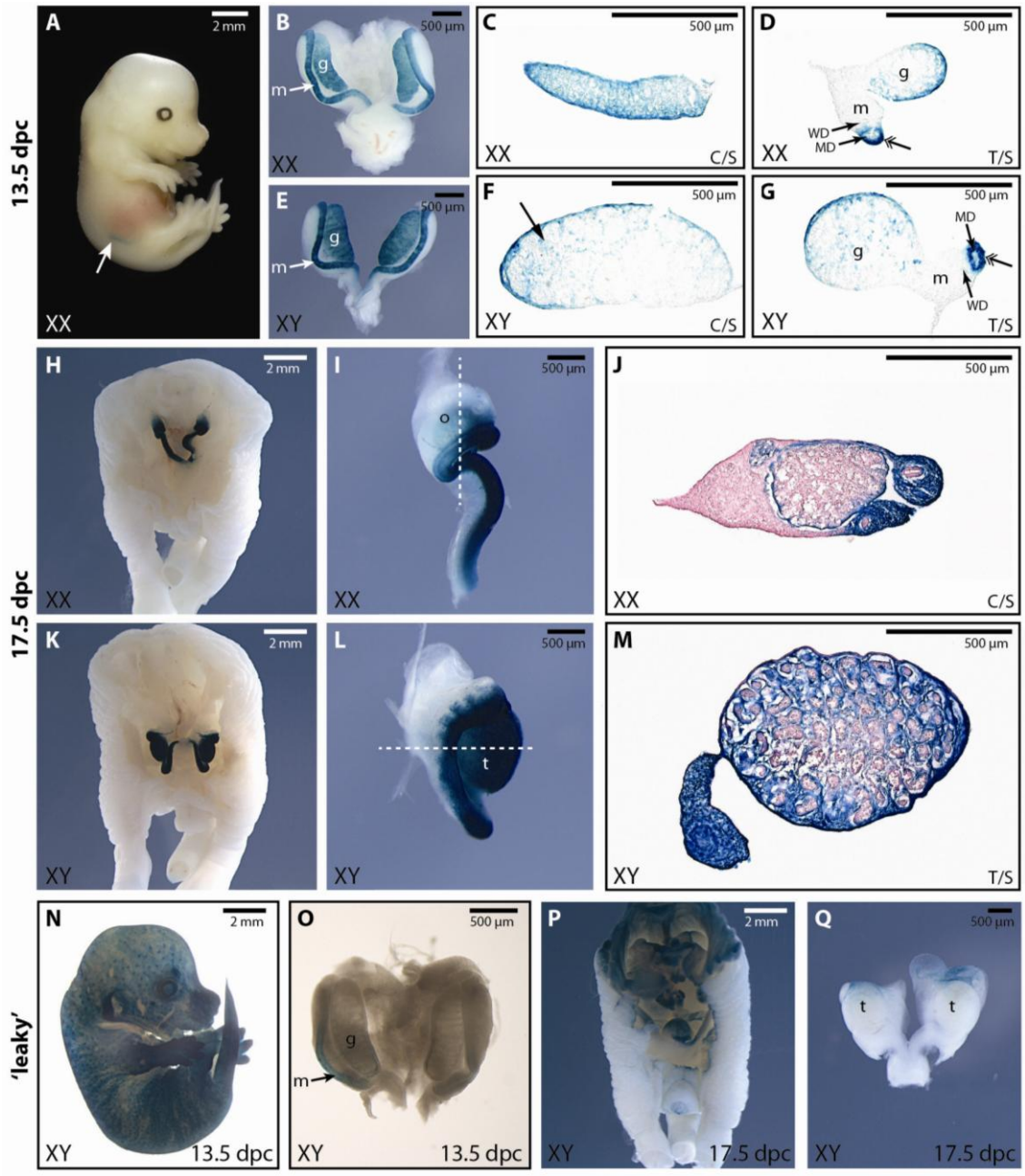

Figure 5.8: Embryonic *Amhr2-Cre* expression profile using β-gal reporter activity
Amhr2-Cre females were mated with R26R males and the embryos collected at 13.5 dpc and 17.5 dpc. (**A**) Following X-Gal staining, β-gal activity was detected solely in the urogenital ridge of the 13.5 dpc embryos (white arrow). No staining was observed in any *Cre*-negative embryos. (**B-G**) This urogenital ridge staining was restricted to the gonad and mesonephros of both male and female embryos. Cryosections in a coronal orientation revealed staining throughout the ovary (C) and in the interstitium of the testis (F). Transverse cryosections revealed strong β-gal activity in the Müllerian duct mesenchyme in the mesonephros of both female (D) and male (G) tissue (double arrows). (**H-M**) At 17.5 dpc, this β-gal activity was strong in the developing oviducts and uterine horns, with less expression in the ovaries of females (H-I). In the males, the Müllerian duct has regressed, but staining still persists in the developing epididymides and vasa deferentia, along with strong expression in the testes (K-L). Cryosection of both the ovary (J) and testis (M) in the orientation shown in (I) and (L), respectively (white dotted lines). (**N-Q**) In some *Cre*-positive embryos, expression was 'leaky'. β-gal activity was detected on the surface of the tissue, but only very weakly internally in the cells that should be expressing *Amhr2-Cre*. This was seen at both 13.5 dpc (N-O) and 17.5 dpc (P-Q). Scale bars are as marked on each image. g, gonad; m, mesonephros; C/S, coronal section; T/S, transverse section; WD, Wolffian duct; MD, Müllerian duct; o, ovary; t, testis.

This ‘leaky’ expression, even though not common, was undesirable because if the *Cre* recombinase was expressed in an unpredictable fashion, it could drive the deletion of *Mapk14* in other locations, potentially producing confounding phenotypic results that make interpretation difficult.

In adult females at 6 weeks of age, β-galactosidase activity was observed in the uterine horns, oviducts, and in the ovary (Figure 5.9A-B). Cryosection data of the ovary revealed *Amhr2-Cre* expression in the granulosa cells of follicles, however, the staining did not penetrate far into the tissue (Figure 5.9C-D). In adult males of the same stage, weak X-Gal staining was seen in the epididymides and vasa deferentia (Figure 5.9E). Cryosection data of the testis revealed that the expression was located around the surface of the epididymis, with some also in the epididymis tubule wall. Some expression was apparent in the surface epithelium of the testis with little, if any, in the interstitium of the testis (Figure 5.9F). The expression observed in the ovaries, oviducts and uterus is consistent with previously published data (Jeyasuria et al. 2004; Jorgez et al. 2004; Hernandez Gifford et al. 2009; Kyrönlahti et al. 2011b). In contrast, expression in the adult testis is reported to be strong in Sertoli cells of the seminiferous tubules and Leydig cells in the interstitium (Jeyasuria et al. 2004; Tanwar et al. 2010; Kyrönlahti et al. 2011a). This discrepancy is most likely a result of impaired penetration of X-Gal into the adult wholemount testis and is likely to be rectified by X-Gal staining of cryosections rather than wholemount tissue. Unfortunately, due to time constraints this avenue could not be pursued.

As discussed in section 5.2.2.1, it should be stressed that expression studies using *LacZ* reporters such as R26R do not necessarily reveal current *Amhr2-Cre* gene expression. Therefore, the weak staining seen in the adult male vas deferens is likely to be a

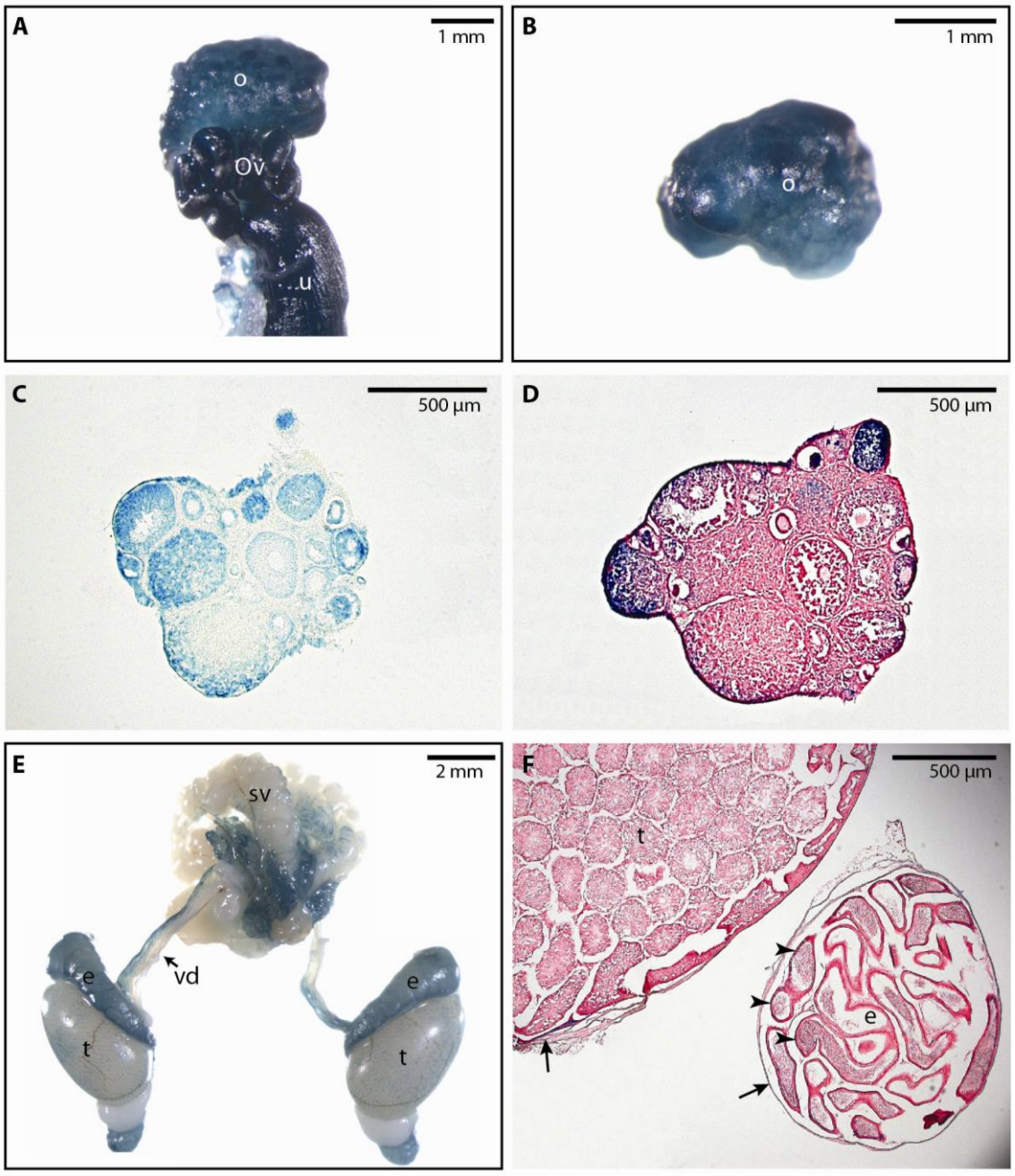

Figure 5.9: Expression of *Amhr2-Cre* in adult tissue as shown by β-gal activity
(**A-D**) Following X-Gal staining of the ovaries, oviducts, uterine horns and uterus body from 6 week old females, strong β-gal activity was observed in the oviducts and outer lining of the uterine horns (A). Expression was also seen in the ovaries (B), cryosections of which show evidence of *Amhr2-Cre* in the granulosa cells of the secondary and tertiary follicles and in the corpus luteum (C). Alternate slides were also stained with a nuclear fast red stain to highlight the ovarian structure; however, the X-Gal staining did not penetrate all the way into the ovary (D). (**E**) Weak β-gal activity was observed in the male testes, epididymides, vasa deferentia and parts of the seminal vesicles. (**F**) Cross-sections stained with nuclear fast red show very weak β-gal expression in the surface epithelium of both the epididymis and testis (arrows). It was difficult to detect expression in the body of the testis, however, expression was apparent in the epididymis wall (arrow heads). o, ovary; Ov, oviduct; u, uterine horn; SV, seminal vesicle; vd, vas deferens; e, epididymis; t, testis.

consequence of previous embryonic expression, rather than current *Amhr2-Cre* expression.

5.2.3.2. Use of Amhr2-Cre to drive Mapk14 deletion

Due to the ability of *Amhr2-Cre* to delete the R26R locus successfully in the majority of cases, and its strong expression in the Müllerian ducts and gonads by 13.5 dpc, the generation of *Mapk14* conditional knockouts driven by the *Amhr2-Cre* recombinase was continued (referred to as *Amhr2Cre-Mapk14*-cKO, or 'mutants' within section 5.2.3 only). The same breeding strategy was followed as for the *Sf1-Cre*-driven deletion; G3 embryos from timed matings between female G2 $Mapk14^{flox/flox}$ and male G2 $Mapk14^{flox}$/+; *Amhr2-Cre*/+ mice were assessed.

5.2.3.3. Assaying for successful recombination

During the $Mapk14^{flox/+}$; *Amhr2-Cre*/+ (G2) colony genotyping, it became apparent that non-specific recombination was occurring. Results from the ear biopsies highlighted some (N = 18, out of 39) G2 individuals that contained the deletion allele, with or without the floxed allele, in *flox*/+; *Cre*/+ samples (Figure 5.10A). This resulted in some mosaic animals in which, presumably, some of the floxed alleles had been deleted in a subset of cells contributing to the ear, but in other cells recombination had not occurred and the floxed allele was still present (N = 12 of 18; refer to blue marked samples in Figure 5.10A). Other animals exhibited complete deletion of the floxed allele in all cells of the ear (N = 6 of 18; refer to red marked samples in Figure 5.10A). This effect was likely due to inappropriate, early and widespread expression of the *Amhr2* promoter of the targeted allele. Due to the potential effects of this non-specific recombination, individuals with the complete deletion genotype (N = 6; referred to as 'G2 DEL' double heterozygotes from here on) were set up in separate timed matings to enable identification and segregation of potentially more severe G3 mutant phenotypes

(referred to as ‘DEL G3’ progeny). The *flox/+*; *Cre/+* individuals that did not carry a deletion allele (N = 21 of 39; referred to from now on as ‘G2 NORM’ double heterozygotes) were used for the matings with G2 *Mapk14*$^{flox/flox}$ individuals to assess the phenotypes of ‘NORM G3’ tissue-specific conditional knockout progeny (refer to Table 5-6 for summary of nomenclature used).

To ensure that the deletion of *Mapk14* was occurring in the Müllerian duct of the G3 progeny, one mesonephros from each embryo was removed and put aside for genotyping, while the other was collected for gene expression analysis along with the gonad (by WMISH). One mesonephros and part of the hindbrain were then genotyped separately per embryo (Figure 5.10B). The deletion allele was always present in the hindbrains of *DEL/flox* embryos from the DEL G3 progeny (when the deletion allele was inherited through the germ line) (red and blue marked samples, Figure 5.10Bii). Moreover, embryos from the DEL G3 progeny that inherited the deletion allele from the G2 DEL father and floxed allele from the mother, and were also *Cre*-positive, did not display complete deletion of the floxed region. Even in the mesonephros sample, the deletion allele was more abundant in comparison to the hindbrain sample, but the floxed allele was also present. A surprising observation was that the deletion allele was also identified in the hindbrain samples of some NORM G3 embryos (red marked sample, Figure 5.10Bi). This suggests that the non-specific recombination was occurring sporadically. As a result, any experimental *Mapk14*$^{flox/flox}$*; Amhr2-Cre/+* embryos from G2 NORM fathers that contained the non-specific deletion allele were grouped with the *Mapk14*$^{DEL/flox}$*; Amhr2-Cre/+* embryos from the DEL G3 progeny and referred to as ‘DEL mutants’. Only embryos that contained the specific recombination in just the mesonephros were considered as normal conditional (tissue-specific) knockouts and are referred to as ‘NORM mutants’ (Table 5-6).

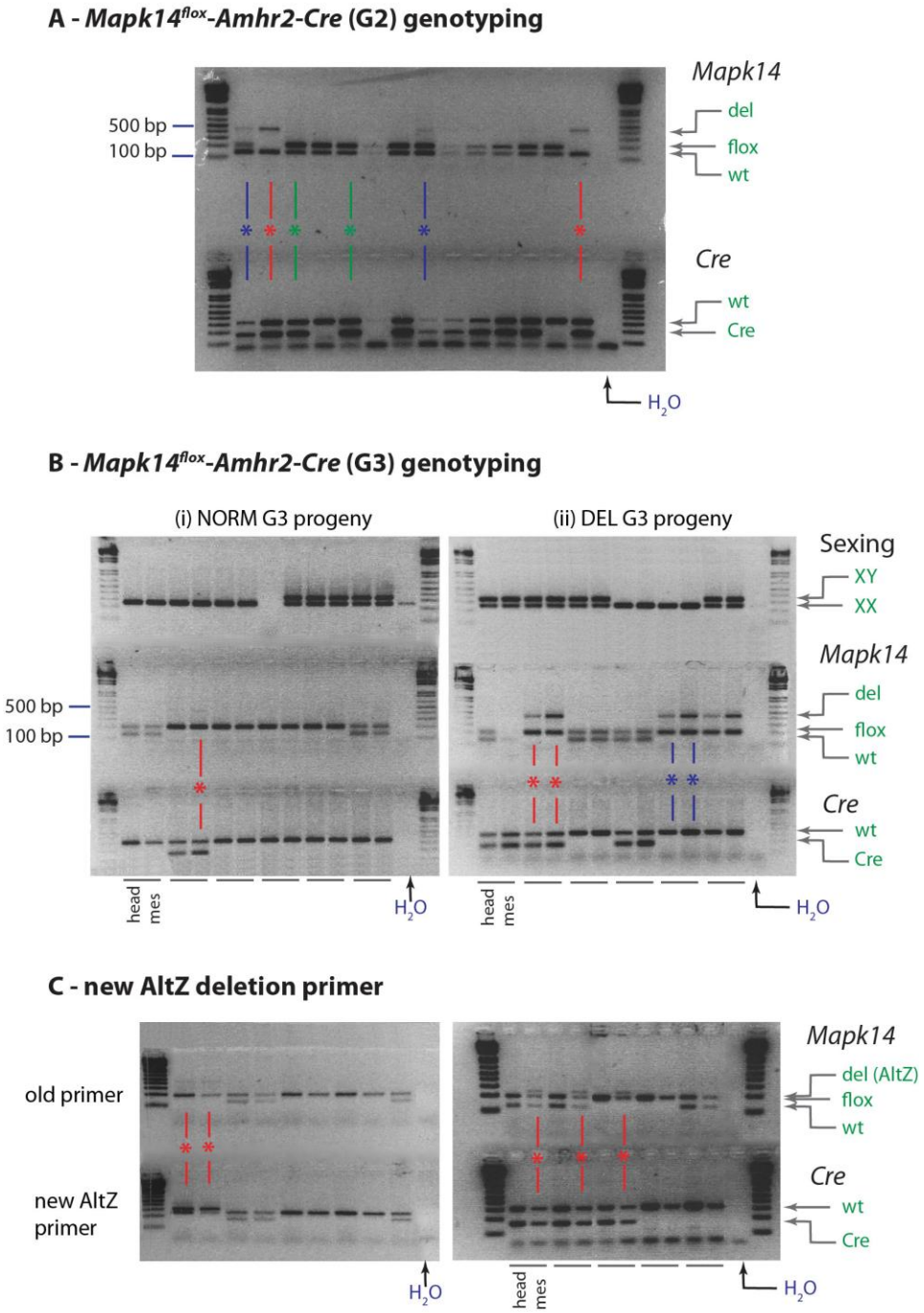

Figure 5.10: *Amhr2-Cre*-directed *Mapk14* knockout G2 and G3 colony genotyping
Standard PCR genotyping assays to determine the *Mapk14* alleles inherited and likelihood of successful recombination. (**A**) During the G2 colony genotying, the deletion allele was observed in the ear biopsy samples of some *Cre*-positive mice. In some cases, apparent mosaicism was detected: some cells contained the deletion allele with the wild-type allele, and other cells contained the floxed allele with the wild-type allele (blue marked samples). Other samples contained the deletion and wild-type alleles, apparently in the vast majority of cells of the ear biopsy (red marked samples), while others displayed the expected double heterozygous genotype (*Mapk14*$^{flox/+}$*; Amhr2-cre/+*) as shown by the green marked samples. (**B**) Genotyping of the G3 progeny. (Bi) The deletion allele was much less abundant in the mesonephros in comparison with the floxed allele (red marked sample) and the deletion allele was also occasionally observed in the head tissue of the embryos. (Bii) The deletion product was very strong in the DEL G3 progeny and was also present in the head tissue. In all samples containing the deletion allele, it is inherited from the father and the presence of *Cre* (red samples) does not cause further ubiquitous deletion, as the floxed allele is still present. The deletion product is stronger in the mesonephros sample than the head in all cases, including *Cre*-negative (blue samples). (**C**) Optimisation of a new deletion primer (AltZ) which produces a stronger product that is easier to detect.

Table 5-6: Description of nomenclature used for *Amhr2Cre-Mapk14*-cKOs
Abbreviations: del, deletion; mes, mesonephros; cKO, conditional knockout.

Mapk14; Amhr2-Cre	**Genotype**	**Description**
G2 NORM	*flox*/+; *Cre*/+	Double heterozygous males
G2 DEL	*Δ*/+; *Cre*/+	Double heterozygous males carrying a del allele
NORM G3		Progeny from matings between G2 NORM heterozygotes and G2 *flox* homozygotes
DEL G3		Progeny from matings between G2 DEL heterozygotes and G2 *flox* homozygotes
NORM mutants	*flox/flox*; *Cre*/+	cKOs from a NORM G3 litter. Del allele restricted to mes
DEL mutants	*Δ/flox*; *Cre*/+	cKOs from a DEL G3 litter OR a NORM G3 litter. Del allele in both hindbrain and mes samples

The *Amhr2-Cre* line was generated and maintained on a mixed C57BL/6J × 129/SvEv background (Jamin et al. 2002) and subsequent studies using this line also maintain the mixed genetic background (Jeyasuria et al. 2004; Jorgez et al. 2004; Kobayashi et al. 2011; Kyrönlahti et al. 2011b). It may be that the increased amount of C57BL/6J in the congenic line used in this study affects the specificity of expression. However, this 'leaky' expression has been reported previously on a mixed genetic background (Hernandez Gifford et al. 2009; Pastorelli et al. 2009). In the work by Hernandez Gifford *et al*, the surprising observation was made that the recombined deletion allele was present in other tissues in addition to the organs that comprise the reproductive tract and pituitary gonadal axis, such as the brain, heart and liver. The work by L.Pastorelli *et al* was carried out using the same allele imported from R.Behringer as used in this chapter, but before the line was congenic on the C57BL/6J background. Thus, the fact that this phenomenon has been observed by an independent research group suggests that the C57BL/6J background is unlikely to be the main contributory factor in "leaky" expression. Although these are the only two reported cases of the leaky *Cre* expression in the literature, many other studies have reported variation in *Amhr2-Cre*-driven recombination efficiency, and the presence of mosaicism in the targeted tissues. For

some reason, neither the variation in efficiency nor the leaky *Cre* expression appear to cause more severe phenotypes in these different studies than that expected with tissue-specific *Cre* activity.

In contrast to the genotyping analysis with the *Sf1-Cre*-driven *Mapk14* deletion, the results with the *Amhr2-Cre*-driven deletion gave a much weaker product for the deletion allele, which was often very difficult to detect. Therefore, the PCR was re-optimised and a new deletion primer designed using the Primer3 programme, giving a smaller product that would therefore be easier to amplify (Figure 5.10C). This was called the AltZ primer.

5.2.3.4. Analysis of Müllerian duct regression in males

If *Mapk14* does have a non-redundant function in either the development of the Müllerian duct in females into the oviducts and uterine horns or the regression of the Müllerian duct from 14.5 dpc in male embryos, or for the function of adult granulosa cells, Leydig cells or Sertoli cells, then the ablation driven by *Amhr2-Cre* should result in a detectable phenotype. In females, this could result in infertility of the adults, whereas in males it could result in a persistent Müllerian duct alongside the Wolffian duct as seen in *Amhr2*$^{-/-}$ mutants (Mishina et al. 1996), or defects in spermatogenesis or testicular descent. In wild-type XY mice, the Müllerian duct regresses from 14.5 dpc (Jamin et al. 2002). Therefore, analysis at 17.5 dpc should determine whether a defect in Müllerian duct regression has occurred since by this stage the duct should be completely absent and only the Wolffian duct should be present. Therefore, embryos from 12 litters were collected at 17.5 dpc; these had normal Mendelian ratios of the expected genotypic classes. Histological analysis of H&E-stained wax transverse sections of the mutant male reproductive tract revealed normal development, with correct regression of the

Müllerian duct, and seminiferous tubules with normal morphology (Figure 5.11A,B). WMISH analysis of *Pax2* expression, which marks both the Müllerian duct and the Wolffian duct, confirmed the presence of a single duct in the mesonephros of male mutants that is the Wolffian duct (Figure 5.11D).

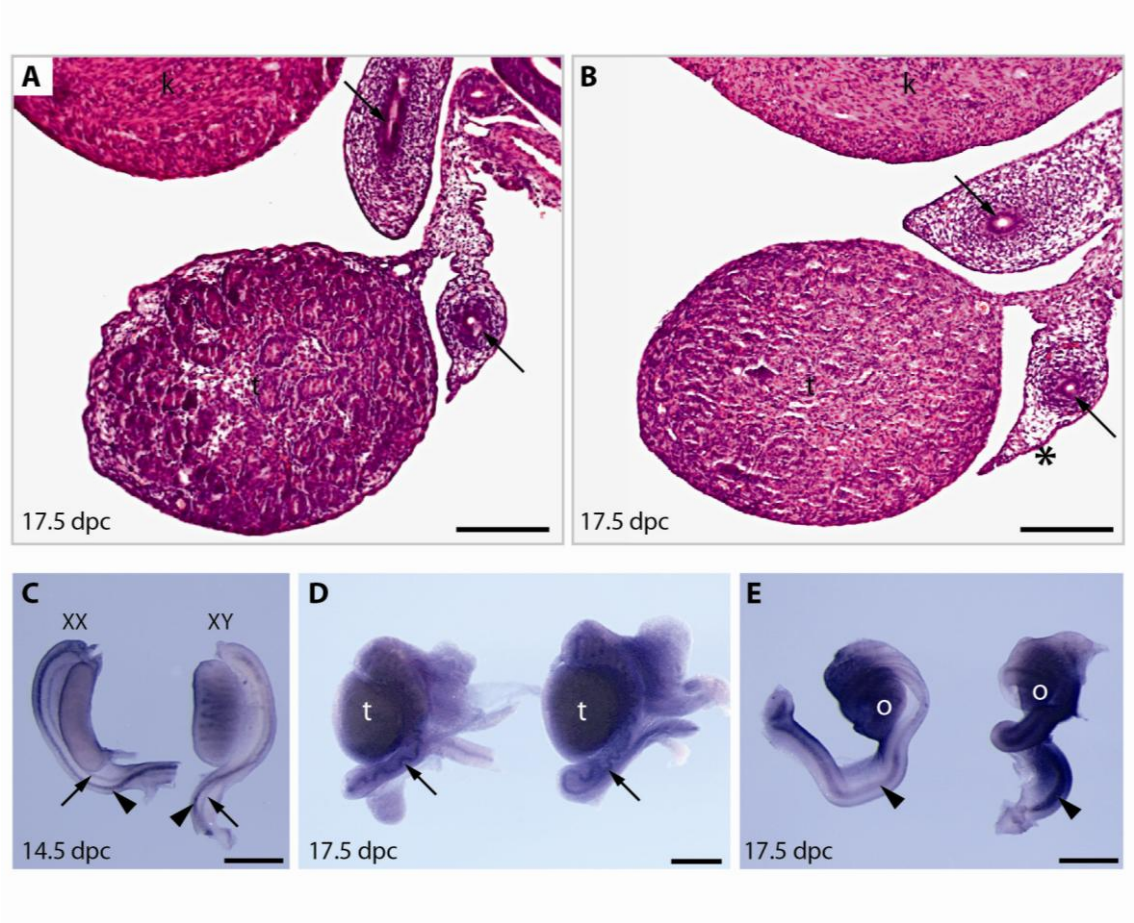

Figure 5.11: Analysis of Müllerian duct regression in male *Amhr2Cre-Mapk14*-cKO
Embryos were collected at 17.5 dpc from NORM G3 litters. *Mapk14*$^{flox/+}$*; Amhr2-Cre/+* embryos were used as controls. (**A-B**) The testes, kidneys and male reproductive tracts were removed for H&E-stained section histology. (A) Seminiferous tubules are clearly visible in the control testes with the epididymis and vas deferens as the only ducts present in the mesonephros (arrows). (B) No obvious defects were visible in the mutants. Seminiferous tubules had developed normally and there was no evidence of a persistent Müllerian duct alongside the Wolffian duct in the mesonephros (site of a persistent Müllerian duct if present is marked by an asterisk). (**C-E**) *Pax2* WMISH expression that marks both the Müllerian duct and Wolffian duct as shown in the 14.5 dpc C57BL/6J wild-type (arrowheads and arrows, respectively, C). At 17.5 dpc only the Wolffian duct was visible in male mutants (right, D) and is comparable with the male controls (left, D). 17.5 dpc females were also analysed, with the Müllerian duct clearly visible in both controls (left, E) and mutants (right, E). Scale bars = 200 µm (A,B), 500 µm (C-E). k, kidney; t, testis; o, ovary; arrows, Wolffian duct; arrowheads, Müllerian duct.

5.2.3.5. Analysis of male and female gonad development

To complete the embryonic phenotypic analysis, gonads were collected at 14.5 dpc and the gene expression patterns of five key sexual development genes were analysed by WMISH. The DEL mutant gonads were analysed separately from the NORM mutant gonads in case of any difference in the phenotype. No obvious defects were seen in the expression patterns of any of the key genes in either male or female NORM mutant gonads, or in the DEL mutant gonads (Figure 5.12).

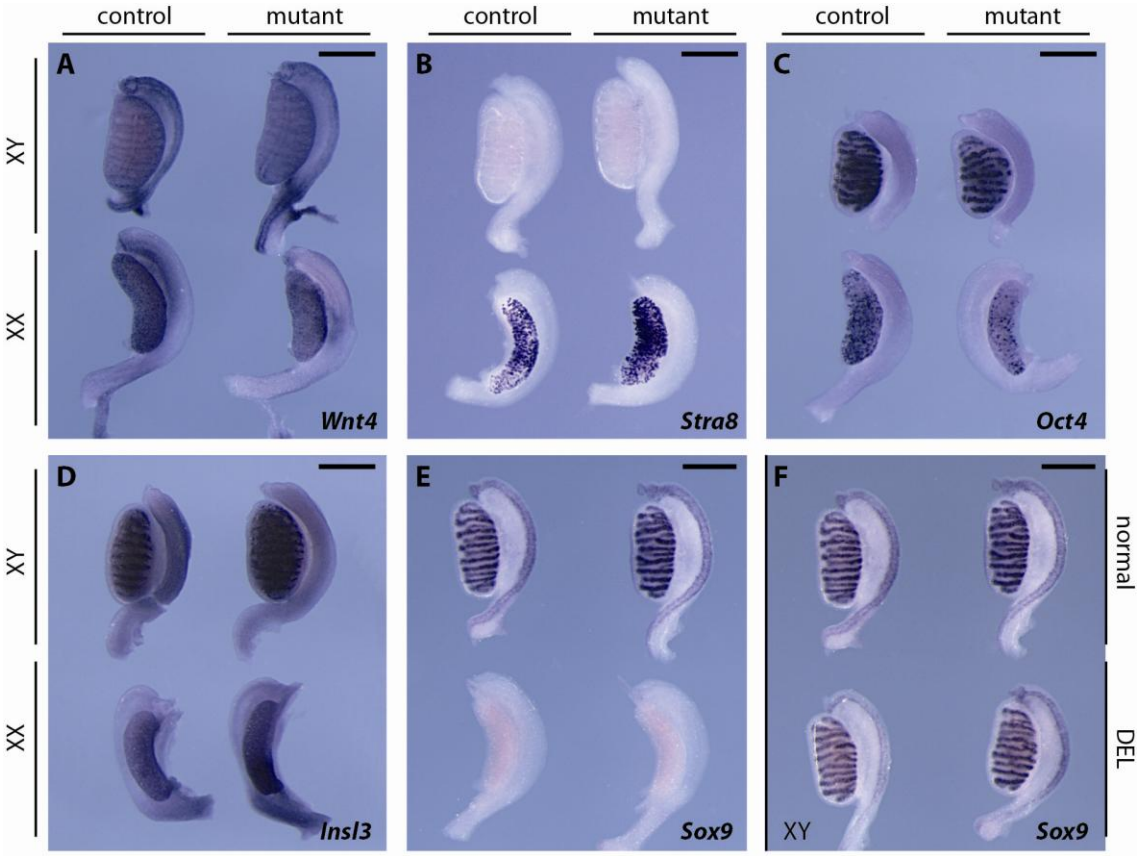

Figure 5.12: Gonadal analysis of *Amhr2Cre-Mapk14*-cKOs
WMISHs performed on 14.5 dpc gonads from NORM G3 litters and from DEL G3 litters. (**A-E**) NORM G3 litter analysis: *Wnt4* (A); *Stra8* (B); *Oct4* (C); *Insl3*, which marks male Leydig cells (D); and *Sox9* (E). The controls (left side of each image) are littermates and are a range of all non-mutant genotypes. Mutants are on the right side with males on the top row and females on the bottom. (**F**) *Sox9* expression in male controls and mutants from NORM G3 litter (top row) in comparison with male controls and mutants from DEL G3 litters (bottom row). No difference was observed in the DEL mutants compared to controls or to NORM mutants with any probe analysed (other marker analysis data not shown). All scale bars = 500 μm.

5.2.3.6. Male fertility and morphology

To ensure there were no morphological defects or male infertility in the *Amhr2Cre-Mapk14*-cKO mice, three mutant males were placed into fertility testing at approximately 8 weeks of age with C57BL/6J females of known fertility for 1 month (Table 5-7). Embryos were collected from pregnant females at 13.5 dpc to determine the litter sizes. Approximately six females were mated with each male during this time. Of the females that were pregnant, an average litter of 7.76 embryos was observed. Although control males were not tested at the same time, comparison with the control males from the *Sf1-Cre*-driven deletion (section 5.2.2.5) suggested that there was a slight decrease in litter size; however, *Amhr2-Cre* mutant males were still fertile, and this decrease was not significant. At the end of the one-month fertility-testing period, males were culled at approximately 13 weeks of age and assessed for any gross morphological defects; however, no gross abnormalities were observed (Figure 5.13).

Table 5-7: Fertility testing results of male mutants
N is number of animals. Values are expressed as average ± SEM

Mapk14; Cre	Sex	*N*	# litters	# of embryos	Average litter size	*p* (t-test) c.f. XY control
flox/flox; *Amhr2-Cre*/+	M	3	17	132	7.76 ± 0.53	0.068
flox/+; *Sf1-Cre*/+	M	6	16	144	9.00 ± 0.38	

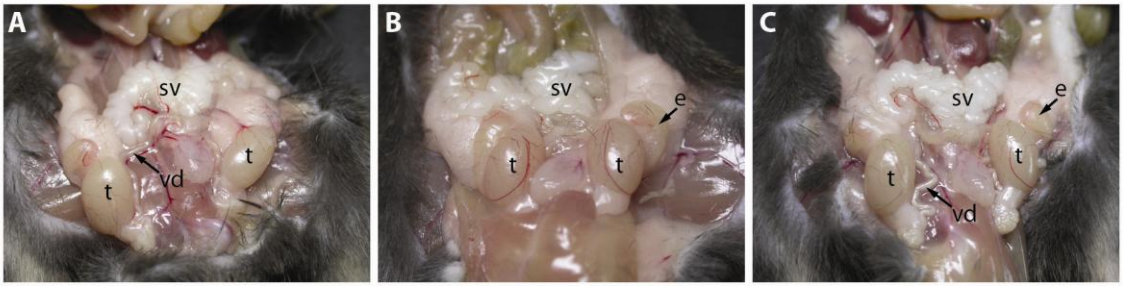

Figure 5.13: Gross morphology of male *Amhr2Cre-Mapk14*-cKO mutants
Three mutants were sacrificed at approximately 13 weeks of age to assess the gross internal morphology of the reproductive organs. All three mutants (**A**-**C**) appeared normal, with normal-sized testes, no evidence of cryptorchidism, and seminal vesicles with normal appearance. Controls were not assessed at the same time. t, testis; sv, seminal vesicle; vd, vas deferens; e, epididymis.

5.2.3.7. Female fertility and histology

If Müllerian duct development was disrupted in any way in female mutant mice this might result in infertility. This conclusion also applies to a defect in granulosa cells if site-directed recombination in these cells affected granulosa cell function and resultant oocyte development and maturation processes. Therefore, females were also mated to test their fertility (Table 5-8). Four mutant females (two NORM mutants and two DEL mutants) and four control females (*flox*/+; *Cre*/+) at approximately 19 weeks were mated with C57BL/6J males. Due to the limited number of female mutants available to test, they were allowed to litter down and newborn pups were counted, and removed. The females were then mated again to produce another litter. This was repeated over the course of two months with the aim of two or three litters per female in that time. At the end of the two-month period, the data were collated. Control females produced an average of two litters each, with 6.5 pups per litter. However, the mutant females produced significantly less. NORM mutants produced one litter between them, containing just three embryos over the whole two-month period; DEL mutants did not produce any litters at all. Due to the way that the matings were set up, the presence of the copulatory plug was not checked. Statistical analysis using a two-tailed student's *t*-test showed that mutant females were significantly less likely to produce a litter, and when they did, it contained significantly fewer pups.

Following the two-month fertility testing, female mutants and controls were sacrificed at approximately 7.5 months of age and analysed for gross morphological defects. The mutants were of an average size and weight and the ovaries appeared normal. However, the uterine horns of some of the mutants appeared shorter and more dilated (Figure 5.14). Histological analysis using H&E-stained sections also showed that the ovaries were undergoing normal follicle cycling, since all stages could be detected (Figure

5.15A-C). Released ova were observed in the oviducts of some mutants confirming normal ovary function (Figure 5.15D-E). One mutant displayed unilateral dilation of a uterine horn that lacked endometrial glands (Figure 5.15C,F,L) and another sample contained a micro-cyst in the oviduct, which is likely to be a cystic endometrial gland (Figure 5.15I). However, these abnormalities were not consistent amongst the four mutant samples and could therefore be normal variation.

Table 5-8: Fertility testing results for female mutants
N is number of mice. Values are expressed as average ± SEM. *for mutant females, litters for the three non-pregnant mice were denoted as having 'zero' pups, to permit statistical analysis. Statistical analysis was performed using a student's *t*-test and *p* value ≤ 0.05 was classed as significant.

Mapk14; Amhr2-Cre	Sex	*N*	Total litters	Total pups	Average litter size*	Litters/female*
flox/flox; *Cre*/+	F	2	1	3	0.75 ± 0.75	0.25 ± 0.25
DEL/flox; *Cre*/+		2	0	0		
flox/+; *Cre*/+	F	4	8	52	6.50 ± 0.82	2.00 ± 0.41
p (*t*-test)					0.005	0.011

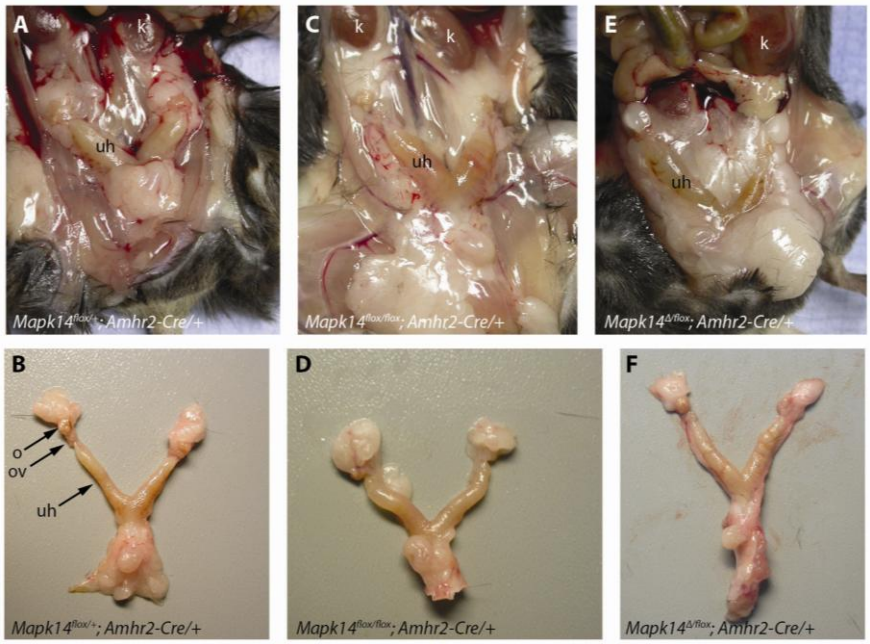

Figure 5.14: Gross morphology of *Amhr2Cre-Mapk14*-cKO females
Females at 7.5 months of age were analysed for gross internal morphology. *Mapk14*$^{flox/+}$*;Amhr2-Cre/+* controls (**A**,**B**) were compared with NORM G3 mutants (**C**,**D**) and DEL G3 mutants (**E**,**F**). The mutant uterine horns from both categories were often shorter and more distended than the control littermates, with one DEL G3 mutant displaying unilateral dilation of the uterine horn to twice the width of the other side (left, E).

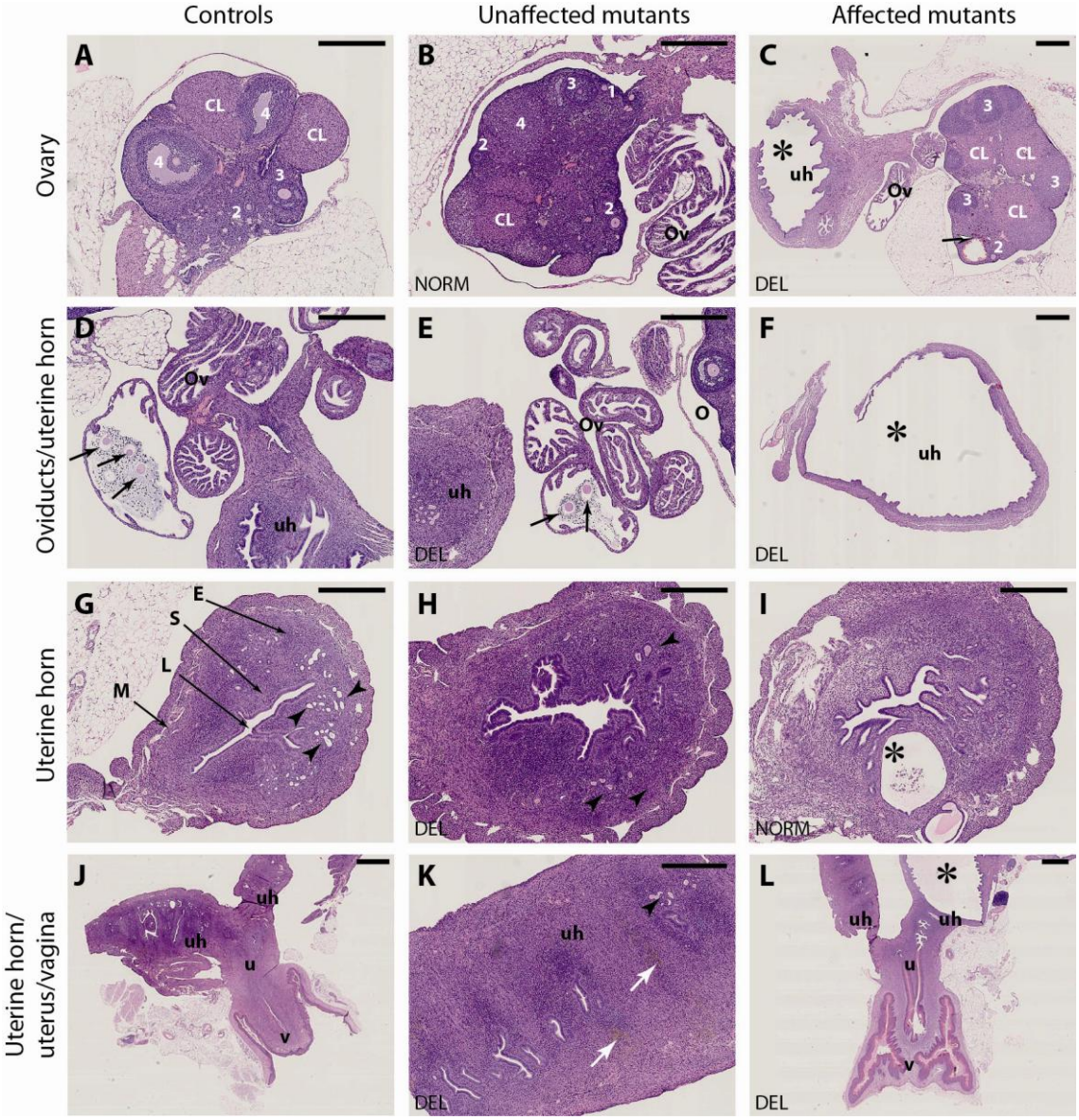

Figure 5.15: *Amhr2Cre-Mapk14*-cKO female histology analysis
H&E-stained histology sections of adult female reproductive tissues to compare NORM and DEL mutants with *Mapk14*$^{flox/+}$; *Amhr2-Cre* heterozygous controls. Most mutants exhibited normal histology (2nd column) but in some samples defects were detected (asterisks, 3rd column). No differences between NORM mutants or DEL mutants were observed. (**A-C**) Analysis of ovaries: control (A) and unaffected mutant (B) displaying normal folliculogenesis, but some haemorrhaging was notable in one affected mutant sample (arrow, C). (**D-E**) The oviducts were unremarkable in the mutants (E), and ova were detected in both control (D) and mutant samples (arrows). (**F-I**) Cross-sections of the uterine horns: Control sample (G) and unaffected mutant sample (H) displaying normal histology with endometrial glands (arrowheads). In one mutant sample (I) an endometrial cyst was detected (asterisk), while another was severely dilated and lacked endometrial glands (asterisk, F). (**J-L**) Longitudinal section of the uterine horns, uterus and vagina: Normal control (J) and mutant (K) uterine horn, with endometrial glands (arrowheads) and haemosiderin pigment (arrows) visible. (L) One mutant displayed unilateral dilation of the uterine horns (asterisk) (this sample is also visible in (C) and (F) sections), however uterus and vagina were normal. Stages of folliculogenesis labelled: 1) Primary follicle; 2) Secondary follicle (preantral); 3) Tertiary follicle (antral); 4) Late tertiary follicle (preovulatory); CL, corpus luteum. Ov, oviduct; uh, uterine horn; o, ovary; L, lumen; S, Stroma; E, endometrium; M, myometrium. Scale bars = 500 µm (A-I,K), 1 mm (J,L).

In an attempt to identify the cause of the observed infertility, three more mutants and three controls were mated with C57BL/6J males at 21 weeks of age. These were plug-checked, and at 2.5 dpc the females were sacrificed and the uterine horns flushed for the collection of morulae. The number of morulae extracted was recorded, and healthy morulae were then cultured to check their ability to develop to the blastocyst stage (Table 5-9). NORM mutant females produced 5 healthy morulae that were able to develop into blastocysts, and 14 unhealthy morulae; controls produced 32 healthy and 6 unhealthy morulae (Figure 5.16). These results show that the mutant females exhibited a normal mating response due to the presence of the copulatory plug and that fertility issues occur after this point. The production of a few healthy morulae suggests the oocytes are maturing normally. Too much weight cannot be placed on the increased number of unhealthy morulae due to the low numbers involved, but it is tempting to speculate that the defects occur before implantation. However, the ability of the morulae to culture to blastocysts suggests that the ova are healthy. Although the ovaries are histologically normal, a defect in function of the granulosa cells to nurture the oocytes cannot be ruled out. Further work will be required to address these questions.

Table 5-9: Results from morula harvest from *Amhr2Cre-Mapk14*-cKO females
Morulae were collected at 2.5 dpc from 21-week old females. The healthy 8-cell morulae were cultured for 72 hours and all, including morulae from the mutants, cultured successfully into hatching blastocysts. A decrease in the number of healthy morula from the mutants was observed, with a higher percentage damaged, unfertilised or 2-cell staged. Due to the low numbers, this was not significant.

Mapk14; Amhr2-Cre	Sex	*N*	Total litters	Total embryos	Healthy 8-cell morulae	% unhealthy
flox/flox; *Cre*/+	F	3	2	19	5	74
flox/+; *Cre*/+	F	5	4	38	32	16
p (*t*-test)					0.270	0.325

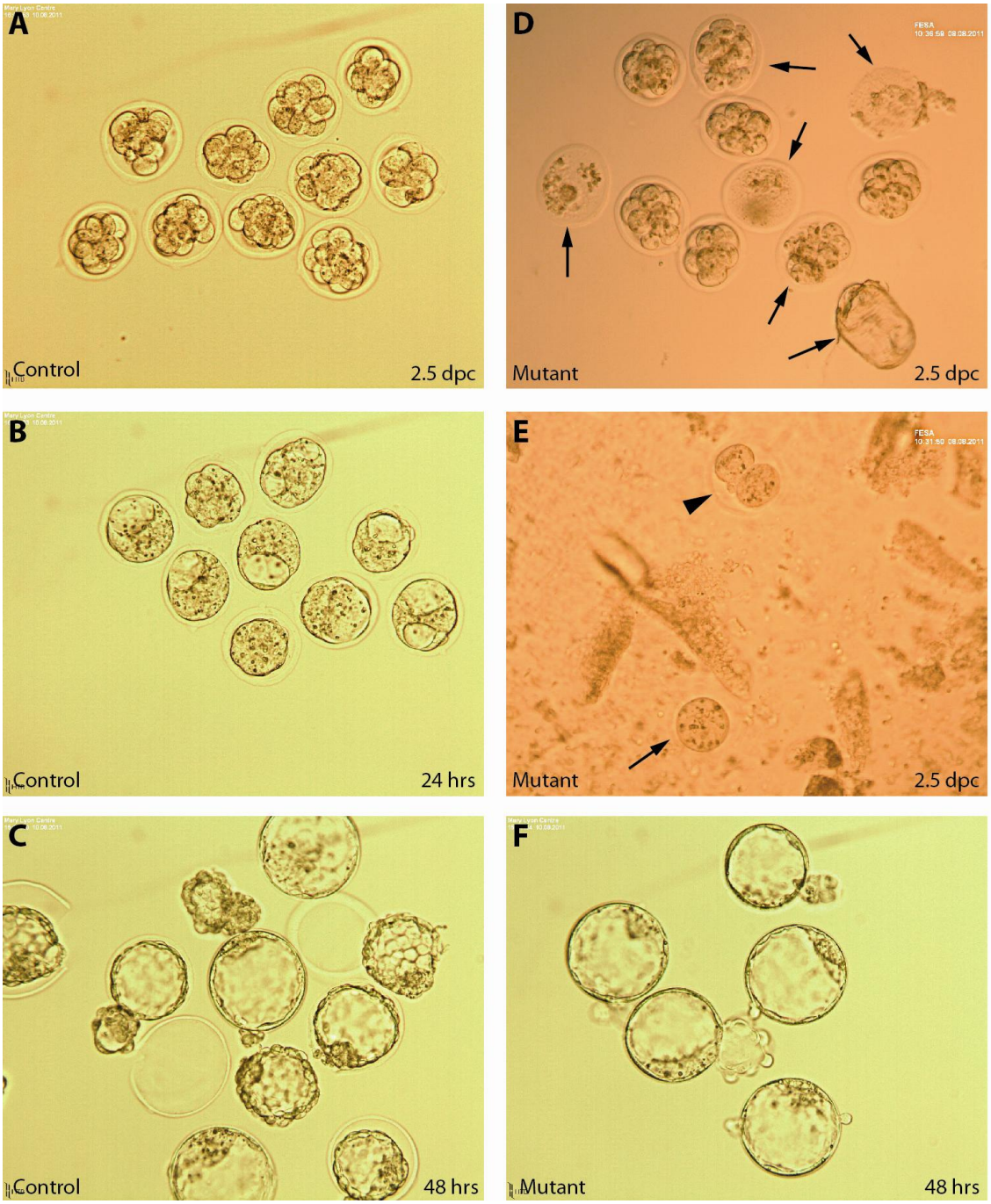

Figure 5.16: Morula collection from *Amhr2Cre-Mapk14*-cKO litters
Morulae were collected at 2.5 dpc from *Mapk14*$^{flox/flox}$*; Amhr2-Cre/+* NORM mutant mothers and *Mapk14*$^{flox/+}$*; Amhr2-Cre/+* controls by flushing out the uterine horns. (**A-C**) 32 healthy morulae from controls were collected (A) and these cultured successfully up to 72 hours to the hatching blastocysts stage (B-C). (**D-F**) Fewer healthy morulae were collected from mutants, with 74% of the morulae damaged (arrows, D), unfertilised (arrow, E) or just two-cell staged (arrowhead, E). The 5 healthy morulae (unmarked, D) cultured successfully for 72 hours until the hatching blastocysts stage (F).

5.3. Discussion

Here, I have shown that deletion of *Mapk14* in either somatic cells of the gonad or Müllerian duct mesenchyme is not detrimental to either gonad or reproductive tract development. In contrast, inhibition of p38α and p38β in organ culture with a specific small-molecule inhibitor at 11.5 dpc resulted in XY somatic and germ cell sex reversal (Bogani et al. 2009; Ewen et al. 2010). Deletion of *Mapk14* using *Amhr2-Cre* did disrupt female fertility, but the exact mechanism behind this defect could not be elucidated.

A role for *Mapk14* in adult ovaries had previously been shown by a deletion in granulosa cells (using *Cyp19-Cre*) that affected gene expression profiles of pre-ovulatory follicles and cumulus cell-oocyte complexes, but did not disrupt fertility (Liu et al. 2010). Small molecule inhibitor studies using either SB203580 or SB202190, which are specific to p38α/β MAPK, have also shown that follicle-stimulating hormone (FSH) can activate the p38 MAPK pathway in rat granulosa cells (Maizels et al. 1998). While these inhibitor studies have been very useful in determining a role for the p38 MAPK pathway in both testis development and ovary function, the results presented in this chapter have provided the first *in vivo* evidence of a critical function in female fertility.

Amhr2-Cre has been documented to drive targeted deletion in granulosa cells previously, resulting in infertility due to the inactivation of follistatin (*Fst*) (Jorgez et al. 2004). Follistatin is a key negative regulator of FSH due to its ability to bind and neutralise activins (Ueno et al. 1987). The phenotype of the resultant conditional knockout female is broadly similar to that observed with the conditional deletion of *Mapk14* using *Amhr2-Cre*. The *Fst* conditional knockout females also produce fewer

litters and have reduced litter sizes, with some females being completely infertile. In immature mice, until 3 months of age, ovarian histology was normal in comparison with controls. However, after 3 months of age defects were observed that were more severe in aged mice, indicating a degeneration of ovarian function with age. At 3 months, follicles were still present within all stages of folliculogenesis, however, fewer antral follicles and corpora lutea were observed. By 6 months, these defects were more severe, and by 8 months of age very few follicles were present at any stage but there was a significant increase in zona pellucida remnants indicating oocyte cell death. The ability of oocytes to be fertilised at 3 weeks and 6 months of age was assessed by this group through superovulation of females and the collection of oocytes and one-cell embryos 20 hours later. At 3 weeks, the conditional knockout females displayed normal fertility in comparison with controls, but at 6 months, a significant decrease was observed in both the number of oocytes released and the number that had developed to the two-cell stage after 24 hour culture.

Although the fertilisation tests I carried out on the *Amhr2Cre-Mapk14*-cKO females were limited due to i) the availability of just three experimental mice (compared to seven of 6-months-of-age in Jorgez *et al.* 2004) and ii) collecting 2.5 dpc morulae after natural matings instead of after superovulation, it is possible that similar results may have been observed if the numbers were higher. Further work would be required to determine whether *Fst* and *Mapk14* operate in the same cellular pathways of female reproductive tract development.

It may be that *Mapk14* has a key role in the development of the female reproductive tracts and targeted deletion in the Müllerian duct mesenchyme driven by *Amhr2-Cre* results in the infertility that is not observed with granulosa cell-specific deletion using

Cyp19-Cre (Liu et al. 2010). The uterine horns were notable for being more dilated in *Amhr2Cre-Mapk14*-cKO mice than in controls, and the ability of healthy morulae from these experimental mice to culture to the blastocyst stage suggests that there are no defects in oocyte production and fertility, but that, alternatively, the oviduct or uterine horns are not providing the right environment for the support of the early-stage embryos.

Other models of female infertility through gene inactivation driven by *Amhr2-Cre* also display similar phenotypes to the inactivation of *Mapk14* in the same cell types. These include the inactivation of *Gata4* (Kyrönlahti et al. 2011b) and of β-catenin (*Ctnnb1*) (Hernandez Gifford et al. 2009). *Gata4* conditional knockouts display reduced fertility but normal morphology and histology up until 6 months of age. After this, differences in both gross and histological appearances of ovarian tissue were apparent, including non-haemorrhagic ovarian cysts. These *Gata4* conditional knockouts appear to have impaired function of granulosa cells exhibited by reduced AMH levels, and also have an impaired response to gonadotrophins. Conditional knockouts of *Ctnnb1* displayed complete infertility at all ages studied, from 2 months through to 8 months. However, the ovarian gross and histological phenotypes appeared to be normal. Instead, oviductal and uteri abnormalities were apparent with failed implantation of the released oocytes, and grossly distended oviducts and disrupted coiling.

GATA4 is reported to be regulated by FSH through increased phosphorylation regulated by FSH-mediated protein kinases, including ERK1/2 and protein kinase A (Kwintkiewicz et al. 2007). In addition, due to similarities between the two *Gata4* and *Ctnnb1* conditional knockouts driven by *Amhr2-Cre*, it is postulated that *Gata4* regulates the β-catenin/WNT pathway in adult ovaries. As FSH also activates p38

MAPK, it is possible that p38α could be involved in the GATA4/β-catenin regulation of granulosa cells and oestrogen production.

Analysis of male *Gata4* conditional knockouts driven by *Amhr2-Cre* also highlights a role for *Gata4* in Sertoli cell function in adult mice (Kyrönlahti et al. 2011a). Males were fertile with no abnormalities until 6 months of age, following which severe testicular atrophy and a decline in fertility were observed. The analysis of male *Amhr2Cre-Mapk14*-cKOs was very limited due to time constraints and the limited number of mice available. Up until 3 months of age there were no obvious abnormalities, but analysis of older mice was not possible. This possibility of age-related defects in these mutant mice would warrant further study.

While the deletion of *Mapk14* using *Amhr2-Cre* has generated an interesting female infertility phenotype, the most notable result, from the perspective of gonad development and the role of the MAPK pathway in testis determination, is that the *Mapk14* deletion driven by *Sf1-Cre* in somatic cells of the early gonad did not disrupt sexual development. Inhibition of p38α and p38β in gonad organ culture using small molecule inhibitors such as SB202190 (Bogani et al. 2009) and SB203580 (Ewen et al. 2010) has provided *in vitro* evidence for a role of these two p38 MAPKs in XY gonad development. The specificity of these small molecule inhibitors has been assessed in detail (Davies et al. 2000). Both inhibitors are pyridinyl imidazoles that inhibit the p38α and p38β MAPKs. SB203580 is very selective towards these kinases, with concentration values required to achieve 50% inhibition (IC_{50}) of 50 nM and 500 nM respectively. However, it does also inhibit LCK, GSK3β and PKBβ protein kinases, albeit with 100-500-fold higher IC_{50} values. SB202190 has very similar inhibitory properties, but with stronger inhibition of p38β, as the IC_{50} values for p38α and p38β

were 50 nM and 100 nM respectively. It also slightly inhibited LCK, PKBβ and GSK3β along with PKA and ROCK-II. Their ability to inhibit upstream kinases (MAP2Ks or MAP3Ks) was not tested. The ability of both drugs to inhibit protein kinases depends on the size of the amino-acid side chain at position 106 (Wilson et al. 1997). In p38α and p38β, a threonine is found at this position. A kinase with a larger residue at this site, such as in p38γ and p38δ, is insensitive to the drug, while a kinase with a threonine, or smaller residue, will also be inhibited by the drug. Despite the fact that JNK kinases are reported to be resistant to inhibition due to the presence of methionine at position 106, one group has reported that some isoforms of JNK2 are slightly inhibited in the presence of SB203580 (Whitmarsh et al. 1997). However, the IC_{50} value was much higher: 10-20 μM inhibitor was required to reduce JNK2β to basal levels and 100 μM for JNK2α, compared with the 1 μM required to reduce p38α to basal levels. Moreover, this inhibition of JNK isoforms was assessed by Eyers *et al* who also identified the slight inhibition, but at 50-500 fold higher IC_{50} than p38α (Eyers et al. 1999). However, they did not find evidence that the phosphorylation of two putative substrates of JNK was affected as a consequence. Therefore, as long as SB203580 and SB202190 are used in the lowest concentration necessary to inhibit p38α and p38β, other non-specific effects should be avoided.

Inhibition with SB202190 as late as 11.5 dpc, significantly later than the initial up-regulation of *Sry* and subsequent activation of *Sox9,* is sufficient to decrease *Sox9* levels and increase *Wnt4* in the somatic cells of the XY gonad. Ewen *et al* suggest that this supports their hypothesis that p38 MAPKs affect the differentiation of germ cells and that inhibition at such a late stage means it is likely that the observed effects are a direct effect on germ cells, rather than an indirect effect through inhibition of *Sry* expression. Perhaps there is an important role for p38 MAPKs in both somatic cells and germ cells

and a global deletion of *Mapk14* in the whole gonad is required to see an effect. A simple way to address this would be to perform embryo-specific *Mapk14* deletion using a *Mox2-Cre* (*MORE-Cre*) driver (Hui et al. 2007; Perdiguero et al. 2007). *More-Cre* is expressed throughout the epiblast following implantation and therefore not in extra-embryonic tissues, avoiding the embryonic lethality observed with the constitutive knockout (Tallquist and Soriano 2000). Expression of the *More-Cre* recombinase is observed from 5 dpc and the *Mapk14* conditional knockout mice survive until postnatal day 4, which would enable analysis of embryonic gonad development. The identification of a gonadal phenotype in this embryo-specific deletion of *Mapk14* would highlight two different hypotheses. Either, i) germ cells play a key role as Ewen *et al* suggest, and it is the affect of *Mapk14* on germ cell differentiation that dictates the sex-specific gonad development pathway in the organ culture model, or ii) the deletion of *Mapk14* much earlier in development, at least earlier than permitted by *Sf1-Cre*, is required to disrupt testis development.

The experiment outlined above would be important for addressing some of the potential reasons why a phenotype is not seen with the *Sf1-Cre*-driven deletion of *Mapk14*, namely, embryonic stage of deletion and/or the contribution of defects in other cell-types. There are also several other potential reasons for the absence of a gonadal phenotype. Functional redundancy amongst the different p38 isoforms could compensate for the loss of *Mapk14* – perhaps *Mapk11* (p38β) is also crucial, as the inhibitor studies may suggest, or *Mapk13* (p38δ), which is strongly expressed in the testis in comparison with the ovary. It could also be that a functionally unimportant MAPK has been targeted and JNK is the vital link between *Map3k4* and testis determination. The main point that needs to be addressed to enable further study in this

area is the exact gonadal cell lineage(s) in which *Map3k4*-activated signalling is required.

The conditional knockout strategy employed in this chapter does have limitations. Firstly, the breeding scheme required inactivation of two floxed alleles simultaneously, which could have delayed the ablation and subsequent onset of a phenotype. It is possible to design a breeding scheme incorporating a null allele in place of the floxed allele in the *flox/+; Cre/+* males in the G2 generation. This would result in *null/flox; Cre/+* experimental offspring in which only one floxed allele needs to undergo site-specific recombination. However, the null allele of *Mapk14* was not initially available and due to time constraints it was not possible to wait for the generation of *null/flox; +/+* mice from the *β-actin-Cre* driven deletion. The significance of the potentially delayed ablation of two floxed alleles is highlighted by a report on the use of *Amhr2-Cre* to drive the tissue-specific deletion of *Ctnnb1* (Deutscher and Yao 2007); the phenotypes observed in the *Amhr2-Cre*; $Ctnnb1^{flox/flox}$ embryos were less severe than those observed in the *Amhr2-Cre*; $Ctnnb1^{flox/-}$ embryos.

Secondly, it was not possible to address the efficiency of the conditional inactivation and the amount of mosaicism resulting from the use of either *Cre* driver. Ideally, the presence or absence of the specific *Mapk14* mRNA transcript and protein would have been detectable in wild-type and conditionally inactivated cells by WMISH and immunohistochemistry. However, due to the floxed region of the *Mapk14* allele only encompassing exons two and three, the *Mapk14* riboprobe for use in WMISH would not differentiate between either the floxed mRNA transcript or the deletion mRNA transcript, unless the stability of the deletion transcript had been significantly disrupted. This is also true for qRT-PCR analysis, as the TaqMan probe used would have to anneal

to the floxed region so that it could differentiate between the wild-type allele and recombined allele; normal expression levels would only be detected from the wild-type allele, whereas the presence of the recombined deletion allele would result in reduced levels of *Mapk14* detected. Detecting p38α protein would have been the most reliable method, but unfortunately I did not have a reliable antibody. Therefore, the success of the recombination was determined by the presence of the deletion allele detected by standard PCR. Unfortunately, the lack of a phenotype does not help confirm the successful recombination and high efficiency. A different method to confirm gene inactivation involves modifying the targeting vector to include a reporter gene in such a way that the inactivation of the targeted gene causes activation of the reporter. The reporter activity can then be detected in the cells with gene inactivation (Kwan 2002). This approach has been reported in limb-specific inactivation of *Fgf8* (Moon and Capecchi 2000), however, reporter activity cannot differentiate between the successful recombination of one allele or both alleles. A variant of this approach was also very recently reported with a *Mapk14* conditional inactivation by Bruchas *et al*, who studied the deletion in parts of the brain to determine the function of the kinase in depression and addiction through a stress-activated response (Bruchas et al. 2011). However, in this case, the reporter was located in a different construct to the floxed allele, and therefore expression only confirmed the presence of functional *Cre*, since it is known that not all floxed loci delete with the same efficiency (see below).

Another limitation to the conditional knockout method, particularly pertinent for the *Sf1-Cre*-driven deletion, is the lag between onset of *Cre* expression and deletion of targeted protein. This is summarised in the diagram below (Figure 5.17), based on Nagy, 2000 (Nagy 2000). The *Cre* recombinase-mediated excision of the target is a stochastic event since it does not occur at the same time in all the cells of the target

lineage. There are a number of different factors that can affect the speed of excision, including the expression characteristics of the *Cre* enzyme, the availability of the floxed sequence, and mRNA and protein half-lives of the target gene. Assessing the expression of the *Cre* enzyme by crossing with the reporter R26R and staining for β-galactosidase activity is very useful for determining the approximate stage when the target is deleted. However, the R26R floxed region is excised very efficiently and often more easily than the experimental floxed region, meaning that the R26R results have to be taken only as a guide. Similarly, *β-actin-Cre* is a very efficient *Cre* deleter, so the resulting excision does not necessarily indicate that the floxed region will be deleted as efficiently by the experimental *Cre* driver. These issues may be more pertinent when studying testis determination, a process which is known to be extremely sensitive to the timing of particular molecular and cellular events. What is required is a way of determining whether *Sf1-Cre* is a suitable *Cre* line for studying the MAP3K4 pathway, independently of questions of functional redundancy. This question is addressed in the next chapter.

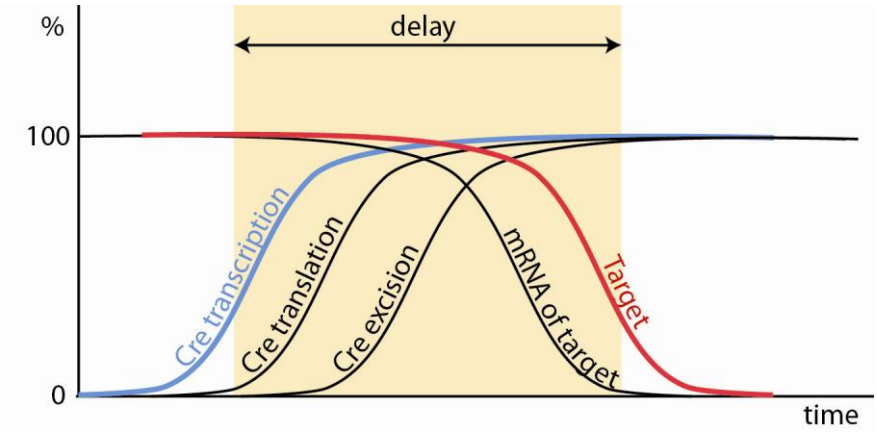

Figure 5.17: Delay of *Cre* action
Graph to show the delay between the activation of the promoter and consequent *Cre* transcription through to the reduction of functional target protein in the *Cre*-expressing cells. This delay includes time from *Cre* transcription to translation of the recombinase protein and recombination of the subsequent targeted sequence. This recombination does not occur in all cells at the same time, so there is a lag in the drop off of target mRNA, and the half-life of the target protein impacts on the time it takes for the levels of the target protein to decrease significantly. Figure adapted from (Nagy 2000).

Chapter 6. Further studies on the mechanism of MAP kinase signalling in gonad development

6.1. Introduction

The conditional inactivation of *Mapk14* driven by *Sf1-Cre* in the somatic cells of the gonad does not affect sex determination or gonadal development, despite the link between chemical inhibition of p38α/β and XY gonadal sex reversal in an organ culture model. This inhibition of p38α and p38β *in vitro* at 11.5 dpc is sufficient to down-regulate the expression of *Sox9* and up-regulate the expression of *Wnt4*. The XY sex reversal is also seen in germ cells as evidenced by the increase in *Stra8* expression in XY samples. As discussed in the previous chapter (section 5.3), there are many potential reasons for the absence of a gonadal phenotype after somatic cell-specific ablation of *Mapk14* in the gonad. These include: possible functional redundancy amongst the different p38 MAPKs; an alternative p38 MAPK, other than *Mapk14*, may be the important regulator; deletion at an earlier embryonic stage may be required; the MAP3K4-activated pathway may be active in a different cell lineage; or, finally, a completely different MAPK may function in testis determination, such as one or more of the JNKs. Work described in this chapter attempts to address these points.

Due to the time-consuming nature of breeding conditional knockouts and the complexity involved with attempting a multiple gene knockout when one of the alleles requires conditional inactivation, other methods to determine whether functional redundancy is an issue were explored. Gene knockdown can provide a valuable insight into function, whilst also providing the flexibility of targeting multiple gene transcripts at the same time, along with the possibility of using either cell or organ culture to exclude the need to generate large numbers of mice. One way to facilitate gene

knockdown is the short interfering RNA (siRNA)-induced activation of the RNA interference (RNAi) pathway to degrade mRNA.

Most siRNAs are exogenous, short 21-25 nucleotide (nt) double-stranded (ds) RNA molecules that are commonly introduced into the cell by viruses in the form of longer dsRNAs. The presence of these dsRNAs in cells triggers the RNAi pathway to facilitate gene silencing, and this process is reviewed extensively by G.Hannon (Hannon 2002). The key initiation of this RNAi pathway is through an RNase III enzyme, Dicer. Dicer recognises long dsRNAs and processes them into siRNAs with 2 nt overhangs at the 3'-ends (Bernstein et al. 2001; Elbashir et al. 2001b). The siRNAs are then incorporated into a RNA-induced silencing complex (RISC), which is comprised of the Argonaute family of proteins, and results in the unwinding of the ds siRNA and subsequent activation of the RISC complex. The activated RISC uses the single-stranded unwound siRNA to direct it to the complementary mRNA target. As a result, the target mRNA is cleaved, preventing the initiation of translation and thus effecting a gene silencing mechanism. The single-strand siRNA/RISC complex can cleave many complementary mRNA sequences in this manner, since the siRNA is not destroyed in the process. This RNAi pathway is conserved across many different species including plants, worms and mammals.

Not only does Dicer process exogenous dsRNAs into siRNAs, but it also processes numerous endogenous small RNAs known as microRNAs (miRNAs). These miRNAs also use the RISC complex to effect gene silencing but through a slightly different mechanism. miRNAs typically have incomplete base pairing to the target gene and consequently cause translational repression of many mRNAs with similar sequences, rather than the mRNA degradation that results from binding of siRNAs that have

complete complementarity to their target. miRNAs are non-coding RNAs transcribed to regulate gene expression through silencing of cognate mRNAs and are essential during development (Sayed and Abdellatif 2011). The primary miRNA transcripts (pri-miRNA) consist of multiple hairpin loops that are processed into a 70 nt stem-loop pre-miRNA by a microprocessor complex. This microprocessor complex consists of an RNaseIII enzyme, Drosha, and a dsRNA-binding protein, Pasha. The pre-miRNAs are transported out of the nucleus by a nuclear transport receptor complex and cleaved by Dicer into a mature ~22 nt ds miRNA with asymmetric 3'-ends. This miRNA is then processed by RISC for translation repression as described above. The importance of gene regulation by this pathway is highlighted by the finding that the knockout of *Dicer1* in mice causes early embryonic lethality by 7.5 dpc (Bernstein et al. 2003).

Due to the function of the RNAi pathway, exogenous dsRNAs (in the form of small-hairpin (sh) RNAs or siRNAs), can be used for targeted gene knockdown in model organisms that have this RNAi machinery. This method of gene silencing has been extensively studied and trialled to avoid the use of time-consuming and expensive knockouts and is reviewed by W-C.Lee *et al* (Lee et al. 2008). It can be induced through the addition of multiple forms of dsRNA including: simple siRNAs, longer dsRNA made from plasmids which will be cleaved by Dicer in the cell into siRNA, or shRNAs introduced into the cell in either a virus or plasmid by transfection. The method chosen depends on the cost (siRNAs are expensive), accessibility (siRNAs may diffuse better than viruses) and the tissue- or cell-type being transfected (for example in mammalian cells, only viruses are taken up without the need of a transfection reagent).

The most common system for the successful application of RNAi is in conventional cell culture. This method of gene knockdown has been used repeatedly to investigate the

function of genes since the first success (Elbashir et al. 2001a). Unfortunately, the use of siRNA for gene knockdown does have limitations (Sledz and Williams 2005). First, the effect is only transient: in cells, the gene silencing and resultant phenotype is not permanent. Second, the efficacy of siRNA-mediated gene silencing depends on many factors, such as the sequence of the siRNA, the half-life of the targeted mRNA and protein, and the presence of any feedback mechanisms within the cell to control expression of the target gene. A third aspect is that non-specific and off-target effects of the RNAi response can be common. Non-specific effects are known to be possible following the observation that siRNAs can activate other dsRNA response elements, leading to the up-regulation of alternative genes such as those associated with innate immune pathways. Off-target effects involve the ability of siRNAs to trigger the miRNA pathway and thus genes other than the target can have altered expression.

Other applications of RNAi have extended to their *in vivo* delivery in mice and also to explant organ culture. The ability to determine the function of a gene during organ development *ex vivo* is very advantageous and the use of siRNA has been reported in the culturing of salivary glands (Sakai et al. 2003), kidneys (Davies et al. 2004), lungs (Gill et al. 2006) and ovaries (Wang and Roy 2006), to name a few examples. Despite these success stories, relatively few reports documenting the successful use of siRNAs in organ culture have been published, and this is particularly so in the case of developing gonad organ culture. Many research groups have tried to develop a reliable technique, but few have succeeded. There are a handful of examples of the use of siRNA in gonad organ culture including: the use of oligofectamine to facilitate Alks and Smads siRNA knockdown in rat urogenital ridges (Zhan et al. 2006); microinjection of *Sox9* shRNA plasmids into the XY 11.5 dpc gonad followed by magnetically-mediated gene transfection ("magnetofection") to induce localised sex reversal (Svingen et al.

2009); and nucleofection of XY gonads in a 'hanging drop' culture to facilitate partial knockdown of *Sox9* using an shRNA plasmid (Ryan et al. 2010). However, all of these methods have limitations, notably technical difficulty, regionalised effects, poor transfection and low efficiency of gene silencing. The use of siRNA in organ culture not only has the limitations previously mentioned, such as protein half-life and feedback mechanisms employed by the cell to maintain expression of a gene, but is also affected by specific problems associated with organ culture itself. This includes the environment of the cells to be transfected, which are tightly packed together in multiple layers in the explanted organ, often acting as barriers or traps to siRNA diffusion. This is in stark contrast to the accessibility of two-dimensional cell cultures. This 'trapping' of siRNA in organ culture has been observed through the preferential targeting of certain cell types by the siRNA or labelled fluorophores. For example, in salivary glands, successful siRNA delivery is associated with epithelial cells more than mesenchymal (Sakai et al. 2003), whereas in kidneys the opposite effect is observed (Davies et al. 2004). Other delivery methods have been trialled to increase the transfection efficiency, such as Lentiviral delivery of shRNAs. However, there are reports that these viruses are incapable of penetrating deep into tissue (Lee et al. 2008).

Despite all of these limitations, the benefits of finding a robust *ex vivo* knockdown method, and thus assessing functional redundancy amongst the different p38 MAPK isoforms, prompted the trial of two different methods.

6.2. Results

6.2.1. Determining the function of p38 MAPKs in gonad development

One explanation for the conditional ablation of *Mapk14*^{flox} in somatic cells of the gonad not resulting in a sexual development phenotype could be that the inappropriate p38 MAPK was targeted. Although it has previously been documented that individual constitutive knockouts of *Mapk11*, *Mapk12*, and *Mapk13* are viable and fertile, these analyses were not always conducted on a C57BL/6J background, and the ratio of male to female mice produced was not reported. Nor were embryonic gonads systematically assessed in these reports. Moreover, some defects are also very subtle and it may require expertise in the study of gonad development to identify them.

For these reasons, the *Mapk11* constitutive knockout mouse was obtained as a kind gift from J.S.Arthur (Beardmore et al. 2005). The initial plan was to generate a double knockout of *Mapk11* and *Mapk14* to recapitulate the p38α/β inhibitor studies. However, the receipt of *Mapk11* mice was delayed substantially and it became impossible to attempt this in the time that was available. The homozygous *Mapk11* mice that were imported (three male and three female) were reported to be predominantly on a C57BL/6J background, although the number of backcrosses was not known. One male was used for IVF to rederive the line into the animal house at MRC Harwell. The remaining mice were mated together while housed in quarantine to generate embryos with which to assess gonad development. Unfortunately, following 4-5 weeks of mating, copulatory plugs were not detected. This could be the result of a variety of factors including: transport to MRC Harwell disrupting normal mating behaviour, the age of the mice (which was unknown), as well as fertility defects. The homozygous

mice were culled 19 weeks after they first arrived and analysed for gross morphological abnormalities of the reproductive organs. No abnormalities were visible (Figure 6.1).

Timed matings were subsequently performed between the rederived *Mapk11*$^{-/+}$ heterozygotes. Embryos were collected at 14.5 dpc from pregnant females. Of the 20 embryos collected from two litters, five were genotyped (using a PCR-based strategy) as homozygous knockouts. Unfortunately, all were phenotypically female with an XX chromosome constitution; no gross morphological abnormalities of ovary development were observed. Due to time constraints no further litters could be collected and therefore testis development in XY homozygotes could not be assessed. However, due to the fact the line is normally maintained as a homozygous colony with no reported fertility issues, and the gross morphology of the adult homozygous males was normal, it is unlikely that any significant embryonic defects would have been observed. Nevertheless, the possibility of subtle defects, such as delayed testis determination, cannot be ruled out because it is not uncommon for embryonic gonads to recover from mild abnormalities, such as in the formation of testes after initial ovotestes development (Washburn and Eicher 1983; Val et al. 2007).

Again, due to time constraints, gonadal development in the two other p38 MAPK gene knockouts could not be determined. The constitutive knockout of *Mapk12* has been reported and is both viable and fertile on a mixed (C57BL/6J × BALB/c) genetic background (Sabio et al. 2005). Given the low overall expression of *Mapk12* during gonad development, it seems unlikely that this gene, on its own, would have a vital role in gonad development.

There are two different targeted alleles of *Mapk13*. The first was bred on the C57BL/6J background and was maintained as a homozygous colony, confirming viability and

fertility of both males and females (Schindler et al. 2009). This line was also used to generate a double knockout of *Mapk13* and *Mapk12*, also reported to be viable and fertile (Sabio et al. 2005). The second targeted allele (Sumara et al. 2009) also results in viable homozygotes on the C57BL/6J background; however, fertility was not reported. Personal communication with the authors of the study confirmed that fertility had not been tested; however, they had not observed an obvious bias in the male to female ratio in the homozygotes produced from heterozygous intercrosses. It is unlikely that they would have genotyped for the sex chromosomes, but rather determined the sex by phenotype, but it is still unlikely that XY sex reversal had occurred. Due to the strong sexually dimorphic expression profile of *Mapk13* during gonad development, it would be interesting to test the fertility of homozygotes since late-onset fertility defects after 6 months of age in both XY and XX mice, as were seen in the deletion of *Gata4* using *Amhr2-Cre* (Kyrönlahti et al. 2011a; Kyrönlahti et al. 2011b), remain a possibility.

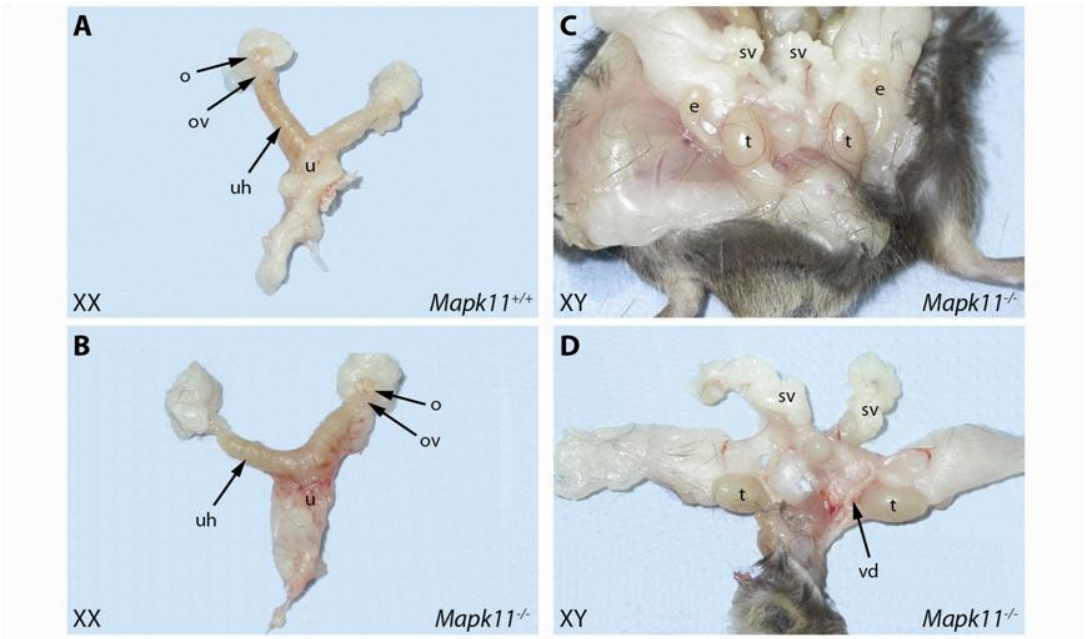

Figure 6.1: Gross morphology of male and female reproductive organs in *Mapk11*$^{-/-}$ mice
Analysis of gross morphology in imported *Mapk11*$^{-/-}$ adult mice revealed no overt abnormalities. (**A**) XX control, (**B**) XX *Mapk11*$^{-/-}$, (**C-D**) XY *Mapk11*$^{-/-}$. Control males were not analysed at the same time. The mice were genotyped for their sex, which corresponded with both the external and internal phenotype. o, ovary; ov, oviduct; uh, uterine horn; u, uterus; sv, seminal vesicles; e, epididymis; t, testis; vd, vas deferens.

6.2.2. Gene knockdown of the p38 MAPKs in gonad organ culture

To further address the role of functional redundancy amongst the different p38 MAPKs, and to establish an approach that could prove very useful in future functional studies in our laboratory, gene knockdown methodologies in gonad organ culture were trialled. As with embryonic kidneys and lungs, gonads at 11.5 dpc are known to culture very successfully (Buehr et al. 1993; Martineau et al. 1997). To validate the organ culture technique in my hands, male (XY) and female (XX) C57BL/6J wild-type gonads with attached mesonephroi were dissected from 11.5 dpc embryos at the bipotential stage and cultured on agar moulds supplemented with foetal calf serum (FCS), L-Glutamine and Ampicillin for 48 hours. The gonads cultured successfully and subsequent analysis by WMISH confirmed expected expression of *Sox9*, a Sertoli cell-specific marker, in a male-specific fashion (Figure 6.2) and testis cord-like structures were present.

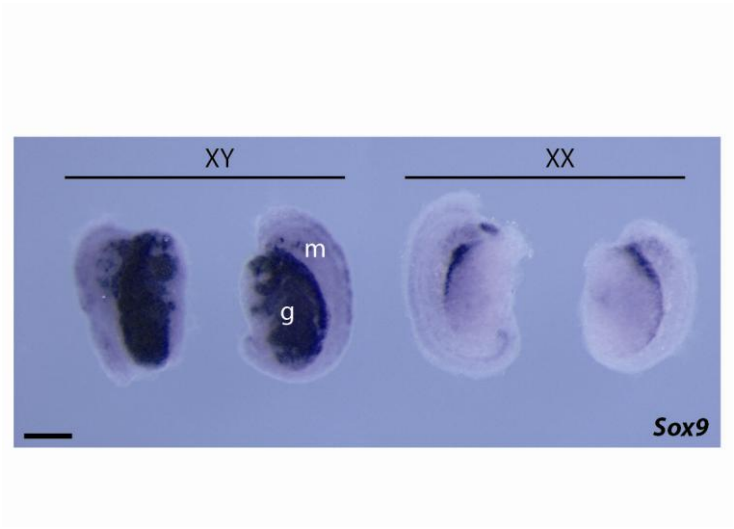

Figure 6.2: Expression of *Sox9* by WMISH in cultured gonads
Embryonic gonads were explanted at 11.5 dpc and cultured in agar grooves, supplemented with serum and ampicillin, for 48 hours. Subsequent analysis of *Sox9* expression by WMISH revealed strong staining in the gonads of XY samples with cord-like structures apparent in some samples. Weak expression was also detected in the mesonephros. In XX samples, *Sox9* was absent from the gonad, but visible at low levels in the mesonephros. These expression patterns compare favourably with those of wild-type 13.5 dpc samples *in vivo*. g, gonad; m, mesonephros. Scale bar = 200 µm.

6.2.2.1. Magnetofection of shRNA

Despite the relative ease of culturing gonads *ex vivo*, not many reports documenting successful gene knockdown within such gonads have been published, as discussed in the Introduction (section 6.1). It is more than likely that this technique has been tried many times, but with limited success. For this reason, establishing a protocol for a successful delivery method to initiate the RNA interference pathway was challenging. A recent publication by Svingen *et al* described the successful delivery of shRNA by the use of magnetofection: a technique involving the microinjection of shRNA molecules (in a vehicle of magnetic beads and lipofectamine) straight into the middle of the 11.5 dpc gonad, and application of a magnetic field to draw the compound directly into cells (Svingen et al. 2009). The benefits of this method over any virus-mediated or siRNA simple diffusion variant included the controlled localised effect of the knockdown within the gonad around the site of injection, providing an internal positive control for normal growth in culture in the regions not injected. This magnetofection method was therefore utilised initially for the injection of an EGFP expression plasmid.

Microinjection of an 11.5 dpc gonad proved challenging. A variety of methods were trialled, including a handheld pipette using pulled glass capillaries, and also a mouth pipette. Subsequent analysis of GFP expression within the gonad following 48 hours of culture revealed conflicting results. Some fluorescence was frequently observed around the site of injection, along with increased levels in the mesonephros. However, comparison with the negative controls, injected with the magnetic beads and lipofectamine but without the expression plasmid, often revealed comparable levels of expression in similar sites. It was concluded that this was a consequence of auto-fluorescence of the magnetic beads in the gonad and/or red blood cells (a well known phenomenon) in the mesonephros (Figure 6.3A-I). A trial injection of an *Sry*-expressing

plasmid (*pcHA-Sry*; a kind gift from P.Koopman) was also performed on XX gonads to determine whether testis-specific gene expression could be induced (Figure 6.3J). However, no evidence of an effect was seen.

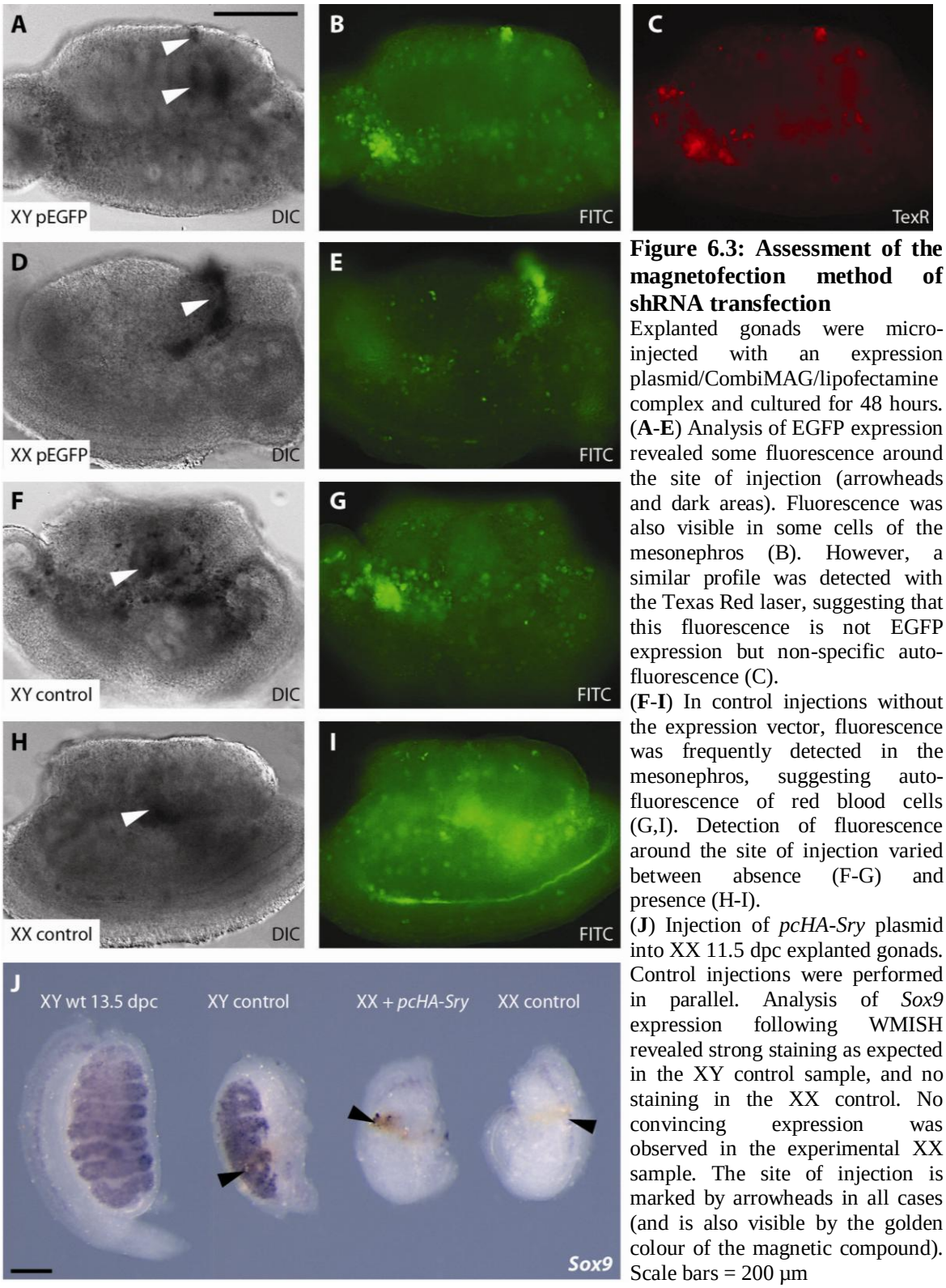

Figure 6.3: Assessment of the magnetofection method of shRNA transfection

Explanted gonads were micro-injected with an expression plasmid/CombiMAG/lipofectamine complex and cultured for 48 hours. (**A-E**) Analysis of EGFP expression revealed some fluorescence around the site of injection (arrowheads and dark areas). Fluorescence was also visible in some cells of the mesonephros (B). However, a similar profile was detected with the Texas Red laser, suggesting that this fluorescence is not EGFP expression but non-specific auto-fluorescence (C).

(**F-I**) In control injections without the expression vector, fluorescence was frequently detected in the mesonephros, suggesting auto-fluorescence of red blood cells (G,I). Detection of fluorescence around the site of injection varied between absence (F-G) and presence (H-I).

(**J**) Injection of *pcHA-Sry* plasmid into XX 11.5 dpc explanted gonads. Control injections were performed in parallel. Analysis of *Sox9* expression following WMISH revealed strong staining as expected in the XY control sample, and no staining in the XX control. No convincing expression was observed in the experimental XX sample. The site of injection is marked by arrowheads in all cases (and is also visible by the golden colour of the magnetic compound). Scale bars = 200 µm

6.2.2.2. Transfection of siRNA

A much simpler method than magnetofection was then trialled, involving transfection of a naked siRNA into the gonad with the use of lipofectamine and no other delivery vehicle. Initial experiments involved transfection of a red Alexa fluor oligonucleotide and subsequent monitoring of levels of uptake into the gonad. Following optimisation, the data indicated a certain level of consistent uptake observed in the experimental samples compared to negative controls; fluorescence was consistently observed in the mesonephros of experimental samples, with accompanying (but variable) levels in the body of the gonad (Figure 6.4). However, the efficiency of uptake was variable. For the negative controls, a standard, non-specific negative control siRNA was used.

6.2.2.3. Sox9 knockdown in gonad explant cultures

Initial knockdown experiments were performed using a *Sox9* siRNA. XY gonads lacking *Sox9* exhibit complete sex reversal, exhibiting expression of female somatic markers *Foxl2* and *Wnt4* (Lavery et al. 2011). Recapitulating this phenotype in gonad culture would validate this knockdown method for use with other genes. Although it is possible to obtain siRNAs that contain a fluorescent tag to monitor the uptake into cells, these are very expensive, so, instead, normal unlabelled siRNAs were used and transfection of the red Alexa fluor oligonucleotide control was performed alongside the experimental siRNAs to assess efficiency of the uptake. Two siRNAs targeting different parts of the *Sox9* transcript were pooled to increase the chances of efficient knockdown. To assess successful knockdown, expression of cell-specific markers was analysed by both WMISH and qRT-PCR. For qRT-PCR analysis, each individual cultured gonad was analysed separately to avoid any potential suppression of a detectable effect if the gonads were pooled due to the variation in efficiency (refer to Materials and Methods sections 2.7.1 and 2.12.2).

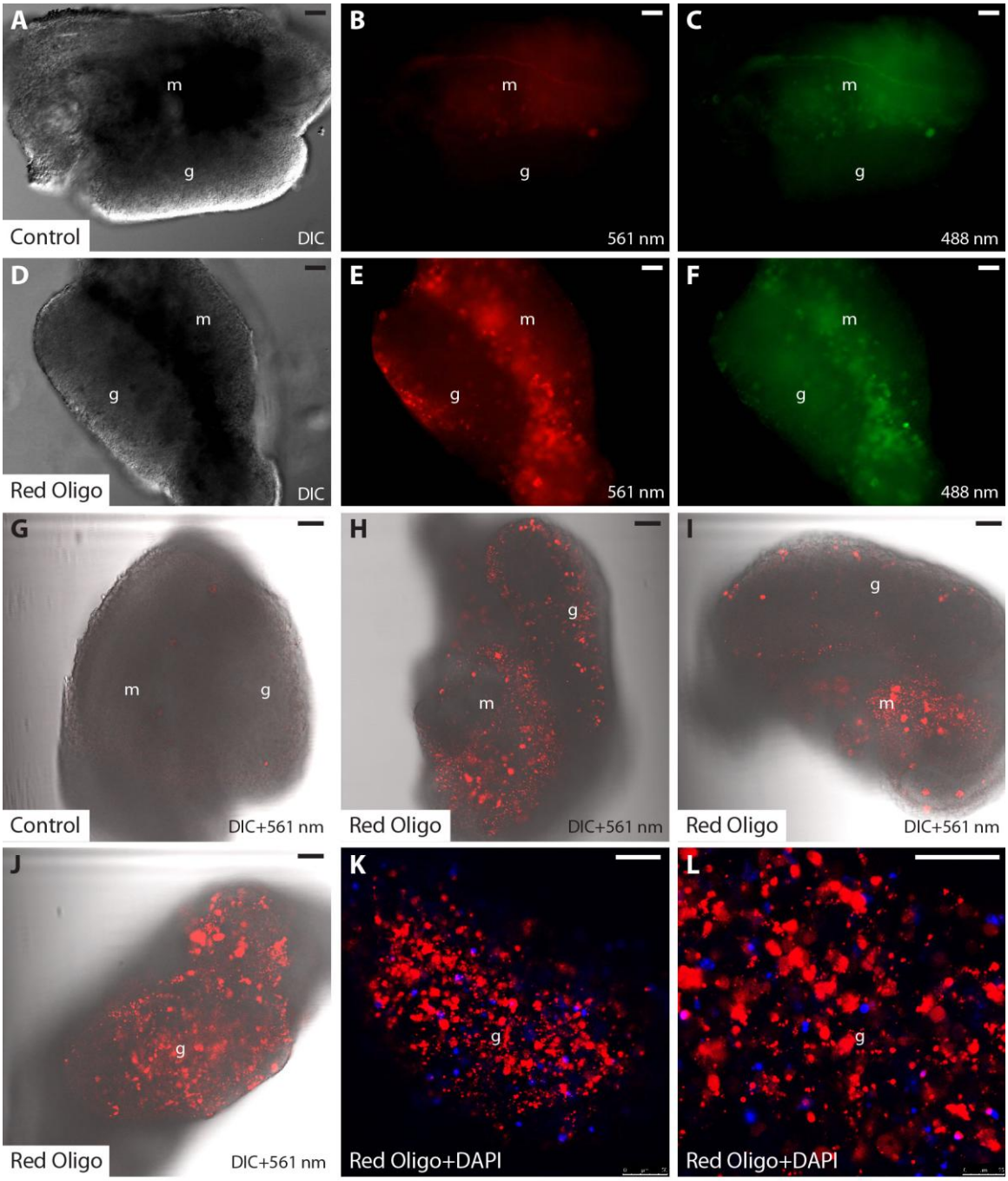

Figure 6.4: BLOCK-iT Red Alexa Fluor oligonucleotide delivery

(**A-F**) Images of cultured gonads were taken using an Olympus IX81 microscope. (A-C) No fluorescence was detected in control gonads transfected with a negative siRNA at either 561 nm (B), corresponding to the Red Alexa Fluor, or 488 nm to detect auto-fluorescence (C). (D-F) Fluorescence was detected in the gonad and mesonephros of samples transfected with 120 pmoles of Red oligo (E) with minimal levels of non-specific fluorescence restricted to the mesonephros (F), suggesting that some mesonephric expression was autofluorescence of red blood cells but gonadal fluorescence was true Red oligo expression.

(**G-L**) Images were taken with a Leica TCS SP5 confocal microscope. (G) Control gonads in which occasional red fluorescent cells were observed, but fluorescence in the mesonephros was limited. (H-I) Variable fluorescence levels were observed in the transfected gonads from a high gonadal percentage of cells transfected (H), to a low amount but with expression still present in the mesonephros (I). (J-L) To assess the transfection efficiency, some gonads were incubated with aqueous DAPI (K-L). However, for reasons unknown, the DAPI expression profile did not appear normal. Unfortunately, this experiment could not be repeated due to time constraints.

Scale bars = 100 µm. m, mesonephros; g, gonad; DIC, differential interference contrast.

Knockdown was initially performed on 11.5 dpc (17 ts) dissected gonads, which were subsequently cultured for 48 hours. Analysis of gene expression revealed variable results. By WMISH, *Sox9* expression was largely unaltered, although some samples had potential localised disruption of expression. One knockdown gonad did show *Foxl2* gain-of-expression, and another knockdown gonad showed a few spots of *Stra8* in the anterior pole (Figure 6.5A-F). By qRT-PCR, analysis of *Sox9*, *Stra8*, *Wnt4*, and *Fst* expression in six experimental samples identified one sample with decreased *Sox9* and increased *Wnt4*, *Fst* and *Stra8* (Figure 6.5G-J).

Knockdown of *Sox9* was also attempted on earlier stage gonads dissected between 10.5 and 11.0 dpc (8-13 ts). Results from these were much more promising. Analysis by WMISH revealed approximately 30% of experimental knockdown gonads exhibiting elevated *Wnt4* expression, decreased *Sox9* expression and also decreased *Hsd3b* expression (Figure 6.6). Analysis by qRT-PCR highlighted approximately 65% of experimental samples exhibiting partial sex reversal, as defined by decreased levels of *Sox9* and *Amh*, and increased levels of *Wnt4* and *Fst* (Figure 6.7).

However, the consequence of culturing from earlier stages was apparent disruption to the development of the XY control samples: elevated *Wnt4* expression was observed by WMISH in some XY control gonads, and using qRT-PCR, approximately 30% showed decreased levels of *Sox9* and *Amh*, and increased levels of *Wnt4* (although not always in the same sample). However, as the experimental samples exhibited a much more dramatic change in marker gene levels (65% compared to 30%), it was considered that *Sox9* knockdown was successful to some degree, with variability between samples. As a consequence of these data, knockdown of p38 MAPK genes was attempted.

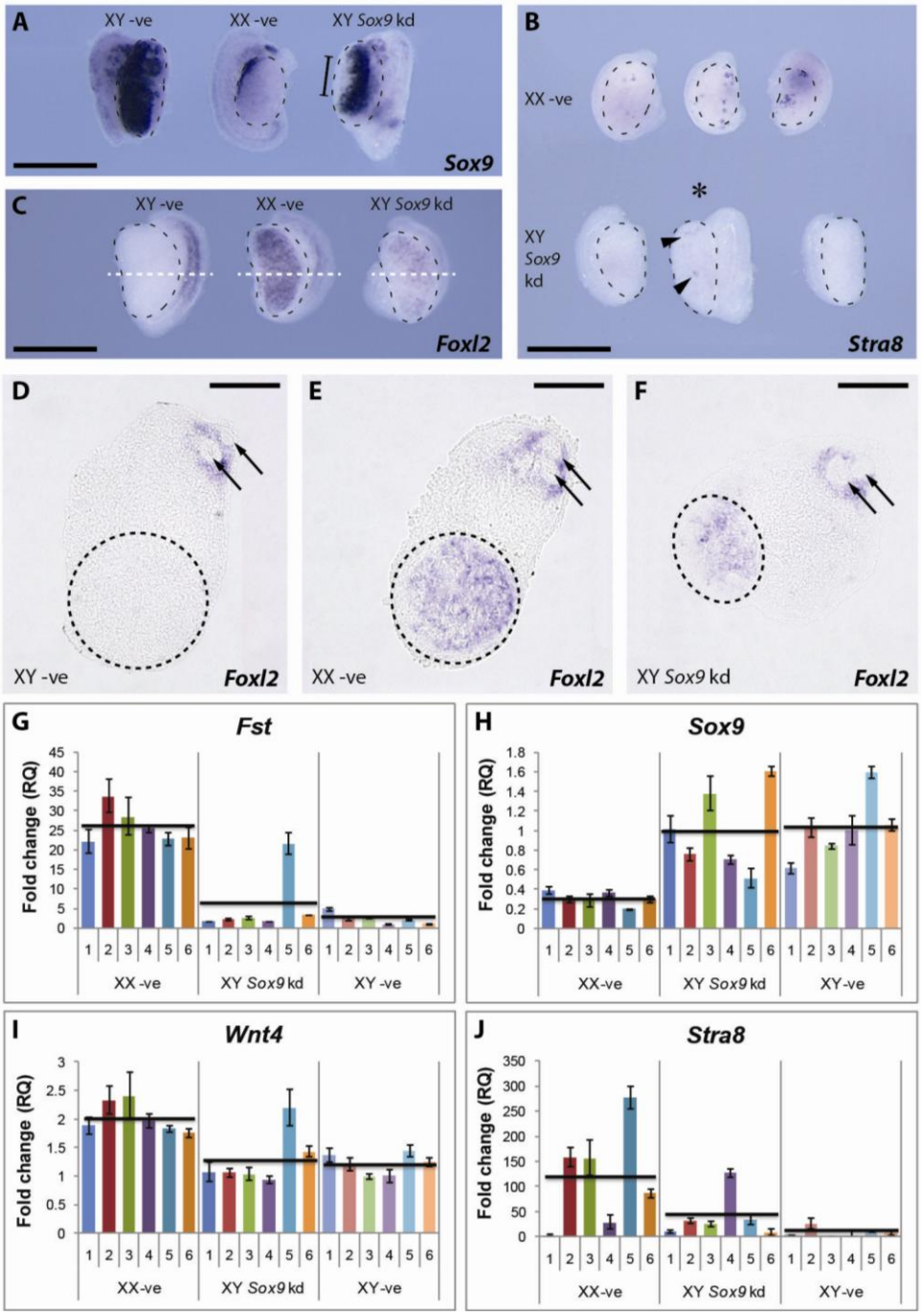

Figure 6.5: Analysis of *Sox9* knockdown (kd) in cultured 17 ts gonads

(**A**-**F**) WMISH analysis of *Sox9* (A), *Stra8* (B) and *Foxl2* (C-F) expression in XY *Sox9* knockdown (kd) gonads versus XY and XX negative controls. Gonadal region is within the black dotted lines in all cases, with mesonephros along one side. (A) *Sox9* expression exhibits localised loss in the centre of the gonad (marked by black bar), while *Stra8* analysis (B) showed presence of a few meiotic germ cells (black arrow heads) in one sample. Expression in the XX negative controls was also sparse however, due to the early stage of the gonad before the majority of germ cells have entered meiosis. (C) *Foxl2* expression was present in one XY *Sox9* kd gonad (out of 6 examined). (D-F) Transverse cryosections (orientation shown by dotted white lines in (C)), confirm *Foxl2* expression in the gonadal region of the XY *Sox9* kd sample. Expression was also seen in the mesenchyme surrounding both the Wolffian duct and Müllerian duct in all samples (arrows). Scale bars = 500 µm (A-C), 100 µm (D-F).

(**G**-**J**) qRT-PCR results for six samples of each category. Sample number and colour correspond to the same sample across the different gene analyses. Black horizontal bars mark the average fold change for each group. A slight trend towards expression levels closer to that of XX controls is seen in the XY *Sox9* kd group for all genes analysed, but this is not significant. XY *Sox9* kd sample #5 appears sex reversed in the expression of *Fst*, *Sox9* and *Wnt4*, and this accounts for the average trend observed. Error bars correspond to RQ min and max.

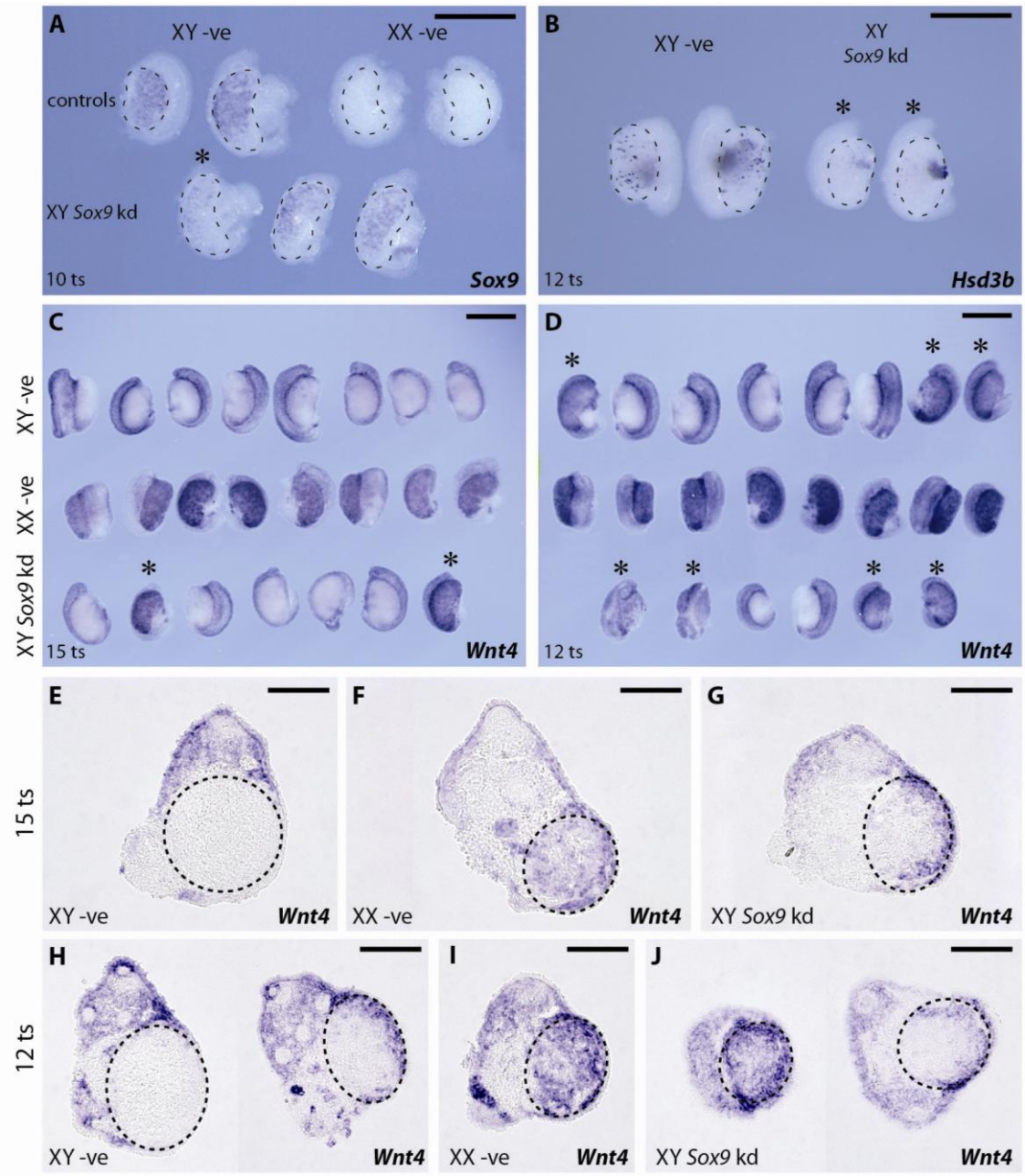

Figure 6.6: WMISH analysis of *Sox9* knockdown (kd) in cultured 10-15 ts gonads
(**A**) *Sox9* expression in XY *Sox9* kd 10 ts gonads was slightly reduced in some samples (asterisk), however, the expression did vary greatly. (**B**) *Hsd3b* expression (which marks testis-specific Leydig cells) was also reduced in 12 ts XY *Sox9* kd gonads compared to XY controls. (**C**-**D**) *Wnt4* expression was present in two XY *Sox9* kd 15 ts gonads (C) and four 12 ts samples (D). However, at 12 ts some XY negative control samples also showed *Wnt4* expression in the gonad (see asterisks). (**E**-**J**) Transverse cryosections confirm *Wnt4* expression in the gonadal region of the 15 ts XY *Sox9* kd samples (G) and also in the 12 ts XY *Sox9* kd samples (J). Some peripheral expression was also present in a XY negative control gonad (right, H). Scale bars = 500 µm (A-D), 100 µm (E-J).
The gonadal region is within the black dotted lines while the mesonephros is either to one side or situated behind the gonad. Asterisks mark affected gonads.

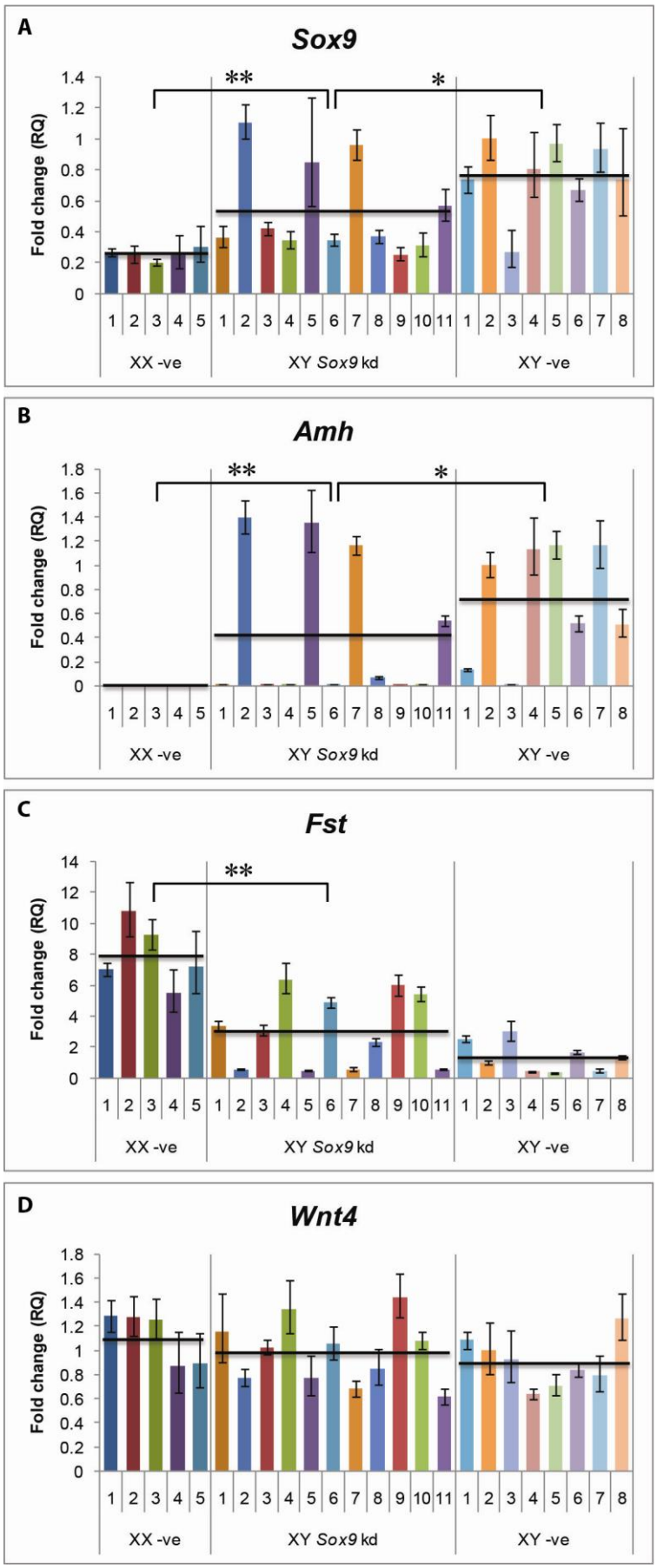

Figure 6.7: qRT-PCR analysis of 9-11 ts XY *Sox9* knockdown (kd) gonads

Sample number and colour correspond to the same sample across the different gene analyses. Black horizontal bars mark the average fold change for each group.

(**A**) *Sox9* expression analysis revealed 65% of XY *Sox9* kd samples with levels similar to that of XX controls (#'s 1, 3, 4, 6, 8, 9 & 10). One XY control sample of 8 also showed decreased expression. A significant average decrease in expression was observed in XY *Sox9* kd samples in comparison with XY controls. However, a significant difference between XY *Sox9* kd and XX controls also remained.

(**B**) *Amh* expression revealed very similar results to that of *Sox9* analysis. The same 7 samples showed a significant decrease in *Amh* expression to levels comparable with XX controls. Two XY controls also showed a decrease in expression to similar levels. The same levels of significance were observed between the three different group averages as with *Sox9* analysis.

(**C**) *Fst* expression confirmed the sex reversal of the 7 XY *Sox9* kd samples as they exhibited a 4-10-fold increase in levels. However, the difference between the XY *Sox9* kd group and the XY controls was not quite significant due to four XY control samples also displaying a modest increase in *Fst* levels.

(**D**) *Wnt4* expression confirmed consistency with the same XY *Sox9* kd samples exhibiting slight increases in expression. However, expression in the XX and XY controls did not differ by much, likely due to the strong mesonephric expression in XY samples.

RQ was calculated following calibration to XY control sample #2. Error bars correspond to RQ min and RQ max. Significance was calculated using a one-tailed student's *t*-test at 95% confidence. *, p value ≤ 0.05; **, p value ≤ 0.005

6.2.2.4. Knockdown of p38 MAPKs in gonad explant culture

Initially, single knockdowns of each gene (excluding *Mapk12*) were conducted to assess the efficiency of the siRNAs on 10-18 ts XY gonads. Again, two siRNAs targeting different parts of the same transcript were pooled together. WMISH analysis of the corresponding p38 MAPK expression was performed: although WMISH is not quantitative, reduced levels of staining indicative of a slight reduction in expression was observed in some samples of *Mapk14* and *Mapk13* knockdown (Figure 6.8A,B,F,G). However, in contrast, qRT-PCR analysis did not reveal convincing knockdown of expression. Data were very variable across all three classes analysed, including XX and XY negative controls, for both *Mapk13* and *Mapk14* knockdowns. No effect of knockdown was visible in the *Mapk14* knockdown gonads at all, despite loss of *Amh* expression and corresponding gain of *Fst* expression in two samples (Figure 6.8C-E). Considering two XY control samples also showed loss of *Amh* expression (*Fst* was not analysed for these two samples), it is likely that these effects are due to early culturing of the gonads which has disrupted the testis development pathway, rather than an effect of the *Mapk14* knockdown. The same phenomena were also observed with the *Mapk13* knockdown experiment; any potential effects were also seen in the XY control group (Figure 6.8H-J).

Pooling of the different p38 MAPK siRNAs for multiple knockdown was attempted. Three different variations were trialled: *Mapk14*, *Mapk13* and *Mapk11* knockdown; *Mapk14* and *Mapk11* knockdown; and *Mapk14* and *Mapk13* knockdown. However, initial analyses did not reveal convincing results as gene expression levels for the different p38 MAPKs varied greatly across all three classes: XY knockdown, XY control and XX control. No consistency or pattern could be deciphered and therefore the experiment was halted. Until the efficacy of the p38 MAPK siRNAs and the efficiency

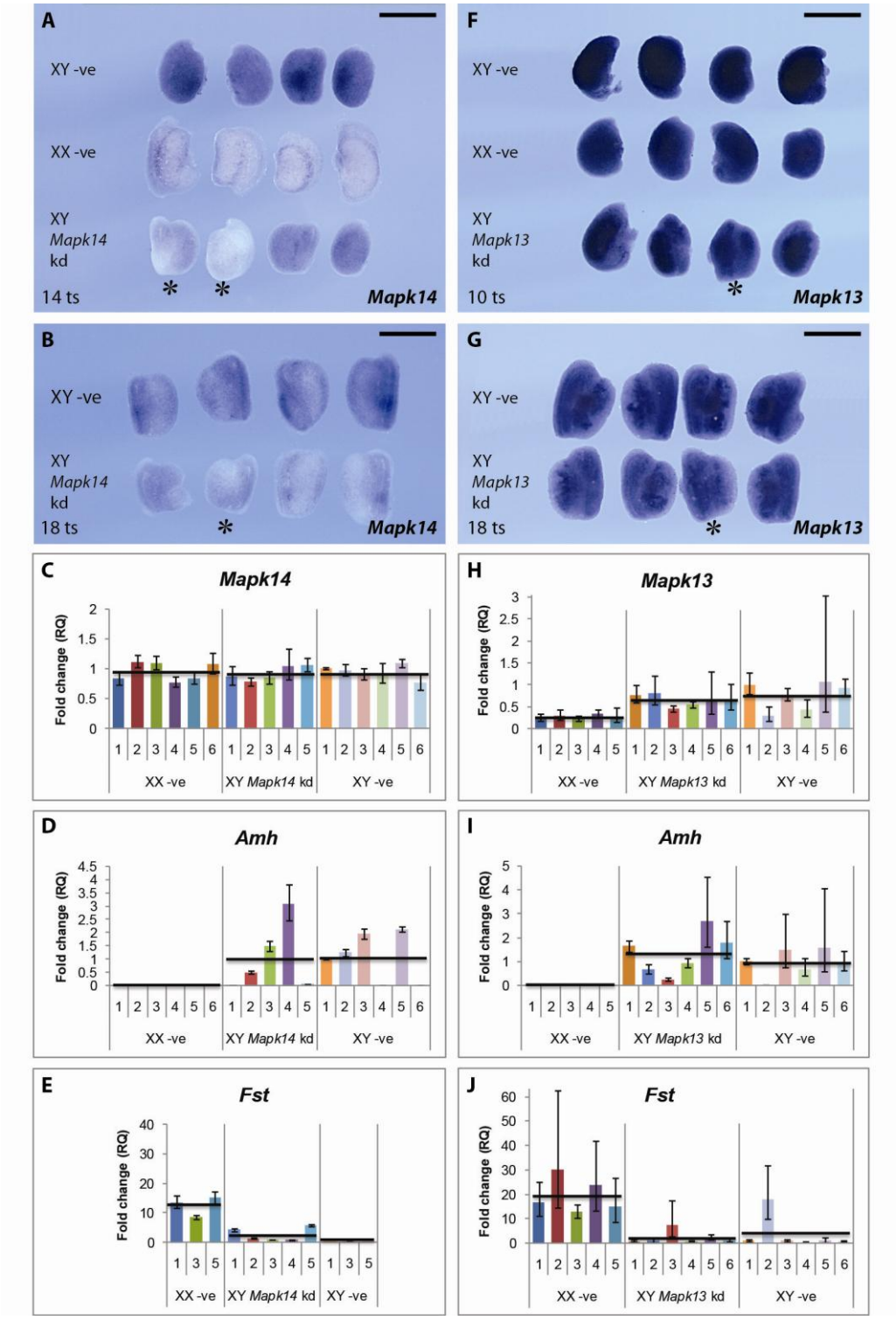

Figure 6.8: Analysis of *Mapk14* and *Mapk13* independent knockdowns
(**A-E**) *Mapk14* knockdowns were performed on 9-18 ts explanted gonads. (A-B) Analysis of *Mapk14* expression by WMISH revealed promising decreases in the XY *Mapk14* kd gonads at both 14 ts (A) and 18 ts (B) – see asterisks. (C-E) Analysis of gene expression levels by qRT-PCR at 10 ts was not so convincing. The levels of *Mapk14* appeared unaltered (C), despite potential samples showing sex reversal through changes in *Amh* (D) and *Fst* (E) expression. 15 ts and 18 ts knockdown stages were also analysed, also with no obvious effects (data not shown). (**F-J**) *Mapk13* knockdowns were also performed on 10-18 ts explanted gonads. (F-G) Assessment of *Mapk13* by WMISH following knockdown highlighted some samples with convincing decreases in expression (see asterisks) at both 10 ts (F) and 18 ts (G). (H-J) Analysis by qRT-PCR on 13 ts gonads revealed variable results, but XY *Mapk13* kd samples displayed the same variation as XY controls. Scale bars = 500 µm. RQ calculated following calibration to XY –ve control sample #1. Error bars indicate RQ min and RQ max.

of the knockdown protocol can be improved, this technique is not reliable enough to use. Unfortunately, due to time constraints no further optimisations could be explored.

6.2.3. Conditional ablation of *Map3k4*

A floxed allele of *Map3k4* became available towards the end of the project (kind gift from H.Chi). This afforded the opportunity to ascertain whether *Sf1-Cre* is a suitable *Cre*-driver to help dissect the MAP3K4 testis-determining pathway and thereby shed light on its stage- and cell-specificity of function, without concerns about functional redundancy. Firstly, to ensure that deletion of the floxed allele (*Map3k4*^{flox}) gave the same phenotype as the constitutive knockout when inactivated ubiquitously, a cross was set up with *β-actin-Cre*. The same breeding programme was followed as in section 5.2.1, which resulted in timed matings between *Map3k4*$^{flox/flox}$ males and *Map3k4*$^{flox/+}$; *β-Actin-Cre/+* females. Embryos were collected at 13.5 dpc from two litters. The genotype and successful recombination was assessed by standard PCR. Twenty embryos were collected, four of which were conditional knockout mutants (20%; *Map3k4*$^{\Delta/\Delta}$; *β-Actin-Cre/+*). Two mutants exhibited either spina bifida or a curly tail, and this variable penetrant phenotype is consistent with the constitutive knockout (Bogani et al. 2009). All four mutants were phenotyped as females due to the ovarian shape and lack of testis cords observed in the gonads. However, all were genotyped as XY, confirming complete XY gonadal sex reversal as was expected (Figure 6.9). Photographs were not taken.

Meanwhile, a cross was also set up with *Sf1-Cre* to allow targeted inactivation of *Map3k4* in the somatic cells of the gonad. Embryos were collected at 14.5 dpc from timed matings between *Map3k4*$^{flox/flox}$ females and *Map3k4*$^{flox/+}$; *Sf1-Cre/+* males. Five litters were collected and no external phenotype was observed in the 40 embryos.

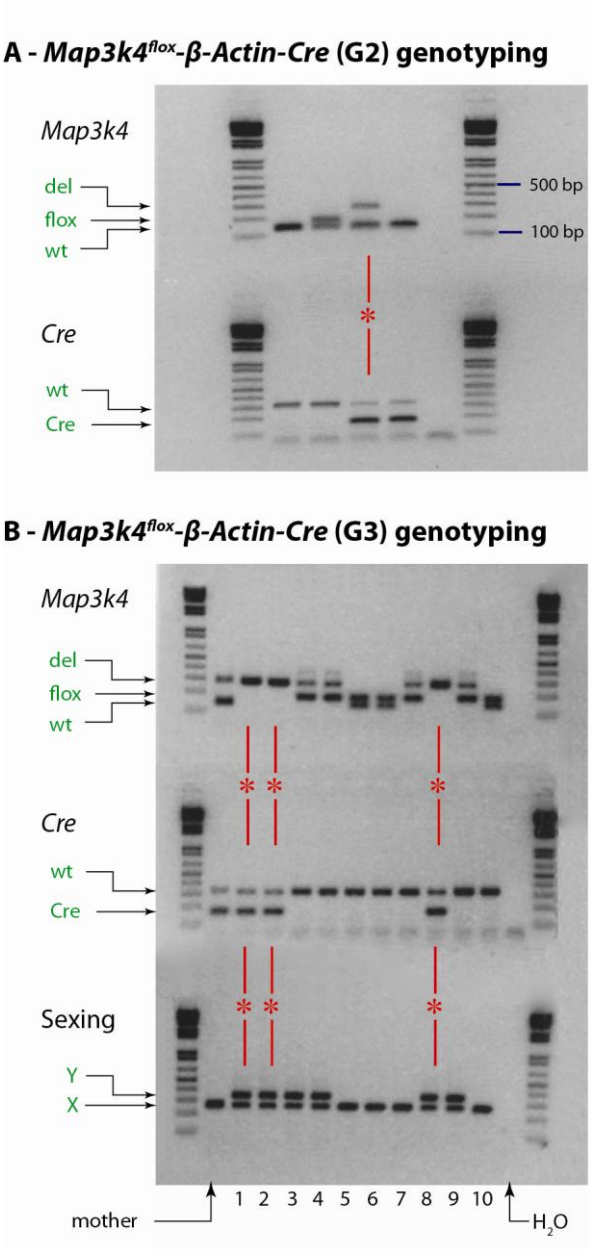

Figure 6.9: *β-actin-Cre*-driven ubiquitous deletion of the *Map3k4^{flox}* allele

(**A**) Example of genotyping of *Map3k4^{flox}* colony to detect recombination of the floxed region in the G2 colony. The four possible genotypes are represented. The sample marked in red is the desired *Map3k4$^{\Delta/+}$*; *β-actin-Cre/+* heterozygote.

(**B**) Genotyping of the G3 progeny. Complete recombination of the floxed allele occurred in the presence of *Cre* in all mutant samples (red marked samples). All mutants were genotyped as XY.

Thirteen embryos were genotyped as homozygous mutants (32.5%; *Map3k4*$^{flox/flox}$; *Sf1-Cre*/+), nine of which were XY (22.5%). One gonad from each embryo from two litters was collected for genotyping to confirm the targeted deletion by presence of the deletion allele, while the other was used for subsequent gene expression analysis. The deletion allele was clearly detected in all gonad samples of *Cre*-positive embryos (60%) and was absent from the hindbrain samples (Figure 6.10A). The phenotypic sex corresponded with the genetic sex in all cases. Therefore, the targeted deletion of *Map3k4*^{flox} in somatic cells of the gonad driven by *Sf1-Cre* did not cause gonadal sex reversal.

WMISH analysis was conducted to assess the expression patterns of *Sox9* and *Stra8* in the mutant gonads (Figure 6.10B-E). *Sox9* expression in the XY mutants was normal in comparison with XY controls (heterozygous *Map3k4*$^{flox/+}$; *Sf1-Cre*/+ and *Map3k4*$^{flox/flox}$; +/+) and no expression was seen in XX mutants. *Stra8* expression was also normal in XX mutants, however, in XY mutants a very small cluster of *Stra8*-positive cells was observed in the posterior pole. This suggests that the targeted deletion of *Map3k4* driven by *Sf1-Cre* in somatic cells could be delaying testis development very slightly, and as a result some germ cells in the posterior pole have entered meiosis. A similar observation is made in other contexts in which testis determination is slightly delayed, such as the C57BL/6J-Y^{AKR} background (Washburn and Eicher 1983).

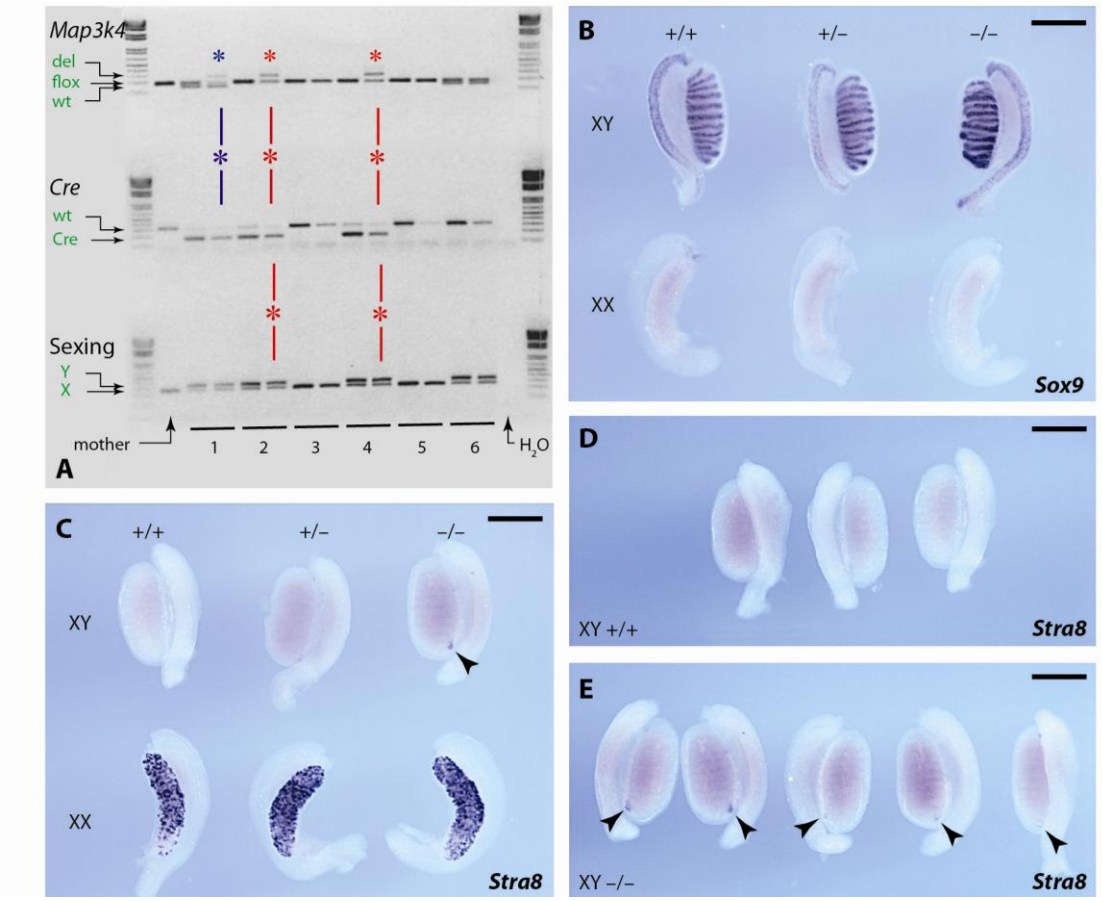

Figure 6.10: *Sf1Cre-Map3k4*-cKO analysis at 14.5 dpc

Gonads were collected from 14.5 dpc embryos from timed matings between male *Map3k4*$^{flox/+}$*; Sf1-Cre/+* and female *Map3k4*$^{flox/flox}$ mice. (**A**) Genotyping was performed by standard PCR assay. Hindbrain sample and one gonad were collected from each embryo and loaded onto the gel in that order. The recombined deletion allele was restricted to the gonad sample of *Cre*-positive embryos confirming successful recombination was occurring. See red marked samples for mutant genotype, blue marked sample for heterozygous control.

(**B-E**) The expression profiles of *Sox9* and *Stra8* were analysed by WMISH in *Cre*-negative controls (+/+), *Cre*-positive controls (+/−) and conditional knockout mutants (−/−) of both XY and XX tissue. (B) *Sox9* was unaltered in the XY mutants and clearly defined the testis cords. No abnormalities were notable in the XX mutants. (C) The expression of *Stra8* was largely unaltered in the XY mutants although a few germ cells in the posterior pole did appear to have entered meiosis (see arrowhead). No change in expression was observed in the XX mutants. Comparison of three XY *Cre*-negative controls (D) with five XY mutants (E), confirms the presence of the *Stra8*-positive cells clustered in the posterior poles of all mutants (arrowheads). Scale bars = 500 µm.

6.3. Discussion

The conditional inactivation of *Map3k4* in somatic cells of the gonad using the *Sf1-Cre*-deleter does not significantly disrupt sex determination. Some evidence of germ cells entering meiosis in a small cluster in the posterior pole of XY mutants was evident, which suggests that the deletion of *Map3k4* in *Sf1*-positive somatic cells may have retarded testis development slightly. However, this would not affect the later development or function of the testis. Clusters of XY meiotic germ cells have been reported previously and attributed to a slight delay in testis development (Warr et al. 2011). *Sry* is expressed initially in the centre of the gonadal primordium and then extends outwards towards the poles (Bullejos and Koopman 2001). This *Sry* expression results in a similar spatiotemporal *Sox9* expression profile a few hours later. However, increased activation and maintenance of *Sox9* expression, particularly at the poles, is required for the subsequent Sertoli cell differentiation and testis cord formation. It is thought that testis development is initiated following the *Sry/Sox9*-induced activation of the gene encoding the secreted molecule, FGF9, in the centre of the gonad. FGF9 then spreads the signal out towards the poles, acting in a positive feedback loop with *Sox9* (Hiramatsu et al. 2010). Any delay of this signal at the poles of the gonad could allow the feminisation of a few cells through failure to antagonise ovary-determining genes such as *Wnt4* and *Foxl2*, thus enabling some germ cells in the vicinity to enter meiosis (Hiramatsu et al. 2009; Wilhelm et al. 2009). This phenomenon, albeit in a more severe form, is observed in *Fgfr2*-null embryos, when ovotestes develop in the absence of the FGF9 receptor (Kim et al. 2007). Indeed, this is the best explanation for all cases of XY ovotestes development in which the gonadal poles are the usual sites of regional sex reversal. While the phenotype observed with the *Map3k4* conditional inactivation in the somatic cells is not this severe, it is possible that the activation of *Sry* has been delayed

very slightly, suggesting that the MAP3K4 pathway does act in the somatic cells, but that deletion using *Sf1-Cre* occurs too late to fully disrupt the expression of *Sry*. Recent reports of the use of *Sf1-Cre* to conditionally delete *Gata4* also support this hypothesis (Manuylov et al. 2011). Using a different *Cre*-driver that is expressed earlier in the somatic cells would help to address this theory. There is a report of an inducible *Wt1-Cre*^{ERT2} which is activated by tamoxifen and has been used to delete *Gata4* in the somatic cells of the 10.5 dpc gonad, which results in complete XY sex reversal and confirms its suitability in comparison with *Sf1-Cre* (Manuylov et al. 2011). The non-inducible, GFP-tagged *Wt1-Cre*^{GFP} also expresses GFP in the urogenital ridge of 9.5 dpc embryos, suggesting it is suitable for early conditional gene inactivation in somatic cells (Zhou et al. 2008).

In light of all the technical difficulties and limitations surrounding siRNA-mediated gene knockdown in organ culture, it was not surprising that the attempt to establish this technique was challenging. However, despite the observation that approximately 30% of cultured XY control gonads younger than 11.0 dpc exhibited evidence of disruption to testis determination, the knockdown of *Sox9* appeared to disrupt testis determination in approximately 65% of XY samples, thus indicating that the knockdown had worked with approximately 30% efficiency. There are reports of successful gonad culturing from as early as 12 ts (Hiramatsu et al. 2010), however, it may be that explanting gonads earlier than this stage and therefore before the initiation of *Sry* expression in the centre of the XY gonad, causes a slight disruption and delay to *Sry* up-regulation and therefore the female pathway is partially activated, as described previously. This is supported by a report by McLaren and Buehr that 10.5 dpc UGRs cultured for 3-5 days contain meiotic germ cells and do not develop testis cords (McLaren and Buehr 1990). The authors identified some differentiated Sertoli cells; however these cells were unable

to support testis cord development, suggesting that a certain stage of differentiation needed to be reached *in vivo* before the cells were capable of supporting further XY gonad development in culture. At the later stage of 17 ts analysed, one XY *Sox9* knockdown sample displayed convincing female development, while the XY controls had gene expression levels within the normal range. Therefore, at this stage, the efficiency of successful knockdown dropped to below 20%; in contrast, explanting gonads at this stage did not affect the culturing process or affect testis development in XY controls.

This variability and general low efficiency of the knockdown methodology meant that actual experiments would be difficult to interpret. The attempted knockdown of the p38 MAPK genes in a range of gonad stages between 10 to 18 ts was not successful. There are methods that could be used to improve the transfection efficiency, such as re-constructed organ cultures. Re-constructed organs are formed from the disaggregation of the organ rudiment so that cells are exposed to the siRNA and then re-aggregated so that organotypic development is still possible. This technique was used successfully in postnatal ovaries to knockdown *Wee1* in separated oocytes and somatic cells (Park et al. 2006), but the disadvantage to this approach is that the gonad structure and organisation is lost after re-aggregation. Whether or not this technique could be applied to embryonic gonads remains to be determined, but it is likely to also depend on the gene that is being analysed.

The generation of a double knockout of *Mapk11* and *Mapk14* was in fact reported very recently and provides evidence for functional redundancy between p38α and p38β during different aspects of mouse development (del Barco Barrantes et al. 2011). These authors generated a double knockout of p38α and p38β by restricting the deletion of

p38α to embryonic, epiblast-derived tissue, using a *Sox2-Cre* line to delete the *Mapk14*^{flox} allele, and crossing these mice to *Mapk11*$^{-/-}$ mutants. Subsequent phenotypic analysis confirmed that functional redundancy between the two p38 MAPKs occurred in some, but not all, tissues. The double knockouts were embryonically lethal by 16.5 dpc and exhibited spina bifida, reduced liver size, and occasional occurrence of exencephaly. These phenotypes were not apparent in the single knockout of either p38 MAPK, suggesting that p38α and p38β act redundantly in these aspects of development. However, in other tissue types, the loss of one cannot be compensated by the expression of the other. For example, in placental tissue, the expression of p38β under the p38α promoter (*p38*β*KI*α; obtained by insertion of *Mapk11* downstream of the *Mapk14* promoter) could not rescue the placental defect and embryonic lethality by 11.5 dpc. In addition, heart defects also observed in the double knockout could not be rescued with the replacement of one of the *Mapk14*^{flox} alleles with the *p38*β*KI*α knock-in, suggesting that while both p38 MAPKs could have a role in heart development, they may be active in different cell types. In contrast, the lung phenotype observed with the single conditional knockout of *Mapk14* (Ventura et al. 2007), was partially rescued by the addition of *p38*β*KI*α to replace one of the *Mapk14*^{flox} alleles, suggesting that the enhanced *Mapk11* expression could compensate for the essential function of p38α in lung development. Another interesting aspect to this study was that the transcriptional regulator properties of GATA4, and a few other transcription factors important during heart development, were also affected, although the actual mRNA expression was not.

While the authors did not report any abnormalities in gonad development in the embryos of these double knockout mice, it is unlikely that they would have looked closely at this tissue, or genotyped for the sex chromosomes to see if they corresponded to the phenotypic sex. They also do not report the sex of the embryos that they

phenotyped. It would therefore be very interesting to determine whether gonad development was disrupted. One phenotype of the double knockout that is noteworthy in the context of sex determination is the spina bifida, which is also observed in the *Map3k4* null mutants (Bogani et al. 2009). The presence of other developmental phenotypes in the double p38α and p38β knockout, which are not common to the *Map3k4* mutant, is not surprising; many different MAP kinase signalling cascades, from a diverse range of extracellular signals, can activate the p38 MAPKs. The lack of detectable developmental phenotypes during the studies of the p38β, p38γ or p38δ MAPK knockouts, therefore, supports the idea of redundant roles amongst the different p38 MAPKs. Therefore, functional redundancy remains an important consideration, if p38 MAPKs are indeed confirmed to be involved in MAP3K4-regulated sex determination.

Despite all of this support for redundant roles amongst the different p38 MAPKs, which could extend to a role in gonad development, there is a strong "take-home message" from the study of the p38α and p38β double knockout: The authors did not observe defects in all aspects of development that were suggested by studies of p38α and p38β function using small molecule inhibitors. The double knockout embryos did not display limb defects, and underwent normal somitogenesis and gastrulation processes (del Barco Barrantes et al. 2011). Therefore, it must remain an open question whether the XY sex reversal observed in our inhibitor studies in organ culture reflects a bona fide role for p38α/β in sex determination, despite the fact that this phenotype was also confirmed by another group (Ewen et al. 2010). When used in high concentrations, the p38α/β inhibitors can also inhibit non-specific proteins as described in the Discussion in Chapter 5; therefore, caution must be taken in the interpretation of any phenotype observed.

Chapter 7. Discussion

7.1. Overview

The molecular and cellular events of sex determination described in this thesis are extremely complex. Researchers have dedicated their careers to this subject for over 50 years, aiming to elucidate the mechanisms involved in the developmental decision to generate ovaries or testes. Yet it has only been in the last 20 years that the molecular basis of sex determination has become clearer, with the identification of *Sry* as the elusive testis-determining gene on the Y chromosome and the downstream targets *Sox9* and *Fgf9*. In ovarian determination, the important discoveries have emerged within the last 10 years, with the identification of the active genetic processes that put paid to the idea that the ovarian pathway was the 'default' pathway. However, much work still needs to be done. The exact mechanism of *Sry* activation is not yet known despite the characterisation of many potential *Sry* transcriptional regulators. The work in this thesis has attempted to characterise a novel signalling pathway important for the activation of *Sry*: the MAP kinase pathway. The overall aim was to investigate the cellular and molecular basis of phenotypic abnormalities observed in the ENU-mutant, *Map3k4*$^{byg/byg}$, and to determine the downstream kinases activated and the mechanism employed for *Sry* activation during the process of sex determination.

7.2. Summary of results

This thesis describes experiments aimed at investigating the cellular and molecular basis of the sex reversal phenotype associated with the XY *Map3k4*$^{byg/byg}$ mutant. Cellular characterisations revealed that morphological development of the testis is disrupted at the earliest identifiable stage of sex determination in XY *Map3k4*$^{byg/byg}$ mutants. This was shown by a defect in male-specific proliferation at 11.5 dpc, which was attributed

to a defect in *Sry* up-regulation. To determine if the expression of one of the potential *Sry* transcriptional regulators was affected in the XY *Map3k4*$^{byg/byg}$ mutants, the protein expression of both Steroidogenic factor 1 (SF1) and activated (phosphorylated) SF1 was examined. However, SF1 expression was not disrupted, suggesting that either SF1 is functionally compromised for some other reason, or alternative molecules should be investigated. Elucidation of the downstream kinases activated by MAP3K4 during sex determination was attempted, with particular focus on identifying a role for the p38 MAP kinases (MAPKs). The mRNA expression pattern of the four different p38 MAPKs was assessed and both p38α and p38δ were found to be strongly expressed in the developing XY gonad. Using a conditional knockout approach to avoid the early lethality of the constitutive p38α knockout, the function of p38α in *Sf1*-positive somatic cells was assessed. However, specific inactivation in these cells did not affect gonad development. Subsequent conditional inactivation of *Map3k4* itself in these *Sf1*-positive cells also did not disrupt gonad development, suggesting that this pathway is either initiated in a different cell lineage or at an earlier stage than deletion driven by *Sf1-Cre* can disrupt. As part of an independent project to determine if p38α had a role in different aspects of sexual development, p38α was also inactivated in the Müllerian duct mesenchyme and gonadal somatic cells that expressed *Amhr2-Cre*. Müllerian duct regression in XY embryos, and gonad development in either XX or XY embryos, was not disrupted. However, fertility testing of XX females at 6 months of age revealed that they were extremely sub-fertile. The cause for this infertility has not yet been identified. Gene knockdown in organ culture was attempted to determine a role for multiple p38 MAPKs in all cell types of the gonad. Functional redundancy amongst the different p38 MAPKs could compensate for the loss of p38α as demonstrated by a recent publication detailing the effect of a double p38α/β knockout (del Barco Barrantes et al. 2011).

Unfortunately it was not possible to optimise a reliable and reproducible knockdown technique within the time I had remaining.

Overall, this thesis has shown that the MAPK pathway is active in the XY gonad very early in development, before the activation of *Sry*. p38 MAPKs are a strong MAPK candidate in this pathway since they are activated at the time of sex determination, and the small-molecule inhibition of p38α/β in organ culture leads to XY sex reversal. The use of *Sf1-Cre* is inappropriate to study the function of the MAPK pathway in sex determination and the investigation of a *Cre* driver that is expressed earlier within the gonad is required.

7.3. Potential mechanisms of MAP3K4-mediated regulation of sex determination from published *in vitro* data

Evidence is accumulating for a positive relationship between MAP kinase signalling and *Sry*/*Sox9* expression in other mouse developmental systems, including chondrocytes (Murakami et al. 2000; Tew and Hardingham 2006) and cultured keratinocytes (Gazel et al. 2008). In chondrocytes, SOX9 is a master regulator of differentiation; heterozygous mutations in *SOX9* cause campomelic dysplasia, a severe dwarfism syndrome caused by cartilage abnormalities (Wright et al. 1995). Fibroblast growth factors (FGFs) are also important during differentiation in chondrocytes, and have been shown to upregulate *Sox9* in this system (Murakami et al. 2000). FGFs signal through tyrosine kinase receptors, which are known to activate the extracellular signal-regulated kinase (ERK) family of the MAP kinase cascade (Schlessinger 2000; Lanner and Rossant 2010), and evidence that the MAP kinase cascade mediates the upregulation of *Sox9* expression by FGF2 has been reported (Murakami et al. 2000). Due to the critical role of FGF signalling in testis-determination, mediated by FGF9 and FGFR2, it

remains a possibility that FGFs could employ the MAP3K4-activated cascade in the gonad to regulate testis-determination. However, support for this model is tempered by the fact that loss of *Fgf9* does not disrupt expression of *Sry* (Colvin et al. 2001). Moreover, XY *byg/byg* gonads were observed to respond to exogenous FGF9 by up-regulation of *Sox9* (Bogani et al. 2009). These observations would seem to position MAP3K4 and FGF9 at different points of the testis-determining pathway. A link between the MAP kinase pathway and *Sox9* was also reported in the gonad, but in this case the MAP kinase pathway mediated the activation of *Sox9* by Vinexin γ, a scaffolding protein of the ERK family of MAP kinases (Matsuyama et al. 2005). However, the targeted disruption of the gene encoding Vinexin γ caused only slight down-regulation of *Sox9* and did not disrupt sex determination.

The interactions between MAP kinase signalling and *Sox9* regulation described above have identified ERK1/2 as the relevant MAPK. However, p38 MAPKs have also been implicated in other relevant *in vitro* studies. p38 MAPK can target *SRY* expression in cultured human keratinocytes (Gazel et al. 2008), regulate IL-1β-induced *SOX9* stabilisation in human articular chondrocytes (Tew and Hardingham 2006), and regulate IL-1α-induced proliferation of cultured Sertoli cells (Petersen et al. 2005). The role of p38 MAPK is further supported by the observations that the MAP kinase pathway can also activate, by phosphorylation, some of the potential transcriptional regulators of *Sry*: SF1 and GATA4. ERK1/2 and p38 MAPK can regulate the binding of GATA4 to DNA in the heart (Tenhunen et al. 2004), while in the mouse prepubertal Sertoli cell line, SMAT1, p38 MAPK has been shown to specifically activate *Gata4* expression (Lasala et al. 2011). In combination with the data from the double p38α/β knockout study, which showed that the transcriptional regulator properties of GATA4 were affected in the heart such that the activation of its target, *Hand2*, was impaired (del Barco Barrantes

et al. 2011), GATA4 therefore remains a very promising candidate as a mediator between the MAP3K4-activated MAP kinase pathway and *Sry* activation in the early gonadal ridge.

Evidence for epigenomic functions of MAP3K4-mediated signalling has previously been reported. During embryonic development of the *Map3k4*$^{ki/ki}$ mutant, Abell *et al* showed that placental disruptions also occurred, which was a result of FGF4-mediated inhibition of JNK and p38 activation in trophoblast stem cells (Abell et al. 2009). Due to these trophoblast defects, further work focusing on trophoblast stem cells isolated from *Map3k4*$^{ki/ki}$ blastocysts (TS^{KI4}) revealed a function for MAP3K4 in the establishment of epigenetic marks (Abell et al. 2011). TS^{KI4} cells underwent an epithelial-mesenchyme transition which was not observed in wild-type TS cells (TS^{WT}). This loss of epithelial phenotype was attributed to the loss of acetylation on histones H2A and H2B. The histone acetyltransferase (HAT) CBP, and a closely related family member p300, were identified following examination of the MAP3K4 signalling network of genes whose targeted disruption resulted in a similar phenotype to those of *Map3k4*$^{ki/ki}$ mutants. This suggested that the loss of H2A/H2B acetylation in TS^{KI4} cells may have been due to altered CBP or p300 activity. Activation of CBP and p300 by phosphorylation can be blocked by a JNK inhibitor, and JNK activity was shown to be reduced in TS^{KI4} cells (Abell et al. 2009). These data suggested that the loss of MAP3K4-activated kinase activity caused the inhibition of H2A/H2B acetylation through JNK-mediated signalling, which affected the properties of trophoblast stem cells (Abell et al. 2011). This implies that MAP3K4-mediated kinase signalling could affect epigenetic regulation of other target genes in different tissues.

If one or more of the p38 MAPKs were indeed the target MAPK in MAP3K4-activated signalling in the gonad, it is possible that disruption of the ability of MAP3K4-mediated signalling to affect epigenetic regulation of target genes could result in impairment of the ability of GATA4 to bind to and transcriptionally activate *Sry* in the gonad, as has been postulated to be the case with GATA4 and its target, *Hand2*, in the heart (del Barco Barrantes et al. 2011).

7.4. MAP kinase signalling and human DSDs

The causes of many cases of human DSDs remain unknown. For example, it has been estimated that around 60-70% of cases of 46,XY gonadal dysgenesis (GD) remain unexplained at the molecular level (Scherer 2002; Ostrer 2008). However, positional cloning studies in patients with 46,XY GD and complete (C) GD have led to the identification of several of the most significant sex-determining genes in mammals. For example, *SRY*, *SOX9*, *SF1*, *WT1* and *WNT4* were all identified in this way. Recently, mutations in *MAP3K1* were also identified as a cause of 46,XY DSD (Pearlman et al. 2010). The phenotypes observed were very variable and included both 46,XY GD and CGD. In addition, the regulation of the downstream MAPKs, p38 and ERK1/2, was found to be disrupted in mutant cell lines derived from these patients. In an effort to determine if *Map3k1* also has a role in mammalian sex determination, we obtained mice carrying a null mutation of *Map3k1* to assess the gonadal phenotype (Warr et al. 2011). *Map3k1* was found to be expressed in the coelomic region of 11.5 dpc gonads, and in the mesonephric tubules and Wolffian duct epithelium. By 13.5 dpc, expression in the XY testis was restricted to the testis cords and was also observed in the mesonephric tubules, Müllerian duct, and Wolffian duct of both sexes. *Map3k1*-deficient mice were viable and fertile on a mixed genetic background; however, on the C57BL/6J

background homozygotes were non-viable and died by 14.5 dpc. Assessment of the XY embryonic gonads at 13.5 dpc on this background revealed that normal testis determination occurred but the gonads were slightly longer in length, and, perhaps as a consequence, some germ cells in the poles were expressing the meiosis marker, *Stra8*. Therefore, the disruption to *Map3k1*-activated MAP kinase signalling does not overtly affect testis determination in the mouse despite the observed role for this gene in human testis determination. There are several explanations for this apparent discrepancy; these include evolutionarily diverged roles of MAP3Ks between humans and mice, or the possibility that the sex-reversing human *MAP3K1* mutations are not simple null alleles, but may act as dominant negatives. However, what these findings do confirm is that there is a conserved role for MAP kinase signalling in sex determination in humans and mice.

7.5. Future experiments

7.5.1. Determining the cell lineage in which disrupted MAP3K4-signalling causes XY gonadal sex reversal

It is necessary to confirm the cell-type specificity of MAP kinase activity during testis determination before the full mechanism of action can be determined. The most conclusive way to do this is through conditional inactivation, targeted to a certain cell type. While this is what I had attempted in this project, it has become apparent that the *Cre* lines used were inappropriate for functional inactivation of the pathway. If it is indeed the case that *Map3k4* (and downstream target gene) deletion needs to be driven earlier than the activities of *Sf1-Cre* allows, it is necessary to consider other *Cre* lines. Despite reports that endogenous *Sf1* is expressed from between 9.0 and 9.5 dpc in the gonadal ridge (Ikeda et al. 1994), *Sf1-Cre* activity, via the activation of β-gal following

recombination of the floxed region in the R26R reporter line to activate *LacZ* expression, is not detected until 10.5 dpc (Bingham et al. 2006), with full gonadal expression not until 11.0 dpc. This difference in timing is likely due to the lag between expression of the *Cre* transgene and expression of the β-gal target protein explained in the Discussion of Chapter 5. In contrast, endogenous *Wt1* is expressed from 9.0 dpc in the somatic cells of the gonadal ridge, and GFP-tagged *Wt1-Cre*^{GFP} expression has been detected from 9.5 dpc (Armstrong et al. 1993; Zhou et al. 2008). An inducible version of this *Cre* line is also available (*Wt1-Cre*^{ERT2}). The inducible *Wt1-Cre*^{ERT2} was used to successfully delete *Gata4*^{flox} at 10.5 dpc, whilst *Sf1-Cre* excised *Gata4*^{flox} too late (Manuylov et al. 2011). The authors also noted that *Sf1-Cre* excision was inefficient in the coelomic epithelium of the gonad, although this was not important for the deletion of *Gata4*. Therefore, using either the inducible or non-inducible *Wt1-Cre* to delete *Map3k4* in the early gonadal ridge might be sufficient to determine if the MAP kinase pathway is required in somatic cells. The use of an inducible, ubiquitously expressed *Cre* may also be useful to confirm the specific time by which *Map3k4* must be deleted to affect testis determination.

An alternative approach to determining the cell lineage in which MAP kinase activity is vital for sex determination involves assessing the cell-type specificity of potential activators of MAP3K4. MAP3K4 is maintained in an auto-inhibitory state and must be activated through the binding of upstream effectors to promote dimerisation, before it can in turn activate a MAP2K (Abell et al. 2007). Effectors that have been identified so far include TRAF4 (tumour necrosis factor receptor-associated factor 4), Axin and GADD45 (growth arrest and DNA damage-inducible 45) proteins. TRAF4 and Axin bind to the C-terminal kinase domain of MAP3K4, whereas GADD45 proteins bind to the N-terminal region (Miyake et al. 2007). The C-terminal kinase domain of MAP3K4

has also been shown to bind to a serine/threonine kinase GSK3β. GSK3β acts as an inhibitor to prevent the dimerisation and is also likely to have important roles during development (Abell et al. 2007). Identification of one of these activators in a specific cell lineage within the gonad during the initial stages of sex determination is likely to identify the site of activation of MAP3K4.

7.5.2. Confirming a role for p38 MAPKs in testis determination

As described above, there are many examples of the ability of p38 MAPKs to regulate known genes involved in sex determination, albeit in other tissues and organ systems. Therefore, a role for p38 MAPKs in testis determination still remains a possibility. Having ascertained that the *Sf1-Cre* line is not a suitable driver for conditional inactivation of MAPK components in the gonad, there are many other options for determining if p38α does indeed have a role in testis determination. The simplest method would be to obtain an epiblast-specific *Cre* line such as MORE-*Cre* to determine if p38α has a role by itself in testis development (Hui et al. 2007; Perdiguero et al. 2007). With the report of the double knockout of both p38α and p38β it might also be possible to collaborate with these authors to assess gonad development in the double knockout mutant embryos (del Barco Barrantes et al. 2011). In addition, identification of a suitable *Cre* driver to drive the deletion of *Map3k4* and recapitulate the XY sex reversal phenotype of *Map3k4*-deficient embryos would enable the opportunity to observe the same cell-specific effects of p38α deletion, or the deletion of other MAP kinase pathway members.

7.5.3. Alternative methods to achieve successful knockdowns

As mentioned in the discussion in Chapter 6, gene knockdowns using organotypic cultures with siRNAs in postnatal ovaries have proved to be relatively successful (Park

et al. 2006). It would be interesting to see if a similar method could be optimised for the use with embryonic gonads. However, the limited reports on successful knockdown in embryonic gonads do suggest most available methods are unreliable. A very recent report has described the use of a new method using conditional RNA interference in transgenic mice (Premsrirut et al. 2011). The authors claim that they have identified a quick way of determining the function of many different genes whose knockdown can be controlled temporally, spatially and is reversible by the addition and removal of doxycycline. Briefly, an expression cassette has been designed to contain several elements that can be manipulated for use with any shRNA, such as a microRNA backbone in which any shRNA sequence can be introduced, a GFP reporter and target sites for the Flp/FRT recombinase system. This is then cloned into embryonic stem (ES) cells that carry a 'homing' cassette; using the site-specific Flp/FRT recombination, the shRNA transgene is inserted into the homing cassette so that it is under the control of a doxycycline (DOX)-inducible promoter. The cassette also includes a selectable marker that is expressed on correct insertion of the shRNA transgene. Mice are then generated from these ES cells following tetraploid embryo complementation, to remove the time needed to screen founder lines for germline transmission. The initiation of shRNA knockdown can then be induced by the treatment of mice with doxycycline either during development or postnatally. The authors suggest that this system could also be used to study the effects of multiple genes at the same time by the insertion of shRNA-targeted alleles into ES cells rederived from transgenic animals. While this method would take longer than the attempted siRNA knockdown in organ culture, it is potentially more robust, and likely to be quicker than producing a double knockout line to address gene function.

7.5.4. Role of other MAPKs in gonad development

Despite the strong associations between p38 MAPKs and sex-determining genes in other tissues, it is of course possible that in the gonad a completely different mechanism directed by a different MAPK is employed to regulate sex determination. Therefore, it would be extremely interesting to assess the expression profiles of other potential MAPKs during early gonad development. Some of the JNK MAPKs have been previously reported to be expressed in the testis, so it is possible that they could also be expressed in the embryonic gonads (Davis 2000).

7.6. Summary

This thesis has presented evidence for a role of MAP3K4 during early gonad development; its inactivation causes XY sex reversal due to *Sry* down-regulation, which disrupts cell proliferation and other cellular events associated with testis development. Further work has attempted to elucidate the exact mechanism of action of this MAP3K4-activated signalling pathway and to identify the downstream components by employing genetic methods. The studies suggest that the MAP kinase signalling pathway is active very early in the gonad and that components of this pathway must be inactivated prior to the upregulation of *Sry* at around 10.5 dpc to disrupt testis determination. Elucidating this mechanism will be important for increasing knowledge about the molecular events that constitute sex determination and thus improve understanding of human DSDs that occur as a result of mutations in these pathways.

References

Abell AN, Rivera-Perez JA, Cuevas BD, Uhlik MT, Sather S, Johnson NL, Minton SK, Lauder JM, Winter-Vann AM, Nakamura K, Magnuson T, Vaillancourt RR, Heasley LE, Johnson GL (2005) Ablation of MEKK4 Kinase Activity Causes Neurulation and Skeletal Patterning Defects in the Mouse Embryo. Mol. Cell. Biol. 25, 8948-8959

Abell AN, Granger DA, Johnson GL (2007) MEKK4 Stimulation of p38 and JNK Activity Is Negatively Regulated by GSK3β. Journal of Biological Chemistry 282, 30476-30484

Abell AN, Granger DA, Johnson NL, Vincent-Jordan N, Dibble CF, Johnson GL (2009) Trophoblast Stem Cell Maintenance by Fibroblast Growth Factor 4 Requires MEKK4 Activation of Jun N-Terminal Kinase. Mol. Cell. Biol. 29, 2748-2761

Abell Amy N, Jordan Nicole V, Huang W, Prat A, Midland Alicia A, Johnson Nancy L, Granger Deborah A, Mieczkowski Piotr A, Perou Charles M, Gomez Shawn M, Li L, Johnson Gary L (2011) MAP3K4/CBP-Regulated H2B Acetylation Controls Epithelial-Mesenchymal Transition in Trophoblast Stem Cells. Cell Stem Cell 8, 525-537

Adams RH, Porras A, Alonso G, Jones M, Vintersten K, Panelli S, Valladares A, Perez L, Klein R, Nebreda AR (2000) Essential Role of p38α MAP Kinase in Placental but Not Embryonic Cardiovascular Development. Molecular Cell 6, 109-116

Allen M, Svensson L, Roach M, Hambor J, McNeish J, Gabel CA (2000) Deficiency of the Stress Kinase P38α Results in Embryonic Lethality. The Journal of Experimental Medicine 191, 859-870

Ananthanarayanan V, Pins MR, Meyer RE, Gann PH (2005) Immunohistochemical assays in prostatic biopsies processed in Bouin's fixative. Journal of Clinical Pathology 58, 322-324

Anttonen M, Ketola I, Parviainen H, Pusa A-K, Heikinheimo M (2003) FOG-2 and GATA-4 Are Coexpressed in the Mouse Ovary and Can Modulate Müllerian-Inhibiting Substance Expression. Biology of Reproduction 68, 1333-1340

Aouadi M, Binetruy B, Caron L, Le Marchand-Brustel Y, Bost F (2006) Role of MAPKs in development and differentiation: lessons from knockout mice. Biochimie 88, 1091-1098

Arango NA, Kobayashi A, Wang Y, Jamin SP, Lee H-H, Orvis GD, Behringer RR (2008) A mesenchymal perspective of müllerian duct differentiation and regression in Amhr2-lacZ mice. Molecular Reproduction and Development 75, 1154-1162

Archambeault DR, Tomaszewski J, Joseph A, Hinton BT, Yao HH-C (2009) Epithelial-mesenchymal crosstalk in Wolffian duct and fetal testis cord development. genesis 47, 40-48

Armstrong JF, Pritchard-Jones K, Bickmore WA, Hastie ND, Bard JBL (1993) The expression of the Wilms' tumour gene, WT1, in the developing mammalian embryo. Mechanisms of Development 40, 85-97

Baarends WM, van Helmond MJ, Post M, van der Schoot PJ, Hoogerbrugge JW, de Winter JP, Uilenbroek JT, Karels B, Wilming LG, Meijers JH (1994) A novel member of the transmembrane serine/threonine kinase receptor family is specifically expressed in the gonads and in mesenchymal cells adjacent to the mullerian duct. Development 120, 189-197

Baarends WM, Hoogerbrugge JW, Post M, Visser JA, De Rooij DG, Parvinen M, Themmen AP, Grootegoed JA (1995a) Anti-müllerian hormone and anti-müllerian hormone type II receptor messenger ribonucleic acid expression during postnatal testis development and in the adult testis of the rat. Endocrinology 136, 5614-5622

Baarends WM, Uilenbroek JT, Kramer P, Hoogerbrugge JW, van Leeuwen EC, Themmen AP, Grootegoed JA (1995b) Anti-müllerian hormone and anti-müllerian hormone type II receptor messenger ribonucleic acid expression in rat ovaries during postnatal development, the estrous cycle, and gonadotropin-induced follicle growth. Endocrinology 136, 4951-4962

Bagheri-Fam S, Sim H, Bernard P, Jayakody I, Taketo MM, Scherer G, Harley VR (2008) Loss of Fgfr2 leads to partial XY sex reversal. Developmental Biology 314, 71-83

Barrionuevo F, Bagheri-Fam S, Klattig J, Kist R, Taketo MM, Englert C, Scherer G (2006) Homozygous Inactivation of Sox9 Causes Complete XY Sex Reversal in Mice. Biol Reprod 74, 195-201

Beardmore VA, Hinton HJ, Eftychi C, Apostolaki M, Armaka M, Darragh J, McIlrath J, Carr JM, Armit LJ, Clacher C, Malone L, Kollias G, Arthur JSC (2005) Generation and Characterization of p38β (MAPK11) Gene-Targeted Mice. Mol. Cell. Biol. 25, 10454-10464

Behringer RR, Cate RL, Froelick GJ, Palmiter RD, Brinster RL (1990) Abnormal sexual development in transgenic mice chronically expressing Mullerian inhibiting substance. Nature 345, 167-170

Behringer RR, Finegold MJ, Cate RL (1994) Müllerian-inhibiting substance function during mammalian sexual development. Cell 79, 415-425

Bernstein E, Caudy AA, Hammond SM, Hannon GJ (2001) Role for a bidentate ribonuclease in the initiation step of RNA interference. Nature 409, 363-366

Bernstein E, Kim SY, Carmell MA, Murchison EP, Alcorn H, Li MZ, Mills AA, Elledge SJ, Anderson KV, Hannon GJ (2003) Dicer is essential for mouse development. Nat Genet 35, 215-217

Bingham NC, Verma-Kurvari S, Parada LF, Parker KL (2006) Development of a steroidogenic factor 1/Cre transgenic mouse line. genesis 44, 419-424

Bogani D, Siggers P, Brixey R, Warr N, Beddow S, Edwards J, Williams D, Wilhelm D, Koopman P, Flavell RA, Chi H, Ostrer H, Wells S, Cheeseman M, Greenfield A (2009) Loss of Mitogen-Activated Protein Kinase Kinase Kinase 4 (MAP3K4) Reveals a Requirement for MAPK Signalling in Mouse Sex Determination. PLoS Biol 7, e1000196

Bouma GJ, Washburn LL, Albrecht KH, Eicher EM (2007) Correct dosage of Fog2 and Gata4 transcription factors is critical for fetal testis development in mice. Proceedings of the National Academy of Sciences 104, 14994-14999

Bowles J, Knight D, Smith C, Wilhelm D, Richman J, Mamiya S, Yashiro K, Chawengsaksophak K, Wilson MJ, Rossant J, Hamada H, Koopman P (2006) Retinoid Signaling Determines Germ Cell Fate in Mice. Science 312, 596-600

Bowles J, Feng C-W, Spiller C, Davidson T-L, Jackson A, Koopman P (2010) FGF9 Suppresses Meiosis and Promotes Male Germ Cell Fate in Mice. Developmental Cell 19, 440-449

Bradford ST, Wilhelm D, Bandiera R, Vidal V, Schedl A, Koopman P (2009) A cell-autonomous role for WT1 in regulating Sry in vivo. Hum. Mol. Genet. 18, 3429-3438

Brennan J, Capel B (2004) One tissue, two fates: molecular genetic events that underlie testis versus ovary development. Nat Rev Genet 5, 509-521

Bruchas Michael R, Schindler Abigail G, Shankar H, Messinger Daniel I, Miyatake M, Land Benjamin B, Lemos Julia C, Hagan CE, Neumaier John F, Quintana A, Palmiter Richard D, Chavkin C (2011) Selective p38α MAPK Deletion in Serotonergic Neurons Produces Stress Resilience in Models of Depression and Addiction. Neuron 71, 498-511

Buaas FW, Val P, Swain A (2009) The transcription co-factor CITED2 functions during sex determination and early gonad development. Hum. Mol. Genet. 18, 2989-3001

Buehr M, Gu S, McLaren A (1993) Mesonephric contribution to testis differentiation in the fetal mouse. Development 117, 273-281

Bullejos M, Koopman P (2001) Spatially dynamic expression of *Sry* in mouse genital ridges. Developmental Dynamics 221, 201-205

Burgoyne PS, Buehr M, Koopman P, Rossant J, McLaren A (1988) Cell-autonomous action of the testis-determining gene: Sertoli cells are exclusively XY in XX↔XY chimaeric mouse testes. Development 102, 443-450

Caffrey DR, O'Neill LAJ, Shields DC (1999) The Evolution of the MAP Kinase Pathways: Coduplication of Interacting Proteins Leads to New Signaling Cascades. Journal of Molecular Evolution 49, 567-582

Cameron FJ, Sinclair AH (1997) Mutations in SRY and SOX9: Testis-determining genes. Human Mutation 9, 388-395

Carroll TJ, Park J-S, Hayashi S, Majumdar A, McMahon AP (2005) Wnt9b Plays a Central Role in the Regulation of Mesenchymal to Epithelial Transitions Underlying Organogenesis of the Mammalian Urogenital System. Developmental Cell 9, 283-292

Chaboissier M-C, Kobayashi A, Vidal VIP, LÃ¼tzkendorf S, van de Kant HJG, Wegner M, de Rooij DG, Behringer RR, Schedl A (2004) Functional analysis of Sox8 and Sox9 during sex determination in the mouse. Development 131, 1891-1901

Chassot A-A, Ranc F, Gregoire EP, Roepers-Gajadien HL, Taketo MM, Camerino G, de Rooij DG, Schedl A, Chaboissier M-C (2008) Activation of β-catenin signaling by Rspo1 controls differentiation of the mammalian ovary. Human Molecular Genetics 17, 1264-1277

Chi H, Lu B, Takekawa M, Davis RJ, Flavell RA (2004) GADD45β/GADD45γ and MEKK4 comprise a genetic pathway mediating STAT4-independent IFNγ production in T cells. EMBO J 23, 1576-1586

Chi H, Sarkisian MR, Rakic P, Flavell RA (2005) Loss of mitogen-activated protein kinase kinase kinase 4 (MEKK4) results in enhanced apoptosis and defective neural tube development. Proceedings of the National Academy of Sciences of the United States of America 102, 3846-3851

Colvin JS, Green RP, Schmahl J, Capel B, Ornitz DM (2001) Male-to-Female Sex Reversal in Mice Lacking Fibroblast Growth Factor 9. Cell 104, 875-889

Combes AN, Lesieur E, Harley VR, Sinclair AH, Little MH, Wilhelm D, Koopman P (2009a) Three-dimensional visualization of testis cord morphogenesis, a novel tubulogenic mechanism in development. Developmental Dynamics 238, 1033-1041

Combes AN, Wilhelm D, Davidson T, Dejana E, Harley V, Sinclair A, Koopman P (2009b) Endothelial cell migration directs testis cord formation. Developmental Biology 326, 112-120

Cool J, Carmona FD, Szucsik JC, Capel B (2008) Peritubular Myoid Cells Are Not the Migrating Population Required for Testis Cord Formation in the XY Gonad. Sexual Development 2, 128-133

Cool J, DeFalco TJ, Capel B (2011) Vascular-mesenchymal cross-talk through Vegf and Pdgf drives organ patterning. Proceedings of the National Academy of Sciences 108, 167-172

Crispino JD, Lodish MB, Thurberg BL, Litovsky SH, Collins T, Molkentin JD, Orkin SH (2001) Proper coronary vascular development and heart morphogenesis depend on interaction of GATA-4 with FOG cofactors. Genes & Development 15, 839-844

Cuevas BD, Abell AN, Johnson GL (2007) Role of mitogen-activated protein kinase kinase kinases in signal integration. Oncogene 26, 3159-3171

Davies JA, Ladomery M, Hohenstein P, Michael L, Shafe A, Spraggon L, Hastie N (2004) Development of an siRNA-based method for repressing specific genes in renal organ culture and its use to show that the Wt1 tumour suppressor is required for nephron differentiation. Hum. Mol. Genet. 13, 235-246

Davies SP, Reddy H, Caivano M, Cohen P (2000) Specificity and mechanism of action of some commonly used protein kinase inhibitors. Biochem. J. 351, 95-105

Davis RJ (2000) Signal Transduction by the JNK Group of MAP Kinases. Cell 103, 239-252

DeFalco T, Takahashi S, Capel B (2011) Two distinct origins for Leydig cell progenitors in the fetal testis. Developmental Biology 352, 14-26

del Barco Barrantes I, Coya JM, Maina F, Arthur JSC, Nebreda AR (2011) Genetic analysis of specific and redundant roles for p38α and p38β MAPKs during mouse development. Proceedings of the National Academy of Sciences 108, 12764-12769

Dérijard B, Raingeaud J, Barrett T, Wu IH, Han J, Ulevitch RJ, Davis RJ (1995) Independent Human MAP Kinase Signal Transduction Pathways Defined by MEK and MKK Isoforms. Science 267, 682-685

Deutscher E, Yao HH-C (2007) Essential roles of mesenchyme-derived beta-catenin in mouse Mullerian duct morphogenesis. Developmental Biology 307, 227-236

Dhanasekaran DN, Kashef K, Lee CM, Xu H, Reddy EP (2007) Scaffold proteins of MAP-kinase modules. Oncogene 26, 3185-3202

Dong C, Yang DD, Wysk M, Whitmarsh AJ, Davis RJ, Flavell RA (1998) Defective T Cell Differentiation in the Absence of Jnk1. Science 282, 2092-2095

Dressler GR, Deutsch U, Chowdhury K, Nornes HO, Gruss P (1990) Pax2, a new murine paired-box-containing gene and its expression in the developing excretory system. Development 109, 787-795

Elbashir SM, Harborth J, Lendeckel W, Yalcin A, Weber K, Tuschl T (2001a) Duplexes of 21-nucleotide RNAs mediate RNA interference in cultured mammalian cells. Nature 411, 494-498

Elbashir SM, Lendeckel W, Tuschl T (2001b) RNA interference is mediated by 21- and 22-nucleotide RNAs. Genes & Development 15, 188-200

Engel FB, Schebesta M, Duong MT, Lu G, Ren S, Madwed JB, Jiang H, Wang Y, Keating MT (2005) p38 MAP kinase inhibition enables proliferation of adult mammalian cardiomyocytes. Genes & Development 19, 1175-1187

Enslen H, Raingeaud Jl, Davis RJ (1998) Selective Activation of p38 Mitogen-activated Protein (MAP) Kinase Isoforms by the MAP Kinase Kinases MKK3 and MKK6. Journal of Biological Chemistry 273, 1741-1748

Ewen K, Jackson A, Wilhelm D, Koopman P (2010) A Male-Specific Role for p38 Mitogen-Activated Protein Kinase in Germ Cell Sex Differentiation in Mice. Biology of Reproduction 83, 1005-1014

Eyers PA, van den Ijssel P, Quinlan RA, Goedert M, Cohen P (1999) Use of a drug-resistant mutant of stress-activated protein kinase 2a/p38 to validate the in vivo specificity of SB 203580. FEBS Letters 451, 191-196

Frevel MAE, Bakheet T, Silva AM, Hissong JG, Khabar KSA, Williams BRG (2003) p38 Mitogen-Activated Protein Kinase-Dependent and -Independent Signaling of mRNA Stability of AU-Rich Element-Containing Transcripts. Mol. Cell. Biol. 23, 425-436

Gazel A, Nijhawan RI, Walsh R, Blumenberg M (2008) Transcriptional profiling defines the roles of ERK and p38 kinases in epidermal keratinocytes. Journal of Cellular Physiology 215, 292-308

Gerwins Pr, Jonathan LB, Johnson GL (1997) Cloning of a Novel Mitogen-activated Protein Kinase Kinase Kinase, MEKK4, That Selectively Regulates the c-Jun Amino Terminal Kinase Pathway. Journal of Biological Chemistry 272, 8288-8295

Gill SE, Pape MC, Leco KJ (2006) Tissue inhibitor of metalloproteinases 3 regulates extracellular matrix--Cell signaling during bronchiole branching morphogenesis. Developmental Biology 298, 540-554

Ginsburg M, Snow MH, McLaren A (1990) Primordial germ cells in the mouse embryo during gastrulation. Development 110, 521-528

Gomperts M, Garcia-Castro M, Wylie C, Heasman J (1994) Interactions between primordial germ cells play a role in their migration in mouse embryos. Development 120, 135-141

Goto H, Tomono Y, Ajiro K, Kosako H, Fujita M, Sakurai M, Okawa K, Iwamatsu A, Okigaki T, Takahashi T, Inagaki M (1999) Identification of a Novel Phosphorylation Site on Histone H3 Coupled with Mitotic Chromosome Condensation. Journal of Biological Chemistry 274, 25543-25549

Gubbay J, Collignon J, Koopman P, Capel B, Economou A, Münsterberg A, Vivian N, Goodfellow P, Lovell-Badge R (1990) A gene mapping to the sex-determining region of the mouse Y chromosome is a member of a novel family of embryonically expressed genes. Nature 346, 245-250

Hacker A, Capel B, Goodfellow P, Lovell-Badge R (1995) Expression of Sry, the mouse sex determining gene. Development 121, 1603-1614

Hammer GD, Krylova I, Zhang Y, Darimont BD, Simpson K, Weigel NL, Ingraham HA (1999) Phosphorylation of the Nuclear Receptor SF-1 Modulates Cofactor Recruitment: Integration of Hormone Signaling in Reproduction and Stress. Molecular Cell 3, 521-526

Hammes A, Guo J-K, Lutsch G, Leheste J-R, Landrock D, Ziegler U, Gubler M-C, Schedl A (2001) Two Splice Variants of the Wilms' Tumor 1 Gene Have Distinct Functions during Sex Determination and Nephron Formation. Cell 106, 319-329

Han J, Lee J-D, Jiang Y, Li Z, Feng L, Ulevitch RJ (1996) Characterization of the Structure and Function of a Novel MAP Kinase Kinase (MKK6). Journal of Biological Chemistry 271, 2886-2891

Hannon GJ (2002) RNA interference. Nature 418, 244-251

Hendzel MJ, Wei Y, Mancini MA, Van Hooser A, Ranalli T, Brinkley BR, Bazett-Jones DP, Allis CD (1997) Mitosis-specific phosphorylation of histone H3 initiates primarily within pericentromeric heterochromatin during G2 and spreads in an ordered fashion coincident with mitotic chromosome condensation. Chromosoma 106, 348-360

Hernandez Gifford JA, Hunzicker-Dunn ME, Nilson JH (2009) Conditional Deletion of Beta-Catenin Mediated by Amhr2cre in Mice Causes Female Infertility. Biology of Reproduction 80, 1282-1292

Hiramatsu R, Matoba S, Kanai-Azuma M, Tsunekawa N, Katoh-Fukui Y, Kurohmaru M, Morohashi K-i, Wilhelm D, Koopman P, Kanai Y (2009) A critical time window of Sry action in gonadal sex determination in mice. Development 136, 129-138

Hiramatsu R, Harikae K, Tsunekawa N, Kurohmaru M, Matsuo I, Kanai Y (2010) FGF signaling directs a center-to-pole expansion of tubulogenesis in mouse testis differentiation. Development 137, 303-312

Hu MCT, Wang Y-p, Mikhail A, Qiu WR, Tan T-H (1999) Murine p38-δ Mitogen-activated Protein Kinase, a Developmentally Regulated Protein Kinase That Is Activated by Stress and Proinflammatory Cytokines. Journal of Biological Chemistry 274, 7095-7102

Hui L, Bakiri L, Mairhorfer A, Schweifer N, Haslinger C, Kenner L, Komnenovic V, Scheuch H, Beug H, Wagner EF (2007) p38α suppresses normal and cancer cell proliferation by antagonizing the JNK-c-Jun pathway. Nat Genet 39, 741-749

Ihle JN (2000) The Challenges of Translating Knockout Phenotypes into Gene Function. Cell 102, 131-134

Ikeda Y, Shen WH, Ingraham HA, Parker KL (1994) Developmental expression of mouse steroidogenic factor-1, an essential regulator of the steroid hydroxylases. Molecular Endocrinology 8, 654-662

Ikeda Y, Luo X, Abbud R, Nilson JH, Parker KL (1995) The nuclear receptor steroidogenic factor 1 is essential for the formation of the ventromedial hypothalamic nucleus. Molecular Endocrinology 9, 478-486

Iwanaga A, Wang G, Gantulga D, Sato T, Baljinnyam T, Shimizu K, Takumi K, Hayashi M, Akashi T, Fuse H, Sugihara K, Asano M, Yoshioka K (2008) Ablation of the scaffold protein JLP causes reduced fertility in male mice. Transgenic Research 17, 1045-1058

Jamin SP, Arango NA, Mishina Y, Hanks MC, Behringer RR (2002) Requirement of Bmpr1a for Mullerian duct regression during male sexual development. Nat Genet 32, 408-410

Jeays-Ward K, Hoyle C, Brennan J, Dandonneau M, Alldus G, Capel B, Swain A (2003) Endothelial and steroidogenic cell migration are regulated by WNT4 in the developing mammalian gonad. Development 130, 3663-3670

Jeske YWA, Bowles J, Greenfield A, Koopman P (1995) Expression of a linear Sry transcript in the mouse genital ridge. Nat Genet 10, 480-482

Jeyasuria P, Ikeda Y, Jamin SP, Zhao L, de Rooij DG, Themmen APN, Behringer RR, Parker KL (2004) Cell-Specific Knockout of Steroidogenic Factor 1 Reveals Its Essential Roles in Gonadal Function. Mol Endocrinol 18, 1610-1619

Jiang Y, Gram H, Zhao M, New L, Gu J, Feng L, Di Padova F, Ulevitch RJ, Han J (1997) Characterization of the Structure and Function of the Fourth Member of p38 Group Mitogen-activated Protein Kinases, p38δ. Journal of Biological Chemistry 272, 30122-30128

Jordan BK, Mohammed M, Ching ST, Délot E, Chen X-N, Dewing P, Swain A, Rao PN, Elejalde BR, Vilain E (2001) Up-Regulation of WNT-4 Signaling and Dosage-Sensitive Sex Reversal in Humans. The American Journal of Human Genetics 68, 1102-1109

Jorgez CJ, Klysik M, Jamin SP, Behringer RR, Matzuk MM (2004) Granulosa Cell-Specific Inactivation of Follistatin Causes Female Fertility Defects. Mol Endocrinol 18, 953-967

Josso N, Picard J-Y, Imbeaud S, Clemente Nd, Rey R (1997) Clinical aspects and molecular genetics of the persistent Müllerian duct syndrome. Clinical Endocrinology 47, 137-144

Josso N, Clemente Nd (2003) Transduction pathway of anti-Müllerian hormone, a sex-specific member of the TGF-β family. Trends in Endocrinology and Metabolism 14, 91-97

Karl J, Capel B (1995) Three-Dimensional Structure of the Developing Mouse Genital Ridge. Philosophical Transactions: Biological Sciences 350, 235-242

Karl J, Capel B (1998) Sertoli Cells of the Mouse Testis Originate from the Coelomic Epithelium. Developmental Biology 203, 323-333

Ketola I, Anttonen M, Vaskivuo T, Tapanainen JS, Toppari J, Heikinheimo M (2002) Developmental expression and spermatogenic stage specificity of transcription factors GATA-1 and GATA-4 and their cofactors FOG-1 and FOG-2 in the mouse testis. European Journal of Endocrinology 147, 397-406

Kim C, Sano Y, Todorova K, Carlson BA, Arpa L, Celada A, Lawrence T, Otsu K, Brissette JL, Arthur JSC, Park JM (2008) The kinase p38α serves cell type-specific inflammatory functions in skin injury and coordinates pro- and anti-inflammatory gene expression. Nat Immunol 9, 1019-1027

Kim Y, Kobayashi A, Sekido R, DiNapoli L, Brennan J, Chaboissier M-C, Poulat F, Behringer RR, Lovell-Badge R, Capel B (2006) Fgf9 and Wnt4 Act as Antagonistic Signals to Regulate Mammalian Sex Determination. PLoS Biology 4, e187

Kim Y, Bingham N, Sekido R, Parker KL, Lovell-Badge R, Capel B (2007) Fibroblast growth factor receptor 2 regulates proliferation and Sertoli differentiation during male sex determination. Proceedings of the National Academy of Sciences 104, 16558-16563

Kobayashi A, Behringer RR (2003) Developmental genetics of the female reproductive tract in mammals. Nat Rev Genet 4, 969-980

Kobayashi A, Stewart CA, Wang Y, Fujioka K, Thomas NC, Jamin SP, Behringer RR (2011) β-Catenin is essential for Müllerian duct regression during male sexual differentiation. Development 138, 1967-1975

Kocer A, Reichmann J, Best D, Adams IR (2009) Germ cell sex determination in mammals. Mol. Hum. Reprod. 15, 205-213

Koopman P, Munsterberg A, Capel B, Vivian N, Lovell-Badge R (1990) Expression of a candidate sex-determining gene during mouse testis differentiation. Nature 348, 450-452

Koopman P, Gubbay J, Vivian N, Goodfellow P, Lovell-Badge R (1991) Male development of chromosomally female mice transgenic for Sry. Nature 351, 117-121

Koopman P (2010) The delicate balance between male and female sex determining pathways: potential for disruption of early steps in sexual development. International Journal of Andrology 33, 252-258

Koshland D, Strunnikov A (1996) Mitotic chromosome condensation. Annual Review of Cell and Developmental Biology 12, 305-333

Koubova J, Menke DB, Zhou Q, Capel B, Griswold MD, Page DC (2006) Retinoic acid regulates sex-specific timing of meiotic initiation in mice. Proceedings of the National Academy of Sciences of the United States of America 103, 2474-2479

Kreidberg JA, Sariola H, Loring JM, Maeda M, Pelletier J, Housman D, Jaenisch R (1993) WT-1 is required for early kidney development. Cell 74, 679-691

Kuan C-Y, Yang DD, Roy DRS, Davis RJ, Rakic P, Flavell RA (1999) The Jnk1 and Jnk2 Protein Kinases Are Required for Regional Specific Apoptosis during Early Brain Development. Neuron 22, 667-676

Kurohmaru M, Kanai Y, hayashi Y (1992) A cytological and cytoskeletal comparison of sertoli cells without germ cell and those with germ cells using the W/Wv mutant mouse. Tissue and Cell 24, 895-903

Kwan K-M (2002) Conditional alleles in mice: Practical considerations for tissue-specific knockouts. genesis 32, 49-62

Kwintkiewicz J, Cai Z, Stocco C (2007) Follicle-Stimulating Hormone-Induced Activation of Gata4 Contributes in the Up-Regulation of Cyp19 Expression in Rat Granulosa Cells. Molecular Endocrinology 21, 933-947

Kyriakis JM, Brautigan DL, Ingebritsen TS, Avruch J (1991) pp54 microtubule-associated protein-2 kinase requires both tyrosine and serine/threonine phosphorylation for activity. Journal of Biological Chemistry 266, 10043-10046

Kyriakis JM, Banerjee P, Nikolakaki E, Dai T, Rubie EA, Ahmad MF, Avruch J, Woodgett JR (1994) The stress-activated protein kinase subfamily of c-Jun kinases. Nature 369, 156-160

Kyrönlahti A, Euler R, Bielinska M, Schoeller EL, Moley KH, Toppari J, Heikinheimo M, Wilson DB (2011a) GATA4 regulates Sertoli cell function and fertility in adult male mice. Molecular and Cellular Endocrinology 333, 85-95

Kyrönlahti A, Vetter M, Euler R, Bielinska M, Jay PY, Anttonen M, Heikinheimo M, Wilson DB (2011b) GATA4 Deficiency Impairs Ovarian Function in Adult Mice. Biology of Reproduction 84, 1033-1044

Lanner F, Rossant J (2010) The role of FGF/Erk signaling in pluripotent cells. Development 137, 3351-3360

Lasala C, Schteingart HF, Arouche N, Bedecarrás P, Grinspon RP, Picard J-Y, Josso N, di Clemente N, Rey RA (2011) SOX9 and SF1 are involved in cyclic AMP-mediated upregulation of anti-Müllerian gene expression in the testicular prepubertal Sertoli cell line SMAT1. American Journal of Physiology - Endocrinology And Metabolism 301, E539-E547

Lavery R, Lardenois A, Ranc-Jianmotamedi F, Pauper E, Gregoire EP, Vigier C, Moreilhon C, Primig M, Chaboissier M-C (2011) XY *Sox9* embryonic loss-of-function mouse mutants show complete sex reversal and produce partially fertile XY oocytes. Developmental Biology 354, 111-122

Lavoie JN, L'Allemain G, Brunet A, Müller R, Pouysségur J (1996) Cyclin D1 Expression Is Regulated Positively by the p42/p44MAPK and Negatively by the p38/HOGMAPK Pathway. Journal of Biological Chemistry 271, 20608-20616

Lee SH, Park J, Che Y, Han P-L, Lee J-K (2000) Constitutive activity and differential localization of p38α and p38β MAPKs in adult mouse brain. Journal of Neuroscience Research 60, 623-631

Lee W-C, Berry R, Hohenstein P, Davies J (2008) siRNA as a tool for investigating organogenesis: The pitfalls and the promises. Organogenesis 4, 176-181

Lei N, Hornbaker KI, Rice DA, Karpova T, Agbor VA, Heckert LL (2007) Sex-Specific Differences in Mouse DMRT1 Expression Are Both Cell Type- and Stage-Dependent During Gonad Development. Biology of Reproduction 77, 466-475

Lengronne A, Pasero P, Bensimon A, Schwob E (2001) Monitoring S phase progression globally and locally using BrdU incorporation in TK+ yeast strains. Nucleic Acids Research 29, 1433-1442

Lewandoski M, Martin GR (1997) Cre-mediated chromosome loss in mice. Nat Genet 17, 223-225

Lin L, Achermann JC (2008) Steroidogenic Factor-1 (*SF-1*, *Ad4BP*, *NR5A1*) and Disorders of Testis Development. Sexual Development 2, 200-209

Liu C-F, Bingham N, Parker K, Yao HHC (2009) Sex-specific roles of β-catenin in mouse gonadal development. Hum. Mol. Genet. 18, 405-417

Liu Z, Fan H-Y, Wang Y, Richards JS (2010) Targeted Disruption of Mapk14 (p38MAPKα) in Granulosa Cells and Cumulus Cells Causes Cell-Specific Changes in Gene Expression Profiles that Rescue COC Expansion and Maintain Fertility. Mol Endocrinol 24, 1794-1804

Luo X, Ikeda Y, Parker KL (1994) A cell-specific nuclear receptor is essential for adrenal and gonadal development and sexual differentiation. Cell 77, 481-490

Maizels ET, Cottom J, Jones JCR, Hunzicker-Dunn M (1998) Follicle Stimulating Hormone (FSH) Activates the p38 Mitogen-Activated Protein Kinase Pathway, Inducing Small Heat Shock Protein Phosphorylation and Cell Rounding in Immature Rat Ovarian Granulosa Cells. Endocrinology 139, 3353-3356

Mandel H, Shemer R, Borochowitz ZU, Okopnik M, Knopf C, Indelman M, Drugan A, Tiosano D, Gershoni-Baruch R, Choder M, Sprecher E (2008) SERKAL Syndrome: An Autosomal-Recessive Disorder Caused by a Loss-of-Function Mutation in WNT4. The American Journal of Human Genetics 82, 39-47

Manuylov NL, Zhou B, Ma Q, Fox SC, Pu WT, Tevosian SG (2011) Conditional ablation of *Gata4* and *Fog2* genes in mice reveals their distinct roles in mammalian sexual differentiation. Developmental Biology 353, 229-241

Martin JH, Mohit AA, Miller CA (1996) Developmental expression in the mouse nervous system of the p493F12 SAP kinase. Molecular Brain Research 35, 47-57

Martineau J, Nordqvist K, Tilmann C, Lovell-Badge R, Capel B (1997) Male-specific cell migration into the developing gonad. Current Biology 7, 958-968

Matson CK, Murphy MW, Sarver AL, Griswold MD, Bardwell VJ, Zarkower D (2011) DMRT1 prevents female reprogramming in the postnatal mammalian testis. Nature 476, 101-104

Matsuyama M, Mizusaki H, Shimono A, Mukai T, Okumura K, Abe K, Shimada K, Morohashi K-i (2005) A novel isoform of Vinexin, Vinexin γ, regulates Sox9 gene expression through activation of MAPK cascade in mouse fetal gonad. Genes to Cells 10, 421-434

McElreavey K, Vilain E, Abbas N, Herskowitz I, Fellous M (1993) A regulatory cascade hypothesis for mammalian sex determination: SRY represses a negative regulator of male development. Proceedings of the National Academy of Sciences 90, 3368-3372

McLaren A, Buehr M (1990) Development of mouse germ cells in cultures of fetal gonads. Cell Differentiation and Development 31, 185-195

McLaren A (1991) Development of the mammalian gonad: The fate of the supporting cell lineage. BioEssays 13, 151-156

Mericskay M, Kitajewski J, Sassoon D (2004) Wnt5a is required for proper epithelial-mesenchymal interactions in the uterus. Development 131, 2061-2072

Miller C, Pavlova A, Sassoon DA (1998) Differential expression patterns of Wnt genes in the murine female reproductive tract during development and the estrous cycle. Mechanisms of Development 76, 91-99

Miller C, Sassoon DA (1998) Wnt-7a maintains appropriate uterine patterning during the development of the mouse female reproductive tract. Development 125, 3201-3211

Mishina Y, Rey R, Finegold MJ, Matzuk MM, Josso N, Cate RL, Behringer RR (1996) Genetic analysis of the Müllerian-inhibiting substance signal transduction pathway in mammalian sexual differentiation. Genes & Development 10, 2577-2587

Miyake Z, Takekawa M, Ge Q, Saito H (2007) Activation of MTK1/MEKK4 by GADD45 through Induced N-C Dissociation and Dimerization-Mediated trans Autophosphorylation of the MTK1 Kinase Domain. Mol. Cell. Biol. 27, 2765-2776

Moniot B, Declosmenil F, Barrionuevo F, Scherer G, Aritake K, Malki S, Marzi L, Cohen-Solal A, Georg I, Klattig J, Englert C, Kim Y, Capel B, Eguchi N, Urade Y, Boizet-Bonhoure B, Poulat F (2009) The PGD2 pathway, independently of FGF9, amplifies SOX9 activity in Sertoli cells during male sexual differentiation. Development 136, 1813-1821

Moon AM, Capecchi MR (2000) Fgf8 is required for outgrowth and patterning of the limbs. Nat Genet 26, 455-459

Morais da Silva S, Hacker A, Harley V, Goodfellow P, Swain A, Lovell-Badge R (1996) Sox9 expression during gonadal development implies a conserved role for the gene in testis differentiation in mammals and birds. Nat Genet 14, 62-68

Mudgett JS, Ding J, Guh-Siesel L, Chartrain NA, Yang L, Gopal S, Shen MM (2000) Essential role for p38α mitogen-activated protein kinase in placental angiogenesis. Proceedings of the National Academy of Sciences 97, 10454-10459

Munger SC, Aylor DL, Syed HA, Magwene PM, Threadgill DW, Capel B (2009) Elucidation of the transcription network governing mammalian sex determination by exploiting strain-specific susceptibility to sex reversal. Genes & Development 23, 2521-2536

Münsterberg A, Lovell-Badge R (1991) Expression of the mouse anti-mullerian hormone gene suggests a role in both male and female sexual differentiation. Development 113, 613-624

Murakami S, Kan M, McKeehan WL, de Crombrugghe B (2000) Up-regulation of the chondrogenic Sox9 gene by fibroblast growth factors is mediated by the mitogen-activated protein kinase pathway. Proceedings of the National Academy of Sciences of the United States of America 97, 1113-1118

Nagy A, Gocza E, Diaz EM, Prideaux VR, Ivanyi E, Markkula M, Rossant J (1990) Embryonic stem cells alone are able to support fetal development in the mouse. Development 110, 815-821

Nagy A (2000) Cre recombinase: The universal reagent for genome tailoring. genesis 26, 99-109

Nef S, Schaad O, Stallings NR, Cederroth CR, Pitetti J-L, Schaer G, Malki S, Dubois-Dauphin M, Boizet-Bonhoure B, Descombes P, Parker KL, Vassalli J-D (2005) Gene expression during sex determination reveals a robust female genetic program at the onset of ovarian development. Developmental Biology 287, 361-377

Orvis GD, Behringer RR (2007) Cellular mechanisms of Müllerian duct formation in the mouse. Developmental Biology 306, 493-504

Ostrer H (2008) 46,XY Disorder of Sex Development and 46,XY Complete Gonadal Dysgenesis. In GeneReviews B.T. Pagon RA, Dolan CR, Stephens K, ed. (Seattle (WA): University of Washington, Seattle; 1993-)

Ottolenghi C, Omari S, Garcia-Ortiz JE, Uda M, Crisponi L, Forabosco A, Pilia G, Schlessinger D (2005) Foxl2 is required for commitment to ovary differentiation. Human Molecular Genetics 14, 2053-2062

Ottolenghi C, Pelosi E, Tran J, Colombino M, Douglass E, Nedorezov T, Cao A, Forabosco A, Schlessinger D (2007) Loss of Wnt4 and Foxl2 leads to female-to-male sex reversal extending to germ cells. Hum. Mol. Genet. 16, 2795-2804

Park C-E, Lee D, Kim K-H, Lee K-A (2006) Establishment of ovarian reconstruction system in culture for functional genomic analysis. Journal of Bioscience and Bioengineering 102, 396-401

Parma P, Radi O, Vidal V, Chaboissier MC, Dellambra E, Valentini S, Guerra L, Schedl A, Camerino G (2006) R-spondin1 is essential in sex determination, skin differentiation and malignancy. Nat Genet 38, 1304-1309

Parr BA, McMahon AP (1998) Sexually dimorphic development of the mammalian reproductive tract requires Wnt-7a. Nature 395, 707-710

Pastorelli L, Wells S, Fray M, Smith A, Hough T, Harfe B, McManus M, Smith L, Woolf A, Cheeseman M, Greenfield A (2009) Genetic analyses reveal a requirement for Dicer1 in the mouse urogenital tract. Mammalian Genome 20, 140-151

Pearlman A, Loke J, Le Caignec C, White S, Chin L, Friedman A, Warr N, Willan J, Brauer D, Farmer C, Brooks E, Oddoux C, Riley B, Shajahan S, Camerino G, Homfray T, Crosby AH, Couper J, David A, Greenfield A, Sinclair A, Ostrer H (2010) Mutations in MAP3K1 Cause 46,XY Disorders of Sex Development and Implicate a Common Signal Transduction Pathway in Human Testis Determination. The American Journal of Human Genetics 87, 898-904

Perdiguero E, Ruiz-Bonilla V, Gresh L, Hui L, Ballestar E, Sousa-Victor P, Baeza-Raja B, Jardi M, Bosch-Comas A, Esteller M, Caelles C, Serrano AL, Wagner EF, Munoz-Canoves P (2007) Genetic analysis of p38 MAP kinases in myogenesis: fundamental role of p38α in abrogating myoblast proliferation. EMBO J 26, 1245-1256

Petersen C, Svechnikov K, Fröysa B, Söder O (2005) The p38 MAPK pathway mediates interleukin-1-induced Sertoli cell proliferation. Cytokine 32, 51-59

Pilon N, Daneau I, Paradis V, Hamel Fdr, Lussier JG, Viger RS, Silversides DW (2003) Porcine SRY Promoter Is a Target for Steroidogenic Factor 1. Biology of Reproduction 68, 1098-1106

Polanco JC, Koopman P (2007) Sry and the hesitant beginnings of male development. Developmental Biology 302, 13-24

Premsrirut PK, Dow LE, Kim SY, Camiolo M, Malone CD, Miething C, Scuoppo C, Zuber J, Dickins RA, Kogan SC, Shroyer KR, Sordella R, Hannon GJ, Lowe SW (2011) A Rapid and Scalable System for Studying Gene Function in Mice Using Conditional RNA Interference. Cell 145, 145-158

Racine C, Rey R, Forest MG, Louis F, Ferré A, Huhtaniemi I, Josso N, di Clemente N (1998) Receptors for anti-Müllerian hormone on Leydig cells are responsible for its effects on steroidogenesis and cell differentiation. Proceedings of the National Academy of Sciences 95, 594-599

Raingeaud Jl, Gupta S, Rogers JS, Dickens M, Han J, Ulevitch RJ, Davis RJ (1995) Pro-inflammatory Cytokines and Environmental Stress Cause p38 Mitogen-activated Protein Kinase Activation by Dual Phosphorylation on Tyrosine and Threonine. Journal of Biological Chemistry 270, 7420-7426

Raymond CS, Murphy MW, O'Sullivan MG, Bardwell VJ, Zarkower D (2000) Dmrt1, a gene related to worm and fly sexual regulators, is required for mammalian testis differentiation. Genes & Development 14, 2587-2595

Ryan J, Ludbrook L, Wilhelm D, Sinclair A, Koopman P, Bernard P, Harley VR (2010) Analysis of Gene Function in Cultured Embryonic Mouse Gonads Using Nucleofection. Sexual Development 5, 7-15

Sabio G, Arthur JSC, Kuma Y, Peggie M, Carr J, Murray-Tait V, Centeno F, Goedert M, Morrice NA, Cuenda A (2005) p38γ regulates the localisation of SAP97 in the cytoskeleton by modulating its interaction with GKAP. EMBO J 24, 1134-1145

Sakai T, Larsen M, Yamada KM (2003) Fibronectin requirement in branching morphogenesis. Nature 423, 876-881

Sambrook, Fritsch, Maniatis (1989) Molecular cloning: a laboratory manual, 2nd ed.

Saxén L (1987) Organogenesis of the kidney. In Developmental and Cell Biology Series, P.W. Barlow, P.B. Green, C.C. White, eds. (Cambridge: Cambridge University Press)

Sayed D, Abdellatif M (2011) MicroRNAs in Development and Disease. Physiological Reviews 91, 827-887

Scherer G (2002) The molecular genetic jigsaw puzzle of vertebrate sex determination and its missing pieces. Novartis Foundation Symposium, 225-236

Schindler EM, Hindes A, Gribben EL, Burns CJ, Yin Y, Lin M-H, Owen RJ, Longmore GD, Kissling GE, Arthur JSC, Efimova T (2009) p38δ Mitogen-Activated Protein Kinase Is Essential for Skin Tumor Development in Mice. Cancer Research 69, 4648-4655

Schlessinger J (2000) Cell Signaling by Receptor Tyrosine Kinases. Cell 103, 211-225

Schmahl J, Eicher EM, Washburn LL, Capel B (2000) Sry induces cell proliferation in the mouse gonad. Development 127, 65-73

Schmahl J, Capel B (2003) Cell proliferation is necessary for the determination of male fate in the gonad. Developmental Biology 258, 264-276

Schmahl J, Kim Y, Colvin JS, Ornitz DM, Capel B (2004) Fgf9 induces proliferation and nuclear localization of FGFR2 in Sertoli precursors during male sex determination. Development 131, 3627-3636

Sekido R, Bar I, Narváez V, Penny G, Lovell-Badge R (2004) SOX9 is up-regulated by the transient expression of SRY specifically in Sertoli cell precursors. Developmental Biology 274, 271-279

Sekido R, Lovell-Badge R (2008) Sex determination involves synergistic action of SRY and SF1 on a specific Sox9 enhancer. Nature 453, 930-934

Sekido R, Lovell-Badge R (2009) Sex determination and SRY: down to a wink and a nudge? Trends in Genetics 25, 19-29

Siggers P, Smith L, Greenfield A (2002) Sexually dimorphic expression of Gata-2 during mouse gonad development. Mechanisms of Development 111, 159-162

Sinclair AH, Berta P, Palmer MS, Hawkins JR, Griffiths BL, Smith MJ, Foster JW, Frischauf A-M, Lovell-Badge R, Goodfellow PN (1990) A gene from the human sex-determining region encodes a protein with homology to a conserved DNA-binding motif. Nature 346, 240-244

Sledz CA, Williams BRG (2005) RNA interference in biology and disease. Blood 106, 787-794

Smith C, Mackay S (1991) Morphological development and fate of the mouse mesonephros. Journal of Anatomy 174, 171-184

Smith L, Willan J, Warr N, Brook FA, Cheeseman M, Sharpe R, Siggers P, Greenfield A (2008) The Maestro (*Mro*) Gene Is Dispensable for Normal Sexual Development and Fertility in Mice. PLoS ONE 3, e4091

Soriano P (1999) Generalized lacZ expression with the ROSA26 Cre reporter strain. Nat Genet 21, 70-71

Sumara G, Formentini I, Collins S, Sumara I, Windak R, Bodenmiller B, Ramracheya R, Caille D, Jiang H, Platt KA, Meda P, Aebersold R, Rorsman P, Ricci R (2009) Regulation of PKD by the MAPK p38δ in Insulin Secretion and Glucose Homeostasis. Cell 136, 235-248

Svingen T, Wilhelm D, Combes AN, Hosking B, Harley VR, Sinclair AH, Koopman P (2009) Ex vivo magnetofection: A novel strategy for the study of gene function in mouse organogenesis. Developmental Dynamics 238, 956-964

Swain A, Lovell-Badge R (1999) Mammalian sex determination: a molecular drama. Genes Dev. 13, 755-767

Takekawa M, Posas F, Saito H (1997) A human homolog of the yeast Ssk2/Ssk22 MAP kinase kinase kinases, MTK1, mediates stress-induced activation of the p38 and JNK pathways. EMBO J 16, 4973-4982

Takekawa M, Tatebayashi K, Saito H (2005) Conserved Docking Site Is Essential for Activation of Mammalian MAP Kinase Kinases by Specific MAP Kinase Kinase Kinases. Molecular Cell 18, 295-306

Tallquist MD, Soriano P (2000) Epiblast-restricted Cre expression in MORE mice: A tool to distinguish embryonic vs. extra-embryonic gene function. genesis 26, 113-115

Tam PPL, Snow MHL (1981) Proliferation and migration of primordial germ cells during compensatory growth in mouse embryos. Journal of Embryology and Experimental Morphology 64, 133-147

Tamura K, Sudo T, Senftleben U, Dadak AM, Johnson R, Karin M (2000) Requirement for p38α in Erythropoietin Expression: A Role for Stress Kinases in Erythropoiesis. Cell 102, 221-231

Tanwar PS, Kaneko-Tarui T, Zhang L, Rani P, Taketo MM, Teixeira J (2010) Constitutive WNT/Beta-Catenin Signaling in Murine Sertoli Cells Disrupts Their Differentiation and Ability to Support Spermatogenesis. Biology of Reproduction 82, 422-432

Tenhunen O, Sármán B, Kerkelä R, Szokodi I, Papp L, Tóth M, Ruskoaho H (2004) Mitogen-activated Protein Kinases p38 and ERK 1/2 Mediate the Wall Stress-induced Activation of GATA-4 Binding in Adult Heart. Journal of Biological Chemistry 279, 24852-24860

Tevosian SG, Albrecht KH, Crispino JD, Fujiwara Y, Eicher EM, Orkin SH (2002) Gonadal differentiation, sex determination and normal *Sry* expression in mice require direct interaction between transcription partners GATA4 and FOG2. Development 129, 4627-4634

Tew SR, Hardingham TE (2006) Regulation of SOX9 mRNA in Human Articular Chondrocytes Involving p38 MAPK Activation and mRNA Stabilization. Journal of Biological Chemistry 281, 39471-39479

Tomizuka K, Horikoshi K, Kitada R, Sugawara Y, Iba Y, Kojima A, Yoshitome A, Yamawaki K, Amagai M, Inoue A, Oshima T, Kakitani M (2008) R-spondin1 plays an essential role in ovarian development through positively regulating Wnt-4 signaling. Human Molecular Genetics 17, 1278-1291

Torres M, Gomez-Pardo E, Dressler GR, Gruss P (1995) Pax-2 controls multiple steps of urogenital development. Development 121, 4057-4065

Tournier C, Whitmarsh AJ, Cavanagh J, Barrett T, Davis RJ (1997) Mitogen-activated protein kinase kinase 7 is an activator of the c-Jun NH2-terminal kinase. Proceedings of the National Academy of Sciences 94, 7337-7342

Ueno N, Ling N, Ying SY, Esch F, Shimasaki S, Guillemin R (1987) Isolation and partial characterization of follistatin: a single-chain Mr 35,000 monomeric protein that

inhibits the release of follicle-stimulating hormone. Proceedings of the National Academy of Sciences 84, 8282-8286

Uhlenhaut NH, Jakob S, Anlag K, Eisenberger T, Sekido R, Kress J, Treier A-C, Klugmann C, Klasen C, Holter NI, Riethmacher D, Schütz G, Cooney AJ, Lovell-Badge R, Treier M (2009) Somatic Sex Reprogramming of Adult Ovaries to Testes by FOXL2 Ablation. Cell 139, 1130-1142

Vainio S, Heikkila M, Kispert A, Chin N, McMahon AP (1999) Female development in mammals is regulated by Wnt-4 signalling. Nature 397, 405-409

Val P, Martinez-Barbera J-P, Swain A (2007) Adrenal development is initiated by Cited2 and Wt1 through modulation of Sf-1 dosage. Development 134, 2349-2358

Ventura JJ, Tenbaum S, Perdiguero E, Huth M, Guerra C, Barbacid M, Pasparakis M, Nebreda AR (2007) p38α MAP kinase is essential in lung stem and progenitor cell proliferation and differentiation. Nat Genet 39, 750-758

Vidal VPI, Chaboissier M-C, de Rooij DG, Schedl A (2001) Sox9 induces testis development in XX transgenic mice. Nat Genet 28, 216-217

Viger RS, Mertineit C, Trasler JM, Nemer M (1998) Transcription factor GATA-4 is expressed in a sexually dimorphic pattern during mouse gonadal development and is a potent activator of the Mullerian inhibiting substance promoter. Development 125, 2665-2675

Wang C, Roy SK (2006) Expression of Growth Differentiation Factor 9 in the Oocytes Is Essential for the Development of Primordial Follicles in the Hamster Ovary. Endocrinology 147, 1725-1734

Warr N, Siggers P, Bogani D, Brixey R, Pastorelli L, Yates L, Dean CH, Wells S, Satoh W, Shimono A, Greenfield A (2009) Sfrp1 and Sfrp2 are required for normal male sexual development in mice. Developmental Biology 326, 273-284

Warr N, Bogani D, Siggers P, Brixey R, Tateossian H, Dopplapudi A, Wells S, Cheeseman M, Xia Y, Ostrer H, Greenfield A (2011) Minor Abnormalities of Testis Development in Mice Lacking the Gene Encoding the MAPK Signalling Component, MAP3K1. PLoS ONE 6, e19572

Washburn LL, Eicher EM (1983) Sex reversal in XY mice caused by dominant mutation on chromosome 17. Nature 303, 338-340

Welshons WJ, Russell LB (1959) THE Y-CHROMOSOME AS THE BEARER OF MALE DETERMINING FACTORS IN THE MOUSE. Proceedings of the National Academy of Sciences 45, 560-566

White S, Ohnesorg T, Notini A, Roeszler K, Hewitt J, Daggag H, Smith C, Turbitt E, Gustin S, van den Bergen J, Miles D, Western P, Arboleda V, Schumacher V, Gordon L, Bell K, Bengtsson H, Speed T, Hutson J, Warne G, Harley V, Koopman P, Vilain E, Sinclair A (2011) Copy Number Variation in Patients with Disorders of Sex Development Due to 46,XY Gonadal Dysgenesis. PLoS ONE 6, e17793

Whitmarsh AJ, Yang SH, Su MS, Sharrocks AD, Davis RJ (1997) Role of p38 and JNK mitogen-activated protein kinases in the activation of ternary complex factors. Mol. Cell. Biol. 17, 2360-2371

Wiggin GR, Soloaga A, Foster JM, Murray-Tait V, Cohen P, Arthur JSC (2002) MSK1 and MSK2 Are Required for the Mitogen- and Stress-Induced Phosphorylation of CREB and ATF1 in Fibroblasts. Mol. Cell. Biol. 22, 2871-2881

Wilhelm D, Englert C (2002) The Wilms tumor suppressor WT1 regulates early gonad development by activation of Sf1. Genes & Development 16, 1839-1851

Wilhelm D, Martinson F, Bradford S, Wilson MJ, Combes AN, Beverdam A, Bowles J, Mizusaki H, Koopman P (2005) Sertoli cell differentiation is induced both cell-autonomously and through prostaglandin signaling during mammalian sex determination. Developmental Biology 287, 111-124

Wilhelm D, Koopman P (2006) The makings of maleness: towards an integrated view of male sexual development. Nat Rev Genet 7, 620-631

Wilhelm D, Hiramatsu R, Mizusaki H, Widjaja L, Combes AN, Kanai Y, Koopman P (2007) SOX9 Regulates Prostaglandin D Synthase Gene Transcription in Vivo to Ensure Testis Development. Journal of Biological Chemistry 282, 10553-10560

Wilhelm D, Washburn LL, Truong V, Fellous M, Eicher EM, Koopman P (2009) Antagonism of the testis- and ovary-determining pathways during ovotestis development in mice. Mechanisms of Development 126, 324-336

Wilkinson MG, Millar JBA (2000) Control of the eukaryotic cell cycle by MAP kinase signaling pathways. The FASEB Journal 14, 2147-2157

Wilson KP, McCaffrey PG, Hsiao K, Pazhanisamy S, Galullo V, Bemis GW, Fitzgibbon MJ, Caron PR, Murcko MA, Su MSS (1997) The structural basis for the specificity of pyridinylimidazole inhibitors of p38 MAP kinase. Chemistry & Biology 4, 423-431

Winter-Vann AM, Johnson GL (2007) Integrated activation of MAP3Ks balances cell fate in response to stress. Journal of Cellular Biochemistry 102, 848-858

Wright E, Hargrave MR, Christiansen J, Cooper L, Kun J, Evans T, Gangadharan U, Greenfield A, Koopman P (1995) The Sry-related gene Sox9 is expressed during chondrogenesis in mouse embryos. Nat Genet 9, 15-20

Yang DD, Kuan C-Y, Whitmarsh AJ, Rinocn M, Zheng TS, Davis RJ, Rakic P, Flavell RA (1997) Absence of excitotoxicity-induced apoptosis in the hippocampus of mice lacking the Jnk3 gene. Nature 389, 865-870

Yang DD, Conze D, Whitmarsh AJ, Barrett T, Davis RJ, Rincón M, Flavell RA (1998) Differentiation of CD4+ T Cells to Th1 Cells Requires MAP Kinase JNK2. Immunity 9, 575-585

Yao HHC, Matzuk MM, Jorgez CJ, Menke DB, Page DC, Swain A, Capel B (2004) Follistatin operates downstream of Wnt4 in mammalian ovary organogenesis. Developmental Dynamics 230, 210-215

Yao Z, Diener K, Wang XS, Zukowski M, Matsumoto G, Zhou G, Mo R, Sasaki T, Nishina H, Hui CC, Tan T-H, Woodgett JP, Penninger JM (1997) Activation of Stress-activated Protein Kinases/c-Jun N-terminal Protein Kinases (SAPKs/JNKs) by a Novel Mitogen-activated Protein Kinase Kinase (MKK7). Journal of Biological Chemistry 272, 32378-32383

Yin Y, Ma L (2005) Development of the Mammalian Female Reproductive Tract. Journal of Biochemistry 137, 677-683

Yoshioka K (2004) Scaffold Proteins in Mammalian MAP Kinase Cascades. Journal of Biochemistry 135, 657-661

Zhan Y, Fujino A, MacLaughlin DT, Manganaro TF, Szotek PP, Arango NA, Teixeira J, Donahoe PK (2006) Müllerian inhibiting substance regulates its receptor/SMAD signaling and causes mesenchymal transition of the coelomic epithelial cells early in Müllerian duct regression. Development 133, 2359-2369

Zhou B, Ma Q, Rajagopal S, Wu SM, Domian I, Rivera-Feliciano J, Jiang D, von Gise A, Ikeda S, Chien KR, Pu WT (2008) Epicardial progenitors contribute to the cardiomyocyte lineage in the developing heart. Nature 454, 109-113

Publications

Bogani D, Siggers P, Brixey R, Warr N, Beddow S, Edwards J, Williams D, Wilhelm D, Koopman P, Flavell RA, Chi H, Ostrer H, Wells S, Cheeseman M, Greenfield A (2009) Loss of Mitogen-Activated Protein Kinase Kinase Kinase 4 (MAP3K4) Reveals a Requirement for MAPK Signalling in Mouse Sex Determination. PLoS Biol 7, e1000196

Warr N, Bogani D, Siggers P, Brixey R, Tateossian H, Dopplapudi A, Wells S, Cheeseman M, Xia Y, Ostrer H, Greenfield A (2011) Minor Abnormalities of Testis Development in Mice Lacking the Gene Encoding the MAPK Signalling Component, MAP3K1. PLoS ONE 6, e19572